Ontario

Ontario Geological Survey
Open File Report 6174

Stratigraphy and Sedimentology of the Mesoproterozoic Sibley Group and Related Igneous Intrusions, Northwestern Ontario: Lake Nipigon Region Geoscience Initiative

2005

Ontario

106-01523/

ONTARIO GEOLOGICAL SURVEY

Open File Report 6174

Stratigraphy and Sedimentology of the Mesoproterozoic Sibley Group and Related Igneous Intrusions, Northwestern Ontario: Lake Nipigon Region Geoscience Initiative

by

B. Rogala, P.W. Fralick and R. Metsaranta

2005

Parts of this publication may be quoted if credit is given. It is recommended that reference to this publication be made in the following form:

Rogala, B., Fralick, P.W. and Metsaranta, R. 2005. Stratigraphy and sedimentology of the Mesoproterozoic Sibley Group and related igneous intrusions, northwestern Ontario: Lake Nipigon Region Geoscience Initiative; Ontario Geological Survey, Open File Report 6174, 128p.

Ontario Prospectors Association

Ontario
Northern Ontario Heritage Fund
Fonds du patrimoine du Nord de l'Ontario

The Lake Nipigon Region Geoscience Initiative is a two-year program of geoscience studies in the Lake Nipigon region operated by the Ontario Prospectors' Association (OPA) and funded through an agreement with the Northern Ontario Heritage Fund Corporation (NOHFC). Projects of this initiative are planned in collaboration with the Ontario Geological Survey (OGS), Lakehead University, mineral industry and government partners.

© Queen's Printer for Ontario, 2005

© Queen's Printer for Ontario, 2005.

Open File Reports of the Ontario Geological Survey are available for viewing at the Mines Library in Sudbury, at the Mines and Minerals Information Centre in Toronto, and at the regional Mines and Minerals office whose district includes the area covered by the report (see below).

Copies can be purchased at Publication Sales and the office whose district includes the area covered by the report. Although a particular report may not be in stock at locations other than the Publication Sales office in Sudbury, they can generally be obtained within 3 working days. All telephone, fax, mail and e-mail orders should be directed to the Publication Sales office in Sudbury. Use of VISA or MasterCard ensures the fastest possible service. Cheques or money orders should be made payable to the *Minister of Finance.*

Mines and Minerals Information Centre (MMIC)
Macdonald Block, Room M2-17
900 Bay St.
Toronto, Ontario M7A 1C3
Tel: (416) 314-3800

Mines Library
933 Ramsey Lake Road, Level A3
Sudbury, Ontario P3E 6B5
Tel: (705) 670-5615

Publication Sales
933 Ramsey Lake Rd., Level A3
Sudbury, Ontario P3E 6B5
Tel: (705) 670-5691(local)
1-888-415-9845(toll-free)
Fax: (705) 670-5770
E-mail: pubsales@ndm.gov.on.ca

Regional Mines and Minerals Offices:

Kenora - Suite 104, 810 Robertson St., Kenora P9N 4J2

Kirkland Lake - 10 Government Rd. E., Kirkland Lake P2N 1A8

Red Lake - Box 324, Ontario Government Building, Red Lake P0V 2M0

Sault Ste. Marie - 70 Foster Dr., Ste. 200, Sault Ste. Marie P6A 6V8

Southern Ontario - P.O. Bag Service 43, 126 Old Troy Rd., Tweed K0K 3J0

Sudbury - Level B3, 933 Ramsey Lake Rd., Sudbury P3E 6B5

Thunder Bay - Suite B002, 435 James St. S., Thunder Bay P7E 6S7

Timmins - Ontario Government Complex, P.O. Bag 3060, Hwy. 101 East, South Porcupine P0N 1H0

Toronto - MMIC, Macdonald Block, Room M2-17, 900 Bay St., Toronto M7A 1C3

This report has not received a technical edit. Discrepancies may occur for which the Ontario Ministry of Northern Development and Mines does not assume any liability. Source references are included in the report and users are urged to verify critical information. Recommendations and statements of opinions expressed are those of the author or authors and are not to be construed as statements of government policy.

If you wish to reproduce any of the text, tables or illustrations in this report, please write for permission to the Team Leader, Publication Services, Ministry of Northern Development and Mines, 933 Ramsey Lake Road, Level B4, Sudbury, Ontario P3E 6B5.

Cette publication est disponible en anglais seulement.

Parts of this report may be quoted if credit is given. It is recommended that reference be made in the following form:

Rogala, B., Fralick, P.W. and Metsaranta, R. 2005. Stratigraphy and sedimentology of the Mesoproterozoic Sibley Group and related igneous intrusions, northwestern Ontario: Lake Nipigon Region Geoscience Initiative; Ontario Geological Survey, Open File Report 6174, 128p.

Contents

Abstract ... xiii

Introduction ... 1
  Purpose ... 1
  Location and Access ... 3
  Regional Geology ... 3
  Previous Work ... 7

Lithofacies Descriptions and Depositional Environment ... 9
  Pass Lake Formation ... 11
    Basal Conglomerate Lithofacies ... 11
    Sandstones ... 12
      Well-Sorted Sandstone Lithofacies ... 14
      Horizontally Laminated Sandstone and Siltstone Lithofacies Association ... 14
      Poorly Sorted Sandstone Lithofacies Association ... 14
      Ripple-Laminated Sandstone Lithofacies Association ... 15
  Rossport Formation ... 15
    Massive Siltstone and Sandstone Lithofacies Association ... 17
    Cyclic Siltstone–Dolomite Lithofacies Association ... 17
    Dolomitic Mudstone Lithofacies Association ... 19
    Stromatolitic Chert–Carbonate Lithofacies Association ... 19
    Intraformational Conglomerate Lithofacies Association ... 21
    Graded, Medium-Grained Sandstone and Siltstone Lithofacies Association ... 22
    Mudstone Lithofacies Association ... 23
    Sandy Siltstone Lithofacies ... 23
    Thinly Laminated, Fine-Grained Sandstone and Siltstone Lithofacies Association ... 23
    Siltstone Lithofacies ... 23
  Kama Hill Formation ... 25
    Horizontally Laminated, Fine-Grained Sandstone and Siltstone Lithofacies Association ... 25
    Mud-Cracked, Fine-Grained Sandstone and Siltstone Lithofacies Association ... 25
    Rippled, Fine-Grained Sandstone and Siltstone Lithofacies Association ... 25
    Horizontally Laminated Mudstone Lithofacies ... 27
  Outan Island Formation ... 27
    Mudstone Lithofacies ... 27
    Laminated Sandstone and Mudstone Lithofacies Association ... 27
    Siltstone Lithofacies Association ... 29
    Sandstone Lithofacies ... 29
    Conglomeratic Lithofacies ... 29
  Nipigon Bay Formation ... 31
    Cross-Stratified Sandstone Lithofacies ... 31
    Horizontally Laminated Sandstone Lithofacies Association ... 32
  Depositional Environments ... 32
    Pass Lake Formation ... 32
    Rossport Formation ... 34
    Kama Hill Formation ... 36

Outan Island Formation 36
Nipigon Bay Formation 37
Summary of Depositional Environments 38

Lithostratigraphy of Sedimentary Units 39
Basin Architecture 39

Stratigraphy of the Nipigon Diabase 45

Contact Metamorphic Effects 57
Discussion 59

Geochemistry 60
Geochronology 64
Isotope Geochemistry 69

Acknowledgments 69

References 70

Appendix 1. Major Element Analyses for the Sibley Group 75

Appendix 2. Geochemical Data for Channel Island Member Carbonate Rocks 79

Appendix 3. Whole Rock Analyses of Sibley Group Shale Samples from Diamond-Drill Hole NB-97-4 92

Appendix 4. Whole Rock Analyses of Sibley Group Shale Samples from Outcrops 95

Appendix 5. Geochemical Data for Soil-Related Carbonates from Various Sibley Group Stratigraphic Units 97

Appendix 6. Geochemical Data for Sibley Group Stromatolites 104

Appendix 7. Geochemical Data for Sibley Group Sulphate Samples 110

Appendix 8. Trace and Rare Earth Element Analyses of Hydrochloric Acid (10%) Soluable Portions of Various Sibley Group Carbonate Rocks 113

Appendix 9. Whole Rock Geochemical Data for Possible Weathered Granite at the Base of Diamond-Drill Hole NB-97-2 115

Appendix 10. Whole Rock Geochemical Data for Possible Weathered Archean Metasedimentary Rocks below Sibley Group in Diamond-Drill Hole NI-92-7 117

Appendix 11. Whole Rock Geochemical Data for Possible Weathered Rove Formation Shale near Pass Lake, Ontario 119

Appendix 12. Whole Rock Analyses of Various Sibley Group Carbonate Rocks 121

Metric Conversion Table 128

FIGURES

1. Location map 2
2. Regional geology 4
3. Drill-hole positions and locations of outcrop where sections were measured 8
4. Generalized stratigraphic section of the Sibley Group 10
5. Paleocurrent trend for 38 measurements of large-scale planar cross-stratified sandstones in the Nipigon Bay Formation. 31

6. Three-dimensional diagram showing the distribution of the Pass Lake Formation 39

7. Three-dimensional diagram showing the distribution of the Rossport Formation 40

8. Three-dimensional diagram showing the distribution of the Kama Hill Formation 41

9. Inset in upper left shows the 3 projected section lines and the positions of the drill holes and outcrop sections (circles) used in creating the cross sections 42

10. Section line A–A' modelled using the bottom (A) and top (B) of the Fire Hill Member of the Rossport Formation as the datum 44

11. General locations of cross sections 46

12. Cross-section locations in the southeastern area 47

13. Cross section from Red Rock, in the northwest, to the Osler Group, in the southeast 48

14. West to east cross section from Red Rock to Kama Hill 48

15. Location of sections in the south-central Sibley Group 49

16. Cross section from the Hele Intrusion, in the southwest, to Moseau Mountain, in the northeast 50

17. West to east cross section from Wolf Lake to Stewart Lake 50

18. Location of cross section in the central basin area 51

19. Cross section from the Seagull intrusion, in the south, to Muskrat Lake, in the north 51

20. Location of cross sections in the northern area 52

21. Cross section from Highway 527, in the northwest, to Black Sturgeon Lake, in the southeast 53

22. North-northwest to south-southeast cross section parallel to the southwest corner of Lake Nipigon 53

23. Furthest north cross section 53

24. Location of the cross section east of Chief Bay 54

25. Cross section from the shore of Chief Bay, in the northwest, to the south shore of Black Sturgeon Bay... 55

26. The location of a section on the southeast side of Lake Nipigon 56

27. Cross section across Pipestone Bay, on the southeastern coast of Lake Nipigon, slightly southeast to Pitjawabik Bay 56

28. Distribution of selected elements away from the heat source in a contact aureole 58

29. A) SiO_2 abundance in medium-grained sandstones from the Sibley Group. B) CaO content in the same sandstone samples as (A) 61

30. A) The chemical index of alteration— $Al_2O_3/(Na_2O + K_2O + CaO + Al_2O_3) \times 100$ —is a common indicator of the degree of weathering in shales. It is applied to medium-grained sandstones here and shows the relative amount of chemical weathering of their constituents. B) the Na_2O/K_2O ratio is also a proxy for degree of weathering as Na will commonly be depleted more effectively than K in the early and mid-stages of chemical weathering 62

31. A) The Zr/V ratio indicates the felsic–mafic ratio of material in the medium-grained sandstones. B) The Nb/Y ratio denotes degree of alkalinity of the detritus 63

32. Stratigraphic variation in the carbon and oxygen isotopic signatures of dolomites in the cyclic facies of diamond-drill hole NB-97-2 in Nipigon Bay. 66

33. Stratigraphic variation in the carbon and oxygen isotopic signatures of dolomite in the cyclic facies of diamond-drill hole NI-92-7 in the south-central Sibley Basin. 67

34. Stratigraphic variation in sulphur isotopic signature and strontium isotopic ratios in the Rossport Formation present in diamond-drill hole NI-92-7. 68

PHOTOS

1. Basal conglomerate lithofacies association 12
2. Sandstone lithofacies association at Pass Lake 13
3. Large-scale cross-stratification of the sandstone lithofacies association of the Pass Lake Formation at Quarry Island 14
4. Cyclic siltstone–dolomite lithofacies association and their cathodoluminescence images 16
5. Gypsum, dolomite, and calcite occurrences within the cyclic siltstone–dolomite lithofacies association . 18
6. Stromatolitic chert–carbonate lithofacies association 20
7. Intraformational conglomerate lithofacies association 22
8. Lithofacies associations of the Kama Hill Formation 24
9. Lithofacies associations of the Outan Island Formation 26
10. Outan Island and Nipigon Bay formations 28
11. Lithofacies of the Nipigon Bay Formation 30

TABLES

1. Stratigraphic summary of lithostratigraphic units in the study area. 5
2. Details of diamond-drill core locations and length. 9

Abstract

The Mesoproterozoic sedimentary rocks of the Sibley Group were deposited in a subsiding, intracratonic basin centred to the south of Lake Nipigon. The Group consists of 5 formations, 3 of which (the Pass Lake, Rossport and Kama Hill) were previously defined, with the remaining 2 (Outan Island and Nipigon Bay) only recently described. The Pass Lake Formation consists of the conglomeratic Loon Lake Member and the commonly sheet-like sandstones of the Fork Bay Member, representing a braided fluvial to shallow lacustrine environment. The Rossport Formation is separated into the Channel Island, Middlebrun Bay and Fire Hill members. The Channel Island Member is a cyclic dolomite–red shale unit, which was deposited in a playa lake. The Middlebrun Bay Member is a stromatolitic unit representing strandline deposits laid down during regression of the lake. The Fire Hill Member consists of mud-cracked red shaly siltstone with mud-chip conglomerates and sand sheets. It probably signifies a change in tectonic style from broad subsidence to active half-graben formation. This interval of subsidence was not related to the Midcontinent Rift, which occurred more than 200 million years later. At this point in the stratigraphy, the paleocurrent trend and provenance of the sediments indicate that the regional paleoslope changed allowing source areas to the south of the basin to replace those in the north. The Fire Hill Member accumulated in a sabkha environment where evaporate minerals grew diagenetically from the saline groundwater in the mudflats. The Kama Hill Formation is composed of purple shales and siltstones with ripple laminated fine-grained sandstones increasing in abundance upward. It represents reflooding of the basin and is transitional to the coarsening-upward deltaic distributary mouth bar complexes of the Outan Island Formation. A regional angular unconformity separates the Outan Island Formation from the eolian sandstones of the Nipigon Bay Formation. The Sibley Group, and underlying Paleoproterozoic and Archean basement, was intruded by Nipigon diabase sills at 1109 Ma. Two thin diabase sheets are present near the base of drill holes in the southernmost Sibley Group subcropping under Nipigon Bay. Sibley Group rocks near the north shore of Lake Superior have one thick sill intruded into the Kama Hill Formation in the east and downramping to the Rossport Formation in the west. This sill thickens toward the central basin area in the region around Muskrat Lake and a second thick diabase sill appears in the stratigraphy. Changes in stratigraphic position and elevation of both the sills and the Sibley Group imply the existence of faults with vertical displacements. The northern area is presently known to contain one thick sill near the contact of the basement with a thin package of strata lithically similar to the Sibley Group. Erosive removal of overlying units and lack of data on the deeper basement make further interpretation speculative. The Sibley Group sedimentary rocks present in the central basin area where the sills are thickest are extensively thermally metamorphosed probably reaching temperatures of approximately 400 to 500°C even tens of metres from the major diabase sills. Paleomagnetic studies conducted on the Sibley Group indicate that diagenetic resetting of the sandstones occurred and is related to the Midcontinent rifting event at approximately 1110 Ma and possibly another event at approximately 1350 Ma. The geochemistry of the Sibley Group clearly shows a trend toward more quartz-rich sandstones upward, more extensive weathering of the sediment upward, more felsic material in the sediment upward and less alkalic material in the detritus upward. Uranium–lead zircon geochronology indicates the lower Sibley Group was deposited between 1.6 and 1.34 Ga and the upper Sibley Group between 1.42 and 1.1 Ga. Isotopic studies suggest the water-mass was lacustrine not marine.

Stratigraphy and Sedimentology of the Mesoproterozoic Sibley Group and Related Igneous Intrusions, Northwestern Ontario: Lake Nipigon Region Geoscience Initiative

B. Rogala[1], P.W. Fralick[2] and R. Metsaranta[3]

Ontario Geological Survey
Open File Report 6174
2005

---

[1] Department of Geological Sciences, Queen's University, Kingston, Ontario K7L 3N6
[2] Corresponding author: Department of Geology, Lakehead University, Thunder Bay, Ontario P7B 5E1
philip.fralick@lakeheadu.ca
[3] Department of Geology, Lakehead University, Thunder Bay, Ontario P7B 5E1

Introduction

This project was undertaken as part of the Lake Nipigon Region Geoscience Initiative (LNRGI): a program operated by the Ontario Prospectors Association and funded through the Northern Ontario Heritage Fund Corporation (NOHFC) with partnerships involving Lakehead University (LU), the Ontario Geological Survey (OGS) and local communities. The Lake Nipigon Region Geoscience Initiative is an effort to better understand the geology of the Nipigon Embayment with the goals of attracting mineral exploration and economic development to the Lake Nipigon region, providing the foundation for informed future land use decisions and to contribute to the geological understanding of the Nipigon Embayment.

PURPOSE

The Sibley Group comprises an approximately 900 m thick assemblage of Mesoproterozoic, siliciclastic and evaporitic sedimentary rocks exposed from the northwest shores of Lake Superior to the area south, west and, to a minor extent, east of Lake Nipigon (Figure 1). These rocks are very well preserved, being generally unmetamorphosed, with the exception of local contact metamorphic effects, and are close to flat lying.

The present study of the Sibley Basin was initiated to increase the understanding of the stratigraphy (including the stratigraphy of the diabase sill complex), physical and chemical sedimentology, age, and the nature of paleohydrologic systems operating both during Sibley Group deposition and postdepositionally. Previous studies have provided analyses of sedimentology, stratigraphy and depositional environments (Franklin 1970; Cheadle 1986a, 1986b). However, due to recent drilling projects in the Nipigon Plate, the opportunity to investigate the basin with data obtained from a combination of 25 drill holes and surface outcrops was available for the first time. This expanded database gave new insight, especially in the area of stratigraphy.

There are several aspects to this study of the Sibley Basin. The most fundamental part is the definition and interpretation of lithofacies associations. Lithofacies associations are groupings of individual lithofacies (i.e., rippled fine-grained sandstone), which are commonly found interbedded together as an association (i.e., rippled fine-grained sandstone and parallel-laminated siltstone). They form the basic building blocks of stratigraphy and the types of these lithofacies and their geographic location are used to define formations. Two new formations have been, at this stage, informally added to the stratigraphy. The first occurs mainly in drill core and consists of 2 members. The second new formation can be found in drill core and on Simpson Island in Lake Superior. Previously existing, formally defined formations and members were also described and refined. This provided the framework for creating a model of the stratigraphy of sedimentary rocks present in the Sibley Basin. The diabase to gabbro sill complexes were then placed within this stratigraphy.

Excellent preservation of depositional and early diagenetic features in these rocks, combined with the diversity of genetically distinct sedimentary rocks, allowed them to be studied from both a physical and chemical sedimentological standpoint. A classic sedimentological approach combined with geochemistry allowed for a more powerful characterization of the paleoenvironmental evolution of the Sibley Group than that which could have been accomplished by traditional sedimentological and stratigraphic studies. Once the sedimentology and stratigraphy were defined, it was possible to begin modelling the basin. Information from 25 drill holes, as well as information from outcrops, was compiled, allowing detailed three-dimensional basinwide analysis of facies trends and distributions.

Formation-scale trends in provenance were investigated with the use of geochemistry and detrital zircon geochronology. Samples of medium-grained sandstone were collected for geochemistry from drill holes spanning the entire thickness of the Sibley Group. These data were then plotted against depth to appraise variations between formations, possibly related to changes in the source areas. Three samples for laser ablation mass spectroscopy (LA-MS), U/Pb, detrital zircon, geochronology were collected from the Sibley Group. In addition, one sample was also collected by R.M. Easton (OGS) from rocks lithically correlative to the Sibley Group and another from probable source rocks in the Rove Formation. Approximately 250 zircons were analyzed providing not only time constraints on deposition, but also information on provenance.

The history of fluid migration in sediments and sedimentary rocks of the Sibley Group was investigated in 3 ways. Firstly, isotopic studies of evaporite minerals in the lower half of the Group provided information on fluid migration during formation of these primary and early diagenetic minerals.

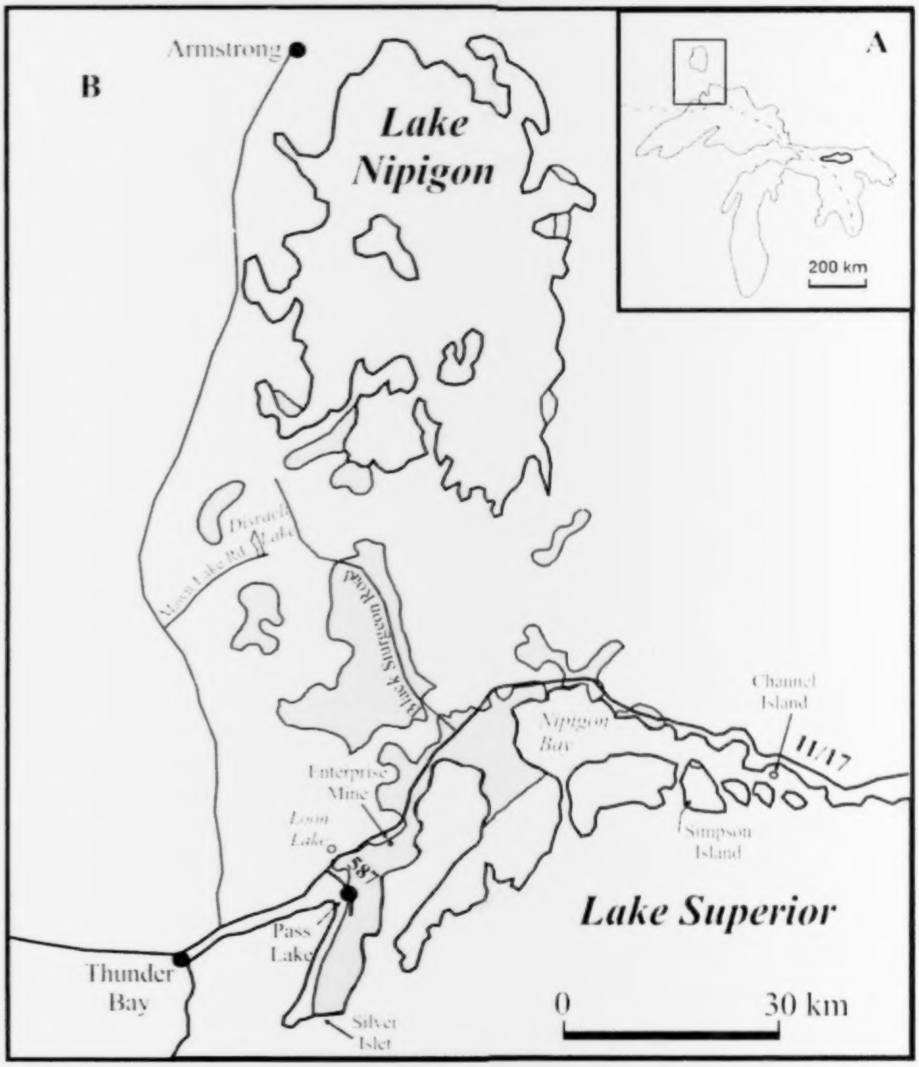
Armstrong
B
Lake Nipigon
A
200 km
Disraeli Lake
Moon Lake Rd
Black Sturgeon Road
Channel Island
Nipigon Bay
11/17
Enterprise Mine
Loon Lake
587
Simpson Island
Pass Lake
Lake Superior
Thunder Bay
0
30 km
Silver Islet

Figure 1. A) The outlined area on the inset map shows the location of the Sibley Basin. B) The shaded area shows the surface distribution of the Sibley Group.

Formation-scale trends in provenance were investigated with the use of geochemistry and detrital zircon geochronology. Samples of medium-grained sandstone were collected for geochemistry from drill holes spanning the entire thickness of the Sibley Group. These data were then plotted against depth to appraise variations between formations, possibly related to changes in the source areas. Three samples for laser ablation mass spectroscopy (LA-MS), U/Pb, detrital zircon, geochronology were collected from the Sibley Group. In addition, one sample was also collected by R.M. Easton (OGS) from rocks lithically correlative to the Sibley Group and another from probable source rocks in the Rove Formation. Approximately 250 zircons were analyzed providing not only time constraints on deposition, but also information on provenance.

The history of fluid migration in sediments and sedimentary rocks of the Sibley Group was investigated in 3 ways. Firstly, isotopic studies of evaporite minerals in the lower half of the Group provided information on fluid migration during formation of these primary and early diagenetic minerals.

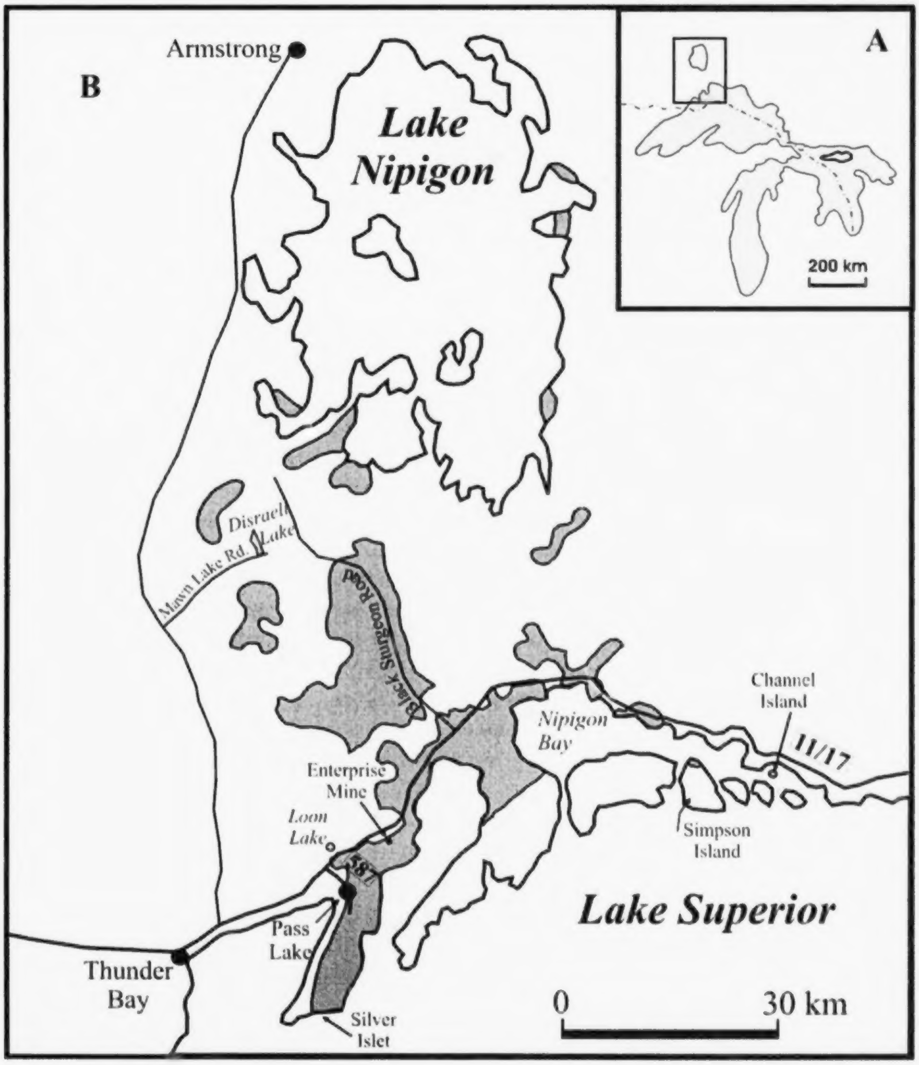
Armstrong
B
Lake Nipigon
A
200 km
Disraeli Lake
Mawn Lake Rd.
Black Sturgeon Road
Channel Island
Nipigon Bay
11/17
Enterprise Mine
Loon Lake
587
Simpson Island
Pass Lake
Thunder Bay
Lake Superior
Silver Islet
0
30 km

Figure 1. A) The outlined area on the inset map shows the location of the Sibley Basin. B) The shaded area shows the surface distribution of the Sibley Group.

The stable isotopes of C, O and S plus the radiogenic isotopes of Sr were employed in this study. Secondly, the mineralogy and geochemistry of contact-metamorphosed sedimentary rocks were investigated to ascertain the mobility of various elements and the generation and movement of fluids. Lastly, paleomagnetic studies were carried out on sandstone samples to ascertain the degree to which their alignment of magnetic minerals had been reset and the approximate timing of the resetting events.

The data sets taken together outline the development of the Sibley Basin, the lateral and vertical organization of the sedimentary fill and the depositional environments it represents, the location of the diabase sheets within this stratigraphic context and the synsedimentary to late postdepositional fluid migration history within this basin.

LOCATION AND ACCESS

The Sibley Basin is an ovoid depression approximately 175 km wide and 400 km long. Rocks filling the basin crop out discontinuously over a 15 000 km^2 area from the northern shore of Lake Superior to the western shore of Lake Nipigon and to Armstrong in the north, as shown in Figures 1 and 2. Outcrops are accessible along Highway 11/17 and Highway 587, as well as along a variety of gravel roads branching off the Black Sturgeon Road and Mawn Lake Road. Outcrops are also accessible by boat along the shore of Lake Nipigon and on several islands in Lake Superior.

The best exposures of the Sibley Group are present in the southern portions of the region near Lake Superior. Contact metamorphic grade increases and exposure quality decreases toward the north where the Sibley Group has been intruded by 2 thick mafic sills of the Keweenawan Nipigon Diabase (cf., Hart and Magyarosi 2004; Hart 2005; Metsaranta and Fralick 2004). Diamond-drill cores from the northern portion of the region show that the Sibley Group subcrops beneath the majority of the area covered by the Nipigon Diabase sheets. The original lateral extent of the Sibley Group is unknown with its preservation largely controlled the presence of erosion resistant overlying igneous rocks and the downdropping of fault blocks during Mesoproterozoic rifting.

REGIONAL GEOLOGY

The Sibley Group is underlain by Archean metavolcanic, metasedimentary and granitic rocks, Paleoproterozoic Animikie Group rocks, and Mesoproterozoic granites and rhyolites. Diabase sills and ultramafic plugs intrude the Sibley Group and the Osler Group overlies it. This succession of stratigraphic units, with rough age constraints, is summarized in Table 1 and the Sibley Group is shown in relation to the regional geology in Figure 2.

Geophysical maps have shown that the greenstone belts of the Mesoarchean to Neoarchean eastern Wabigoon Subprovince extend beneath the Proterozoic units of the Sibley Group in the northern and central areas of Lake Nipigon (Blackburn et al. 1991). Supracrustal rocks and synvolcanic granitoid batholiths dominate the eastern Wabigoon Subprovince (Blackburn et al. 1991). The Neoarchean volcanism, consisting of metamorphosed mafic, felsic and ultramafic rocks, ranges from $2769\ ^{+6}/_{-5}$ Ma (Anglin et al. 1988) to 2722±1 Ma (Tomlinson et al. 2003). Clastic sediments represent alluvial fan, fluvial, and turbiditic sequences (Barrett and Fralick 1985, 1989; Devaney and Williams 1989; Fralick and Barrett 1995; Eriksson, Krapez and Fralick 1994, 1997). The Wabigoon Subprovince has been subjected to 3 phases of folding and shearing. The earlier phase includes imbrication and shallow-plunging folds, followed by belt-parallel, upright to steeply dipping folds. The final structures are due to brittle-ductile shearing, and are related to post-accretion convergence (Blackburn et al. 1991). A more detailed examination of the structure present in the southeastern portion of Wabigoon Subprovince is given by Lafrance, DeWolfe and Stott (2004).

The southern portion of the Sibley Group is predominantly underlain by rocks of the Quetico Subprovince. The Quetico Subprovince is principally composed of metamorphosed turbiditic sediment, derived from neighbouring subprovinces such as the Wabigoon (Williams 1991; Fralick, Jinhua and Williams 1992; Fralick and Kronberg 1997). Igneous rocks are typically felsic to intermediate intrusives, with rare mafic and felsic extrusives, and an even rarer suite of gabbroic and ultramafic rocks (Williams 1991). Detrital zircon ages range from 3.0 to 2.7 Ga (Williams 1991). The boundary between the Wabigoon and Quetico subprovinces is defined by the Blackwater fault, an extension of which the Sibley

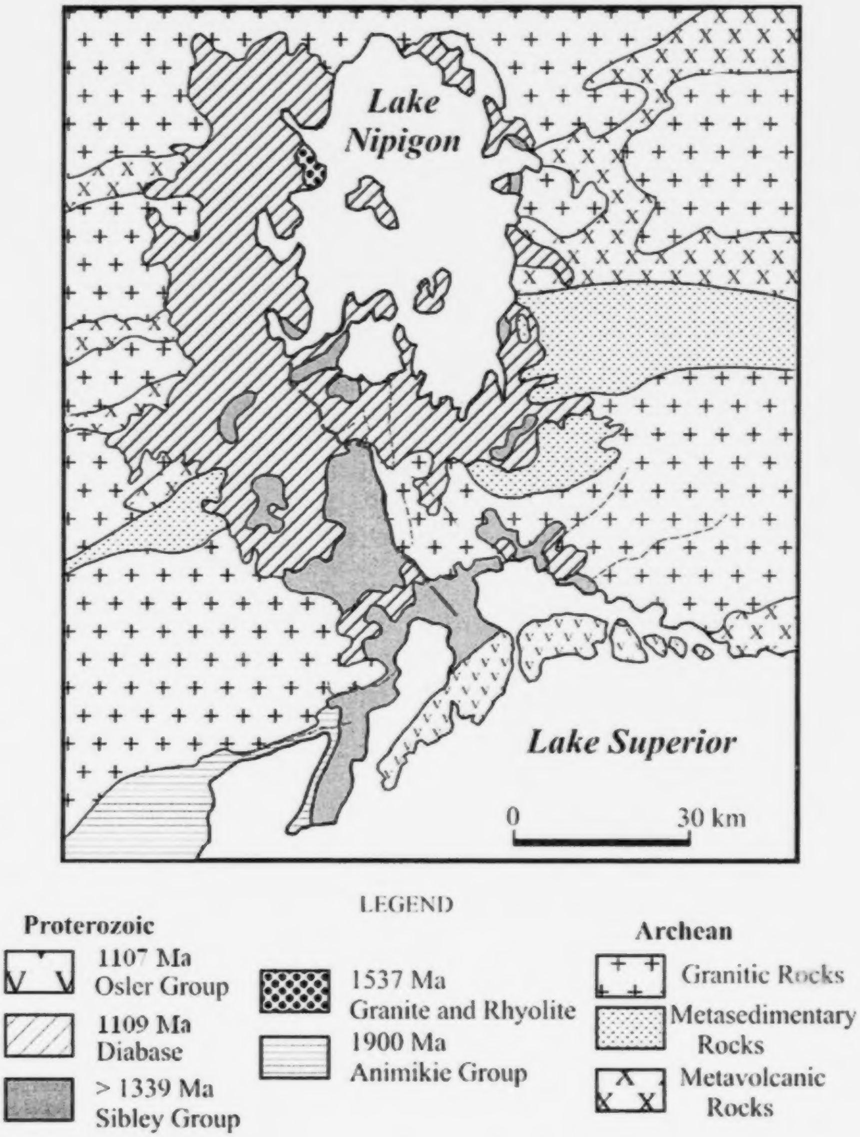
Lake Nipigon
Lake Superior
0
30 km
LEGEND
Proterozoic
1107 Ma Osler Group
1109 Ma Diabase
> 1339 Ma Sibley Group
1537 Ma Granite and Rhyolite
1900 Ma Animikie Group
Archean
Granitic Rocks
Metasedimentary Rocks
Metavolcanic Rocks

Figure 2. Regional geology of the study area. Some minor faults are shown as thin grey lines composed of small dashes. The thick grey line composed of big dashes is the Black Sturgeon fault.

Table 1. Stratigraphic summary of lithostratigraphic units in the study area.

			Age (Ma)
Osler Volcanic Group			1107
Diabase sills			1110 – 1114
Ultramafic to mafic intrusions			1110 – 1124
Sibley Group	Nipigon Bay Formation		1339 – 1537
	Outan Island Formation	Hele Member	
		Lyon Member	
	Kama Hill Formation		
	Rossport Formation	Fire Hill Member	
		Middlebrun Bay Member	
		Channel Island Member	
	Pass Lake Formation	Fork Bay Member	
		Loon Lake Member	
English Bay complex			1537 – 1547
Animikie Group	Rove Formation		1878
	Gunflint Formation		
Quetico Subprovince			2700
Wabigoon Subprovince			2650 – 3000

Group probably overlies to the southwest of Lake Nipigon. There are also 4 deformational events, involving shearing and folding, that affect the Quetico (Williams 1991). The first event is in the form of soft-sediment deformation and slumps, followed by bedding-parallel shearing that produced steep to variable-plunging folds. The third deformational event created upright to inclined shallow-plunging folds. The final deformation event is in the form of small-scale shear zones, representing compression from the south to southeast. The Quetico Subprovince underwent 2 stages of metamorphism. The early stage is a high-pressure metamorphic event that is rarely preserved. This was followed by regional high-temperature metamorphism (Williams 1991).

The Gunflint and Rove formations of the Animikie Group can be found sporadically underlying the Sibley Group between Thunder Bay and Loon Lake (*see* Figure 1). The Animikie Basin was formed on the southern margin of the Superior Province (Pufahl and Fralick 2000) and comprises a southward-thickening wedge deposited on a shelf during transgressive–regressive–transgressive cycles (Fralick and Barrett 1995; Fralick, Davis and Kissin 2002; Pufahl and Fralick 2004). The sediments consist of basal conglomerate, black shales to slates, ferruginous carbonate, chert, jasper, and hematite–magnetite grainstones of the Gunflint Formation (Sutcliffe 1991). The Rove Formation, a thick turbiditic black shale–sandstone sequence, overlies the Gunflint Formation.

There is some debate as to the formation of the basin. Some researchers suggest that the Animikie Basin developed as a foreland basin (Ojakangas, Morey and Southwick 2001; Schneider et al. 2002), whereas others suggest a back-arc basin setting (Fralick, Davis and Kissin 2002). A euhedral zircon population from tuffaceous units in the Gunflint Formation gave a U/Pb age of 1878.3±1.3 Ma (Fralick, Davis and Kissin 2002). The Animikie Basin was deformed and truncated to the south by the Paleoproterozoic Penokean Orogeny. A series of igneous intrusions were emplaced during the termination of the orogenic event.

The English Bay complex is located on the western shore of Lake Nipigon (*see* Figure 2), directly underlying a thin sandstone lithically correlative with the Sibley Group (Davis and Sutcliffe 1985; Hollings, Fralick and Kissin 2004). A lower age bracket of 1537 $^{+10}/_{-2}$ Ma (Davis and Sutcliffe 1985) is defined by U/Pb zircon age determinations obtained from the Redstone Point granite of the English Bay complex. A caldera structure found on the northern part of Lake Nipigon may be associated with its emplacement (Sutcliffe 1991).

A minimum depositional age for the middle portion of the Sibley Group is provided by a Rb/Sr whole rock age of 1339±33 Ma (Franklin 1978) that was obtained from the siltstones of the Rossport and Kama Hill formations. The English Bay complex has been used to define an upper age limit, though this is problematic as, though the overlying thin sandstone to siltstone succession is similar to the basal Sibley Group at locations to the south, a lithological correlation does not necessarily imply a chronostratigraphic correlation.

The Keweenawan Supergroup typically refers to a group of mafic volcanic and sedimentary rocks deposited during a period of active magmatism and rifting, known as the Midcontinent Rift event. Eruptions occurred between 1109 and 1087 Ma (Ojakangas, Morey and Green 2001). Gravity maps have recently been used to infer the presence of felsic intrusive rocks within the mafic volcanic rocks along the northern margin of the Midcontinent Rift (Thomas and Teskey 1994). Keweenawan Supergroup rocks can be found in an arcuate band from Kansas up to Lake Superior, and down to Lake Erie (Ojakangas, Morey and Green 2001). The rift encompasses a series of axial blocks, bounded by high-angle listric faults, with sedimentary basins forming in the half-grabens flanking them (Ojakangas, Morey and Green 2001). The southernmost portion of the Sibley Basin was dissected by this rifting event (*see* Figure 2).

A series of intrusions were emplaced shortly before or contemporaneously with Keweenawan-age volcanism and sedimentation. Several gabbroic intrusions have been emplaced into rocks of the Animikie Group and Keweenawan Supergroup (Sutcliffe 1991). Two main series of sills have also been reported: the Logan sills and the Nipigon sills in the vicinity of Lake Nipigon. The latter intrude the Sibley Group. The Nipigon sills were determined to have an age of $1108.8\ ^{+4}/_{-2}$ Ma based on U/Pb geochronology on zircon and baddeleyite from a composite sample (Davis and Sutcliffe 1985). Uranium–lead geochronology work done on baddeleyite from both the Logan and Nipigon sills, as part of the Lake Nipigon Region Geoscience Initiative, yielded ages in the range of 1115 to 1110 Ma (Heaman and Easton 2005; Heaman et al. 2005).

In the area of the Sibley Group, the Keweenawan Supergroup is represented by the Osler Group. The Osler Group is a 2.75 km thick sequence (Ojakangas, Morey and Green 2001), comprised predominantly of subaerial tholeiitic basalts, with some andesite, rhyolite, and interflow sediments (Sutcliffe 1991). Directly above the Sibley Group, the Osler Group occurs as a series of rhyolite flow rocks with an age of 1107.5 Ma (Davis and Sutcliffe 1985). Above this, there are sporadic occurrences of conglomerate, rich in porphyritic clasts, as well as lenses of cross-bedded sandstone and siltstone. Interflow sediments are most common in the lower part of the Osler Group, whereas the top of the sequence is dominated by basaltic flow rocks (Sutcliffe 1991).

The bedrock in the region is sporadically covered by tills, glaciofluvial sands, and glaciolacustrine laminated mudstone deposited during Pleistocene glaciation and deglaciation. Ice receded from the tip of the Keweenaw Peninsula by 9500 years ago. As deglaciation proceeded, catastrophic floods drained through the Nipigon Basin into the Lake Superior Basin (Barnett 1991). Over the next 500 years, water level fluctuations due to these flooding events in Lake Superior stabilized (Barnett 1991), though eustatic rebound continued to effect the shoreline.

PREVIOUS WORK

Logan (1863) was the first to discuss the Sibley sediments. He included them with the Upper Copper-bearing Series of the Lake Superior region, tentatively calling them Lower Silurian based on a possible stratigraphic correlation with the Potsdam sandstone in Michigan. This was followed by geological surveys undertaken by Robert Bell between 1866 and 1869 (Bell 1870). Hunt (1873) later divided the Upper Copper-bearing Series into the Animikie and Keweenaw groups, with the Sibley sediments being placed in the latter. Disagreements still arose as to the age of the Sibley. Van Hise and Leith (1909) supported a Precambrian age, whereas Wilson (1910) argued for a Paleozoic age. Tanton (1931) incorporated the Animikie and Keweenaw groups into the Kaministikwa Group, which was subdivided into the lower Animikie Series, central Sibley Series, and an upper Osler Series. Comprehensive mapping by McIlwaine (1971a, 1971b, 1975) and Coates (1972) led to the investigations of the Sibley Group by Franklin (1970, 1978) and Franklin et al. (1980).

Franklin (1970) originally divided the Sibley Group into 7 lithological units. These were (from bottom to top) conglomeratic lenses, sandstone, lower red sandy mudstone, stromatolite–chert, upper red limey mudstone, purple mudstone, and limestone. They were described based on their mineralogy and sedimentology. In 1980, Franklin et al. allocated the present names to the units in the Sibley Group: the Pass Lake, Rossport, and Kama Hill formations. Their (1980) Pass Lake Formation consisted of conglomeratic lenses overlain by sandstones. They divided the Rossport Formation into Lower, Central, and Upper members. The Lower Member was described as sandstone beds interlayered with hematitic dolomite beds. The Central and Upper members are, respectively, correlated with the stromatolite chert and upper red limey mudstone units of his previous division.

Cheadle (1986a, 1986b) described the formations in great detail and refined the depositional environments attributed to each. He subdivided the Pass Lake Formation into the Loon Lake and Fork Bay members, and the Rossport Formation into the Channel Island, Middlebrun Bay, and Fire Hill members (Cheadle 1986b). The Loon Lake Member replaced the conglomeratic facies from the Pass Lake Formation, as defined by Franklin et al. (1980). The sandstone unit of the Pass Lake Formation was renamed the Fork Bay Member (Cheadle 1986b). The Channel Island, Middlebrun Bay, and Fire Hill members supplanted the Lower, Middle, and Upper members of the Rossport Formation.

There is some ongoing debate as to the origin of the Sibley Basin. Franklin et al. (1980) suggested that the basin was created as a failed arm of the Midcontinent Rift system. Cheadle (1986a) disagreed with this theory and suggested two alternative possibilities. Although he pointed out inconsistencies between the Sibley Group and rift-related basins, he tentatively suggested that the Sibley Basin might have developed due to extension associated with an earlier Elsonian rifting event (circa 1400 Ma). However, Cheadle's (1986a, 1986b) preferred theory was that the Sibley Basin was a result of lithospheric stretching related to the very earliest extensional phases of the Midcontinent Rift. Hollings, Fralick and Kissin (2004) proposed that the Sibley Basin was created during broad subsidence following thermal doming related to plume activity, which had resulted in the formation of the English Bay rhyolite-granite complex at 1537 Ma.

The Nipigon diabase sills, which intrude the Sibley Group, were also worked on extensively during the mid 1980s. Sutcliffe conducted a program of regional mapping, petrology and geochemistry of these bodies culminating with production of his PhD thesis (Sutcliffe 1986).

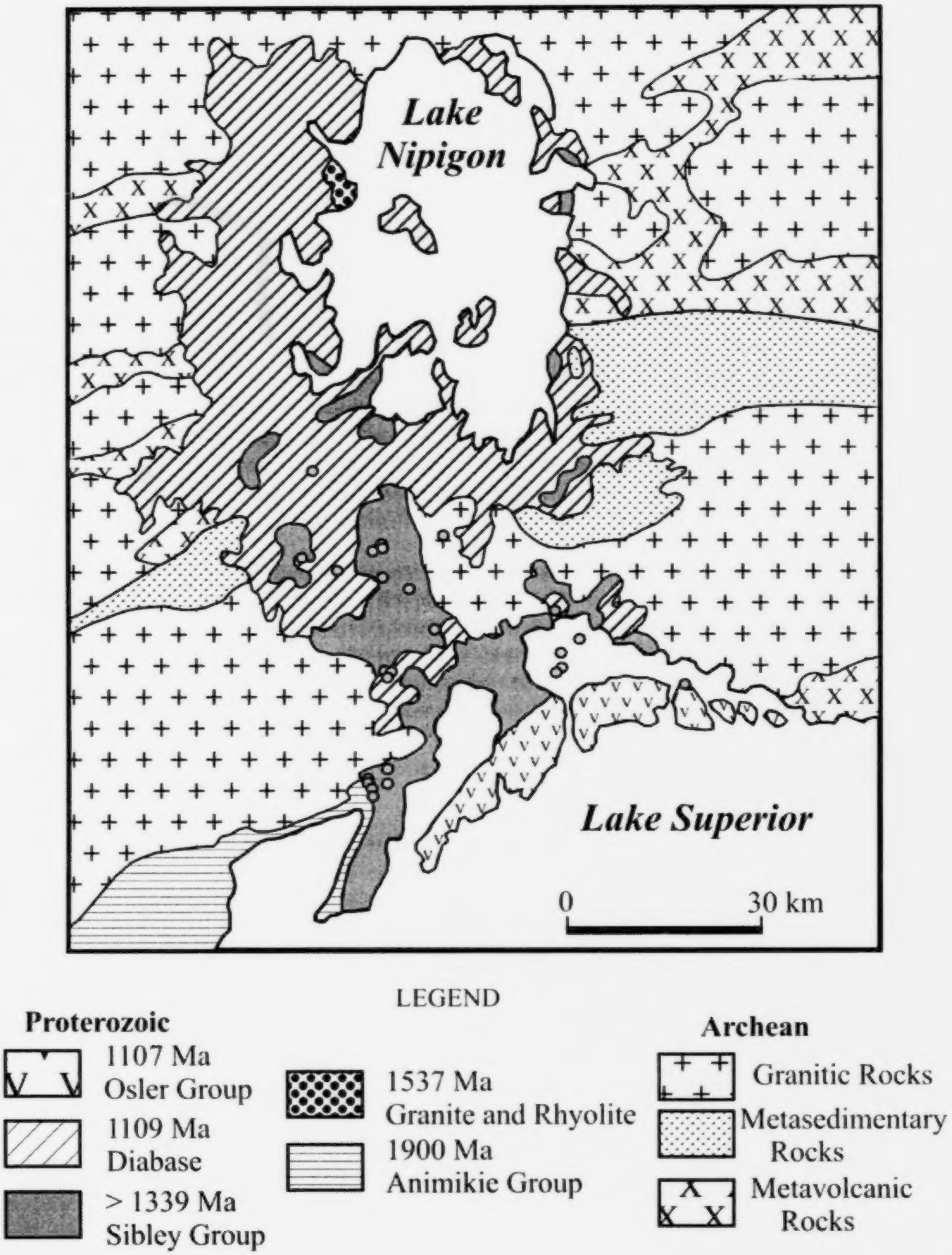
Lake Nipigon
Lake Superior
0
30 km
LEGEND
Proterozoic
1107 Ma Osler Group
1109 Ma Diabase
> 1339 Ma Sibley Group
1537 Ma Granite and Rhyolite
1900 Ma Animikie Group
Archean
Granitic Rocks
Metasedimentary Rocks
Metavolcanic Rocks

Figure 3. Drill-hole positions and locations of outcrop where sections were measured in areas of good exposure are shown as filled circles.

Table 2. Details of diamond-drill core locations and length.

Drill Hole	UTM Co-ordinates (NAD27, Zone 16)		Length (m)	Elevation (m asl)
	Easting (m)	Northing (m)		
SB-101	377950	5383500	177.31	297
SB-102	377900	5383300	163.80	293
SO-1	384150	5433950	53.26	343
SO-2	384150	5433950	109.08	343
DO-82-1	377500	5410100	16.97	369.8
DO-82-2	377500	5410070	22.91	360.7
DO-82-3	377410	5410900	21.03	352.1
DO-82-4	377300	5410100	20.72	339.4
DO-82-5	377410	5409890	29.25	333.6
DO-82-6	377660	5410100	15.21	359.8
DO-82-7	378850	5410870	48.12	316.4
DO-82-8	377670	5410030	22.01	356.8
NI-92-5	356750	5468310	42.38	381
NI-92-7	353850	5443000	151.15	404
CYP-96-1	432500	5419940	464.5	183
NB-97-2	426990	5416241	677.8	183
NB-97-4	425430	5410540	1015.6	183
NB-97-5	427140	5411800	744.2	183
HE-02-01	391250	5423148	253.62	403
HE-02-02	393007	5449701	245.00	402
SR-02-01	363501	5439302	287.00	316
DDH-1	376365	5437493	120.81	290
DDH-2	376371	5446449	86.63	297
DDH-3	346299	5446449	53.75	297
DDH-5	373679	5444646	39.30	290

Lithofacies Descriptions and Depositional Environment

The lithostratigraphy and the depositional environments, which controlled the three-dimensional development of that stratigraphy, were investigated by conducting detailed examination of outcrops and drill core from the study area. Considerable recent drilling has been undertaken by various companies within the area of the Nipigon Plate to access mineral potential. Substantial amounts of the drill core from these projects is located in the Ministry of Northern Development and Mines Conmee and James Street core libraries in Thunder Bay. Cores from 25 drill holes were logged and are summarized in Table 2. The positions of the drill holes are shown in Figure 3. Logs of all of the drill holes are given in Appendix A of Rogala (2003).

The Sibley Group now includes 5 formations (Rogala 2003) (Figure 4). The Pass Lake Formation is the basal unit, consisting of the Loon Lake and Fork Bay members. Cheadle (1986a) noted that sandstones, correlated with the Pass Lake Formation, have been found intercalated with rhyolites of the English Bay complex. The Rossport Formation, comprising the Channel Island, Middlebrun Bay, and Fire Hill members, overlies the Pass Lake Formation. The Kama Hill Formation is unsubdivided and overlies the Rossport Formation. These 3 formations were formerly defined by Franklin (1970), Franklin et al. (1980) and Cheadle (1986a, 1986b). Drill holes in Lake Superior have intersected upper units not previously recognized on the mainland. This has resulted in the identification of two new formations. The Outan Island Formation overlies the Kama Hill Formation and has been divided into 2 members: the Lyon Member and the Hele Member. The Outan Island Formation is overlain by the Nipigon Bay Formation, which is not subdivided.

Some problems occur when attempting to describe the Sibley Group within the confines of these formations due to overlap of lithofacies associations among them. This is particularly evident when trying to distinguish the Channel Island Member from the Fire Hill Member of the Rossport Formation, as defined by Cheadle (1986a) and Franklin et al. (1980). Therefore, the Sibley Group will be described here by formation and subdivided into lithofacies associations, some of which are similar to those described by Cheadle (1986b). These will later be put into the context of the members and formations formerly defined by Cheadle (1986a).

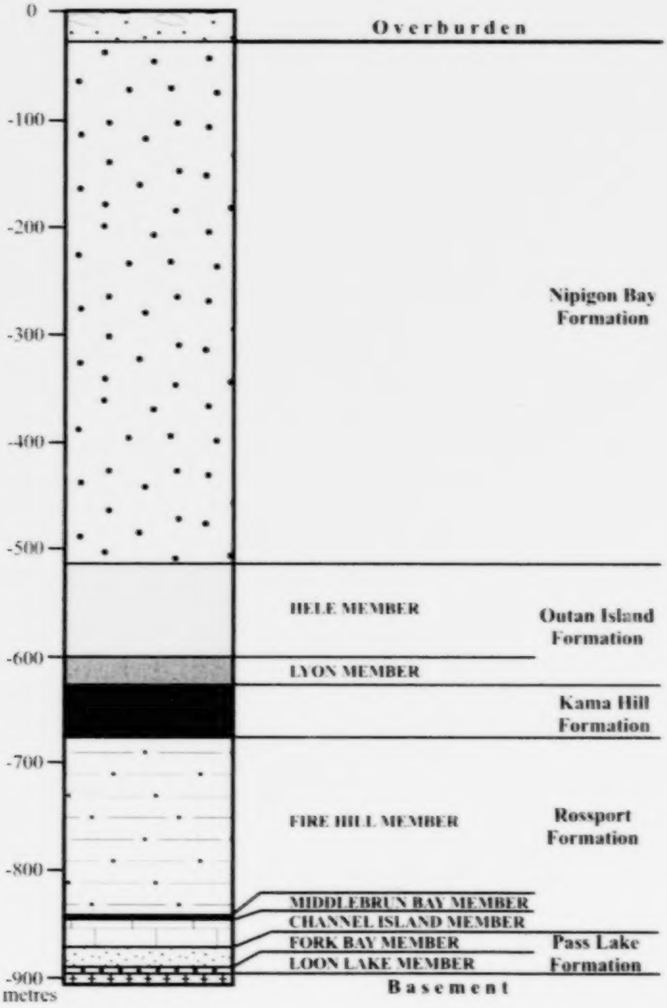
0
-100
-200
-300
-400
-500
-600
-700
-800
-900
metres
Overburden
Nipigon Bay Formation
HELE MEMBER
Outan Island Formation
LYON MEMBER
Kama Hill Formation
FIRE HILL MEMBER
Rossport Formation
MIDDLEBRUN BAY MEMBER
CHANNEL ISLAND MEMBER
FORK BAY MEMBER
LOON LAKE MEMBER
Pass Lake Formation
Basement

Figure 4. Generalized stratigraphic section of the Sibley Group.

PASS LAKE FORMATION

The Pass Lake Formation crops out sporadically throughout the Sibley Basin, with the thickest accumulations occurring in the central part of the basin. It thins toward the southeast. When present, the formation can reach a thickness of 100 m, although it is more typically 5 to 25 m thick. Paleocurrents trend toward the southeast (Cheadle 1986a).

The Pass Lake Formation consists of the Loon Lake Member and the Fork Bay Member. Cheadle (1986a) described the Loon Lake Member as a basal conglomerate facies, which is also the definition applied here. The Fork Bay Member was divided by Cheadle (1986a) into 3 facies: 1) heterolithic, 2) cross-bedded, and 3) plane-bedded sandstone facies. However, the large-scale features that these associations are based on are difficult to identify in drill core, so these facies descriptions will be slightly modified to take this into account. The division between these members is defined as the point where the conglomerates of the Loon Lake Member give way to the sandstones of the Fork Bay Member. This transition is typically sharp, although some gradational pebbly sandstones do occur. These pebbly sandstones have been included with the Fork Bay Member, in accord with Cheadle (1986a). The Loon Lake Formation can reach a thickness of 15 m, and the Fork Bay Member is 0 to 80 m thick.

Basal Conglomerate Lithofacies

The basal conglomerate occurs sporadically in drill core and outcrops in a patchy semicircle along the southern margin of the basin, filling topographic lows. Its thickest accumulation is in the southeast. The conglomerate can reach a thickness of 15 m, but is more typically only a few metres thick.

The basal conglomerate can appear tabular to lensoid, and may be matrix supported to clast supported, with well-rounded clasts up to 40 cm in diameter (Photo 1). Some outcrops are clast-supported at the base and matrix-supported at the top. An outcrop on La Grange Island in Lake Superior shows large-scale cross-stratification. Clasts are predominantly jasper, taconite, and shale derived from the underlying Gunflint and Rove formations. Where the conglomerate overlies Archean granites, clasts of granite and quartzite dominate with some metavolcanic clasts (Cheadle 1986b).

Cheadle (1986a) noted that cross-bedded medium-grained sandstone and dolomitic mudstone lenses are present in some outcrops. These are typically erosively cut by large scour-and-fill structures by overlying conglomerate. Caliche crusts and clast-coatings were also observed by Cheadle (1986a).

An excellent exposure of this member occurs in a railway cut near Loon Lake. Here, massive clast-supported, polymictic, cobble to boulder conglomerates form large lenses in sandstones and siltstones. Most sandstones are themselves composed of stacked lenses with sandstone lenses also present internally in conglomerates. Carbonate cement and well-developed caliche horizons are prominent in this assemblage. Good exposure of the Loon Member also occurs at Pass Lake (*see* Figure 1). At this locality, approximately 1 to 2 m of conglomerate overlie a weathering profile developed on Rove Formation shales. The majority of the outcrop contains a single thick layer consisting of a clast-supported, massive, polymictic, cobble conglomerate with a sandy hematite-rich matrix. Quartz-rich sandstones of the Fork Bay Member sharply overlie the conglomerate at this locality.

Sandstones

The sandstone lithofacies association is divided into several types of individual lithofacies based on drill core analysis, including well-sorted massive sandstone, poorly sorted massive sandstone, silty sandstone, laminated siltstone and sandstone, and rippled sandstone. These units commonly grade into each other. Combinations of these lithofacies would be correlative with Cheadle's (1986a) plane-bedded (Photo 2), cross-bedded (Photo 3), and heterolithic facies. These facies seem to be organized with the heterolithic facies at the bottom, overlain by the cross-bedded facies, which is overlain by the plane-bedded facies (Cheadle 1986a).

Cheadle (1986a) described the plane-bedded facies as being primarily composed of horizontal laminae and thin beds, with secondary planar cross-beds and oscillation ripples. He also noted that, at Silver Islet, these are accompanied by scour-and-fill structures with coarser sandstone deposited within them. The coarse-grained sandstones filling scours are erosively overlain by the sandstones of the plane-bedded facies. Interbeds of calcareous and dolomitic mudstone and siltstone can also be found there. The well-sorted sandstone, horizontally laminated sandstone and siltstone, and silty sandstone facies described here may be representative of the plane-bedded facies of Cheadle (1986a).

The cross-bedded facies described by Cheadle (1986a) consists of a 5 to 30 m thick unit of large-scale planar cross-beds. These cross-beds can be wedge-shaped or tabular, with individual sets reaching thicknesses of 1 to 10 m. Cheadle (1986a) noted that, at Channel Island, the cross-beds are interbedded with the plane-bedded facies, which partially overlies scour surfaces with pebbly sandstone infills.

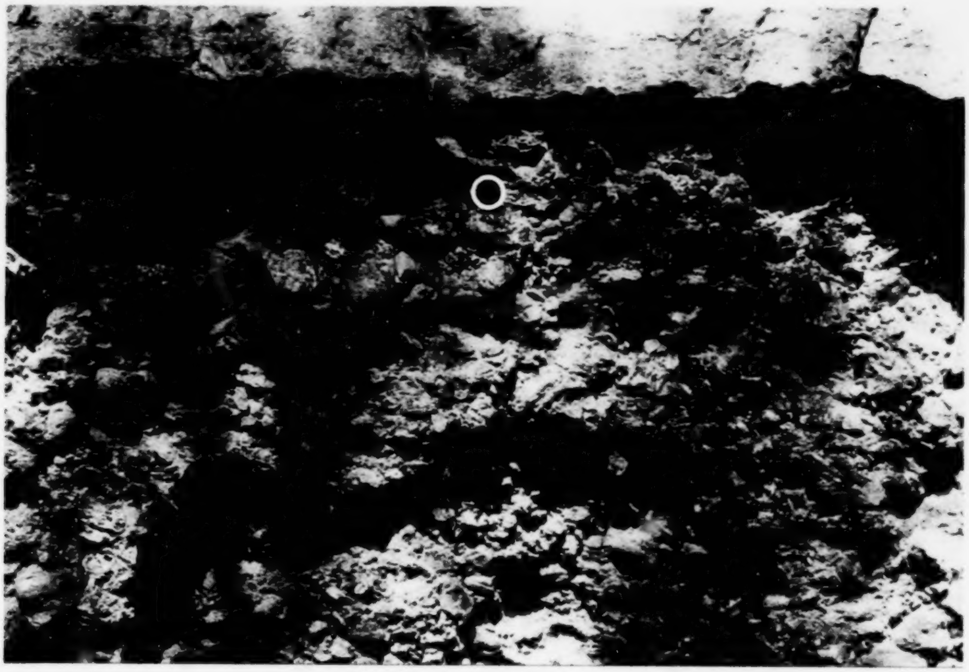

Photo 1. This picture shows the contact of the basal conglomerate lithofacies association with the sandstone lithofacies association at Pass Lake. Note the roundness, size, and lack of sorting of the clasts. A lens cap, outlined in white, is shown for scale.

The heterolithic facies of Cheadle (1986a), which only crops out on Channel Island, is composed of interbedded medium to very coarse-grained feldspathic wackes, arenites, and black shale. This facies may correlate with the poorly sorted sandstone facies.

Based on drill core, the lower Fork Bay Member is dominated by interbedded, well-sorted and poorly sorted, massive sandstone facies. The upper portion of the Fork Bay Member contains interbeds of the well-sorted, massive sandstone facies, the horizontally laminated siltstone and sandstone facies, and the ripple-laminated sandstone facies.

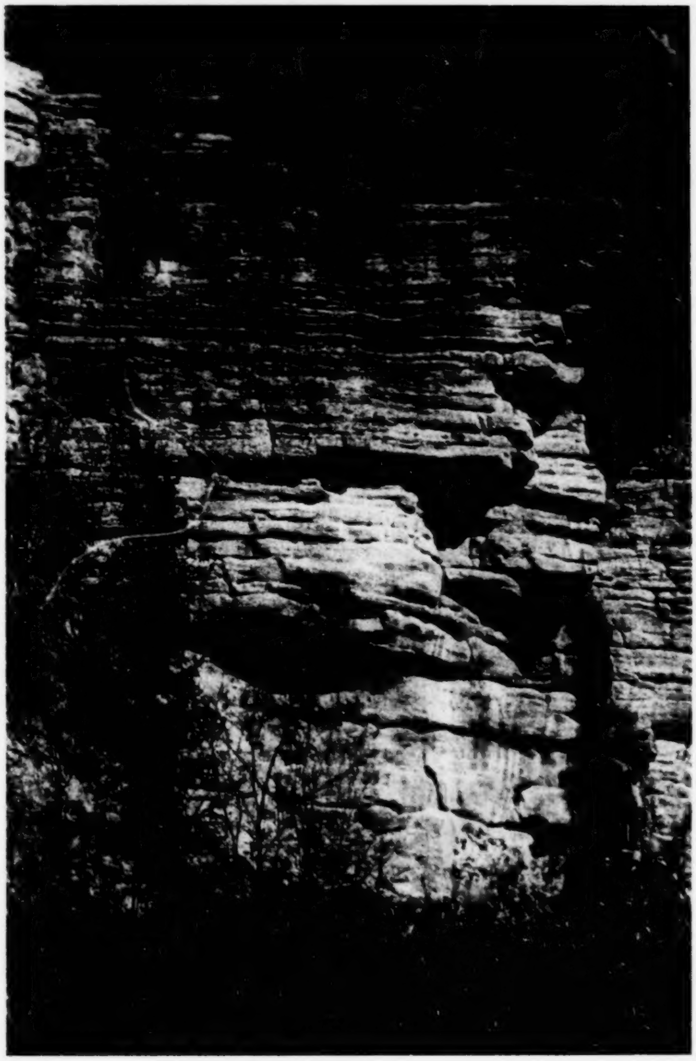

Photo 2. Sandstone lithofacies association at Pass Lake. These plane-bedded sandstones overlie the basal conglomerate shown in Photo 1. Notice the upward thinning of the sandstone beds.

WELL-SORTED SANDSTONE LITHOFACIES

This facies is the most abundant unit of the Pass Lake Formation. It is a relatively well-sorted, purplish brown, medium-grained sandstone that appears to be faintly horizontally laminated. Some larger feldspar grains occur that range from 1 to 3 mm in diameter. Rare ripple laminae are also present. Series of well-sorted massive sandstone beds range from 10 to 600 cm in thickness. This lithofacies is interbedded with the poorly sorted massive sandstone lithofacies.

HORIZONTALLY LAMINATED SANDSTONE AND SILTSTONE LITHOFACIES ASSOCIATION

This lithofacies association is predominantly sandstone layers composed of medium- to fine-grained sandstone that may be graded, or have horizontal or low-angle laminae. These beds can range from 1 to 600 cm in thickness. Massive siltstone beds, intercalated with the sandstone units, range from 1 to 50 cm in thickness. Areas of finely, horizontally laminated siltstone to sandy siltstone also occur. Individual layers of sandy siltstone are well sorted and range from 1 to 100 cm thick.

POORLY SORTED SANDSTONE LITHOFACIES ASSOCIATION

This unit typically consists of purplish brown to buff medium-grained sandstone, although coarse to very coarse sandstone layers are present. Reduced spots, layers and areas are abundant. The sandstone contains copious amounts of small, elongate mud chips, 2 to 3 mm in length. Occasionally, mud chips may reach 1 to 2 cm in length. The poorly sorted sandstone beds vary in thickness from 5 cm to 10 m, averaging 1 m.

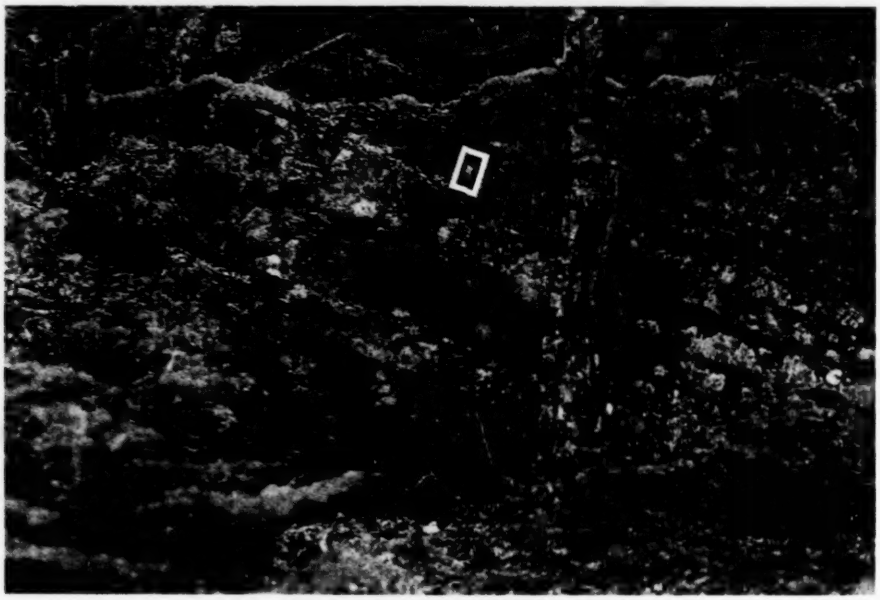

Photo 3. Large-scale cross-stratification of the sandstone lithofacies association of the Pass Lake Formation is shown in an outcrop from Quarry Island. Handheld global positioning system (GPS) unit for scale, outlined in white.

RIPPLE-LAMINATED SANDSTONE LITHOFACIES ASSOCIATION

This unit consists of ripple-laminated medium- to fine-grained sandstone. Some ripple forms are preserved and laminae are covered with mudstone drapes. Individual laminae have a maximum thickness of 1 cm. Although a series of ripple-laminated sandstones can range from 5 to 40 cm thick, most tend to be between 35 and 40 cm thick. This facies is interbedded with the well-sorted sandstone lithofacies association and the horizontally laminated siltstone and sandstone lithofacies association.

These lithofacies and lithofacies associations are arranged into both fining and thinning-upward, and coarsening and thickening-upward successions, though the former is by far the most common. The coarsening and thickening-upward successions are limited to Copper Island in the extreme southeast of the outcrop area. The base of this section is characterized by thinly bedded green siltstone and lensoid sandstone beds with wave or current rippled tops. The sandstones become coarser, thicker and more laterally continuous upward. Throughout this section, the sandstone beds display either grading, trough cross-stratification, parallel lamination or hummocky cross-stratification. Loaded basal contacts are common on sandstone beds as are green mud-chip conglomerates at the base of beds. Siltstone partings at the tops of sandstone beds are common and display abundant syneresis cracks, which have been mistaken in the past for fossils.

The most pronounced fining and thinning-upward succession is present at Pass Lake (*see* Photo 2). Overall, this section is characterized by an upward decrease in bedding thickness as well as increasing frequency of interbedded red siltstones. Sedimentary structures evident near the base of the section include upper flow regime parallel lamination, low-angle cross-stratification and wave-rippled bed tops. The top of the section is composed of red siltstones containing 30 to 80 cm massive to parallel-laminated sandstone beds with wave-rippled tops.

ROSSPORT FORMATION

The Rossport Formation is the most complex of the formations. The thickest accumulations of this formation, approximately 100 m, occur in the central portion of the basin, with prominent thinning toward the east. Cheadle (1986a) measured paleocurrent trends toward the east.

The lower contact of the Rossport Formation is designated as the point in the stratigraphy where the sandstones of the Pass Lake Formation become less significant than the dolomitic mudstones of the Channel Island Member. Thus, there is commonly a transitional contact between the Pass Lake Formation and Rossport Formation lithologies.

The Rossport Formation has been subdivided into 10 facies associations: massive siltstone and sandstone; cyclic siltstone–dolomite; dolomitic mudstone; stromatolitic chert–carbonate; intraformational conglomerate; graded medium-grained, sandstone and siltstone; mudstone; sandy siltstone; thinly laminated, fine-grained sandstone and siltstone; and siltstone lithofacies associations. The lower portion of the Rossport Formation has a well-defined facies sequence. Above the contact with the Pass Lake Formation, there is typically a succession of lithofacies associations consisting of massive siltstone, sandstone, and dolomitic mudstone, followed by the cyclic siltstone–dolomite. The massive siltstone and sandstone lithofacies association may not be present if the Rossport Formation directly overlies the basement. The distribution of facies tends to be more varied above the cyclic siltstone–dolomite lithofacies association. The most common succession begins with the dolomitic mudstone lithofacies association overlying the cyclic facies. This is followed by the sandstone and mudstone lithofacies association, stromatolitic lithofacies association, and a return to the sandstone and mudstone lithofacies

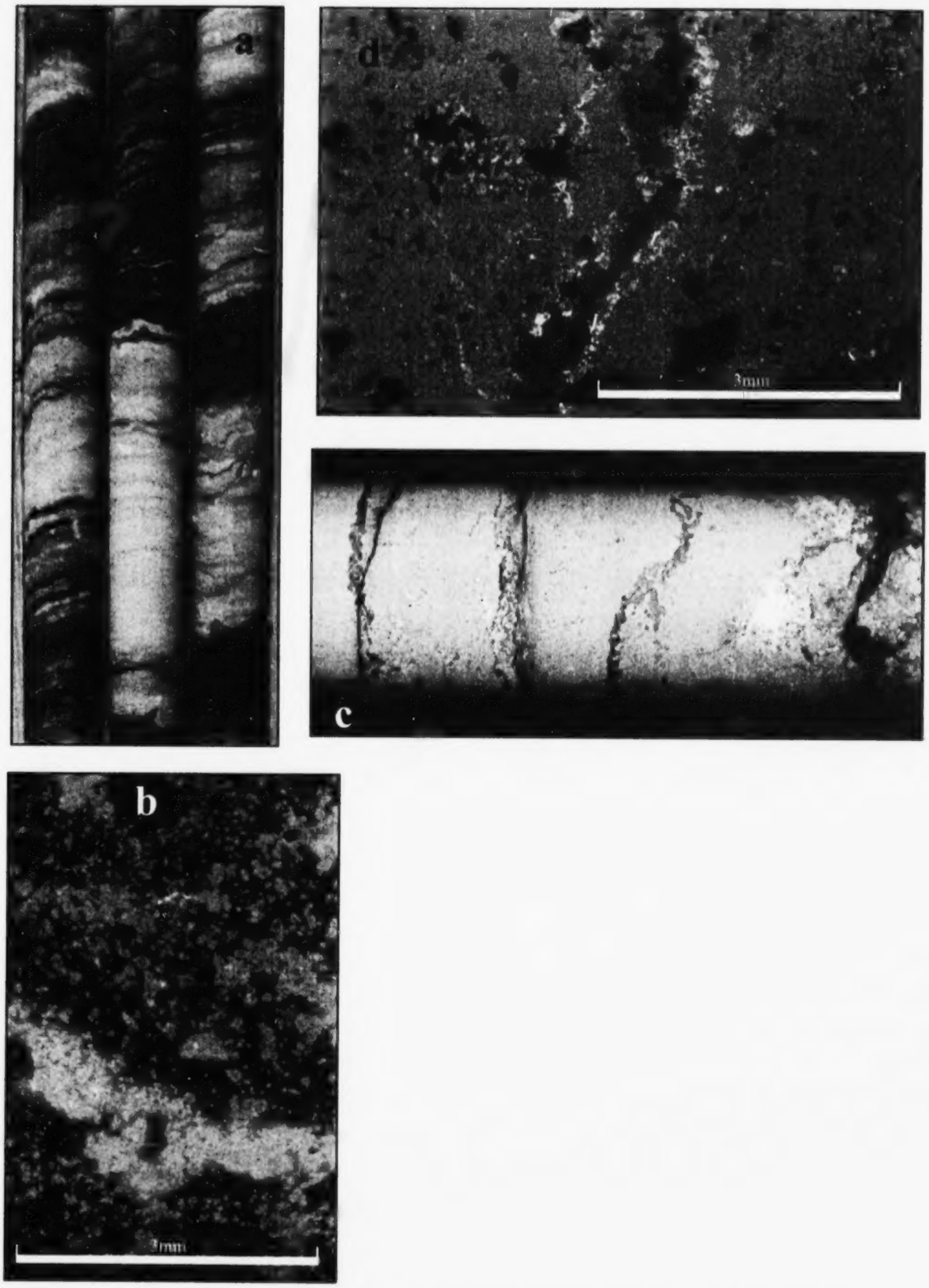

Photo 4. These pictures show the end members of a cyclic siltstone–dolomite lithofacies association and their cathodoluminescence images. a) This is a typical section, demonstrating the cyclicity of the siltstone and dolomitic mudstone end members. Below, in (b), is a cathodoluminescence image from a similar section. Dolomite is indicated by the light hues, while siliciclastics appear black. c) This photo is a closer view of the dolomitic mudstone end member, with a representative cathodoluminescence photo (d). There is abundant very fine-grained dolomite throughout the section (background medium grey) with calcite (white), quartz (dark grey), and siliciclastics (black). The darker linear feature is a gypsum vein. Gypsum does not luminesce, but reflects light from nearby luminescent minerals. Photos are of core from drill hole NI-92-7.

association. The mud-chip conglomerate lithofacies association, and sometimes the conglomerate lithofacies association, is interbedded with the upper sandstone and mudstone lithofacies association. Both of these lithofacies associations are overlain by interbeds of the sandy siltstone, laminated fine-grained, sandstone and siltstone, and siltstone lithofacies associations, but there is often an interbedded transition between them. Although the sandy siltstone, laminated, fine-grained sandstone and siltstone, and siltstone lithofacies associations interbed, there tends to be a general progression from sandy siltstone dominated to siltstone-dominated lithofacies associations.

The main variations of the above sequence centre on the first introduction of the sandstone and mudstone lithofacies association. In some instances, the sandstone and mudstone lithofacies association is first introduced in the middle of the cyclic siltstone–dolomite lithofacies association. In this case, there is the cyclic siltstone–dolomite lithofacies association, usually with the dolomitic mudstone lithofacies association accompanying it, occurring both below and above the first sandstone and siltstone layers. The sandstone and mudstone lithofacies association may also first occur below or above the stromatolitic lithofacies association. The mud-chip conglomerate lithofacies association and conglomerate lithofacies association may occur near the introduction of the sandstone and mudstone lithofacies association or farther up in the succession.

Massive Siltstone and Sandstone Lithofacies Association

This lithofacies association is dominated by massive siltstone. The siltstone layers tend to be light to medium brick red with some reduction spots. In some cases, dolomitic siltstone is present, mixing with non-dolomitic siltstone in swirly wisps. The siltstone may also contain coarser horizons of medium-, coarse- and very coarse-grained sandstone. Mudstone units can be 45 to 450 cm thick, and are interbedded with poorly sorted, medium-grained sandstone units that are 1 to 31 cm thick. Sandstone units are buff to greyish, with some pinkish tinges. Some of the medium-grained sandstone layers contain coarser grains, whereas others are dominantly coarse-grained sandstone. A few of these sandstone layers are dolomitic, particularly where they are near the contact with the cyclic siltstone–dolomite lithofacies association.

Cyclic Siltstone–Dolomite Lithofacies Association

The cyclic siltstone–dolomite lithofacies association is unique within the Sibley Group. It consists of variations between 2 end members that are intimately interbedded (Photos 4a and 4c). For the purpose of logging the diamond-drill core, the cyclic siltstone–dolomite lithofacies association is generally divided into intervals dominated by one end member or the other, or by approximately even amounts of each. One end member is a red shale to siltstone, and the other is a dolomitic mudstone or dolomitic fine-grained sandstone that is typically a shade of pink to cream coloured. The dolomitic fine-grained sandstone member usually occurs in marginal areas of the basin.

The shale and siltstone end member is commonly well consolidated, although thicker areas have friable sections. It is usually represented by a brick red silty shale, although both siltstone and shale occur. Rare areas of very coarse sandstone may also occur. Laminae within this member are seldom flat and are often disrupted by loaded carbonate layers, and diagenetic carbonate and gypsum veins (*see* Photo 4a). Shale and siltstone layers tend to be distorted around carbonate blobs and sink into cracks in the intercalated dolomitic mudstone laminae. Individual layers range from millimetre scale to approximately 15 cm thick. Interlayered cyclic facies sections dominated by the shale and siltstone end member average 10 to 30 cm thick, but may be up to 130 cm thick.

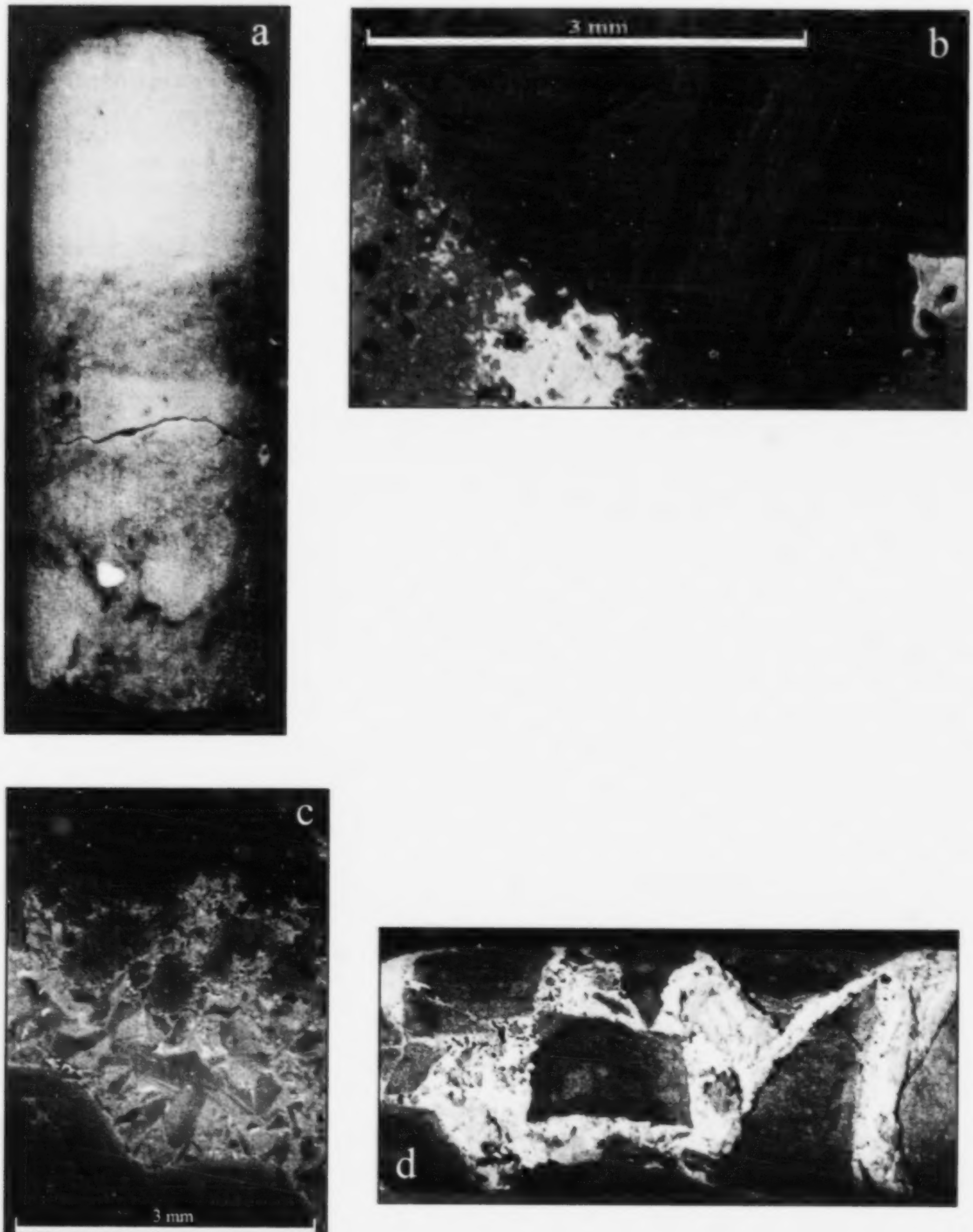

Photo 5. Gypsum, dolomite, and calcite occurrences within the cyclic siltstone–dolomite lithofacies association. a) Gypsum layers can occasionally be found within this lithofacies association, ranging between 1 and 5 cm in thickness. This layer is 5 cm thick. b) This is a cathodoluminescence picture of dolomitic mudstone (light grey) with calcite (white). The elongate crystals in the upper portion of this photo are gypsum. The growth patterns suggest that they grew on top of the dolomite. c) This photo is a close-up of a dolomite and calcite vein in mudstone (black) under luminescence. It shows the intergrowths of calcite and dolomite, as well as the infiltration of dolomite into the mudstone. d) This photo shows a siltstone breccia that has been cemented by gypsum (white). Photos are of core from drill hole NI-92-7.

The dolomitic mudstone end member is cream coloured, whereas the dolomitic fine-grained sandstone end member tends to be buff. These layers frequently contain diagenetic calcite blobs and stringers, as well as bladed gypsum crystals. Cathodoluminescence studies showed some gypsum crystals growing on dolomitic mudstone, suggesting that some gypsum crystals may have formed as growths on the substrate (Photo 5b). Gypsum also rarely forms 1 to 5 cm layers within the dolomitic mudstone layers (*see* Photo 5a). Mud stringers and granular looking bands may also be found within individual layers, probably indicating that they are actually multiple layers. The granular bands are typically found in dolomitic mudstone and consist of medium-sized quartz grains, although some coarse to very coarse grains also occur. The dolomitic mudstone fines away from these coarse bands. A few dolomitic mudstone layers near the bottom of the assemblage also have coarse siliciclastic horizons at the tops of the layers. In these cases, the extrabasinal granules can reach 5 mm in diameter and may be clast supported.

Dolomitic Mudstone Lithofacies Association

This lithofacies association seems to be restricted to directly below or directly above the cyclic siltstone–dolomite lithofacies association. It is often similar in appearance to the cyclic siltstone–dolomite lithofacies association in that it commonly has both off white to pink dolomitic mudstone and dark to medium brick red mudstone layers. However, it is completely dominated by mudstone, at times exclusively mudstone or shale in composition, and lacks the periodicity of the true cyclic siltstone–dolomite lithofacies association. The mudstone or shale beds typically range from 10 to 230 cm in thickness, averaging 50 cm thick, although they may occur on a millimetre scale, and are interbedded with dolomitic or carbonaceous mudstone in sections up to 75 cm thick. Some shale layers have increasing carbonate content up through them. The dolomitic mudstone beds range from millimetre-scale laminae to 60 cm thick beds, averaging approximately 20 cm in thickness. Dolomite-rich mudstone layers increase as the cyclic siltstone–dolomite lithofacies association is approached.

Stromatolitic Chert–Carbonate Lithofacies Association

This lithofacies association is dominated by stromatolitic chert and carbonate laminae. It was thought, by Franklin et al. (1980) and Cheadle (1986a, 1986b), to be a fairly continuous layer and, hence, a marker bed. However, while it occurs locally as laterally extensive layers in outcrop, it has proven to be quite sporadic in drill core. Cheadle (1986a) divided this lithofacies association into 4 lithological elements: massive interbedded black chert and light grey carbonate, chert–carbonate sharpstone conglomerates, chert–carbonate cryptalgal laminites and columnar stromatolites, and evaporite minerals. The cryptalgal laminites have been identified as *Stratifera* (Cheadle 1986a) and the columnar stromatolites have been identified as *Conophyton metula* (Cheadle 1986a). Cheadle (1986a) also identified pseudomorphs of sulphate minerals and halite within the crinkly laminae, and observed that the chert appears to be an early replacement of carbonate, as well as noting the presence of pyrite and organic carbon within the chert.

All of Cheadle's (1986a) lithological elements have been found in drill core and outcrops. The cryptalgal laminites and columnar stromatolites are the most easily identifiable elements in drill core. The cryptalgal laminites (Photo 6c) are usually not silicified, whereas the columnar stromatolites (*see* Photo 6d) are frequently silicified. Both gypsum crystals and halite pseudomorphs have been found. The stromatolitic facies is 0.8 to 1.4 m thick. Fine carbonate sandstone layers are interbedded with the cryptalgal laminites.

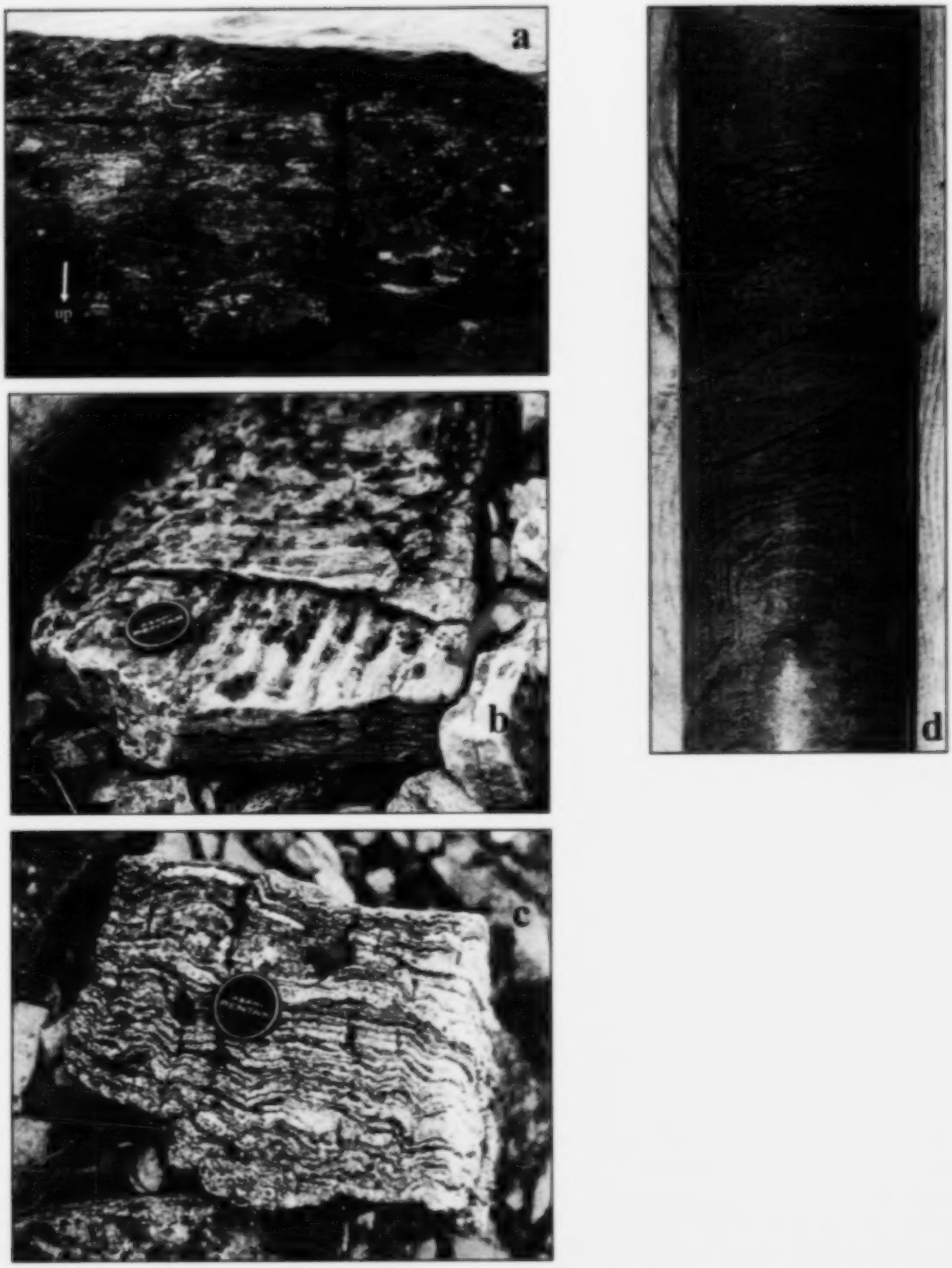

Photo 6. Stromatolitic chert–carbonate lithofacies association. The Channel Island sequence consists of a) upward-thinning sandstone beds and b) rippled fine sandstone, overlain by c) the crinkly laminae of the stromatolitic carbonate lithofacies association. The crinkly laminae are intercalated with fine carbonate grainstone laminae. d) A silicified stromatolite from drill hole HE-02-02 is also shown.

An outcrop on Channel Island in Lake Superior (*see* Figure 1) preserves the facies contacts between the stromatolitic lithofacies association and underlying units. The sequence begins with laminated medium-grained sandstone, with laminations fining upward (*see* Photo 6a). Draping foresets of trough cross-stratification indicate large wave ripples (*see* Photo 6b). Above this unit is a fine-grained sandstone unit, characterized by low-angle cross-stratification and undulatory surfaces. The layers are not graded, but often have thin, fissile mud caps. Overall, the fine-grained sandstone unit increases in siltstone content upward. The siltstone unit is trough cross-stratified near the base. Some layers are internally stratified, but overall become blocky, and more massive upward. The stromatolitic limestone unit lies directly above the siltstone unit. It is dominated by crinkly mat structures (*see* Photo 6c), and some tepee structures were observed. The stromatolitic layers are several millimetres thick, but may occur in packages of layers up to 2 cm thick. These layers and packages of layers are intercalated with very fine-grained carbonate grainstone layers that are millimetre scale to 15 cm thick. The carbonate layer has a friable, weathered upper surface and is overlain by a poorly sorted siltstone with matrix-supported intraformational clasts.

Another outcrop of the stromatolitic facies, on Mawn Lake Road, southeast of Shillabeer Lake (*see* Figure 1), preserves an intraformational conglomeratic unit in close proximity to the stromatolite unit. Both outcrops are low and rubbly and occur on opposite sides of the road from each other, making precise stratigraphic positioning difficult. The conglomeratic unit appears to consist of marly, fine-grained sandstone and some stromatolitic pieces with a chert matrix. The intact stromatolitic chert–carbonate lithofacies association consists of stromatolitic layers, and packages of layers, intercalated with very fine-grained carbonate sand lenses and layers. These are similar to the sections at Channel Island (*see* Photo 6c), only those tend to be more silicified and less well preserved. Other outcrops throughout the study area repeat the theme of the stromatolitic carbonate having an altered upper surface and being overlain by intraformational conglomerates or siltstones exhibiting extensive red and yellow mottling.

Intraformational Conglomerate Lithofacies Association

The intraformational conglomerate lithofacies association consists of two slightly different conglomeratic lithofacies, although these differences are not significant enough to preclude them being considered one lithofacies association. For descriptive purposes, one facies is referred to as a mud-chip conglomerate (Photo 7b) and the second is simply termed conglomerate (*see* Photo 7a).

The mud-chip conglomerate is relatively rare compared to most of the other lithofacies, although it is more common than the stromatolitic and conglomeratic facies. The mud-chip conglomerate usually has a mudstone matrix and is matrix supported, although clast-supported areas can be found. It consists predominantly of mud chips and blocks, but may also contain dolomitic and gypsiferous clasts, as well as an occasional semilithified clast from the sandstone units. Blocks within the conglomerate are rounded and often elongate, although they tend to be less elongate when sandstone clasts are present. Some of the clasts have preserved layering within them. When present, they are crumpled and deformed, indicating soft sediment deformation. The mud-chip conglomerate layers are 10 to 25 cm thick and may occur as isolated layers or in a series of layers. Individual clasts are millimetre scale to 2 cm in diameter. The mud-chip conglomerate may also appear in close proximity to the conglomeratic lithofacies association.

The conglomerate facies is an intraformational conglomerate, consisting of clasts of siltstone, fine-grained sandstone, shale, and dolomite. Many clasts have preserved laminations within them. Clasts sizes are quite varied, ranging from pebble size to boulder size. Boulder-sized clasts are extremely difficult to distinguish in drill core, but are clearly seen in an outcrop on Mawn Lake Road, southeast of Shillabeer Lake, stratigraphically above the stromatolitic chert–carbonate lithofacies association. Here, the conglomerate beds reach tens of centimetres to 1 m in thickness. The matrix is generally composed of sandy siltstone. Overall, sorting is quite poor. Many of the conglomerates are matrix supported, although some may be locally clast supported and a few of the clast-supported beds become matrix supported upward.

Graded, Medium-Grained Sandstone and Siltstone Lithofacies Association

This lithofacies association is dominated by buff to pinkish red, massive, medium-grained sandstone. Sandstone units may also be fine, coarse, or very coarse grained and may be graded and massive or cross-stratified. Massive graded beds constitute the majority of the sandstone beds. Some climbing ripples have been found at the base of, and grading into, the cross-stratified units. Many of the sandstones have carbonate cements, particularly those sandstones near the contact with the cyclic facies. The sandstone beds range from 5 to 400 cm in thickness, averaging approximately 40 cm thick. Successive sandstone layers may reach thicknesses of several metres before being interrupted by a siltstone bed. This lithofacies association is interbedded with siltstone beds of the siltstone lithofacies association, as well as the dolomitic mudstone lithofacies association and, to a lesser degree, the silty shale lithofacies association. The sandstone and siltstone lithofacies association is confined to the section of the Rossport Formation directly above the cyclic siltstone–dolomite or dolomitic mudstone lithofacies associations and below the mudstone, sandy siltstone and laminated fine-grained sandstone and siltstone lithofacies associations.

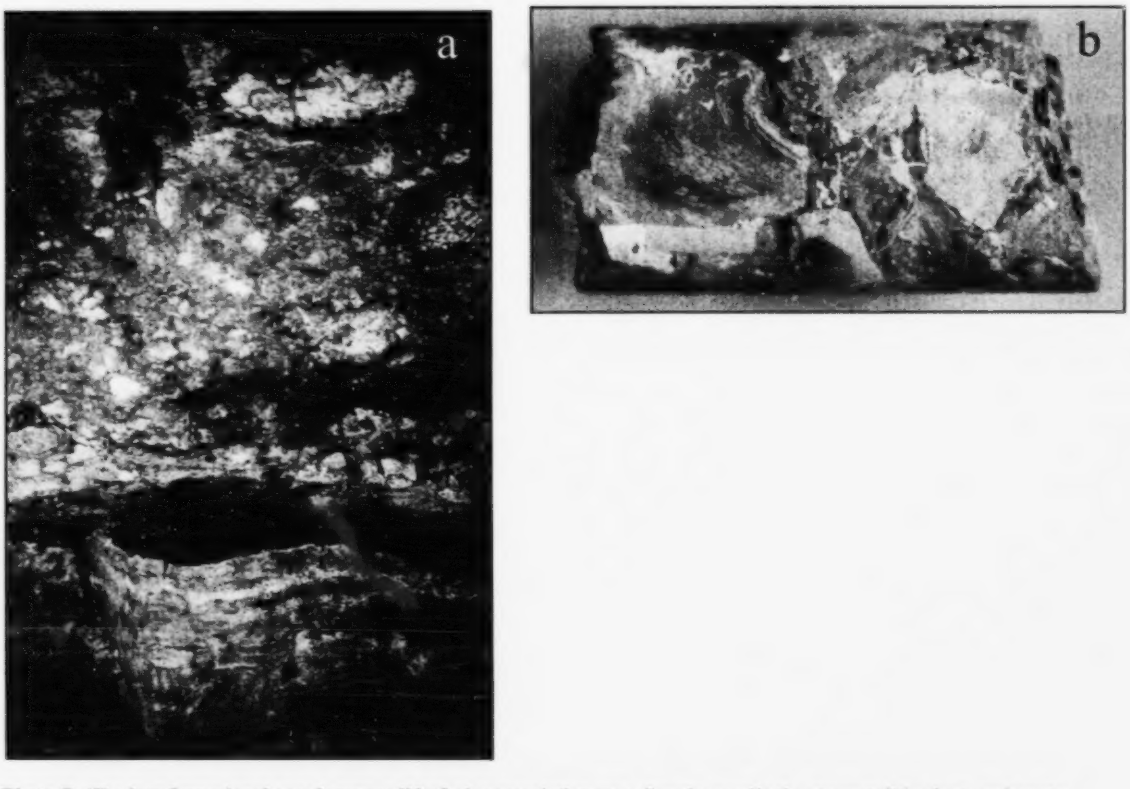

Photo 7. The intraformational conglomerate lithofacies association may directly overlie the stromatolitic chert–carbonate lithofacies association, as seen in (a), an outcrop on Channel Island. b) The drill core is from NB-97-2 and shows a mud-chip conglomerate unit. Notice the gypsum growth between some of the clasts.

Mudstone Lithofacies Association

The mudstone lithofacies association is relatively rare in the stratigraphy, but quite distinct. It consists of dark purplish brick red shale and mudstone intercalated with carbonate-rich layers. Individual layers within it are on the millimetre scale, and the entire unit averages only 5 cm, although it can be up to 30 cm in thickness. The mudstone lithofacies association is interbedded with the siltstone and sandy siltstone lithofacies association.

Sandy Siltstone Lithofacies

The sandy siltstone lithofacies is typically massive, although some areas have vague horizontal laminae preserved. These laminae are generally obliterated by extensive mottling from reduced areas and distortion related to carbonate nodules crystallized within the sediment. The reduced areas tend to be irregular in shape, with only some constrained to reduction spots. There are abundant carbonate nodules, ranging from millimetre scale up to 5 cm in diameter. Many areas of the sandy siltstone lithofacies association have high carbonate contents. Portions of this unit appear to have sections that may represent soil horizons. These sections begin with a carbonate-rich sandy siltstone that progresses upward to sandy siltstone with nodular carbonate layers, topped with friable, dark purple shaley siltstone. The sandy siltstone lithofacies ranges from 30 to 400 cm thick, and is interbedded with the siltstone, mudstone, and laminated siltstone and fine-grained sandstone lithofacies associations. Some conglomerate and mud-chip conglomerate beds may extend up into this lithofacies.

Thinly Laminated, Fine-Grained Sandstone and Siltstone Lithofacies Association

This lithofacies association is composed of fine-grained sandstone layers that often grade to siltstone and are capped by dark red mudstone. The fine-grained sandstone layers are lighter in colour, often contain some dolomite, and may be associated with carbonate nodules. Intervals of laminated fine-grained sandstone and siltstone are generally 5 to 90 cm thick. Individual beds of fine-grained sandstone and siltstone are centimetre scale. This unit is predominantly interbedded with the siltstone facies, and occurs at approximately 3 m intervals throughout the siltstone section above the sandy siltstone lithofacies association.

Siltstone Lithofacies

All of the lithofacies associations above the cyclic siltstone–dolomite, dolomitic mudstone and stromatolitic lithofacies associations are interbedded with the siltstone lithofacies. It can be thought of as forming the background sediment in this section of the formation which contains all other lithofacies. The siltstone lithofacies is composed of siltstone to silty shale, and is generally massive or contains fine laminae. Areas with relatively high shale content tend to be highly friable, although the majority of this facies has limited friability. Reduction spots are relatively abundant, although reduced areas may spread out into large mottles. The siltstone facies commonly reaches a thickness of 300 cm, but may range from 50 cm to 10 m thick. This facies is gradational with the facies of the Kama Hill Formation.

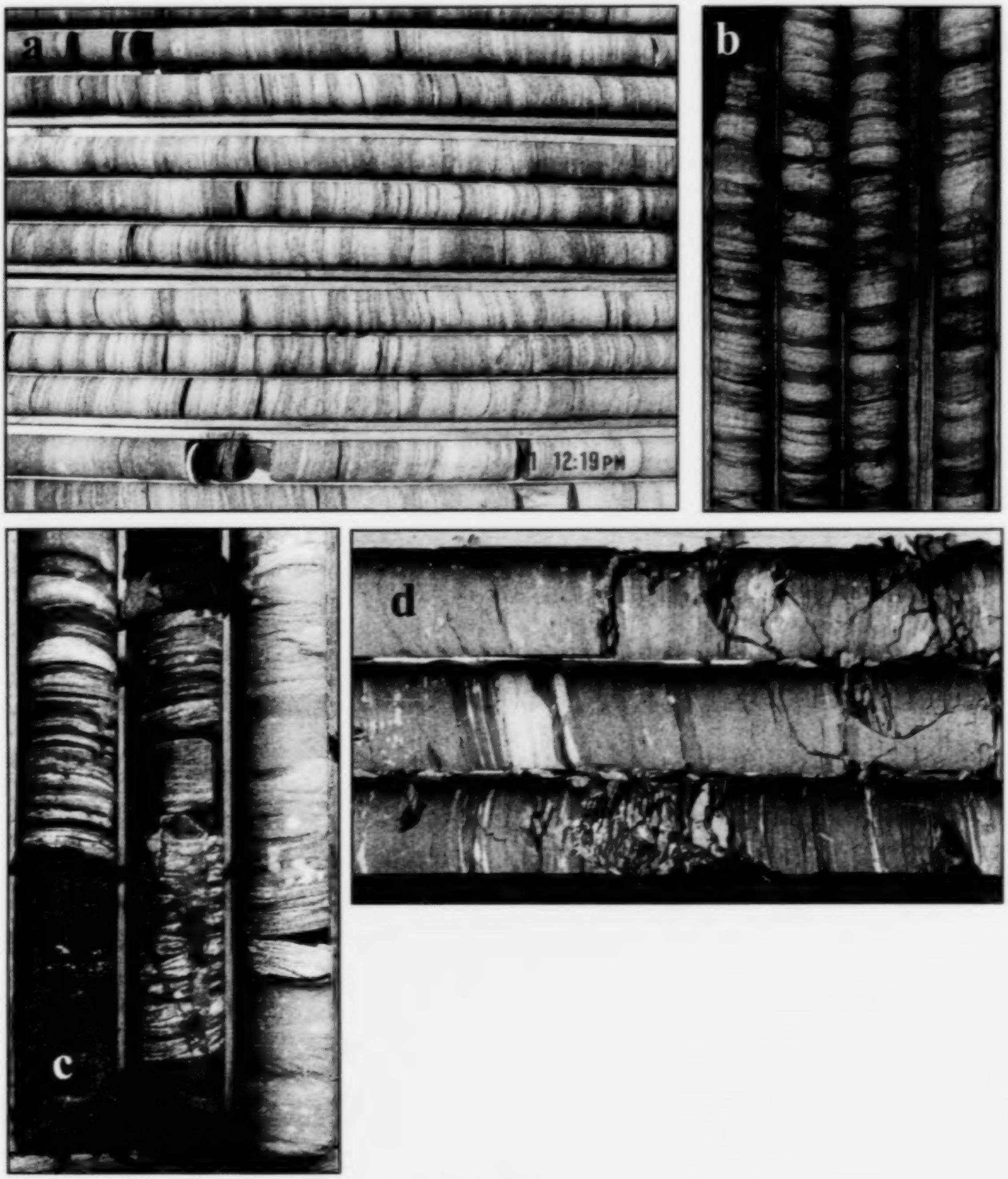

Photo 8. The Kama Hill Formation is dominated by the horizontally laminated, fine-grained sandstone and siltstone and the mud-cracked, fine-grained sandstone and siltstone lithofacies associations, as shown in a) and b). c) The rippled, fine-grained sandstone and siltstone and d) the horizontally laminated mudstone lithofacies associations can be locally abundant. All photos are taken in natural sunlight without filters of core from drill hole NI-92-7.

KAMA HILL FORMATION

The Kama Hill Formation is approximately 10 to 50 m thick. According to Cheadle (1986a), the paleocurrents for this formation trend toward the east. The Kama Hill Formation is divided into 4 lithofacies associations, and is dominated by the horizontally laminated, fine-grained sandstone and siltstone lithofacies association and the mud-cracked, fine-grained sandstone lithofacies association. The rippled fine-grained sandstone and siltstone lithofacies association and horizontally laminated mudstone lithofacies association are less common, with the latter being the least common. The lithofacies associations tend to form successions of horizontally laminated, fine-grained sandstone and siltstone, rippled fine-grained sandstone, and rippled siltstone with mud drapes. Occasionally, intervals of thick silt, horizontally laminated shale and mudstone, and friable siltstone and shale layers occur. In some of the drill core, intervals of mud-cracked sandstone and siltstone and horizontally laminated mudstone are prevalent directly above the Rossport Formation, whereas the rippled sandstone facies dominates the top of the Kama Hill Formation.

Horizontally Laminated, Fine-Grained Sandstone and Siltstone Lithofacies Association

This lithofacies association consists of layers of horizontally laminated, fine-grained sandstone and fine-grained sandstone grading to siltstone, which commonly have horizons of very small mud chips (Photo 8a). Some siltstone layers are contorted, have disruptive mottling, or contain contorted or folded mud wisps. Layers may have distinct boundaries or may be only distinguishable by slight changes in grain size. The individual fine-grained sandstone to siltstone layers range from 1 to 2 cm in thickness. Units of horizontally laminated, fine-grained sandstone and siltstone range from 5 to 800 cm, but are more typically 60 cm thick.

Mud-Cracked, Fine-Grained Sandstone and Siltstone Lithofacies Association

This lithofacies association is dominated by fine-grained sandstone to siltstone, with layers separated by thin, millimetre-scale, purple mud laminae. Individual fine-grained sandstone and siltstone laminae are typically 3 to 5 mm thick. Some thicker muddy siltstone layers do occur. The mud-cracked fine-grained sandstone lithofacies association has extensive mud cracks that often extend through multiple sediment layers (*see* Photos 8a and 8b), obscuring the original layering. Mud-cracked areas often extend for 2 to 10 cm. Elongate mud chips, 1 to 20 mm in diameter, tend to occur in a roughly horizontal alignment at the bases of some sandy layers. Units of the mud-cracked, fine-grained sandstone and siltstone lithofacies association range from 3 to 95 cm thick, but are more commonly 5 to 10 cm thick.

Rippled, Fine-Grained Sandstone and Siltstone Lithofacies Association

Ripples may be found in units up to 25 cm thick, as individual layers, or isolated ripples in fine-grained sandstone or siltstone interlayered with mudstone (*see* Photo 8c). Packages of rippled sandstone and siltstone may dominate over sections up to 120 cm thick. Individual layers are generally 1 to 2 cm thick. The ripples tend to be in fine-grained sandstone lower in the Kama Hill Formation, becoming rippled siltstones higher in the succession. The thickness of the mud caps on the ripples also increases upward, from several millimetres to 2 cm thick.

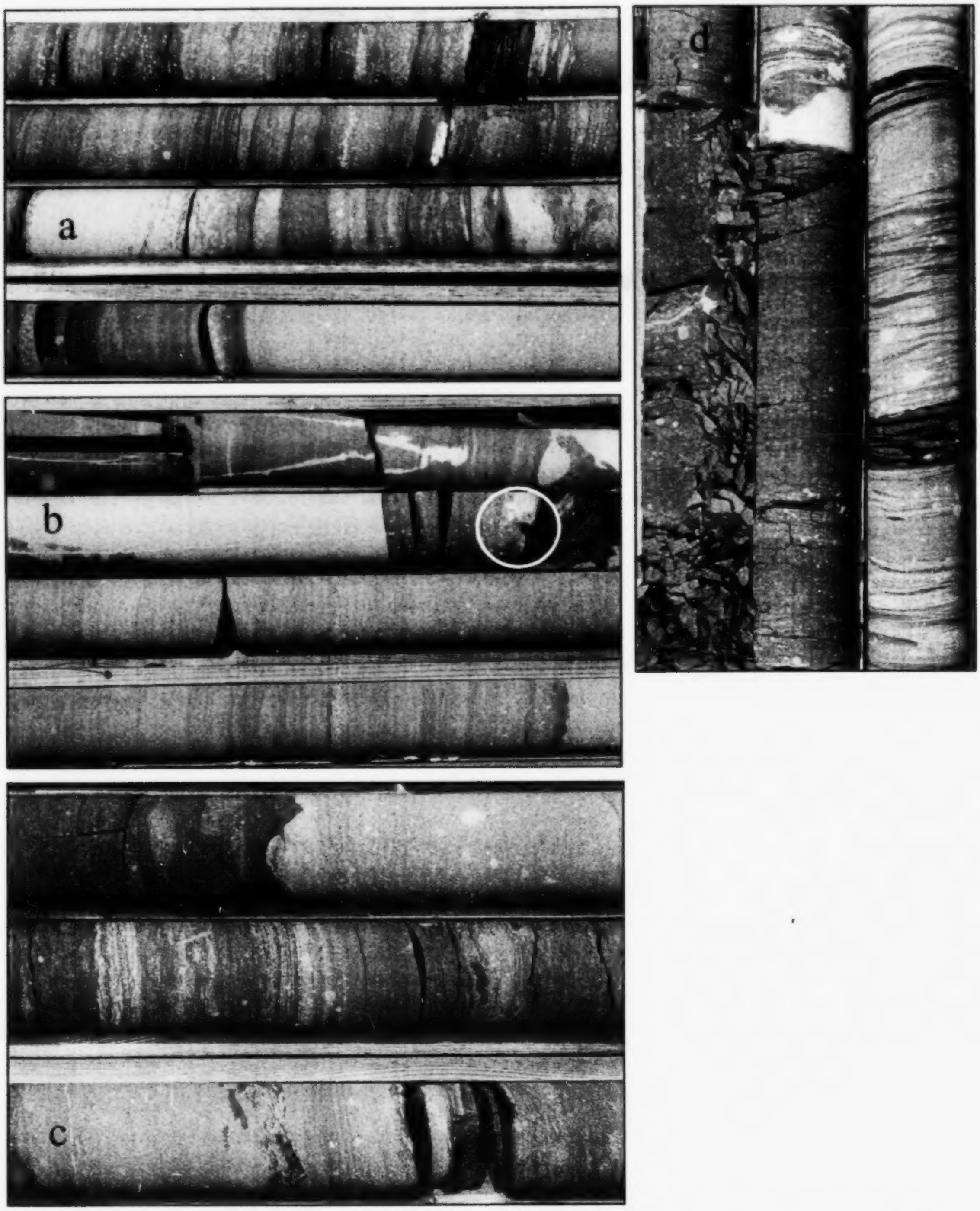

Photo 9. Lithofacies associations of the Outan Island Formation. The contacts between the sandstone lithofacies and the laminated sandstone and mudstone lithofacies association (a, c) and the mudstone lithofacies association (the core below the circled area in b) are shown. b) An intraformational conglomerate is shown in the circled area; c) rip-up clasts can be seen; and d) rippled units are shown. Pictures are of core from drill hole NB-97-2.

Horizontally Laminated Mudstone Lithofacies

This facies consists of thinly laminated to massive mudstone, with individual laminae typically on the millimetre scale, although they may range from 2 to 10 cm thick. Many of these layers are extremely fissile (*see* Photo 8d), whereas others are contorted or folded.

OUTAN ISLAND FORMATION

The Outan Island Formation is a new addition to the Sibley Group stratigraphy. It was identified in 5 drill cores in the southeastern area of the Sibley Basin. One of the drill cores that samples this formation was drilled in Hele Township, whereas the other drill holes are located in Nipigon Bay. However, the Nipigon Bay Formation has already been used to describe the topmost formation of the Sibley Group, so this formation is named after Outan Island, the closest named feature to a complete representation of the formation. Since its discovery in drill core, outcrops of it have been found at the west end of Black Bay, south of Red Rock; and at high elevations inland (Hart 2005). This formation has a maximum thickness of 250 m.

The Outan Island Formation has been divided into 5 lithofacies associations: the mudstone, laminated sandstone and mudstone, siltstone, sandstone, and conglomerate lithofacies associations. The lower Outan Island Formation is dominated, in decreasing order of importance, by the siltstone, mudstone and laminated sandstone and mudstone lithofacies associations.

The upper Outan Island Formation is dominated by thick units of the sandstone lithofacies association with minor alternations of the siltstone, mudstone, and laminated sandstone and mudstone lithofacies associations. The conglomerate lithofacies association is only found alternating with the sandstone lithofacies association, and seems to be present both above and below the transition between the upper and lower Outan Island Formation with the units consisting of large blocks occurring lower in the section. Some units of the sandstone lithofacies association occur in the lower Outan Island Formation, but are typically only 10 cm and rarely reach 150 cm, whereas they are 100 to 1500 cm thick in the upper Outan Island Formation.

Mudstone Lithofacies

The mudstone lithofacies consists of very finely laminated light red to peach shale and bright red mudstone alternating with massive mudstone. Within the laminated units, some of the mudstones grade vertically into shale laminae, whereas other mudstone and shale laminae are distinctly separated. Individual layers may have shale chips floating at the base and some have silicifed carbonate nodules near the tops of the layers. These units range from 6 to 35 cm in thickness.

Laminated Sandstone and Mudstone Lithofacies Association

This unit consists of fining-upward layers of buff fine-grained sandstone to reddish siltstone capped with brick red mudstone (Photo 9). The sandstone and mudstone layers are approximately the same thickness throughout most of the laminated sandstone and mudstone lithofacies association, although the mudstone laminae may be shaley partings instead. Very small rip-up mudstone clasts are frequently found at the base of the sandstone layers. Deep mud cracks are occasionally found penetrating through several layers.

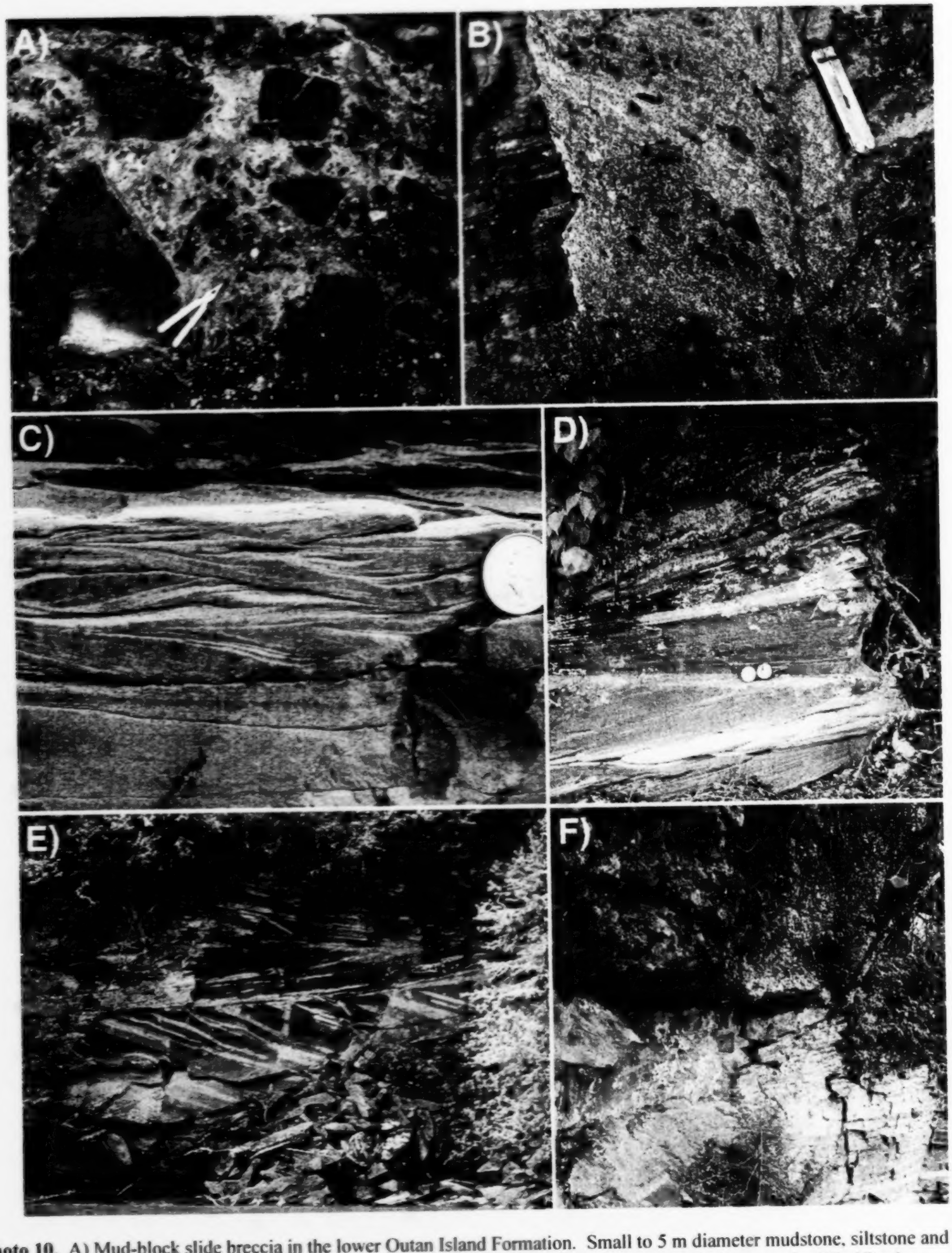

Photo 10. A) Mud-block slide breccia in the lower Outan Island Formation. Small to 5 m diameter mudstone, siltstone and sandstone blocks are present in a medium- to coarse-grained sand matrix (B). This outcrop is 1 km south of Red Rock on Nipigon Bay. C) Hummocky cross-stratification to wave ripple lamination in a slumped sandstone block. Same location as (A) and (B). D) Toesets of large-scale planar cross-stratification in Nipigon Bay sandstone on north-central shore of Simpson Island. E) Large-scale planar cross-stratified Nipigon Bay sandstone. Same location as (D). F) Unconformable contact between the Nipigon Bay sandstones and basal conglomerates of the Osler Group (northeastern shore of Simpson Island).

Siltstone Lithofacies Association

The siltstone lithofacies association is dominated by brick red siltstone with abundant reduction spots. It is typically massive with rarer muddy areas, consisting of horizontal laminae and shale, mud wisps, and layers of mud blocks. Sections of the siltstone lithofacies association also have very fine-grained sandstone that commonly exhibits ripple lamination. Ripple lamination can also be found in these siltstones. These facies of the siltstone lithofacies association can generally occur in 2 specific associations. One sequence begins with sandy siltstone with ripple lamination and is overlain by horizontally laminated mudstone, whereas the other sequence is sandy siltstone with ripple lamination, overlain by ripple-laminated siltstone, overlain by massive siltstone with mud wisps. Contacts are sharp at the base of these layers and they often contain mud rip-up clasts from underlying laminae, although sandy areas sometimes have loaded contacts. The siltstone successions are several metres thick, but individual layers within it are no more than 2 cm thick.

Sandstone Lithofacies

The sandstone lithofacies consists of coarse- and medium-grained sandstones with muddier areas defining layer boundaries. The sandstones are predominantly massive, some of which are normally or reversely graded. Horizontal laminations and rarer ripple laminations also occur. Some of the sandstones contain large blocks of mudstone and mud chips. The mud blocks fall into 3 categories based on differences between them and their position within the sandstone units. The first category consists of basal mud chips derived from rip-up clasts from underlying layers. They are angular and blocky and some of the mud laminae remain intact. The second category is mud chips that appear to float in the centre of a sandstone layer. These mud chips are angular and elongate to blocky with no mud laminae associated with them. The third mud-chip category seems to be restricted to the tops of the sandstone units. In these cases, there are mudstone layers overlying the sandstone unit. Here, sections of the lower mudstone laminae appear to have been delaminated and sunk into the sandstone surface. Some mudstone layers have been pulled apart or contorted, whereas other mudstone layers simply have wispy tendrils that penetrate into the underlying sandstone layer. The sandstone layers often have wavy mud caps. Some of the sandstone units are associated with thin laminae of very coarse-grained sandstone that ranges in thickness from that of a single very coarse sand grain to 1 cm thick. The sandstone lithofacies association can reach 16 m, but is more typically 1 to 2 m thick. Individual sandstone layers are 16 to 100 cm thick. The sandstone-rich areas in the lower member are arranged into coarsening and thickening-upward successions metres to a few tens of metres thick with the successions separated by shaley siltstone. The sandstone-dominated areas of the upper formation have individual beds organized into fining and thinning-upward successions separated by various fine-grained lithofacies.

Conglomeratic Lithofacies

The conglomeratic lithofacies is intraformational, usually consisting of matrix-supported clasts of mud chips and blocks grading upward to a clast-supported conglomerate with clasts of mudstone and sandstone. A few of the conglomerates are not intraformational and contain mafic and granitic clasts. The basal mud chips are angular, whereas the larger mud fragments are rounded. The matrix is siltstone grading upward to medium sandstone. The matrix may have faint laminations, particularly around the basal mud blocks. Clasts range from millimetre scale to 5 m in diameter, and are commonly poorly sorted (Photo 10A). Some conglomerates may have fining or coarsening-upward trends in clast size. Other conglomerates strictly consist of millimetre-scale clasts, whereas another type are isolated occurrences of small clasts at the contacts between sandstone layers (*see* Photos 10A and 10B). In these cases, the sandstone layers are depressed around the clasts. The conglomerate lithofacies ranges between 5 cm and 20 m thick.

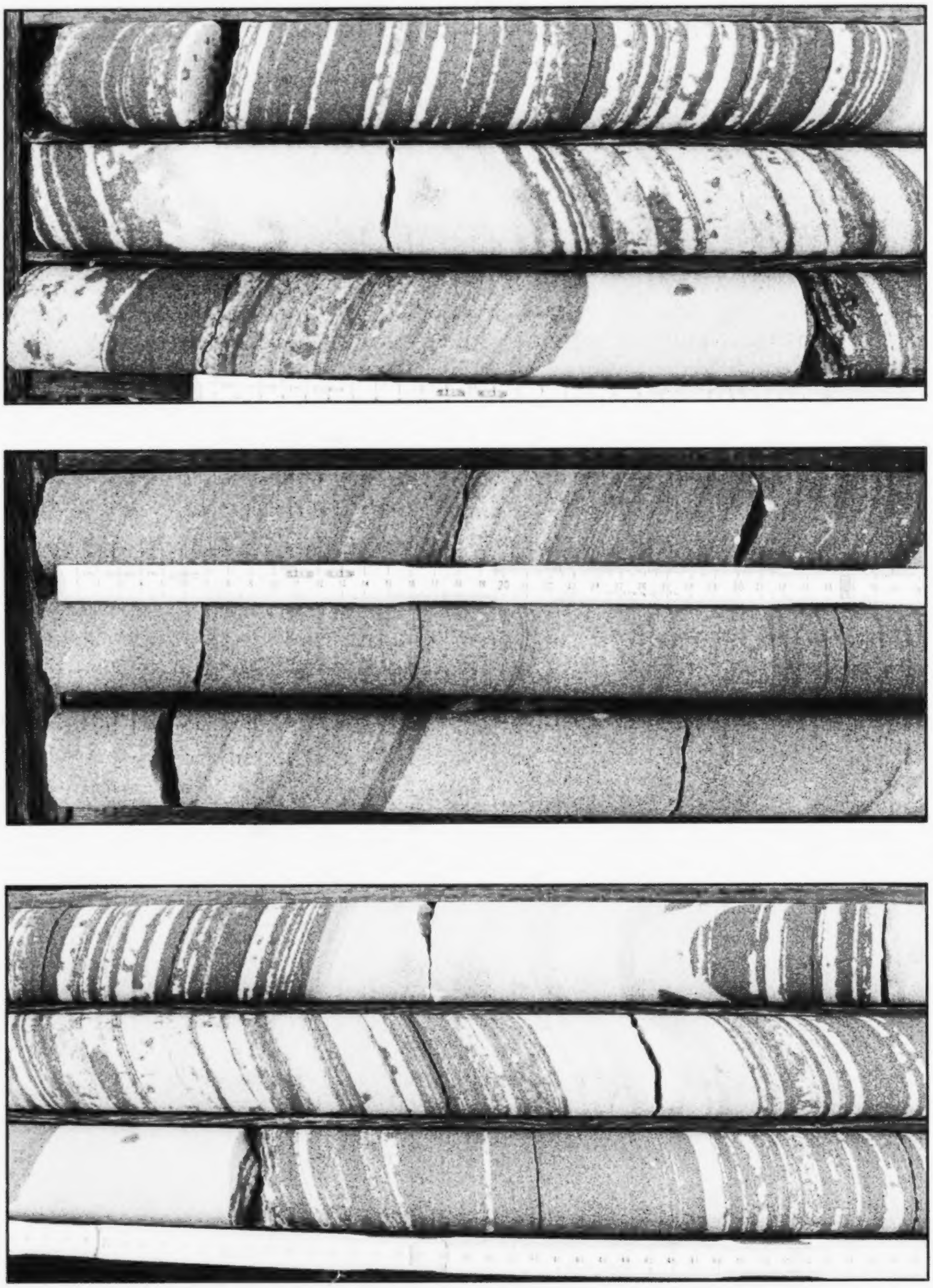

Photo 11. Three photographs are shown, representing the cross-stratified sandstone lithofacies of the Nipigon Bay Formation. Pictures are of core from drill hole NB-97-2.

NIPIGON BAY FORMATION

The Nipigon Bay Formation is also a relatively new addition to the Sibley Group stratigraphy. It is only present in cores from 2 drill holes in Nipigon Bay and one outcrop on a small part of Simpson Island. The total thickness appears to be 450 to 500 m, based on drill core analysis. It has been divided into 2 lithofacies associations: the cross-stratified sandstone lithofacies association and the horizontally laminated sandstone lithofacies association. The cross-stratified lithofacies association dominates the Nipigon Bay Formation.

Cross-Stratified Sandstone Lithofacies

The cross-stratified sandstone lithofacies consists of alternating units of high-angle and low-angle cross-stratified medium-grained quartzarenite (Photo 11). Occasionally, some of the sandstone layers show reverse grading. Individual cross-stratified laminae are distinguished by faint colour variations, and are typically 1 to 3 cm thick. The surfaces of cross-sets are often oxidized to a reddish purple colour, whereas the majority of the sandstones are buff. Some mottling may occur across layers. Individual sets of high-angle cross-stratification dominate this lithofacies, and range from 50 to 350 cm thick, averaging approximately 100 cm thick. Unoriented cross-stratification in drill core contains ripple layers within the high-angle facies that are completely reversed relative to one another. These sets are typically stacked in 4 to 40 m thick units, but are generally 10 m thick. The low-angle cross-stratified facies ranges from 13 to 230 cm thick, and averages approximately 30 cm thick. Stacked sets of this facies are usually 10 m thick, but can reach a thickness of 70 m. Occasionally, ripple forms are preserved along layer contacts. There is a gradational succession from the horizontally laminated sandstone to the low-angle cross-stratified sandstone to the high-angle cross-stratified sandstone.

The one outcrop of the Nipigon Bay Formation, on Simpson Island, preserves a large-scale dune-form. This dune-form is approximately 15 m in height and comprises medium-grained sandstone cross-beds ranging from 10 to 50 cm thick. A toeset wedge is preserved within the outcrop (Photo 10D). Paleocurrents were measured in outcrops on Simpson Island and gave a flow direction to the southwest (Figure 5).

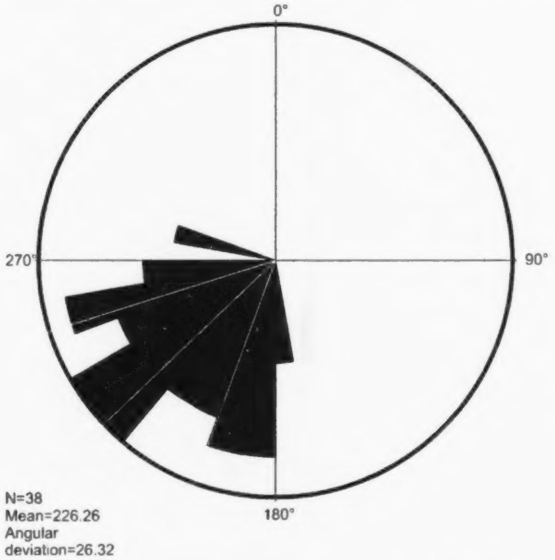

Figure 5. Paleocurrent trend for 38 measurements of large-scale planar cross-stratified sandstones in the Nipigon Bay Formation.

Horizontally Laminated Sandstone Lithofacies Association

This lithofacies association is dominated by medium-grained sandstone, although coarse-grained sandstones and some clay-rich sandstones are not uncommon. These units are 1 to 80 m thick, but are commonly 3 m thick. Individual laminae are a few millimetres to a couple of centimetres thick. Clay-rich sandstone laminae tend to be slightly thinner, have a reddish colouration, and may be fissile. Massive sandstone beds may also be interbedded, ranging from decimetres to 3 m thick. The horizontally laminated sandstone lithofacies association is more likely to be mottled than the cross-stratified sandstone lithofacies association.

DEPOSITIONAL ENVIRONMENTS

Cheadle (1986a, 1986b) gave interpretations for the Loon Lake and Fork Bay members of the Pass Lake Formation, the Channel Island, Middlebrun Bay and Fire Hill members of the Rossport Formation, and the Kama Hill Formation. Here, the depositional environments are examined by formation to maintain continuity with the previous section, although subenvironment divisions will become apparent and be assigned to the members. Some of his interpretations are still valid, whereas others have been modified in light of the new three-dimensional understanding of the Sibley Basin derived from drill core. Depositional environment interpretations for the Outan Island and Nipigon Bay formations will also be discussed. This new analysis of depositional environments should assist in reconstructing the basin architecture and history of the Sibley Group.

Pass Lake Formation

Cheadle (1986a, 1986b) suggested that the Pass Lake Formation represents an alluvial fan. He identified the Loon Lake Member as consisting of debris flow deposits. This was based on the basal conglomerate's muddy matrix, disrupted framework, and lack of stratification. However, Cheadle (1986a, 1986b) also noted that some of the Loon Lake Member conglomerates were graded from clast supported to matrix supported, which he took to indicate waterlain bed-load deposits. Miall (1996) noted that matrix-supported and graded conglomerates indicate debris flows, whereas clast-supported and stratified conglomerates suggest fluvial influences. Cheadle suggested that these latter conglomerates were episodic sheetfloods rather than forming in alluvial channels, due to the lack of internal cross-stratification and the presence of caliche crusts.

Cheadle (1986a, 1986b) considered the heterolithic facies of the Fork Bay Member to be laterally equivalent to the Loon Lake Member. Because of this, as well as the textural immaturity of the sandstones and the existence of medium-scale cross-beds, ripple cross-stratification, and plane-bedded structures, Cheadle (1986a, 1986b) interpreted the heterolithic facies to be turbidites. These would have formed in a lacustrine environment, proximal to the alluvial fan. However, no sedimentological evidence has been found to support the presence of turbidites.

The cross-bedded and plane-bedded facies of Cheadle (1986a, 1986b) were thought to have formed on the alluvial fan under different flow conditions during sheetfloods. The cross-bedded facies was thought to indicate an ephemeral braided stream deposit based on the association of horizontally laminated sandstones, low-angle cross-sets, and a coarse pebble lag. Cheadle (1986a) also noted that the ripple-form laminations that are present within the cross-bedded facies suggest a subaqueous environment, as they are seldom preserved in eolian dunes. He envisioned the horizontally laminated sandstones developing during the initial ebbing of a flood, under upper flow regime conditions. With continued ebbing, low-angle cross-beds would form in transverse bars. Later reworking in a subaerial environment that prevailed in between flood events would result in a deflation pebble lag, which Cheadle (1986a) hypothesized to be a relict desert pavement.

The plane-bedded facies represents rapid deceleration of unchannelled sheetfloods and the formation of alluvial fan sand flats (Cheadle 1986a), which produced sequences of scoured bases, planar laminations, planar cross-beds, ripple cross-laminations, oscillation ripples and a suspension cap. This sequence records a cycle that progresses from upper flow regime to lower flow regime to standing water (Cheadle 1986a; Collinson 1996), similar to the sand-flat cycles of the Upper Triassic red beds in Nova Scotia (Hubert and Hyde 1982). The presence of desiccation cracks, halite casts, and caliche layers suggest subaerial exposure in a semiarid environment (Collinson 1996). The plane-bed facies becomes more abundant basinward, as would be expected from other braided rivers, such as the Platte River (Smith 1970). Suspension deposits become more evident further toward the basin centre and upsection. Cheadle (1986a) suggested that the Silver Islet outcrop represents reworking of the distal alluvial fan by an expanding lacustrine body.

The original interpretation of these units by Franklin (1970) and Franklin et al. (1980) seems more plausible. Franklin (1970) hypothesized that the basal conglomerate was derived from weathering and wave action against Archean basement or an uplifted fault scarp of Gunflint Formation rocks. He suggested the presence of a fault scarp based on the extreme angularity of the Gunflint Formation clasts, very poor sorting, and concentration of the coarsest material in the southwest conglomerates. The maturity of the conglomeratic material in the Lake Nipigon area was thought to indicate a low-energy weathering environment. Franklin et al. (1980) believed that the conglomerate lenses were deposited during rapid, fluvial sedimentation in topographic lows on the pre-Sibley surface. The outcrops near Loon Lake are a good example of deposits formed by this type of depositional system. Franklin (1970) interpreted the presence of ripple-marked and cross-bedded strata interbedded with other conglomerates as indicating a littoral zone, similar to that of some shallow clastic seas (Johnson and Baldwin 1996). Wave action prevents coarse-grained sediment from being transported offshore. In a transgressive succession, the coarse material is overlapped by sand sheets that become reworked by waves (Johnson and Baldwin 1996), similar to the sequence seen in the Sibley Group where the conglomerate layers are overlain by the sandstone lithofacies association, for example, the succession of beds at Pass Lake.

The most convincing evidence to support the lacustrine model proposed by Franklin (1970) and Franklin et al. (1980) is in the sedimentary structures of the sandstone lithofacies association. Franklin et al. (1980) notes the presence of very low-angle cross-beds within the lower 5 m of the sandstone units and the dominance of oscillation ripples throughout the Pass Lake Formation. These features seem to indicate the existence of a beach at the base of the sandstone lithofacies association, overlain by subaqueous sheet flows, interpreted as turbidites by Cheadle (1986a), over a shallow lacustrine basin. Franklin et al. (1980) thought the upward decrease in bed thickness was due to progressive expansion of the lake during a northward strandline migration. They originally hypothesized a northern transport direction based on the presence of chert grains with algal microfossils, similar to those in the Gunflint Formation, found in northern outcrops of the Pass Lake Formation. However, Cheadle (1986a) showed that paleocurrent directions indicate a transport direction toward the southeast.

In summary, Cheadle (1986a) envisioned an alluvial fan forming off of topographic highs and thinning toward the basin centre, where it encountered an expanding water body. Franklin (1970) and Franklin et al. (1980) thought that most of the conglomerates were formed near fault scarps and reworked by waves, although some of them were deposited by fluvial systems in topographic lows. These are overlain by subaqueous sand sheets that were deposited in a lake, thinning upward as the water mass expanded. Evidence for the existence of most of the environments described above is present, though the existence of fault scarps during deposition of the Pass Lake Formation is unlikely (Cheadle 1986a).

Rossport Formation

Cheadle (1986a, 1986b) interpreted the Rossport Formation as representing a lacustrine environment. The cyclic siltstone–dolomite lithofacies association is common to many ancient saline lake deposits, reflecting the cyclic variations in lake hydrology (Talbot and Allen 1996). The calcitic blebs, chert nodules, evaporite minerals (gypsum), and pseudomorphs found within the cyclic siltstone–dolomite lithofacies and overlying dolomitic mudstone lithofacies are common in playa lakes, such as the Ebro Basin in Spain (Salvany, Muñoz and Pérez 1994), and the Officer Basin in Australia (White and Youngs 1980). The presence of the sandstone facies reflects either basin margins where the creation of accommodation space at a greater rate than sediment delivery formed a fining and thinning-upward succession during transgression, for example, outcrops at Pass Lake, or a sediment delivery rate greater than the rate of accommodation space development, which formed coarsening and thickening-upward successions during depositional regressions, for example, outcrops on Copper Island. The finer grained facies occur toward the basin centre (Smoot and Castens-Seidell 1994). It is common for sand sheets to develop in broad unconfined channels on plains bordering playa lakes, and these would have been particularly predominant over channelized flows in the absence of vegetation (Schumm 1963; Miall 1985, 1996).

Desiccation cracks, gypsum nodules, adhesion ripples, and friable mudstones become prevalent above the cyclic siltstone–dolomite lithofacies association. This succession has been interpreted as a damp mud flat by Cheadle (1986b), but may more accurately be compared to a sabkha. The dolomitic mudstones above the cyclic siltstone–dolomite lithofacies association contain solution load structures, growth faults and polygonal deformation structures. In modern systems, these are associated with evaporite crusts on mud flats surrounding playa lakes (Smoot and Castens-Seidell 1994) and are common in sabkha sediments (West, Ali and Hilmy 1979). The presence of gypsum and chert nodules, as well as hematitic soil and caliche layers, also supports the sabkha interpretation. Hematitic soils form in arid environments, appearing as brownish-yellow horizons overlying red, brown or ochre clay that is commonly illuviated (Collinson 1996). In semiarid environments, fersiallitic soils dominate. The weathering in these soils is less complete than in ferruginous soils, and may produce calcitic nodules, similar to those found in the Rossport Formation. These nodules are caliche horizons and may occur as veins or elongate nodules, forming nearly continuous layers as maturity increases (Machette 1985).

Cheadle (1986a) speculated that the dolomitic mudstones were deposited in ephemeral playa lakes, and the mudstones settled out during flash flood events. The overall paucity of coarse sediments through these units, except around marginal zones may indicate that the basin was shallow with low relief, similar to the Mercia Mudstone Group of Great Britain (Talbot and Allen 1996). The Mercia Mudstone is dominated by dolomitic red mudstone containing vague horizontal laminae, desiccation structures, and nodular gypsum horizons. Silt-sized grains have been found within dolomitic mudstone layers and have been interpreted as wind-blown sediment. Further away from the cyclic siltstone–dolomite lithofacies association, there is an abundance of sand patch fabric, which has been interpreted as eolian lags by Smoot and Castens-Seidell (1994). These sediments closely resemble the units of the Rossport Formation, suggesting that they also were deposited in a shallow, semiarid basin with wide alluvial plains.

Above this succession of clastic and chemical sabkha deposits, there is a sudden influx of massive sand beds, which may occur directly below, but more commonly above, the stromatolitic facies of the Middlebrun Bay Member. Based on the distribution of these sandstone units in drill core, they have been used to distinguish the lower boundary of the Fire Hill Member. This boundary is different from that of Cheadle (1986a), who preferred to include the sandstones with the Channel Island Member.

Cheadle (1986a, 1986b) thought that the stromatolite lithofacies occurred during a period when clastic input was restricted. He believed that there was one shallow lake that may have reached pH of 9 to 10, based on the early silicification of the stromatolites. Cheadle (1986b) also pointed to halite pseudomorphs to indicate alkalinity fluctuations. However, the stromatolitic facies is much more isolated than Cheadle (1986a, 1986b) speculated. It is probable that the stromatolites occurred along the shorelines of partially restricted bays where alkalinity reached optimal conditions rather than throughout the entire shallow lake. These restricted conditions could have been caused by the influx of sand sheets into the basin, which initially occurred around the same time and may have provided the barriers to isolate parts of the lake, where the stromatolites would have formed during periods of low sedimentation between sheet floods. This would also account for the stromatolites occurring at slightly different stratigraphic horizons. Truc (1978) described a similar sequence of an isolated stromatolite unit found above an evaporitic sequence during the final fill stages of the basin. He suggested that this was due to the decreasing rate of subsidence and the near-full stage of the basin. The Sibley Basin appears to record a similar history with the upper layers of the stromatolitic facies commonly exhibiting a paleoweathered and diagenetically altered surface probably formed by exposure to meteoric water. This is overlain by a *terra rosa* (soil horizon) in places and subaerial debris flows in other areas.

According to Cheadle (1986b), clastic sedimentation resumed, due to the onset of a wetter climate or uplift. He pointed to the lack of coarse sediment fractions and the absence of evidence for subaerial exposure as suggesting deposition away from lacustrine margins. Cheadle (1986b) suggested that the conglomerates within the upper portion of the Rossport Formation could represent intrusive sedimentary breccias.

However, the examination of drill core reveals that Cheadle's (1986a, 1986b) observation about the lack of coarse sediment is not quite correct. Thick sand beds can be found extending vertically all the way to the Kama Hill Formation, although the drill core shows that the majority of the sand sheets are confined to directly above the stromatolitic facies. These sand sheets are also interbedded with the mud-chip and intraformational conglomerates that Cheadle (1986b) noticed in the Fire Hill Member and proposed to be intrusive sedimentary breccias. However, many of them appear to be debris flows, particularly in the case of the extensive outcrop on Mawn Lake Road, described previously. The poor sorting, matrix support, and lack of stratification in the conglomerates indicate a debris-flow deposit (Collinson 1996; Rust 1978). The mud-chip conglomerates sometimes include dolomitic and gypsiferous mud blocks, and indicate reworking of the basinal strata by slump events.

Cheadle (1986a) was also mistaken about the lack of subaerial exposure. Soil horizons, preserved as caliche layers and diagenetic gypsum nodules, attest to subaerial exposure. Perhaps the best example of subaerial exposure is the sequence on Channel Island, which progresses from subaqueous rippled sandstone to the stromatolitic carbonate unit to subaerial caliche layers and intraformational conglomerates. Some of the stromatolites contain tepee structures, as well as gypsum and halite casts, that are suggestive of hypersaline conditions shortly after deposition being replaced by total desiccation.

Some of the conglomerates noticed by Cheadle (1986a) and Franklin et al. (1980) are true sedimentary breccias and sand sills, for example, south of Pass Lake. Cheadle (1986a) suggested that these formed due to abnormally high fluid pressures associated with lithological barriers. He hypothesized that the mudstones and dolomites of the Channel Island Member, as well as the chert–carbonates of the stromatolitic lithofacies association, would have trapped water within the Pass Lake Formation. Fluid expulsion would then be triggered by earthquake activity creating conduits through the overlying barrier. These sedimentary breccias are frequently found within fault zones (Cheadle 1986a) and microfaults have been noticed in the mudstones of the Fire Hill Member and Kama Hill Formation.

Kama Hill Formation

Cheadle (1986a, 1986b) suggested that the Kama Hill Formation represented a change from a lacustrine environment to a subaerial mud flat, where deposition occurs in a similar way to flood plains although there is a distinct lack of channel deposits. Some channel deposits are interbedded with the Kama Hill Formation near the contact with the Outan Island Formation, but the majority of the Kama Hill Formation is a result of unchannelized sheet flows and settling out of suspension. Cheadle (1986a) based his interpretation on the abundance of desiccation cracks and the absence of carbonates. The horizontally laminated mudstone lithofacies association was interpreted as a suspension deposit primarily associated with mud-flat ponds. The lack of carbonates and quartz nodules indicates a change in hydrological conditions (Cheadle 1986a).

The Kama Hill Formation is dominated by horizontally laminated, fine-grained sandstone and siltstone and mud-cracked, fine-grained sandstone and siltstone, similar to the flood plain along the Beatton River (Nanson 1980). This represents sheetflood and suspension deposits followed by subaerial exposure. The rippled, fine-grained sandstone and siltstone lithofacies association formed during flood events (Nanson 1980). Laminated muds, some associated with wave-rippled siltstone, found in the Kama Hill Formation, represent mud-flat ponds that periodically covered parts of the basin. The presence of thicker units of laminated shale and siltstone, sometimes associated with wave ripples and no subaerial indicators, such as mud cracks, suggests that some of these ponds remained for an extended period of time. This flooding trend must become more pronounced higher in this succession as the next formation is totally subaqueous.

Outan Island Formation

Interpretations of depositional environments for the Outan Island Formation are hindered by the limited amount of surface exposure and drill core that intersected it. The lower Outan Island Formation is thought to represent a deltaic environment, and has been designated the Lyon Member. This unit is restricted to Nipigon Bay and has been named after nearby Lyon Township. The upper Outan Island Formation corresponds with a fluvial environment and has been named the Hele Member, after the township it was found in.

The Lyon Member coarsens upward and is dominated by siltstone and mudstone laminae with some sandstone beds near its base. Coarsening and thickening-upward sequences are common in the grading from red mudstone with fine-grained ripple laminated sandstone near their base to trough and hummocky cross-stratified medium-grained sandstones near their tops. In some drill core, low-angle cross-stratification occurs between the Lyon Member and the Hele Member. This combination of lithofacies associations resembles a muddy deltaic environment, similar to the Upper Carboniferous Westphalian deltaic unit described by Haszeldine (1984), and the Acheloos delta in Greece (Piper and Panagos 1981).

The siltstone and laminated siltstone and mudstone are similar to the fine-grained turbidites deposited in interdistributary areas during floods and in distal delta deposits (Piper and Panagos 1981; Haszeldine 1984; Reading and Collinson 1996). The coarsening and thickening-upward successions are very similar to prograding distal bars to distributary mouth bars present in both modern (Coleman and Prior 1980) and ancient (Fralick and Miall 1989) delta systems. The low-angle cross-stratified sandstones are, most likely, beach deposits (Reading and Collinson 1996). In summary, the Lyon Member displays a typical coarsening-upward, prograding deltaic sequence from the muds and silts in the distal portions of the delta and deeper interdistributary areas to the progradational distal and distributary mouth bars. In some areas, thin beach deposits cap the sequence.

The majority of the Hele Member is dominated by cross-stratified sandstone and normal- or inverse-graded sand beds, topped with mud caps. Mud-chip horizons and broken, contorted mud laminae are common. Many of these sandstones are incorporated into fining-upward sequences from massive or parallel-laminated sandstone to rippled fine-grained sandstone, rippled siltstone, and laminated mudstone. Intraformational conglomeratic units containing subrounded mud blocks are present at the base of some sandstone units, and midway through others.

Allen (1970) described 6 facies in a typical fluvial deposit: conglomeratic, large-scale cross-stratified sandstones, flat-bedded sandstones, small-scale cross-stratified sandstones, alternating beds of siltstone and sandstone, and siltstone facies. All but the large-scale cross-stratified sandstones have been identified in the Hele Member, although lack of the latter may only be due to lack of outcrop exposure. Channel sequences have erosive bases and, generally, a channel lag of matrix-supported intraformational conglomerates (Allen 1970; Miall 1977). In the Hele Member, the fining-upward sequence overlies the channel lag and corresponds to waning flow conditions, similar to abandoned channel sediments (Allen 1970). The siltstones and laminated siltstone–mudstone units, with some ripple laminae, were deposited on the river's flood plain. The presence of mud chips and small mud cracks suggests subaerial exposure on the flood plain (Nanson 1980). Massive sandstones, that may be normal or reverse graded, are interbedded with the siltstones of the flood plain. These represent crevasse-splay deposits (Allen 1964; Miall 1985), caused by a river breaking through its levee and carrying bed-load sediment onto the flood plain. Occasionally, laminated shales are found interbedded with the siltstone lithofacies association, representing flood-plain ponds.

The Hele Member resembles a meandering river system rather than a braided stream, although distal sand-dominant braided rivers can be difficult to distinguish from meandering rivers (Rust 1978). It is particularly difficult to differentiate between the two when outcrops are not available to examine large-scale bed forms, as is the case in the Hele Member.

Nipigon Bay Formation

The Nipigon Bay Formation is believed to be an eolian system. This is suggested by several factors. Most striking is the one outcrop of the Nipigon Bay Formation on Simpson Island (*see* Figure 1), which preserves a distinct, large-scale, remnant dune topography. This dune feature is approximately 15 m in height, which is excessive for most fluvial environments (Collinson 1996; Miall 1977) although large-scale cross-beds can be found in fluvial systems, such as the giant cross-beds of Jones and McCabe (1980) that reached a thickness of 35 m. Kocurek (1996) stresses the importance of the identification of paleotopographic features for identifying eolian dune systems. In drill core, the Nipigon Bay sets tend to be 50 to 400 cm thick, with co-sets ranging from 4 to 40 m thick. The very large-scale cross-beds and high-angle sets indicate an eolian environment (Clemmensen and Abrahamsen 1983; Bigarella 1972).

Besides the initial, large-scale dune features, smaller sedimentary features within the outcrop and in drill core accentuated the similarities between the Nipigon Bay Formation and eolian systems. Most eolian dunes are primarily composed of steeply dipping, concave-upward laminae with plane or curved bounding surfaces (Bigarella 1972). The drill core contains 450 to 500 m of predominantly high-angle cross-stratification, interbedded with some low-angle and horizontally laminated beds. The Simpson Island outcrop contains curved and planar bounding surfaces. The angle of dip on the dune surface should decrease downslope (Bigarella 1972), which is seen in the outcrop and could possibly be indicated by the gradual change from high- to low-angle cross-stratification in drill core.

Another criterion for eolian sand deposits is the high degree of sorting relative to subaqueous sandstones (Bigarella 1972), which is also seen in the Nipigon Bay Formation. However, in some cases, coarse grains are present in the sandstones, which is not typically associated with eolian sand dunes. Clemmensen and Abrahamsen (1983) observed coarsening-upward, granule-rich horizons and incipient granule ripples interbedded with plane-bed laminae near the margins of the Arran Basin. They suggest that the coarse fraction is related to very high wind velocities and note that inverse grading is well known in migrating wind ripples. However, the coarse grains here are more commonly interbedded with the high-angle cross-strata. This indicates that the coarse horizons represent a deflation lag, which is typically found at the bottomsets of dunes (Kocurek 1996; Clemmensen and Abrahamsen 1983). One unusual feature is the rare, preserved ripple-forms in the Nipigon Bay Formation. These are typically absent in eolian dunes, but have been noted in Paleozoic and Mesozoic sandstones of the Colorado Plateau (Bigarella 1972) and the Arran Basin (Clemmensen and Abrahamsen 1983).

The horizontally laminated beds represent the interdune areas. Bigarella (1972) showed that the flat-lying laminae of the interdune area were gradational with low-angle laminae as the base of a dune is approached. The Nipigon Bay horizontal laminae are sometimes associated with silty material, suggesting that they were deposited in low-lying areas that were probably occasionally moist. Kocurek (1996) notes that interdune-flat accumulations are seldom preserved in dry environments, and this would be particularly true in the Mesoproterozoic with no vegetation to stabilize interdune areas. Therefore, the Nipigon Bay Formation was probably a semiarid to arid desert.

Summary of Depositional Environments

The Loon Lake Member represents braided fluvial deposits in low-lying areas on the bedrock surface overlain by transgressive reworked beach deposits. The heterolithic facies of the Fork Bay Member was considered by Cheadle (1986a) to be chronologically equivalent, denoting the subaqueous continuation of debris flows in the form of turbidites. However, these should not be considered true turbidites, but should be termed subaqueous sheet flows. The sandstone beds thin basinward and become interbedded with siltstone beds accumulating during quiet periods in the shallow lake that was forming within the basin.

The lacustrine sandstones of the Pass Lake Formation interfinger with the mud flat and marginal saline lake shales and mudstones of the Rossport Formation. Cyclic siltstone–dolomite beds formed within the saline lake, cycling with lake level fluctuations. Clastic material was restricted to fine sediment settling out during flash-flood events that recharged the basin, while sabkha-like sequences formed in the surrounding mud flats. After a prolonged period, the shallow saline lake began to dry further, forming extensive damp sabkha-like mud flats and allowing sand sheet incursions to penetrate farther into the basin centre. The transition from subaqueous dolomites and siltstones to subaerial conditions is marked by the presence of strandline stromatolitic carbonates. Soils and subaerial mudflows commonly overly these shoreline deposits.

The subaerial mud flats of the Fire Hill Member had a high saline groundwater table as attested to by the abundant diagenetic gypsum nodules. The Kama Hill Formation represents a change to a more humid climate and the gradual reflooding of the basin. The Kama Hill Formation and the lower member of the Outan Island Formation form a prograding deltaic system into a basin that was subaqueous. The delta system was subjected to slope failures which produced large slump-block breccias. This was followed by fluvial deposition on the delta top. There was a hiatus and rotation of the underlying basement blocks creating an angular unconformity between the Outan Island Formation and the Nipigon Bay Formation, after which a thick sequence of eolian sands was deposited.

Lithostratigraphy of Sedimentary Units

The lithostratigraphy of the Sibley Basin has been modelled using RockWorks™ version 99 software, which incorporated 25 complete drill logs, as well as outcrop data. Collar elevations and Universal Transverse Mercator (UTM) co-ordinates were used to place the drill-core logs in the correct spatial positions relative to one another. Models and projected sections have been generated using north to south directional weighting. The model covers the southern half of the Sibley Basin, as insufficient data were available for the northern reaches proximal to Lake Nipigon.

BASIN ARCHITECTURE

Three-dimensional data plots of the Sibley Basin (Figures 6, 7 and 8) were constructed using formation thicknesses obtained from drill-core logs and some outcrop data. The area covered is shown in the inset in Figure 9 and covers the outcrop area of the Sibley Group south of Lake Nipigon. The most striking feature on all of the three-dimensional reconstructions (*see* Figures 6, 7 and 8) is the downdropping trace of the 3 formations in the southeast area underlying Nipigon Bay. This is where the thick successions of

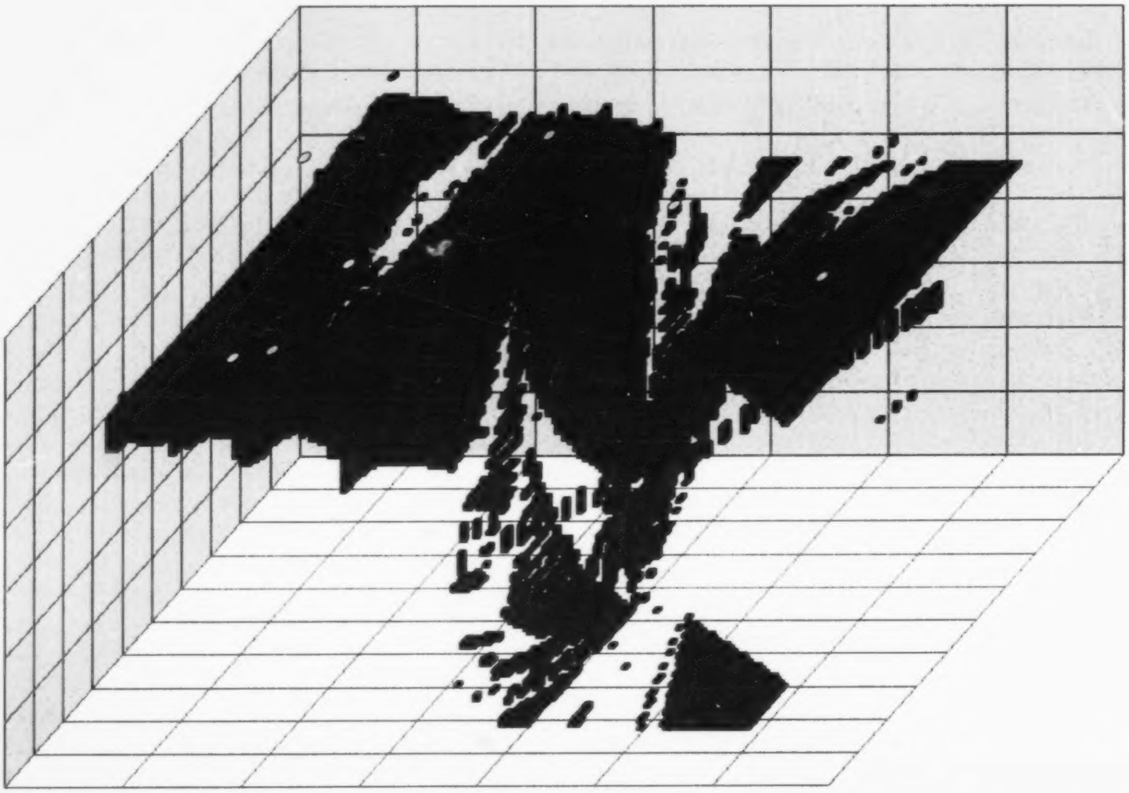

Figure 6. A three-dimensional diagram showing the distribution of the Pass Lake Formation, based on the Fork Bay Member (dark grey), developed using data from drill holes and outcrops. The light grey ellipses denote the positions of the Loon Lake Member of the Pass Lake Formation and the black ellipses signify the positions of the Middlebrun Bay Member of the Rossport Formation.

the Outan Island and Nipigon Bay formations overlie the strata of the Sibley Group (*see* Figures 6, 7 and 8). This deepening trend reflects the down-to-the-southeast tilting of the underlying basement block during Keweenawan rifting. Thus, it is a secondary overprint caused by postdepositional tectonism in the area. Some of the basement subsidence in the southeast may have occurred during formation of the Sibley Basin, but this is difficult to evaluate and cannot be evaluated from diagrams such as these, which use as a datum modern elevations. The three-dimensional diagrams do show the present-day distribution of the lower 3 formations of the Sibley Group and, in addition, show changes in thickness of each of the units. Where the formation is nonerosively overlain by the next unit, as is the case for most of the Pass Lake and Rossport formations, these thickness trends are related to sedimentation patterns. However, where the top of the formation has been eroded, i.e., much of the Kama Hill Formation, the thickness variation will simply reflect degree of erosion. It is interesting to note that all models, but especially the Rossport Formation model (*see* Figure 7), infer the existence of faults with vertical displacements running from northeast–southwest to north–south. Whether these fault-like structures are an artifact of the program or are a true representation of the geology of the area is difficult to evaluate.

Figure 6 depicts the Pass Lake Formation data plot, based on the Fork Bay Member. The Loon Lake Member is too sporadic to be used in the modelling program, but the light grey ellipses in Figure 6 indicate the drill core and outcrop locations where it was found. The thickest occurrences of the Loon

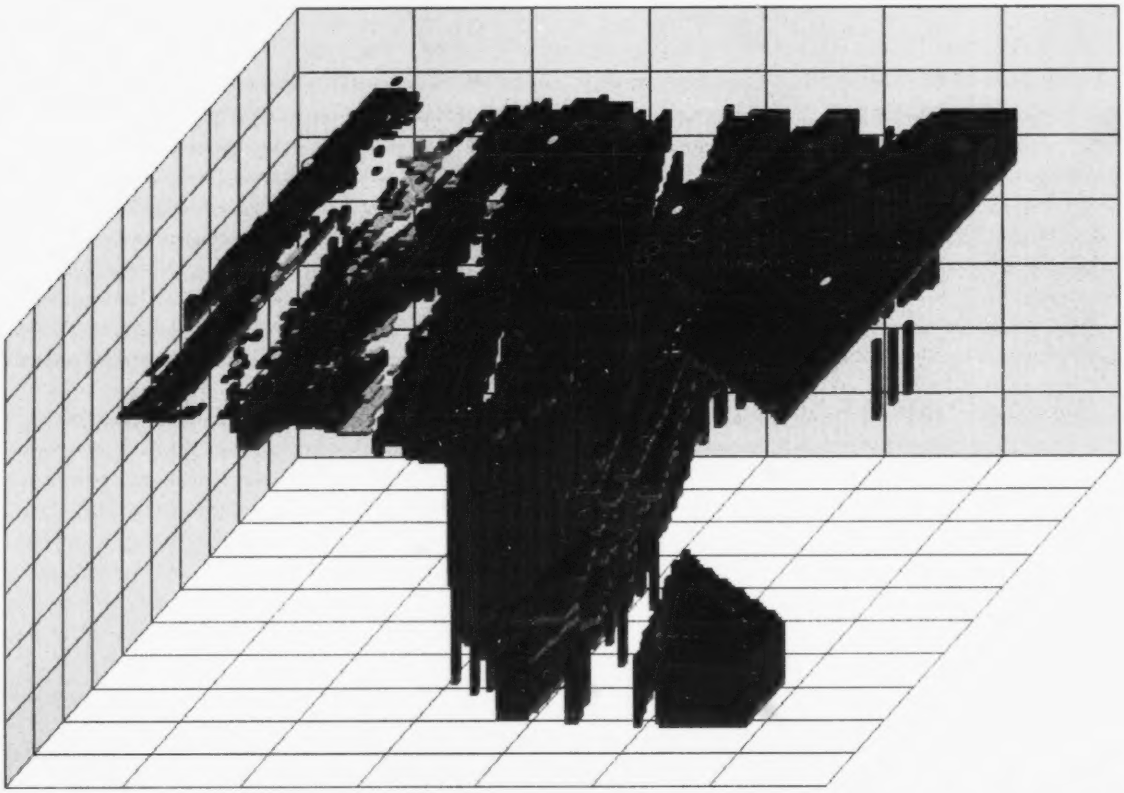

Figure 7. A three-dimensional diagram showing the distribution of the Rossport Formation developed using data from drill holes and outcrops. Datum is present elevation. The light grey ellipses denote the positions of the Loon Lake Member of the Pass Lake Formation and the black ellipses signify the positions of the Middlebrun Bay Member of the Rossport Formation.

Lake Member are along the exposed southern portion of the basin. The Fork Bay Member has a relatively uniform thickness across the basin, although slightly thicker accumulations occur in the topographic lows of the basement.

The three-dimensional data plot for the Rossport Formation is show in Figure 7. The Channel Island Member has a relatively uniform thickness, although it is slightly thicker over topographic lows. The Middlebrun Bay Member is only found as discrete occurrences and is indicated by black ellipses. The Middlebrun Bay Member is observed near the eastern and western margins of the basin. The Fire Hill Member constitutes the majority of the Rossport Formation, and is thickest overlying the downtilted block.

The distribution of the Kama Hill Formation is shown in Figure 8. It is the thickest along the western to northwestern margin of the Sibley Basin, and becomes progressively thinner toward the centre in the basin. The Outan Island Formation laps onto the Kama Hill Formation within the centre of the basin and downtilted southeastern edge. The Nipigon Bay Formation is restricted to the southern portion of the downtilted southeastern block.

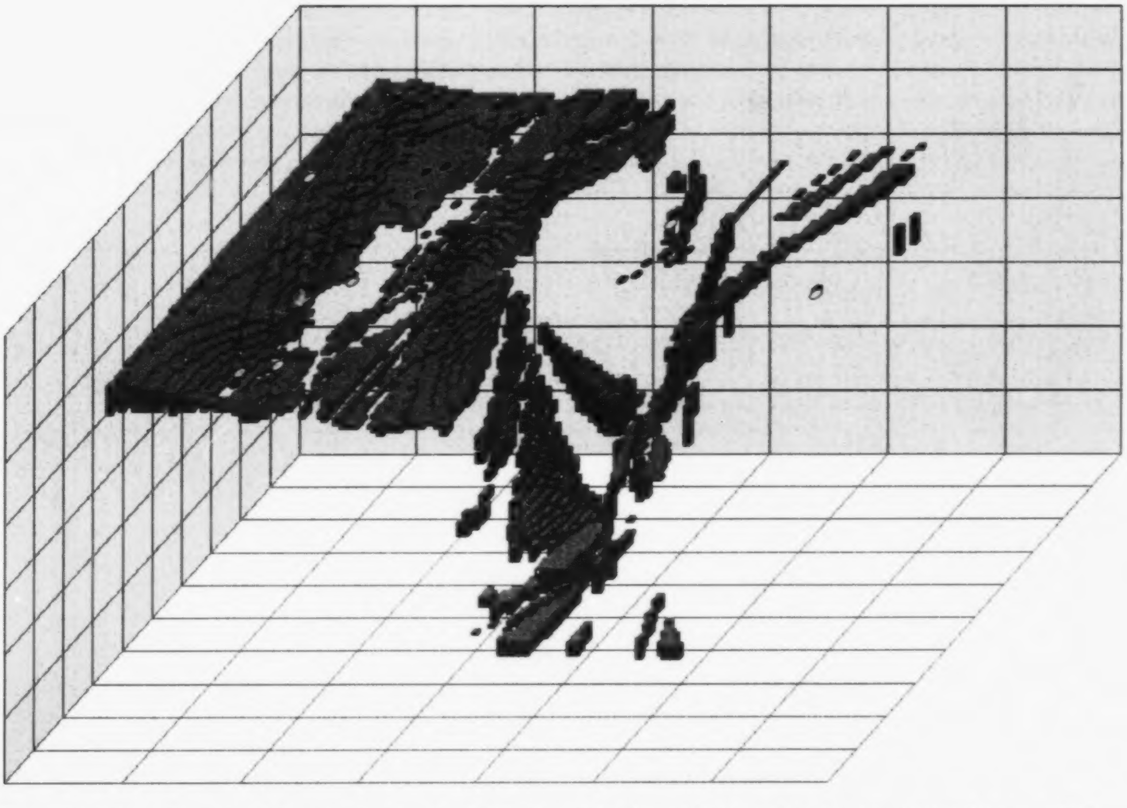

Figure 8. A three-dimensional diagram showing the distribution of the Kama Hill Formation developed using data from drill holes and outcrops. Datum is present elevation. The light grey ellipses denote the positions of the Loon Lake Member of the Pass Lake Formation and the black ellipses signify the positions of the Middlebrun Bay Member of the Rossport Formation.

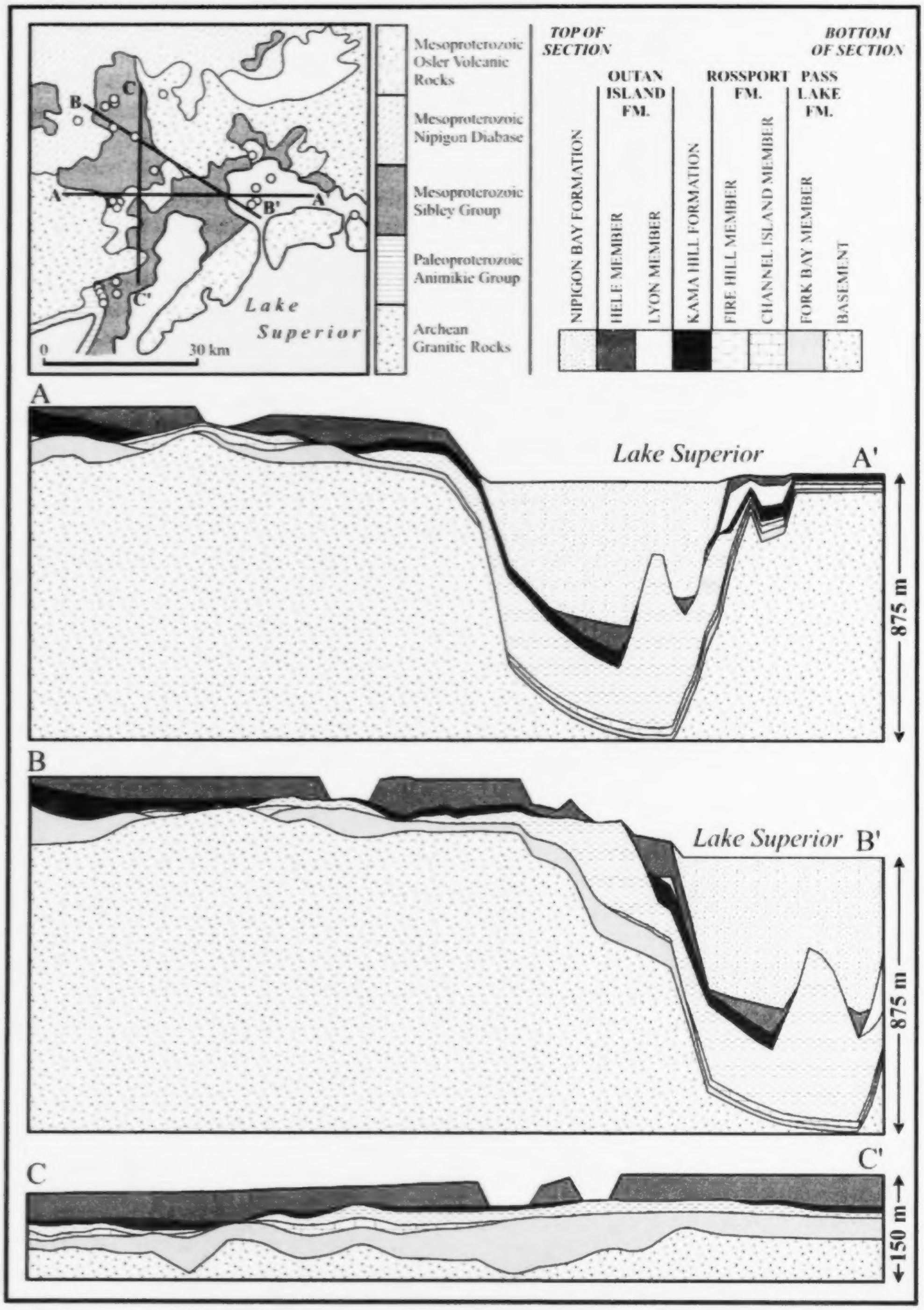
B
C
A
A'
B'
C'
Lake
Superior
0
30 km
Mesoproterozoic Osler Volcanic Rocks
Mesoproterozoic Nipigon Diabase
Mesoproterozoic Sibley Group
Paleoproterozoic Animikie Group
Archean Granitic Rocks
TOP OF SECTION
BOTTOM OF SECTION
OUTAN ISLAND FM.
ROSSPORT FM.
PASS LAKE FM.
NIPIGON BAY FORMATION
HELE MEMBER
LYON MEMBER
KAMA HILL FORMATION
FIRE HILL MEMBER
CHANNEL ISLAND MEMBER
FORK BAY MEMBER
BASEMENT
A
Lake Superior
A'
875 m
B
Lake Superior
B'
875 m
C
C'
150 m

Figure 9. Inset in upper left shows the 3 projected section lines and the positions of the drill holes and outcrop sections (circles) used in creating the cross sections. The 3 section lines are hung on the datum of present elevation. Thus, the modelled sections are a representation of the present distribution of the rock units.

The basin architecture can also be shown using a series of cross sections. A map of the Sibley Basin (*see* Figure 9, inset) shows the lines used for the projected stratigraphic sections depicted in Figures 9A, 9B and 9C. Datum for these 3 sections is current elevation, i.e., the same datum as the three-dimensional plots. Thus, these sections are showing present distribution of the formations with the cumulative effects of all tectonism over the last approximately 1.5 billion years.

These sections illustrate the relationships between the members of the Sibley Group along west–east (A–A′ in Figure 9A), northwest–southeast (B–B′ in Figure 9B), and north–south section (C–C′ in Figure 9C) lines. The Loon Lake Member of the Pass Lake Formation and the Middlebrun Bay Member of the Rossport Formation are not included due to their sporadic and limited extent. The Hele Member causes some problems in the modelling program in the western part of the basin because it is primarily found on the downtilted block and only has one occurrence in the west, which the program interprets as a relatively uniform member across the entire western section.

The west–east and northwest–southeast projected stratigraphic sections clearly show the downdropped block, which was present in the three-dimensional modelling. Here, we have a better view of its geometry, which appears to consist of a downfaulted block underlying western Nipigon Bay. Its location strongly indicates that the majority, if not all, its downward movement was probably Keweenawan in age. The Outan Island Formation and Nipigon Bay Formation are preserved in this downdropped area and probably once covered a much larger region.

The west–east and northwest–southeast projected section lines also clearly show the Fork Bay Member onlapping, but not burying, a topographic high of basement rock in the north. This indicates the effect of localized basement topography on distribution and thickness of the Fork Bay Member sandstones. The northwest–southeast and north–south sections reveal a similar relationship for the Channel Island Member. These lacustrine strata are not capable of completely burying the topographically highest basement hills and, as Figure 9C clearly demonstrates are, in places, isolated in depressions with flanking sandstones of the Pass Lake Formation. The Fire Hill Member also appears to be thicker in some of the topographic lows, although it is thickest in the large downtilted area forming the deep trough under Nipigon Bay, which may indicate that this was a deeper portion of the Sibley Basin during deposition of this unit. This is also supported by the distribution of paleocurrent directions of the Pass Lake and Rossport formations (Cheadle 1986a) that show transport directions converging toward this area. However, erosive removal and thinning in the northern and western areas could have also lead to this thickness pattern.

The effects of subsidence during deposition of the Sibley Group can be modelled by choosing as datums internal stratigraphic surfaces in the sedimentary assemblage. This, in effect, creates a flat plain surface at the top of the chosen sedimentary unit, which can be thought of as representing the flat surface of the earth as deposition of that sedimentary unit ended. Two horizons were selected: the first at the base of the Fire Hill Member and the second at the top of the Fire Hill Member (Figures 10A and 10B, respectively). These were selected to emphasize the change in basin dynamics during the deposition of the Fire Hill Member. Prior to the deposition of the Fire Hill Member, the basin had a relatively uniform depth. The Pass Lake Formation and Channel Island Member of the Rossport Formation fill topographic lows and drape over topographic highs along section line A–A′ (west to east) across the basin (*see* Figure 9A). However, during Fire Hill Member deposition, subsidence is much greater in the east, coinciding with the position of what strikingly appears to be a downfaulted half graben with the main boundary fault on the east side of the basin.

This has some implications for the formation and depositional history of the basin. The original surface of the Sibley Basin was irregular with the greatest topographic variability occurring in the southern section, whereas the central portion was relatively flat. During the first phase of sedimentation the basin formed a broad, gently subsiding area. The conglomeratic facies of the Loon Lake Member was deposited in depressions, and onlapped local topographic highs. The Fork Bay Member blanketed the topography, aside from the occasional basement hill that protruded through it. The sediment was transported from the northwest (Cheadle 1986a). The climate was semiarid during this time, as suggested by caliche layers and halite casts.

The Channel Island Member represents the saline lake of the Rossport Formation. This member appears continuous in Figures 10A and 10B, although Figure 9C reveals that higher elevation areas in the central basin were not completely flooded. The lake may not have been laterally continuous for this entire time span. It could possibly have occurred as a series of medium-sized saline lakes or it could have been one lake that became divided into many during prolonged arid periods. The stromatolitic facies of the Middlebrun Bay Member occurs above the Channel Island Member, forming as the shoreline of the lake moved through an area during the final drying phase. The incursion of sand sheets and debris-flow intraformational conglomerates, as well as the injection of sedimentary breccias and change in basin hydrology (Cheadle 1986a), from open lake to high groundwater table mud flats, could indicate tectonic activity within the basin. This is supported by the apparent formation of a half graben before or during the deposition of the Fire Hill Member (*see* Figure 10B). This series of events is probably related to the change in paleocurrent direction seen in the Kama Hill Formation, with flow in this unit coming from the south (Cheadle 1986a). Other indicators of tectonic activity at this time are tensional pull-apart structures in the underlying Channel Island Member and a thick succession of conglomerates with Sibley Group and Archean clasts, as seen in drill core from a hole drilled through the Sibley Group to the immediate west of the Black Sturgeon fault zone, which may be the structure defining the eastern edge of the half graben. This episode of tectonic activity considerably predates (200 my) the Midcontinent Rift. The Rossport Formation is characterized by a semiarid environment, as suggested by carbonate and gypsum precipitation and desiccation features. A weathering surface exists above the Middlebrun Bay Member and a hiatus may exist here. Thus, the probable graben formation phase of the Fire Hill Member may be separated from the underlying units in time.

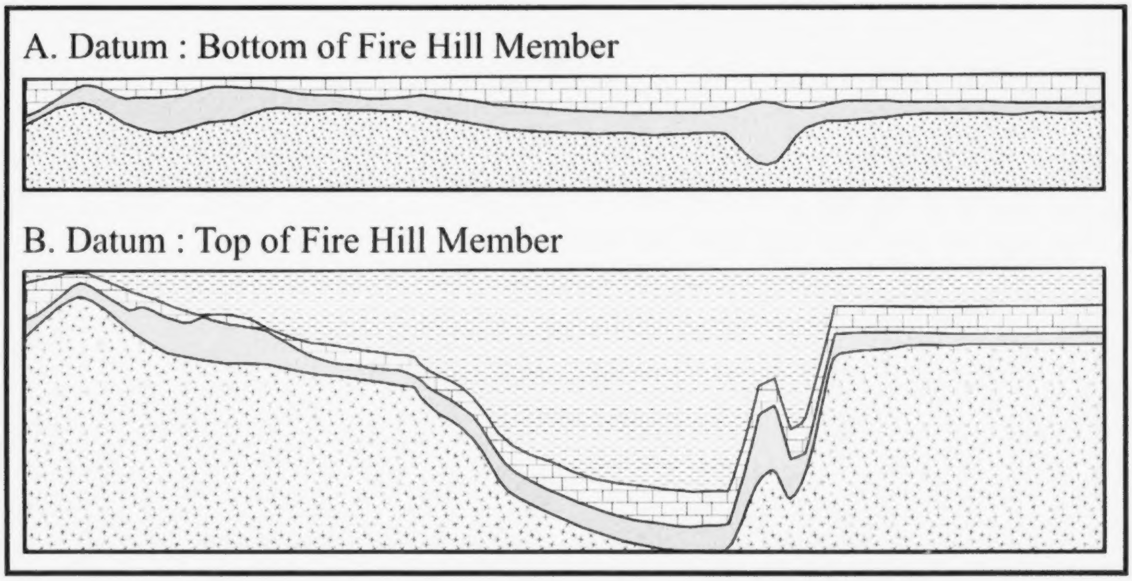
A. Datum : Bottom of Fire Hill Member
B. Datum : Top of Fire Hill Member

Figure 10. Section line A–A' (Figure 9) modelled using the bottom (A) and top (B) of the Fire Hill Member of the Rossport Formation as the datum. This is an attempt to restore the section to what it would have looked like at the beginning and end of Fire Hill deposition. However, the presence of areas of later erosive removal of the Fire Hill Member complicate the interpretation. Legend as for Figure 9.

Flooding of the basin occurs during deposition of the Kama Hill Formation. The thickest accumulation of this unit occurs in the west and pinches out toward the east. In places, the Kama Hill Formation is interbedded with the Outan Island Formation, suggesting that they were coeval. The presence of the lower Outan Island Formation in the southeast, the apparent lateral equivalent of the Kama Hill Formation (*see* Figures 9A and 9B), is in agreement with the lower Outan Island Formation representing wave-modified distributary mouth bars of a delta system with the Kama Hill Formation forming the distal bar to prodelta facies. Paleocurrents for the Kama Hill Formation trend toward the northwest, a complete reversal from the Pass Lake and Rossport formations, but in accord with the shore-proximal lower Outan Island Formation in the southeast grading into the deeper water Kama Hill Formation in the northwest (*see* Figures 9A and 9B). The upper portion of the Outan Island Formation, the Hele Member, was deposited by a fluvial flood plain–channel system, presumably the delta top system as there does not appear to be a break in sedimentation between this unit and the underlying Lyon Member.

There is an angular unconformity between the Outan Island Formation and the Nipigon Bay Formation. The Nipigon Bay Formation is an eolian sand dune system and indicates development of an arid environment. This unit is restricted to the area of the downdropped basement block underlying the west end of Nipigon Bay. It has southwest-trending paleocurrent directions (*see* Figure 5) and was probably at one time much more laterally extensive then it is at present.

Stratigraphy of the Nipigon Diabase

The general stratigraphic positioning of the sills of Nipigon Diabase intruding Sibley Group sedimentary units is very well documented in Hart and Magyarosi (2004), Hart (2005), MacDonald (2004), and MacDonald, Tremblay and Easton (2005), especially the cross sections supplied with these volumes. The chapter presented here is meant to be an overview of the general positions of sills intruded into Sibley Group rocks and the reader is referred to the above volumes for a more detailed analysis.

Numerous faults are depicted on the diagrams presented here. These faults are inferred, from the data collected on surface and from drill holes, but were not observed. Their exact locations are, in some instances, likely inaccurate and some faults may not exist at all. The diabase sills are generally concordant, but up and downramping is not uncommon, and that, combined with an irregular basement topography leading to variable thickness of Sibley Group units, may explain some changes in stratigraphic positioning of sills rather than faulting.

The location of the 10 schematic cross sections presented here are shown in Figure 11. The southernmost outcrop area of the Sibley Group, along the south shore of Nipigon Bay (Figure 12), is near the southern limit of extent of the sill complex. The 900 m of cored stratigraphic section of the Sibley Group present here contains two, in places very thin, sills at or near the base of section (*see* Figures 12 and 13). The lower sill is a typical Nipigon diabase in composition, but the upper sill has a different chemistry (T.R. Hart, OGS, personal communication, 2005). The north shore of the bay contains a few very thin sills in the Rossport Formation, which are geochemically similar to the ultramafic intrusions, but the major sill is a minimum of 90 m thick and is intruded into the Kama Hill Formation (*see* Figures 12, 13 and 14). It does not extend to the other side of Nipigon Bay, though it is continuous along the north shore.

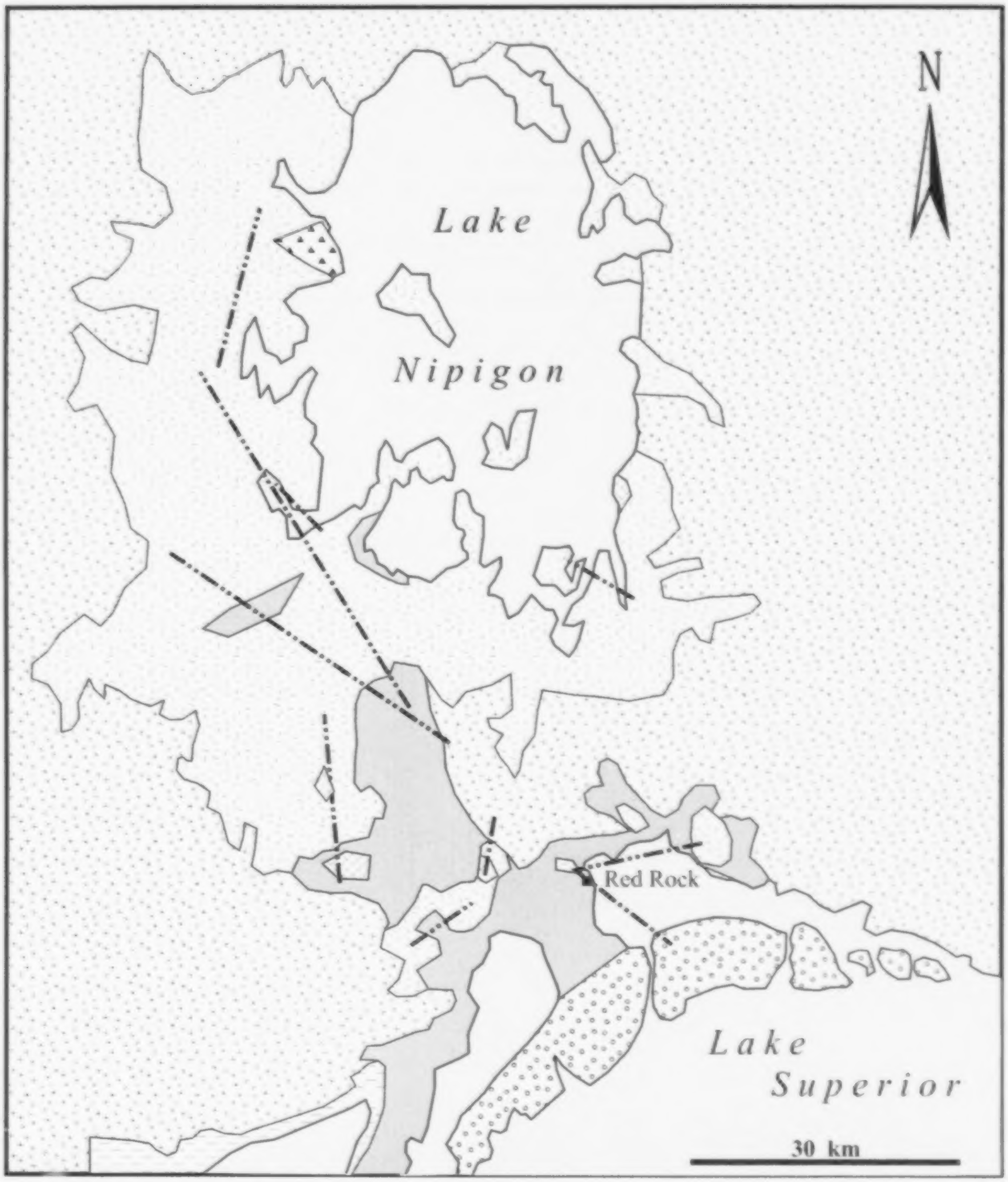

Figure 11. General locations of cross sections (heavy dashed-dotted lines) presented in this section; southeast to northwest, more detailed locations are shown in Figures 12, 15, 18, 20, 24 and 26. Legend: plus symbols (+) are Archean felsic intrusive rocks; horizontal dashes (–) are the Paleoproterozoic Animikie Group; dark grey is the Sibley Group; cross-hatch pattern are ultramafic intrusive rocks; randomly oriented short dashes (- -) are the Nipigon Diabase sills; open circles (o) are the Osler Group; and filled triangles (▲) are the English Bay complex.

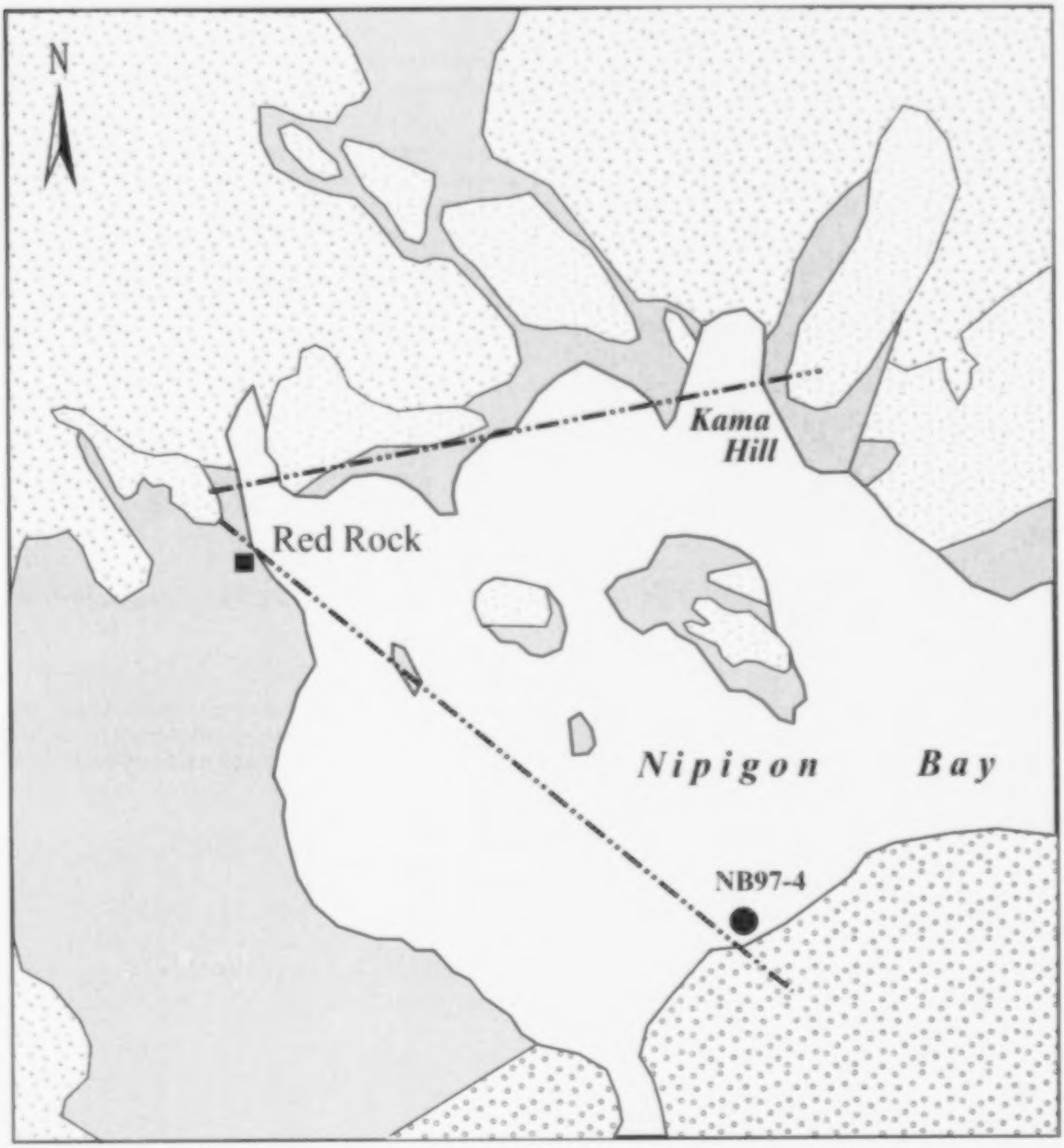

Figure 12. Cross-section locations (heavy dashed-dotted lines) in the southeastern area. The cross section from Red Rock to drill hole NB97-4 is shown in Figure 13; the cross section from Red Rock to Kama Hill is shown in Figure 14. Legend: black dot is the drill hole location; plus symbols (+) are Archean felsic intrusive rocks; dark grey is the Sibley Group; randomly oriented short dashes (- -) are the Nipigon Diabase sills; and open circles (o) are the Osler Group.

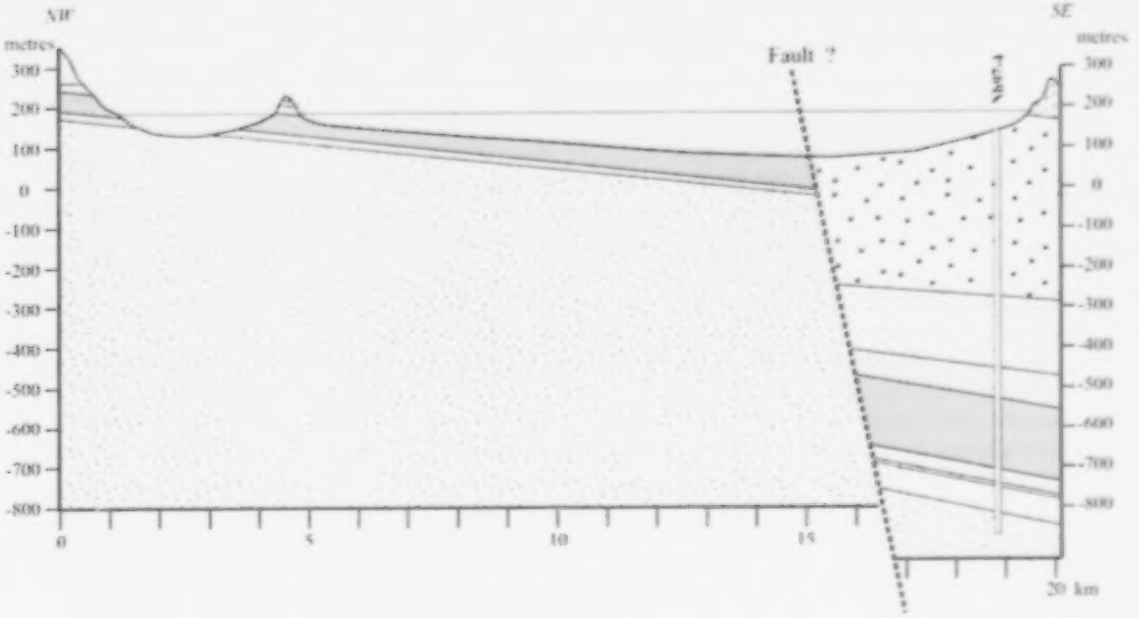
NW
SE
metres
metres
Fault ?
NB97-4
300
200
100
0
-100
-200
-300
-400
-500
-600
-700
-800
0
5
10
15
20 km

Figure 13. Cross section from Red Rock, in the northwest, to the Osler Group, in the southeast; location shown in Figures 11 and 12. The fault is not necessary as the average dip allows the continuity of the layers. It is shown as computer assisted interpretation of stratigraphic data indicates it may be present. Legend: plus symbols (+) are Archean granitic rocks; randomly oriented dashes (- -) are diabase sills; small dots (•) are the Pass Lake Formation; dark grey is the Rossport Formation; cross-hatch pattern is the Kama Hill Formation; randomly oriented pattern of letter "v" are the Outan Island Formation; larger, widely spaced dots (●) represent the Nipigon Bay Formation; and open circles (o) are the Osler Group.

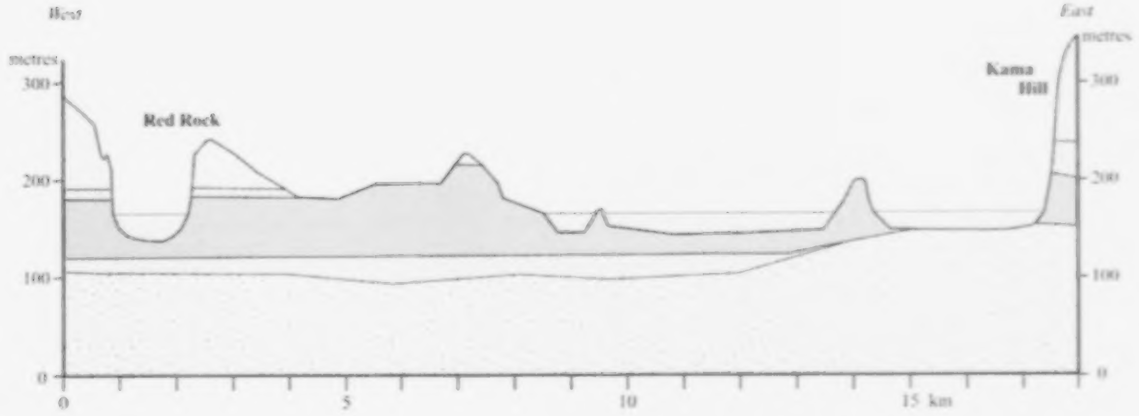
West
East
metres
metres
Red Rock
Kama Hill
300
200
100
0
0
5
10
15 km

Figure 14. West to east cross section from Red Rock to Kama Hill; location shown in Figures 11 and 12. Symbols as for Figure 13.

This same intrusion can be traced along the north shore of Nipigon Bay, onto Verte Island and further to the west through Moseau Mountain (Figures 15 and 16). It appears to be stratigraphically correlative to the Hele ultramafic intrusion. The Hele intrusion lines up with the diabase sill flanking it both to the east (*see* Figure 16) and west (Figure 17). This, of course, is odd as the Hele and Nipigon intrusions are different geochemically and are not genetically related. Further to the west of the section depicted in Figure 16 and to the northwest of the one in Figure 17, in the vicinity of the Seagull intrusion (*see* Figures 11 and 18), 2 sills are present in the Rossport Formation (Figure 19). These sills substantially thicken over a short distance under and to the immediate north of the Disraeli intrusion. To the south of Muskrat Lake, they have reached a combined thickness of over 400 m. The intervening sediments are extensively thermally metamorphosed.

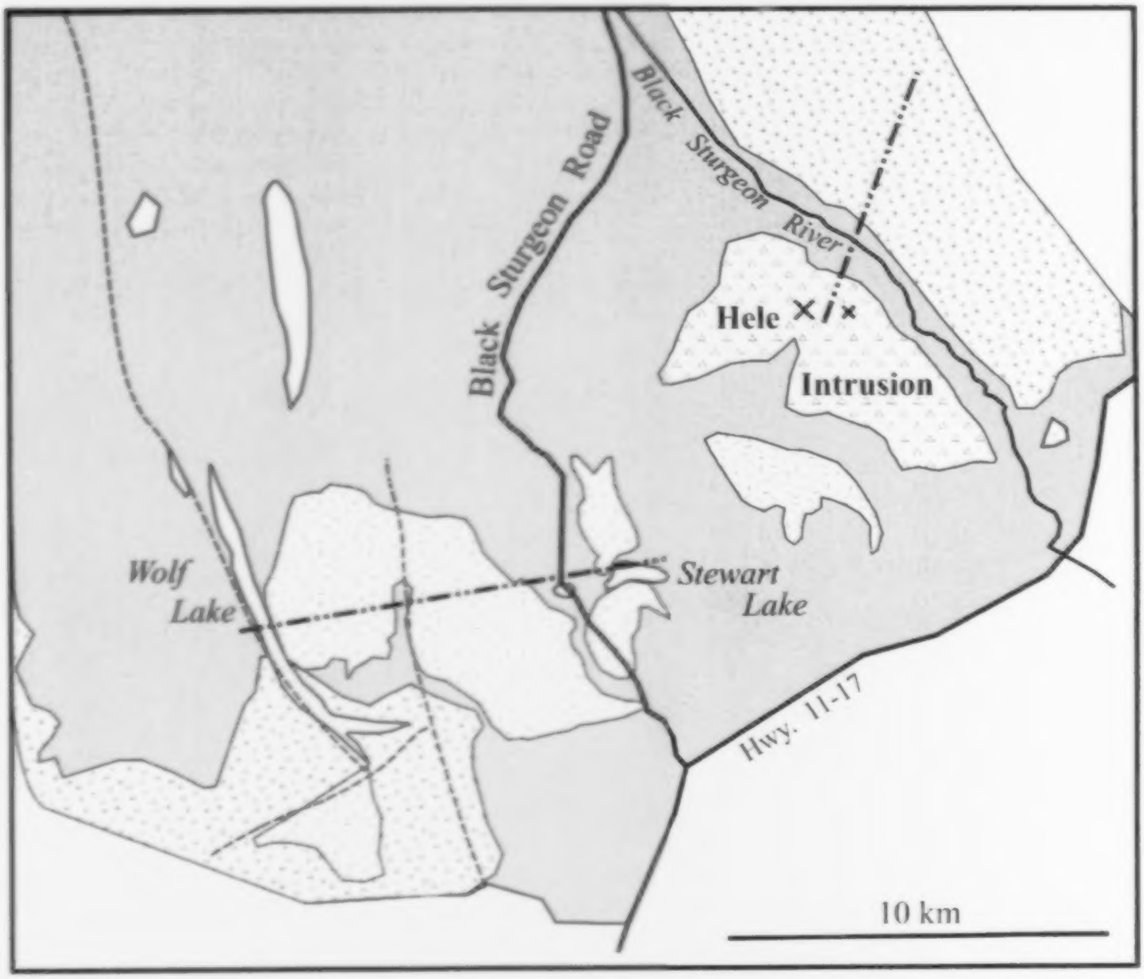

Figure 15. Location of sections in the south-central Sibley Group. The southwest to northeast cross section is shown in Figure 16; the cross section from Wolf Lake to Stewart Lake is shown in Figure 17. Legend: X are drill hole locations; plus symbols (+) are Archean felsic intrusive rocks; dark grey is the Sibley Group; randomly oriented short dashes (- -) are the Nipigon Diabase sills; and open triangles (Δ) are ultramafic intrusive rocks.

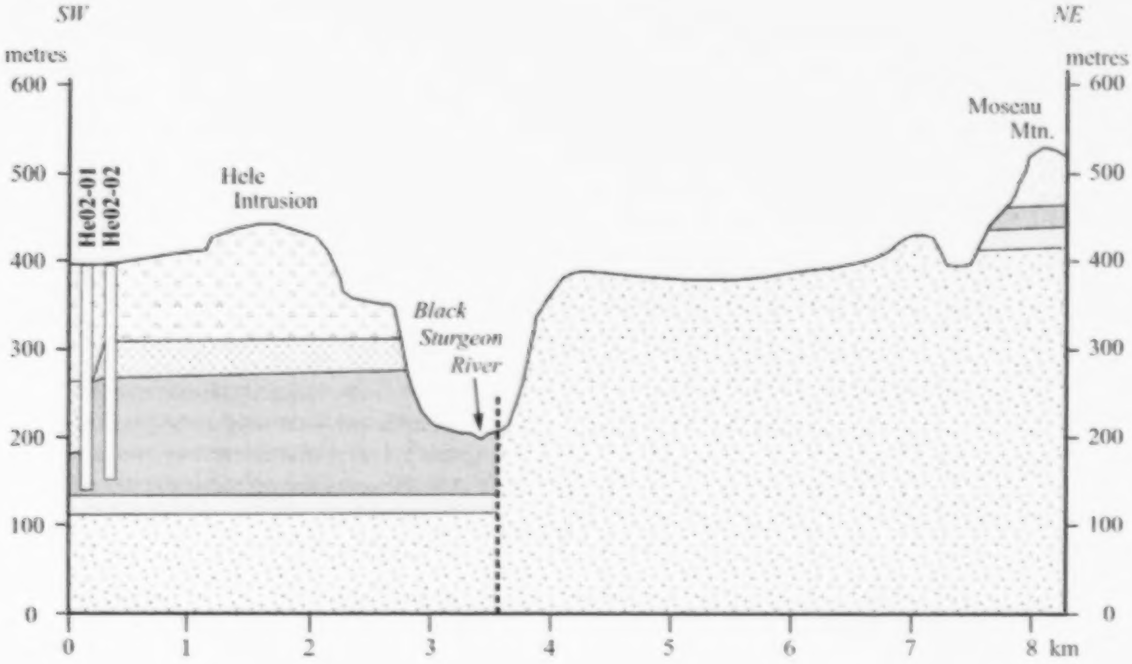
SW
NE
metres
metres
600
500
400
300
200
100
0
He02-01
He02-02
Hele
Intrusion
Black
Sturgeon
River
Moseau
Mtn.
0
1
2
3
4
5
6
7
8 km

Figure 16. Cross section from the Hele Intrusion, in the southwest, to Moseau Mountain, in the northeast; location shown on Figures 11 and 15. Legend: plus symbols (+) are Archean granitic rocks; randomly oriented dashes (- -) are diabase sills; small dots (•) are the Pass Lake Formation; dark grey is the Rossport Formation; cross-hatch pattern is the Kama Hill Formation; and open triangles (Δ) are ultramafic intrusive rocks.

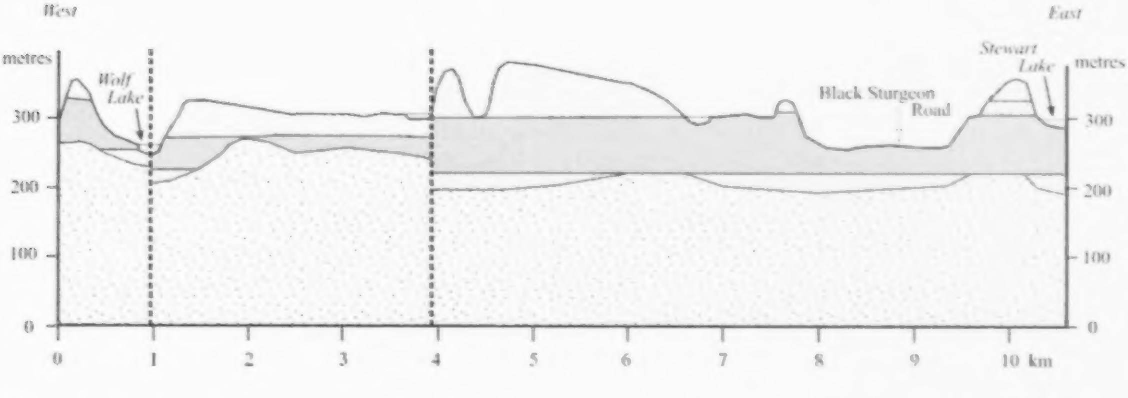
West
East
metres
metres
Wolf
Lake
Stewart
Lake
Black Sturgeon
Road
300
200
100
0
0
1
2
3
4
5
6
7
8
9
10 km

Figure 17. West to east cross section from Wolf Lake to Stewart Lake; location shown on Figures 11 and 15. Symbols as for Figure 16.

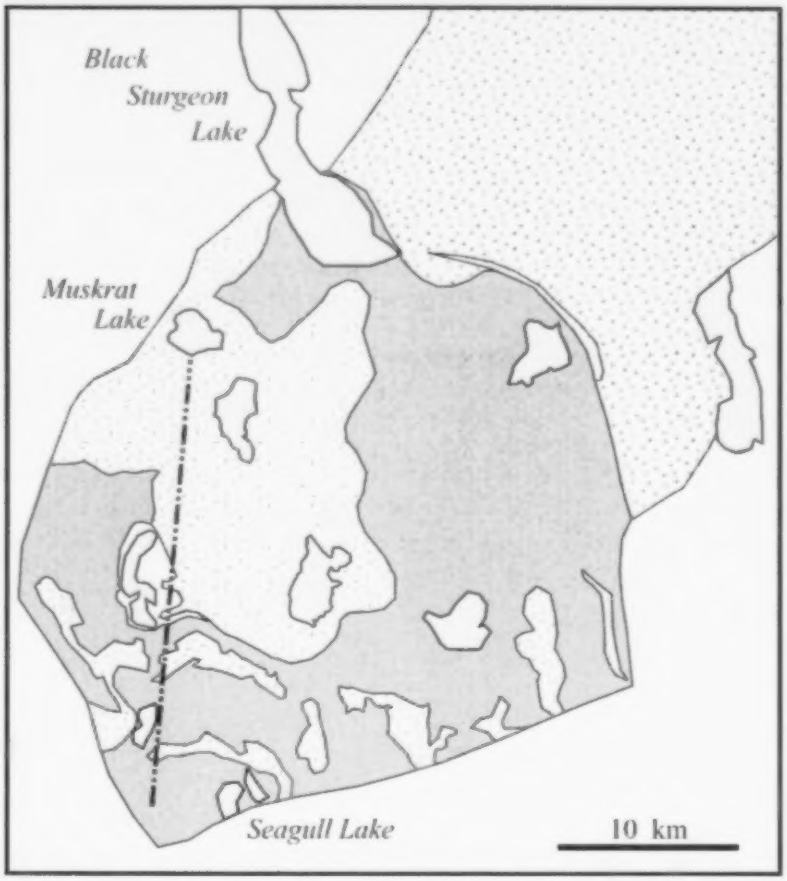
Black Sturgeon Lake
Muskrat Lake
Seagull Lake
10 km

Figure 18. Location of cross section, shown in Figure 19, in the central basin area (*after* Magyarosi et al. 2004). Legend: plus symbols (+) are Archean felsic intrusive rocks; dark grey is the Sibley Group; and randomly oriented short dashes (- -) are the Nipigon Diabase sills.

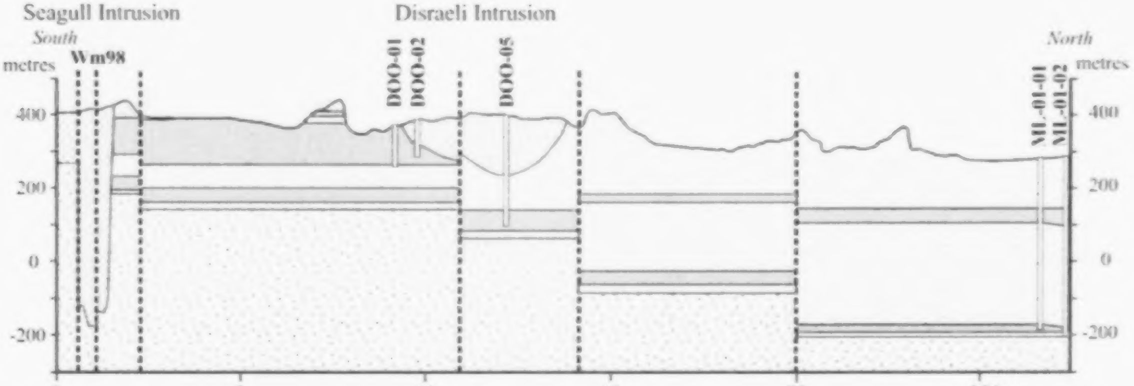
Seagull Intrusion
South
metres
Wm98
Disraeli Intrusion
DOO-01
DOO-02
DOO-05
North
metres
ML-01-01
ML-01-02
400
200
0
-200
0
5
10
15
20
25 km

Figure 19. Cross section from the Seagull intrusion, in the south, to Muskrat Lake, in the north (*from* Magyarosi et al. 2004); location shown on Figures 11 and 18. Legend: plus symbols (+) are Archean granitic rocks; randomly oriented dashes (- -) are diabase sills; small dots (•) are the Pass Lake Formation; dark grey is the Rossport Formation; and cross-hatch pattern are ultramafic intrusive rocks.

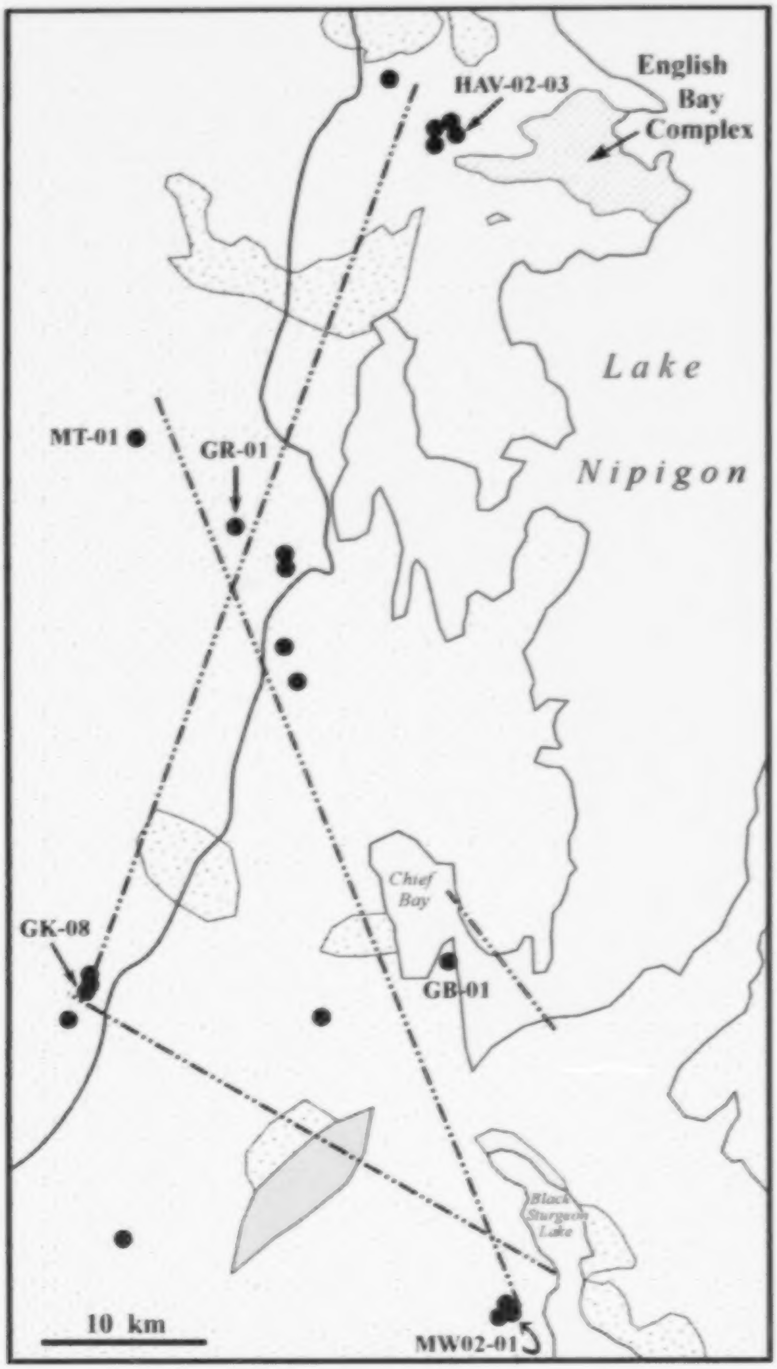
English Bay Complex
HAV-02-03
Lake Nipigon
MT-01
GR-01
Chief Bay
GK-08
GB-01
Black Sturgeon Lake
10 km
MW02-01

Figure 20. Location of cross sections in the northern area. The cross section from Black Sturgeon Lake to drill hole GK-08 is shown in Figure 21; the cross section from drill holes MT-01 to MW02-01 is shown in Figure 22; and the cross section from drill holes HAV-02-03 to GK-08 is shown in Figure 23. The location of the short cross section east of Chief Bay is shown in further detail in Figure 24, with its cross section shown in Figure 25. Legend: large black dots are drill-hole locations; plus symbols (+) are Archean granitic rocks; randomly oriented dashes (- -) are diabase sills; small dots (•) are the Pass Lake Formation; dark grey is the Rossport Formation; and cross-hatch pattern is the English Bay complex.

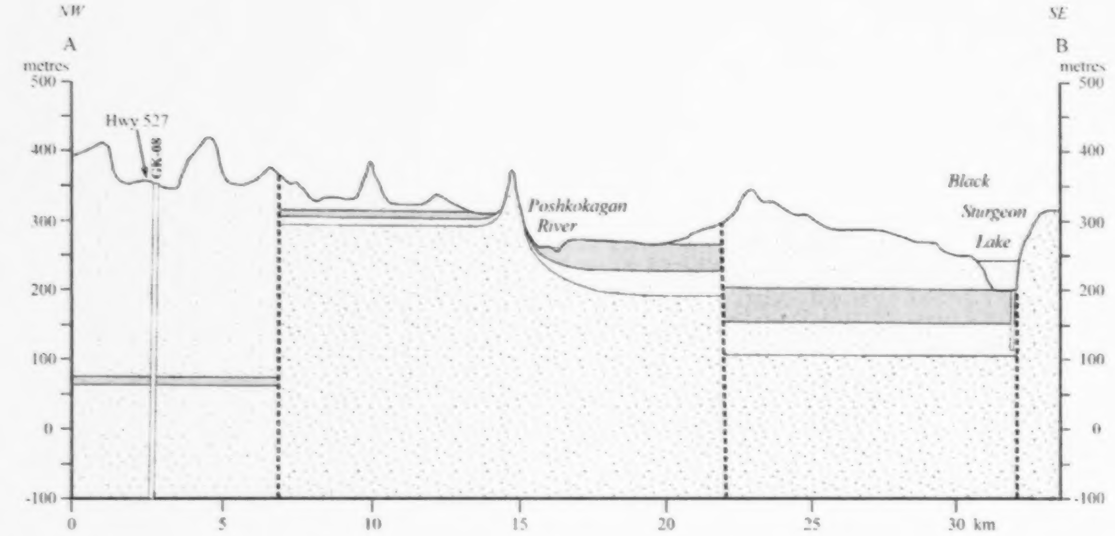
NW
A
metres
500
400
300
200
100
0
-100
Hwy 527
GK-08
Poshkokagan River
Black Sturgeon Lake
SE
B
metres
500
400
300
200
100
0
-100
0
5
10
15
20
25
30 km

Figure 21. Cross section from Highway 527, in the northwest, to Black Sturgeon Lake, in the southeast; location shown in Figures 11 and 20. Symbols are the same as in Figure 13 except the randomly oriented pattern of letter "v" here represent mafic volcanic (?) rocks forming the basement. Legend: plus symbols (+) are Archean granitic rocks; randomly oriented dashes (- -) are diabase sills; small dots (•) are the Pass Lake Formation; dark grey is the Rossport Formation; and randomly oriented pattern of letter "v" are mafic volcanic (?) rocks forming the basement.

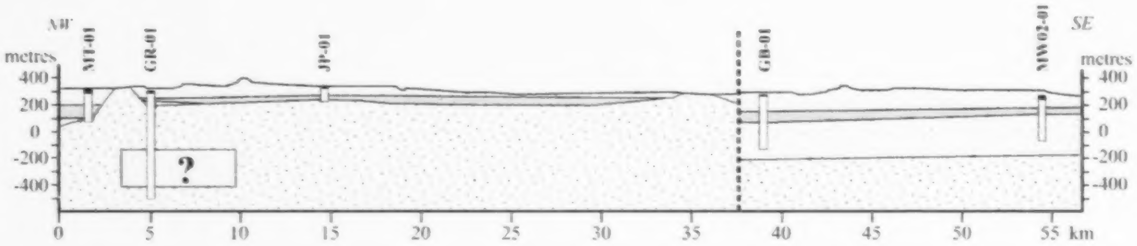
NW
metres
400
200
0
-200
-400
MT-01
GR-01
JP-01
?
GB-01
MW02-01
SE
metres
400
200
0
-200
-400
0
5
10
15
20
25
30
35
40
45
50
55 km

Figure 22. North-northwest to south-southeast cross section parallel to the southwest corner of Lake Nipigon; location shown in Figures 11 and 20. Symbols as for Figure 21.

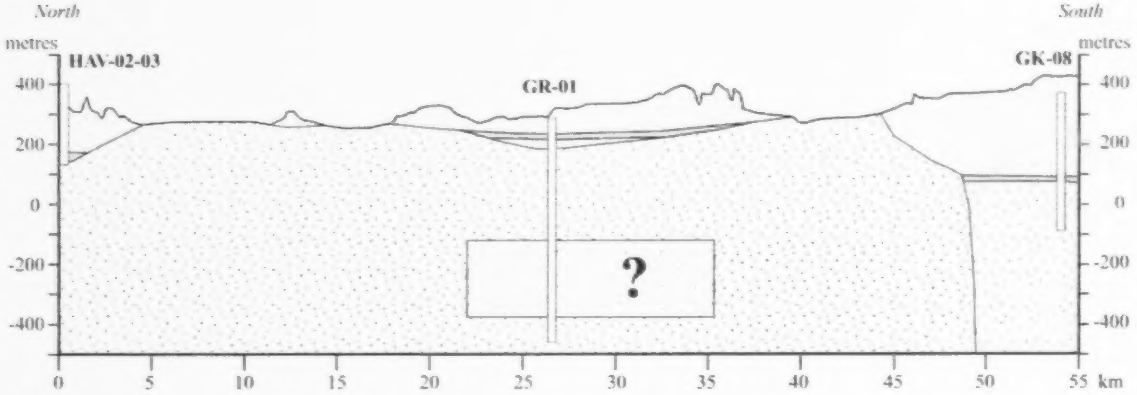
North
metres
400
200
0
-200
-400
HAV-02-03
GR-01
?
GK-08
South
metres
400
200
0
-200
-400
0
5
10
15
20
25
30
35
40
45
50
55 km

Figure 23. Furthest north cross section; location shown in Figures 11 and 20. Symbols as in Figure 21.

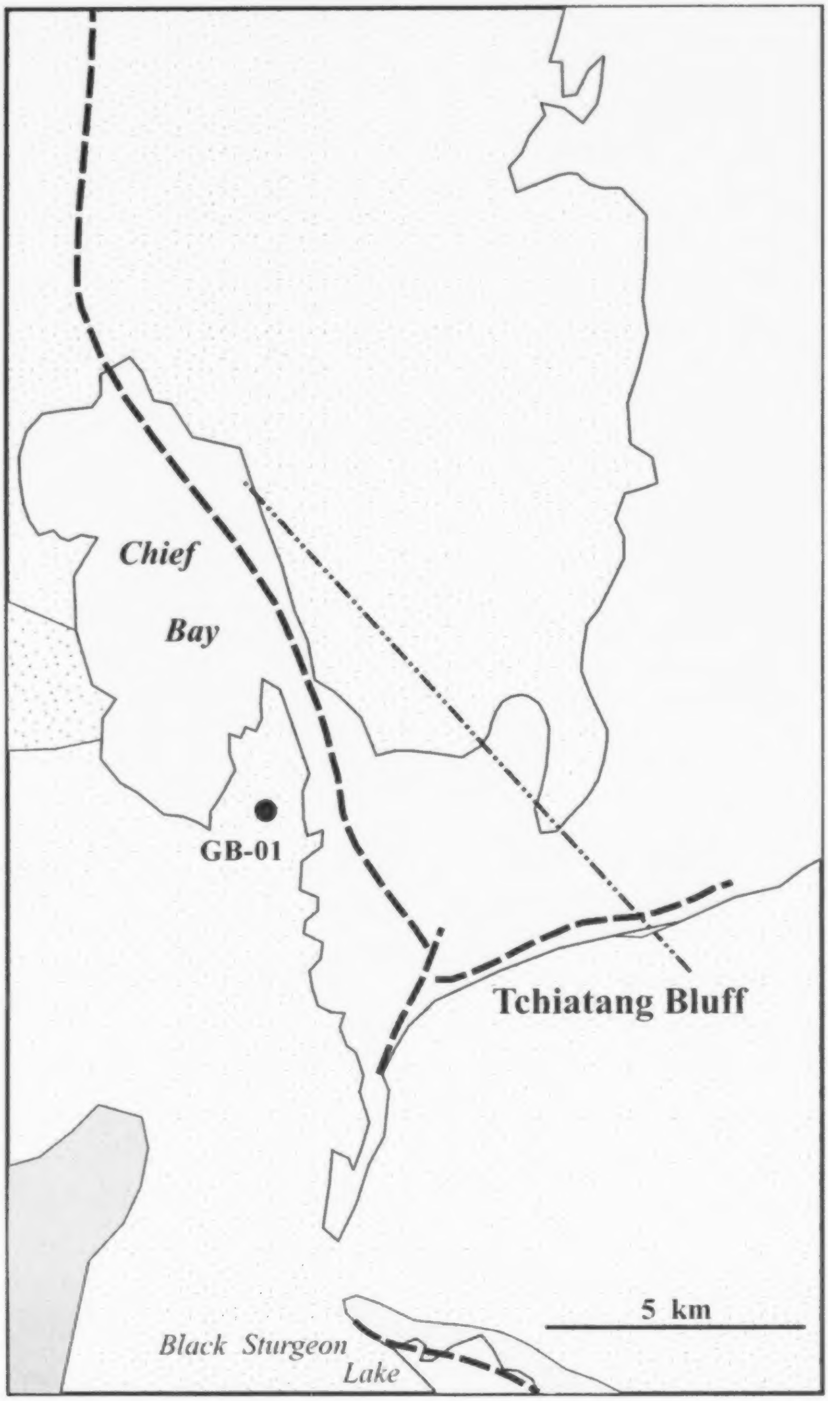
Chief
Bay
GB-01
Tchiatang Bluff
5 km
Black Sturgeon
Lake

Figure 24. Location of the short cross section, shown in Figure 25, east of Chief Bay.

The section lines developed for the northern area are depicted in Figure 20. The section extending from the shores of Black Sturgeon Lake to the northwest (Figure 21) contains the 2 sills in the Rossport Formation at its southeastern end, but the lower sill progressively thins and is interpreted to wedge out to the northwest. This end of the section is anomalous as it has what is probably a mafic volcanic unit as basement and the single sill here is over 450 m thick. Another section line extending north-northwest from near Black Sturgeon Lake exhibits a similar trend with the lower sill terminating to the north-northwest (Figure 22). Erosive removal of the upper portion of the upper sill has resulted in only a thin remnant of it being present in the north. Another diabase body is also present at depth. This was only intersected in one drill hole and, thus, its shape is unknown. The north-northeast to south-southwest section (Figure 23), extending from the area of probable mafic volcanic basement to west of the English Bay Complex (*see* Figure 20), also exhibits a single sill in the Rossport Formation. Erosive outliers of diabase surrounded by felsic intrusive rocks categorize this northern section. An alternative interpretation for this northern region is that the lower sill near Black Sturgeon Lake does not wedge out, but instead correlates with the sill intersected, to the northwest, in Archean basement. Insufficient data exist to select the correct interpretation. A short section to the immediate east of Chief Bay exhibits the displacement on a fault, which probably runs parallel to Tchiatang Bluff (Figures 24 and 25). The last section is on the east side of Lake Nipigon, south of the Kitto intrusion (Figure 26). Here, a thick sill was intruded near the basement–Sibley Group contact (Figure 27).

The regional distribution of sills appears to follow a simple distribution with only a few thin sills present near or at the base of the Sibley Group on the south side of Nipigon Bay. One thick sill is present in the southern portion of the basin. It intrudes the Kama Hill Formation in the east and moves down to the Rossport Formation in the west. Progressing north to the central basin area near Muskrat Lake, 2 sills appear and their thickness greatly increases. This is an area of intense thermal metamorphism of the Sibley Group sedimentary rocks. The 2 sills appear to continue north of Muskrat Lake for approximately 15 km where the lower sill either wedges out or cuts down into the Archean basement. Between here and the English Bay area, one sill exists intruding the Rossport Formation. Interpretations of the sill stratigraphy in the northern area are complicated by the erosive removal of the entire diabase sheet in many places.

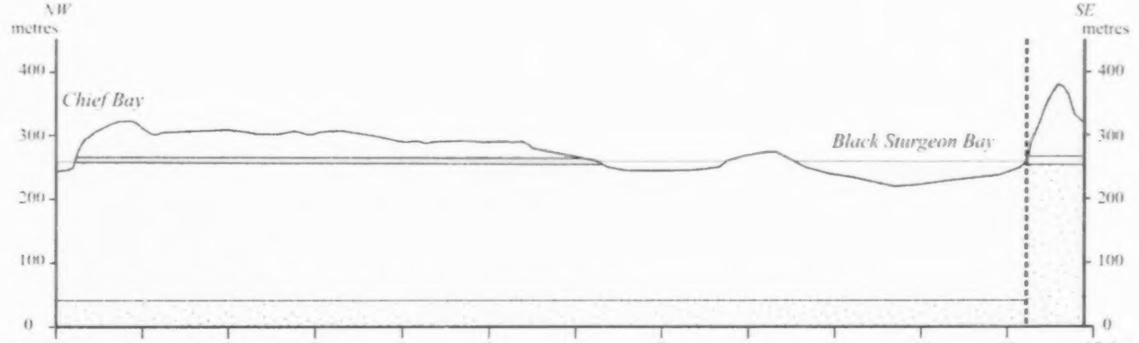

Figure 25. Cross section from the shore of Chief Bay, in the northwest, to the south shore of Black Sturgeon Bay; location shown in Figures 11, 20 and 24. Legend: plus symbols (+) are Archean granitic rocks; randomly oriented dashes (- -) are diabase sills; small dots (•) are the Pass Lake Formation; and dark grey is the Rossport Formation.

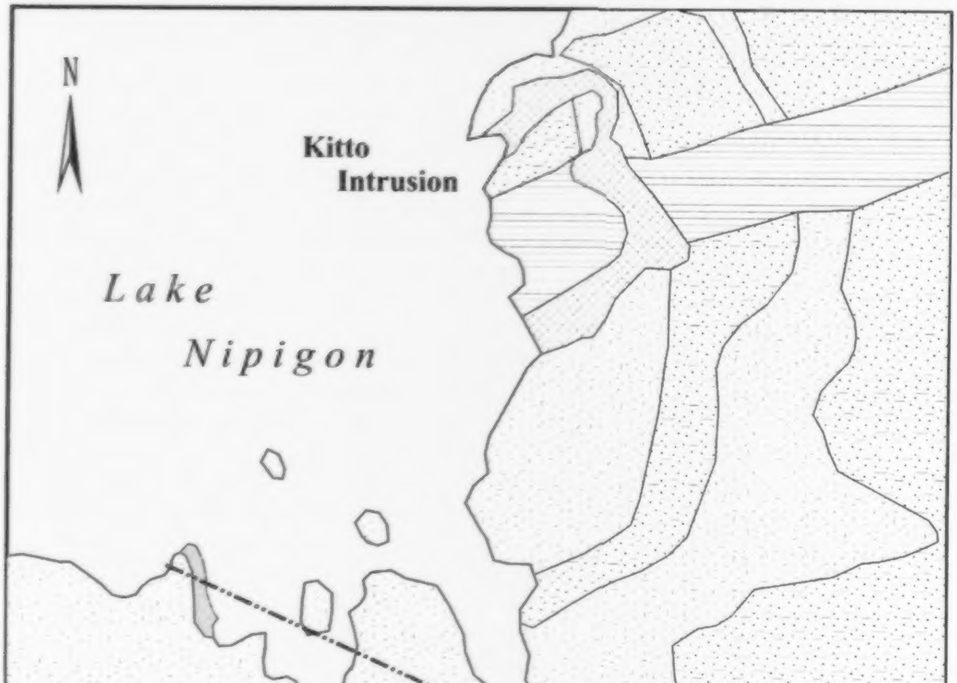
N
Kitto
Intrusion
Lake
Nipigon
5 km

Figure 26. The location of a short section, shown in Figure 27, on the southeast side of Lake Nipigon. Heavy black dashed line is a fault. Legend: randomly oriented dashes (- -) are diabase sills; dark grey is the Rossport Formation; cross-hatch pattern is an ultramafic intrusion; horizontal lines are a discordant unit of diabase; and mixed pattern of dots and horizontal dashes are Archean supracrustal units.

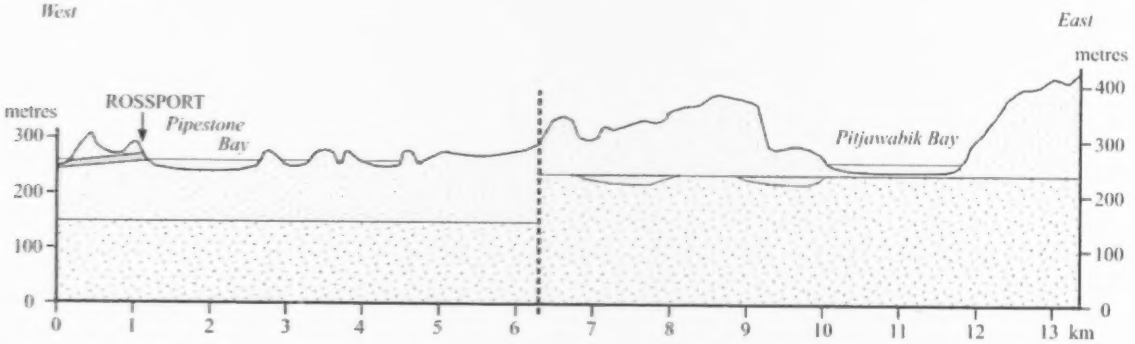
West
East
metres
metres
ROSSPORT
Pipestone
Bay
Pitjawabik Bay
300
200
100
0
400
300
200
100
0
0
1
2
3
4
5
6
7
8
9
10
11
12
13 km

Figure 27. Cross section across Pipestone Bay, on the southeastern coast of Lake Nipigon, slightly southeast to Pitjawabik Bay; location shown in Figures 11 and 26. A thin layer of Rossport Formation splits the sill on the west side of Pipestone Bay and is probably the reason for the name of the bay. Legend: plus symbols (+) are Archean granitic rocks; randomly oriented dashes (- -) are diabase sills; small dots (•) are the Pass Lake Formation; and dark grey is the Rossport Formation.

Contact Metamorphic Effects

Rogala (2000) investigated the effects contact metamorphism, which was induced by the intrusion of thick Nipigon Diabase sills, had on the sediments of the lower Sibley Group. An 80 m thick succession of strata extending away from a thick diabase sill was examined in detail and sampled for geochemical and petrologic analyses by X-ray fluorescence (XRF), X-ray diffraction (XRD), inductively coupled plasma atomic emission spectroscopy (ICP–AES), scanning electron microscope electron dispersive spectrometry (SEM–EDS) and for C–H–N analysis. The strata in question are in diamond-drill core NI-92-5, which was drilled in the central basin area approximately 15 km south of the southwest corner of Lake Nipigon. Twenty-one samples were collected from NI-92-5. At most sample sites, both light (evaporate-rich) and dark (siliciclastic-rich) layers were sampled and the results averaged. This resulted in 11 points that could be plotted on the vertical section. Six samples were also taken from the same stratigraphic interval in diamond-drill hole NI-92-7, located approximately 5 km south of NI-92-5, in which the samples had not been metamorphosed.

The strata sampled belong to the cyclic facies of the Channel Island Member of the Rossport Formation. The amount of interbedded clastic material increases up section. Sporadic sandstone layers occur in the central portion of the section and increase in number and thickness upward. The 20 m of sedimentary rock immediately above the diabase sill is composed of light greenish and cream coloured layers that are millimetres to centimetres thick. Red, hematite-rich clastic layers appear near the top of this succession. The next 30 m of core is not well preserved due to the combination of the original presence of larger amounts of soluble mineral phases and the core being stored outside. Colour variations can occur in sections up to 2 m in length, commonly grading from purple or peach to pink. In these sections, the deterioration of the core increases upward, suggesting increasing carbonate content. Sandstone units, up to a metre thick, are interbedded with siltstone and carbonate layers throughout the upper 30 m of core. In general, the amount of carbonate-rich layers increases upward for approximately two-thirds of the total succession, then decreases in the upper portion as siliciclastic components become more important.

The mineralogy was investigated using X-ray diffraction (XRD) and scanning electron microscopy coupled with energy dispersive spectrometry (SEM–EDS). Examination of peaks for x-ray diffraction uncovered the presence of sodium and potassium varieties of pargasite in addition to tremolite, talc, clinochlore and calcite. Scanning electron microscopy revealed relatively large amounts of barite with varying amounts of hematite and minor amounts of apatite, halite, sylvite, gypsum, and dolomite.

The intrusive contact zone contains a thin layer of predominantly pyrite, with chalcopyrite, magnetite, ilmenite and galena. Above this contact, stratigraphic intervals dominated by pargasite, tremolite, or talc, occur in order (upward): pargasite, tremolite, pargasite, tremolite, talc, tremolite, talc. All of the phases are intimately associated with clinochlore and calcite. At a smaller scale, alternation occurs between pargasite + tremolite + talc + clinochlore and relatively pure calcite layers. Toward the top of the sequence, feldspar, usually in the form of microcline, and some plagioclase may dominate some layers.

The pargasite is euhedral, with a very similar crystal shape to that of a dolomite rhomb, although no dolomite cores were found in it. Dolomite-cored calcite is rarely associated with it. Pargasite may have growth rings and be rimmed by sylvite with some halite association, particularly near the intrusion at the base of the drill core. Pargasite only occurs in the bottom third of the sequence. Of the major mineral phases, tremolite is the most common. It takes the form of thin, fibrous grains, with no apparent internal zoning. Some areas of iron-rich tremolite or actinolite do occur. Tremolite can be found within the top two-thirds of the drill core. Talc occurs within the top third of the core and is subhedral to euhedral. It often forms between calcite grains. Clinochlore is platy and usually euhedral. It may contain some iron, but is magnesium dominated.

Calcite is the main carbonate phase, occurring through the entire succession. There is evidence for calcite recrystallization. Some magnesite may be found associated with dolomite- and halite-rich areas. Calcite is generally magnesium deficient, but can contain magnesium-rich calcite or dolomite cores. The amount of dolomite increases upward. Calcite layers seem to be the primary hosts for salts and barite.

Barite content is highly varied throughout the core. Grain size also fluctuates irregularly from micrometre to millimetre scale. It is commonly associated with calcite-rich areas and less frequently with pargasite, tremolite, talc, and clinochlore grains. The barite is usually situated along grain boundaries or within open-spaces.

Several evaporate minerals are present, such as halite, sylvite and gypsum. These minerals may occur as discrete euhedral crystals up to 15 µm, but primarily occur as inclusions. The inclusions are associated with calcite and apatite, although apatite is more frequently free of inclusions. They can be found sporadically throughout the core, but are concentrated approximately 40 to 60 m above the intrusion.

Hematite content is extremely varied between individual layers, but noticeably increases up section. When the core is well preserved, hematite tends to concentrate in distinct, clastic-dominated layers. Apatite is consistently present, but is chlorine enriched in the bottom half of NI-92-5, and decreases in chlorine upward. Within the top 15 m of core, monazite is the dominant phosphate mineral. The monazite occurs in veinlets or clusters.

For contrast, stratigraphically comparable sections of Noranda's NI-92-7 core were also examined. The mineralogy was quite different. The sections were predominantly dolomite with clastic layers of plagioclase, alkali feldspars, and clay minerals. Talc, gypsum, and barite were present. Barite was relatively rare compared to the sections from NI-92-5.

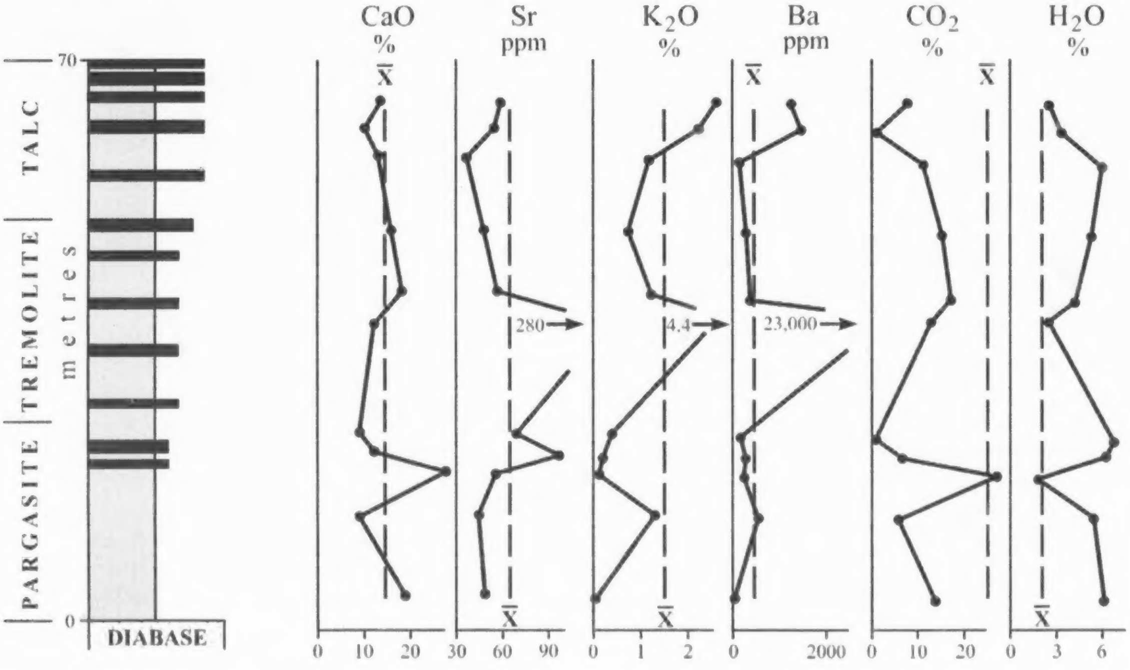

Figure 28. Distribution of selected elements away from the heat source in a contact aureole. The $\overline{X}$ dashed lines represent the average content of the element in non-metamorphosed Sibley Group cyclic facies.

The geochemistry of the sedimentary rocks was analyzed using ICP–AES (TiO_2, Al_2O_3, Fe_2O_3, MnO, MgO, CaO, Na_2O, K_2O, P_2O_5, Ba, Sr, Y, Zr, Nb, Zn, V and Co), XRF (SiO_2) and C–H–N (CO_2 and H_2O). The results for the metamorphosed succession in drill hole NI-92-5 core were compared to the average values of the samples analyzed from the unmetamorphosed cyclic facies in NI-92-7. This provides an indication of mass loss or gain of each element due to metamorphism. The average content of most elements (SiO_2, TiO_2, Al_2O_3, Fe_2O_3, MnO, MgO, CaO, Na_2O, P_2O_5, Y, Zr, Nb, Zn, V and Co) is similar in the unmetamorphosed and metamorphosed sections (i.e., CaO in Figure 28). Strontium and barium show erratic large enrichments on a background of possible slight depletion in the metamorphosed rock. Potassium values in the metamorphosed section are generally low with maximum depletion near the sill (*see* Figure 28). The most interesting effect is observed in the data for the volatiles. Carbon dioxide shows considerable depletion even 70 m away from the sill and H_2O has the opposite trend being enriched even far from the sill (*see* Figure 28).

DISCUSSION

The cyclic facies of the Rossport Formation contains clastic layers interbedded with dolomite and gypsum (Cheadle 1986a). The cyclic facies in NI-92-5 differs from this because of metamorphic reactions induced by the intrusion of a diabase sill.

The mineral assemblage of NI-92-5 differs from the typical assemblage present in metamorphosed carbonate rocks (Winkler 1974; Tracy and Frost 1991; Letargo, Lamb and Park 1995) in that it contains pargasite rather than diopside. The metamorphic grade, from highest to lowest, is represented by pargasite, tremolite, and talc. This is a fairly atypical assemblage, with relatively few documented cases. One such case occurs as an aureole around the Boulder batholith in Montana, which is generally potassium rich (Rice 1977). Skippen and Trommsdorff (1986) conducted experiments on the influence of halite and sylvite in carbonate metamorphism. They conclude that variations in salinity can lead to isograd fluctuations. This could be an explanation for large-scale mineral variations, such as seen by the pargasite–tremolite–pargasite trend in the lower section of NI-92-5. Therefore, evaporate minerals, such as sylvite and halite, probably influenced the presence of pargasite. It should be noted that the pargasites in the samples are either potassic or sodic varieties. Evaporite minerals are a likely source for the potassium and sodium because halide minerals are highly soluble. A complimentary trend of chlorine in apatite is developed as well. Apatite minerals are chlorine rich near the base of the sequence, but decrease significantly with decreasing metamorphic grade up section.

The small-scale layering, such as calcite–tremolite couplets, has a rhythmic nature. Aleksandrov (1996) attempts to provide an explanation for this phenomenon in a variety of aureoles in calcitic and dolomitic skarn deposits. One of Aleksandrov's (1996) suggestions is that the rhythms form by metasomatic zoning based on magnesium levels of the carbonates, and that the calcium and magnesium in each layer is preserved. He proposes that, at least in some situations, a carbonate layer would only form after a layer of magnesium silicate. Aleksandrov (1996) believes that the banding reflects rhythmic influxes of metasomatic fluids. Aleksandrov (1996) may be correct about the retention of calcium and magnesium, but the rhythmic layering in NI-92-5 is probably a result of the original cyclicity of the Channel Island Member sediments rather than pulses from the sill.

Several reactions have been proposed to explain the metamorphism of dolomite to talc and tremolite. Pargasite reactions can be inferred by the addition of halite. These reactions are listed below, in order of increasing metamorphic grade. The reactions require the presence of H_2O in the fluid phase, as well as SiO_2 and Al_2O_3 in the host sedimentary rocks (Tracy and Frost 1991). This is potentially provided by quartz and clay. Fluid temperatures for these reactions seem to be between 400 and 600°C (Skippen and Trommsdorff 1986; Rice 1977; Letargo, Lamb and Park 1995). These temperatures are based on experiments and fluid inclusion studies in metamorphosed carbonate sequences with similar metamorphic mineral assemblages.

$$3\ \text{Dolomite} + 4\ \text{Quartz} + H_2O = \text{Talc} + 3\ \text{Calcite} + 3\ CO_2 \quad (1)$$

$$5\ \text{Dolomite} + 8\ \text{Quartz} + H_2O = \text{Tremolite} + 3\ \text{Calcite} + 7\ CO_2 \quad (2)$$

$$3\ \text{Dolomite} + 2\ Al_2O_3 + \text{Halite} + 6\ SiO_2 + H_2O = \text{Pargasite} + 2\ \text{Calcite} + 3\ CO_2 \quad (3)$$

Equations 1-3. Equations (1) and (2) from Bucher and Frey (2002, p.199); and Equation 3 is a hypothetical explanation for the production of pargasite. In reality, it is probably much more complex.

The change in volatile content of the metamorphosed succession is directly related to the mineralogic changes. As dolomite is destroyed, CO_2 is released (see general equations). This produces CO_2-charged fluid which will migrate away from the heat source. The general equations also predict that H_2O will be taken up in the amphiboles. Commonly, metamorphism leads to devolatilization of H_2O; however, in these rocks, because the primary evaporate minerals in this system are not hydrous and the metamorphic amphiboles are, the H_2O content of the rock increases due to metamorphism.

Geochemistry

The major, minor and trace element composition of the Sibley Group sediments, plus the isotope ratios of C, O, S and Sr, were investigated to acquire information on the source of the sediments, the geochemical changes due to weathering that occurred in the sediments and the composition of the surface and groundwater during deposition of the unit. The isotopic data are also valuable in deciphering the detailed stratigraphy. Uranium–lead geochronology was also conducted on detrital zircons in 5 samples of sandstone to assist in constraining the age of the Sibley Group and provide further evidence on the provenance of the sediments.

Geochemical trends vertically through the stratigraphy were assessed by collecting samples of medium-grained sandstone at approximately 20 m intervals spanning the entire Sibley Group. These samples were analyzed using ICP–AES following dissolution of powder with nitric and hydrofluoric acids. Samples of dolomite were collected from the cyclic facies, stromatolites, soil carbonate horizons and carbonate nodules in the sabkha mud flats. Isotopic ratios of carbon and sulphur were measured in these samples at the facilities of Dr. T.K. Kyser, Department of Geology, Queen's University in Kingston, Ontario. The same samples were also leached with acid and analyzed for major and trace elements using the ICP–AES at Lakehead University. Gypsum from the cyclic facies and the sabkha mud flats of the Rossport Formation were sampled for sulphur isotopic analyses. These were also conducted at the laboratory of Dr. Kyser. The same gypsum samples were leached with distilled water and their major and trace element contents were analyzed by ICP–AES. Selected gypsum and carbonate samples were also analyzed for the isotopes of strontium at the laboratory of Dr. B.L. Cousens, Department of Earth Sciences, Carleton University in Ottawa. Samples were collected through weathering profiles in basement rocks directly underlying the Sibley Group. The basement lithologies sampled include Archean granite and metasandstone, plus Paleoproterozoic black shale. These samples were analyzed by ICP–MS at the Ontario Geological Survey Geoscience Laboratories (Geo Labs) in Sudbury. Additional samples of red mudstone from the cyclic facies of the Rossport Formation and acetic acid leached dolomites were also analyzed at this laboratory. The results of all these analyses are presented in Appendixes 1 to 12.

Samples of medium-grained sandstone were collected from the Pass Lake Formation at Pass Lake and the Outan Island Formation and Nipigon Bay Formation in drill core from a hole drilled in Nipigon

Bay. In addition, Dr. R.M. Easton collected a sandstone sample from a thin unit interlayered between volcanic flows south of Armstrong, and a sample of the Rove Formation from southwest of Thunder Bay. Uranium–lead (detrital zircon) geochronology was conducted on these samples by Dr. L.M. Heaman using a laser ablation mass spectrometer at the University of Alberta (*see* "Geochronology").

Geochemical trends up section, through the Sibley Group, are quite pronounced (Figure 29A). The SiO_2 content increases upward from the Pass Lake Formation to the Outan Island Formation indicating an increase in sediment maturity over this interval. The SiO_2 content continues this trend by jumping to higher levels across the unconformity between the Outan Island Formation and the Nipigon Bay Formation. This indicates that the Nipigon Bay Formation is dominated by a very mature sandstone with the maturity remaining relatively constant up through this interval.

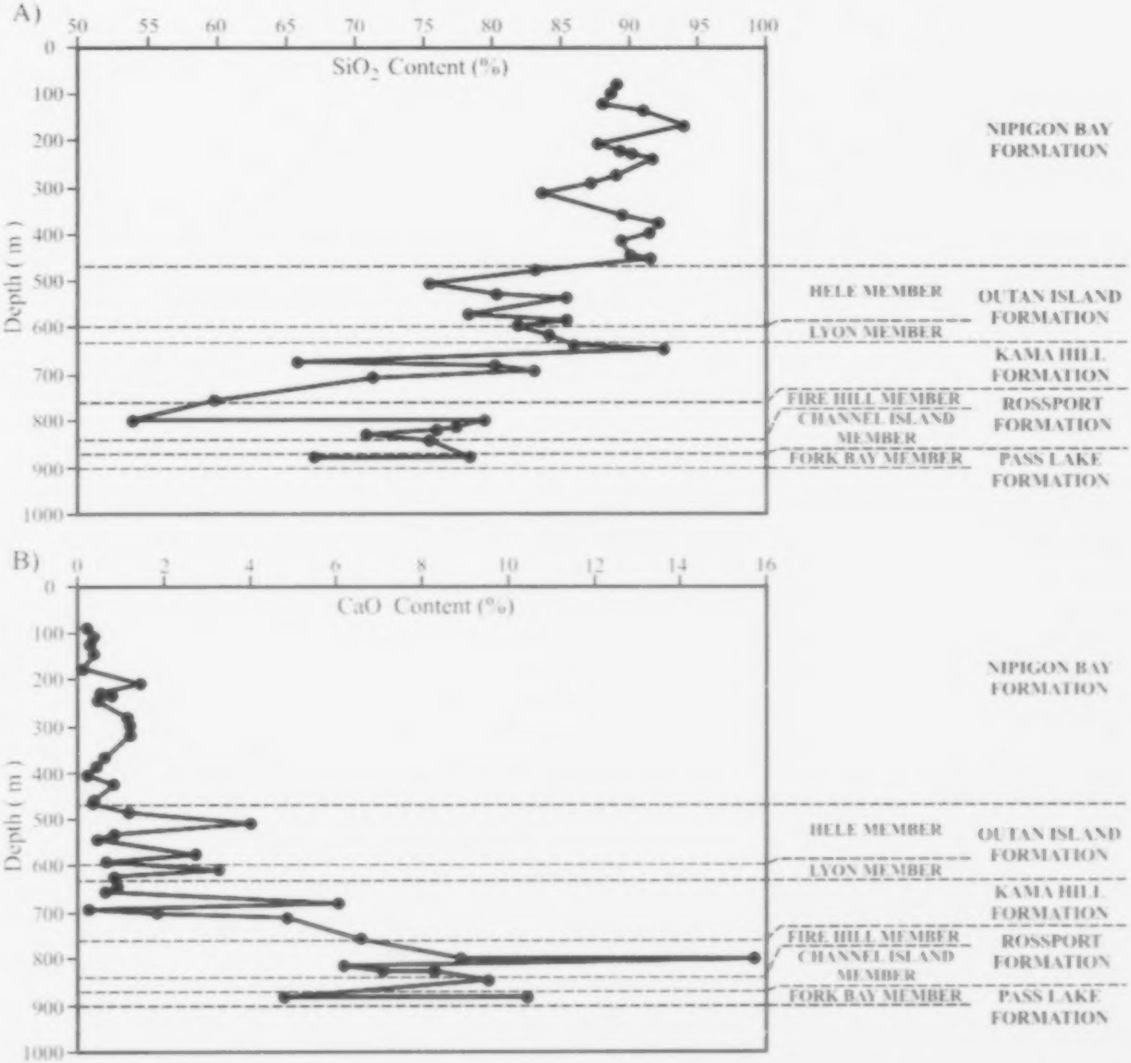

Figure 29. A) SiO_2 abundance in medium-grained sandstones from the Sibley Group. The SiO_2 content exhibits a general increase from the Pass Lake to Outan Island Formations and is higher and less variable in the overlying Nipigon Bay Formation. B) CaO content in the same sandstone samples as (A). The CaO abundance reflects the presence of carbonate cements and is a proxy for the chemistry of the pore waters.

The Ca and CO_2 contents primarily depend on the amount of carbonate in the sandstones. A plot of the CaO content (*see* Figure 29B) shows how the calcium concentration is high in the Pass Lake Formation and Channel Island Member of the Rossport Formation. These 2 units in the core represent the open-water playa lake conditions. The Fire Hill Member also has high CaO values. As it was deposited in a sabkha setting with a high groundwater table precipitating evaporite minerals, dolomitic cements in sandstones of this unit are to be expected. The CaO content decreases substantially through the Kama Hill Formation

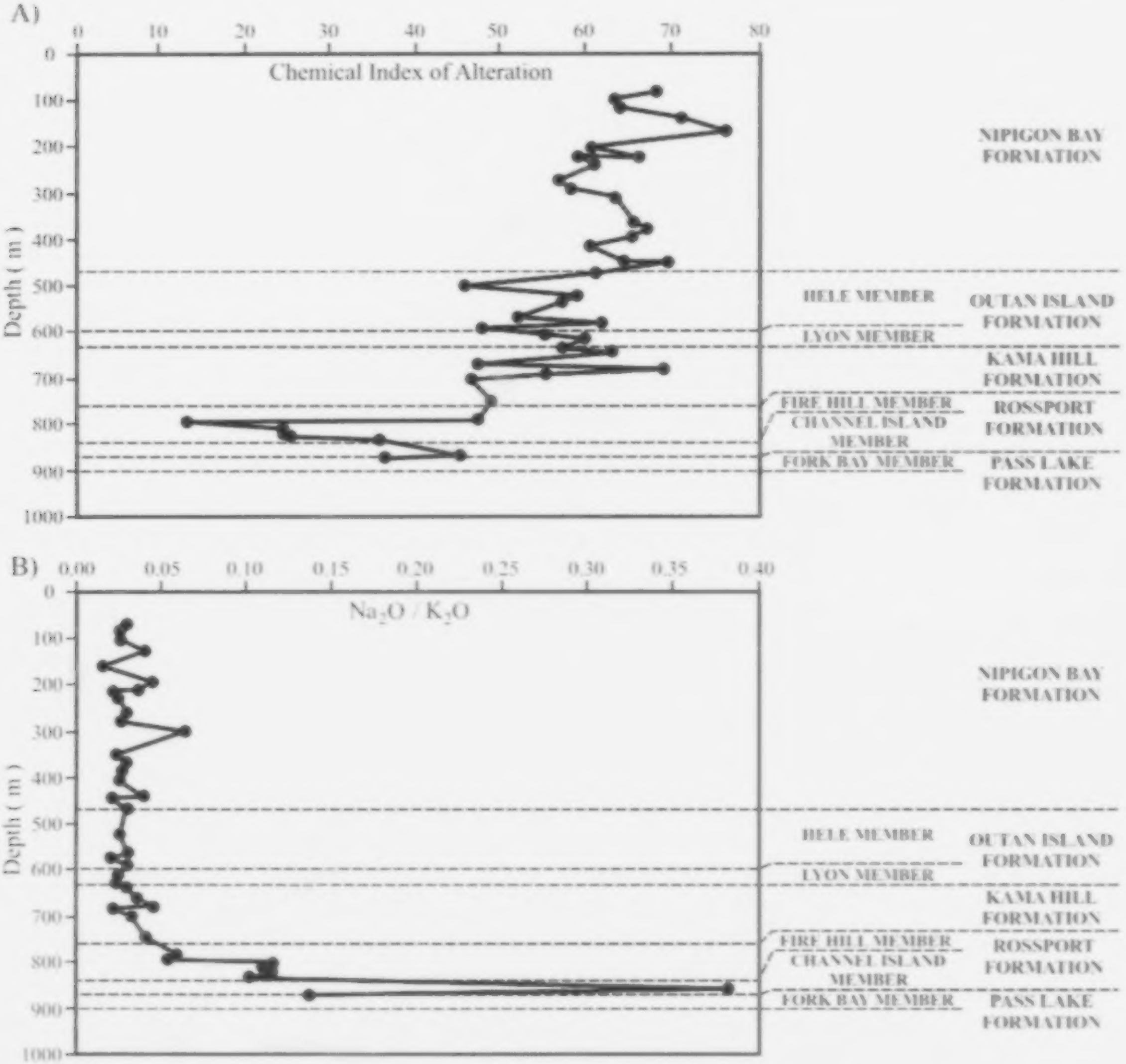

Figure 30. A) The chemical index of alteration— $Al_2O_3/(Na_2O + K_2O + CaO + Al_2O_3) \times 100$ —is a common indicator of the degree of weathering in shales. It is applied to medium-grained sandstones here and shows the relative amount of chemical weathering of their constituents. Fresh igneous rock will have an index of 40 to 50, whereas extremely weathered clay will be near 100. The very low values are the result of the presence of carbonate cements, which has not been corrected for. A strong trend toward increased weathering up section in the Sibley Group is indicated. B) the Na_2O/K_2O ratio is also a proxy for degree of weathering as Na will commonly be depleted more effectively than K in the early and mid-stages of chemical weathering. The trend present indicates that Na depletion was greater than K depletion in the lowest 3 formations. Sodium and K depletion rates reach the same magnitude in the upper Kama Hill Formation and are consistent upward from there. This implies increasing weathering with an increasing amount of K depletion relative to Na through the lower half of the section.

indicating a decrease in the salinity of the pore waters. The Outan Island Formation has generally low values with only 2 slightly elevated. This is in accord with its open-water, storm-modified, deltaic to fluvial setting. The Nipigon Bay Formation has very low CaO abundances. Obviously, the arid setting of this unit suppressed formation of early cements, which in other units contain calcium. The decreasing Ca content exhibits an inverse relationship to SiO_2 indicating that the up-section increase in SiO_2 may be driven by a change from calcium-bearing cements to siliceous ones. However, after accounting for the influence a decreasing Ca up-section content will have on SiO_2, there is still a remnant SiO_2 increase up section.

The degree to which the sediments have undergone chemical weathering can be judged by calculating the chemical index of alteration (CIA). This is Al_2O_3 content of a shale sample divided by its $((NaO+K_2O+CaO+Al_2O_3) \times 100)$ content (Nesbitt and Young 1982). The samples utilized here are

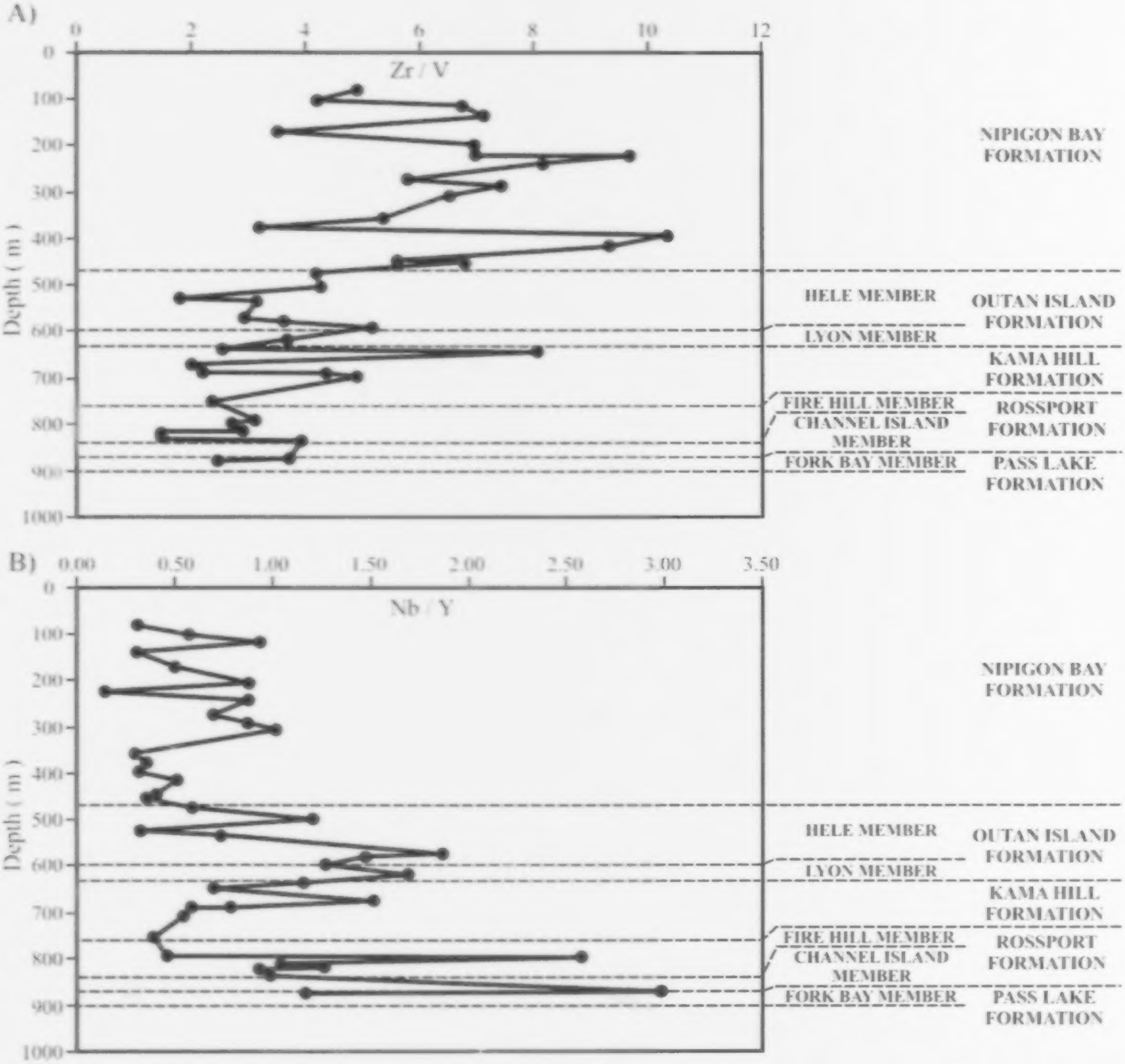

Figure 31. A) The Zr/V ratio indicates the felsic–mafic ratio of material in the medium-grained sandstones. The Sibley Group may slightly increase in felsic content upward from the Pass Lake Formation to the Outan Island Formation. The Nipigon Bay Formation is composed of more felsic-derived detritus. B) The Nb/Y ratio denotes degree of alkalinity of the detritus with higher values reflecting more alkaline sediment. There appears to be an overall decrease in alkalinity upward.

medium-grained sandstones rather than shales and this will result in the CIA values being lower than they would be if shales were sampled. However, the values of the individual samples can still be compared to ascertain trends. It is clear from Figure 30A that there is a trend toward more intense weathering up section from the Pass Lake Formation to the Outan Island Formation. The CIA moves to even higher values in the overlying Nipigon Bay Formation. The Na_2O/K_2O ratio (*see* Figure 30B) will also give an indication of the degree of chemical weathering. Sodium is commonly depleted by chemical weathering more efficiently than potassium. Thus, the early stages of chemical weathering will be characterized by a drop in the abundance of sodium and, in later stages, potassium depletion will begin to catch up with sodium loss. Figure 30 exhibits a trend of increasing sodium depletion up section through the Pass Lake, Rossport and Kama Hill formations. Above this, the rate of potassium depletion balances sodium depletion. This, again, graphically illustrates the increase in chemical weathering up through this portion of the section.

Changes in the provenance of the sediment can also be investigated using geochemistry. The ratio Zr/V is controlled by the amount of felsic (high in Zr) versus mafic (high in V) material in the sandstone. A plot of this ratio (Figure 31A) up through the stratigraphic section establishes a trend from less felsic detritus near the base of the succession to more felsic in the upper portion. In actuality, the succession may be divisible into 2 parts. The Pass Lake through Outan Island formations represent the lower portion, which may have a slightly more felsic debris upward trend. The overlying Nipigon Bay formation is more felsic than the underlying strata, but does not have an internal trend.

The Nb/Y ratio is an indication of the amount of debris from alkaline rocks that is in the sandstones. Higher Nb values reflect higher alkalinity (Winchester and Floyd 1977). Though there is a large amount of variability in the Nb/Y values of the samples, a trend toward decreasing alkalinity with stratigraphic height can be ascertained (Figure 31B).

GEOCHRONOLOGY

Detrital zircon geochronology can also provide insight into the provenance of sedimentary units. As part of the Lake Nipigon Region Geoscience Initiative, 5 sedimentary units were studied by L.M. Heaman of the Department of Earth and Atmospheric Sciences at the University of Alberta. Preliminary results of these studies have been provided in abstract form in Heaman and Easton (2005) and Heaman et al. (2005), and are summarized in this section. Final results will be presented in a peer-reviewed journal. This section is summarized from these publications as well as internal Lake Nipigon Region Geoscience Initiative reports.

All selected samples were pulverized using a jaw crusher and Bico disk mill. Heavy minerals, such as zircon and baddeleyite, were isolated using a series of mineral separation steps including a Wilfley table, Frantz™ isodynamic separator and heavy liquids. For detrital zircon studies, the samples are not processed through the final magnetic separation stages so that there is no sample bias introduced by the sample preparation procedure. Stringent cleaning procedures were employed at all stages to reduce as much as possible the chance for laboratory contamination. The analyzed zircon and baddeleyite crystals were individually selected using a binocular microscope and only the best quality grains were chosen (i.e., generally only those grains that are devoid of fractures, inclusions and turbidity).

All detrital zircon fractions were analyzed using multi-collector NuPlasma™ inductively coupled plasma mass spectrometry (MC-ICP–MS). For these analyses, approximately 100 grains were selected, mounted in epoxy pucks, and polished with 5 µm aluminum oxide powder. The laser ablation was conducted using a 213 nm Nd:YAG Mercantek laser. The diameter of each laser analysis spot was 40 µm and the accuracy of isotopic ratios was controlled by analyzing an in-house Precambrian zircon standard

(LH94-15) after every 12 unknowns. Lead isotopic fractionation was normalized by simultaneously analyzing a thallium solution. The ^{238}U and ^{235}U decay constants used are 1.55125×10^{-10} yr $^{-1}$ and 9.8485×10^{-10} yr $^{-1}$, respectively. The uncertainty associated with age determinations presented in this report are quoted at 2 sigma (2σ).

The Pass Lake Formation has a zircon population that extends from a Mesoarchean zircon (3034 Ma) to a youngest zircon of approximately 1600 Ma, based on 53 analyzed grains. The large concentration of zircons (11 grains) in the age bracket between 1840 and 1900 Ma corresponds with the age of igneous rocks associated with the development of the Penokean convergent margin to the south. There is also a grouping of zircons (5 grains) at approximately 2.4 Ga, roughly the age of Huronian volcanism. The grouping of zircons (6 grains) near 2.7 Ga corresponds in age to the main igneous and deformational phase of the Kenoran Orogeny. A source for the 1.6 to 1.8 billion year old zircons does not exist in Superior Province to the north. These zircons may be originating further to the east or west, or were derived from intrusions of this age to the south. Paleocurrents in the Pass Lake Formation, generally indicating flow from the north, require the Mesoproterozoic debris to be eroded in the south and transported northward prior to sedimentation of the Sibley Group if the source of the Mesoproterozoic debris was in the south where rocks of this age are common.

A sandstone sample, collected by R.M. Easton (OGS) and analyzed by L.M. Heaman (University of Alberta), from an interflow, fine-grained sandstone in the Mesoproterozoic Pillar Lake Volcanics, north of the English Bay Complex, has a distribution of U/Pb, detrital zircon ages similar to the Pass Lake Formation, based on analysis of 50 grains. It contains more Archean zircons, which is understandable considering it is surrounded by rocks of this age. The peak of the Paleoproterozoic zircon population is slightly younger than the zircons from the Pass Lake Formation and the interflow sandstone only possesses 2 Mesoproterozoic zircons that are in the age range of the English Bay Complex (Geon 15). The ages of the zircon population from the interflow sandstone are very similar to the age population distribution of a sample of Rove Formation sandstone collected by R.M. Easton (OGS) from an outcrop of this Paleoproterozoic sedimentary unit south of Thunder Bay. Paleocurrents for the Rove Formation indicate flow was from the north and, as this unit was deposited immediately following the Trans-Hudson Orogeny, it is reasonable to assume that this was the source of the sediment. The best estimate for a maximum depositional age of the greywacke from the upper Rove Formation is provided by a 1777 Ma concordant detrital zircon grain, as the youngest grain in the sample, at 1731 Ma, is 5% discordant (Heaman and Easton 2005). This interpretation is supported by the abundance of grains (n=10) between 1796 to 1777 Ma, and is consistent with U/Pb ash bed ages of 1836±5 and 1832±3 Ma from the basal Rove Formation (Addison et al. 2005). It is evident, based on the striking similarities between the Rove Formation and Mesoproterozoic sandstone sample, that the interflow sandstone was probably mainly derived by erosion of the Rove Formation. The interflow sandstone and the associated volcanics are clearly younger than the English Bay Complex.

The U/Pb, detrital zircon population for sandstone samples collected from the Outan Island Formation is very different from the rest of the samples, and is based on analysis of 62 grains. It contains zircons ranging in age from approximately 1450 to 2750 Ma, but does not have a distinct peak in the age distribution. A significant proportion of the zircons in this sample are younger in age than the Paleoproterozoic, Penokean and Trans-Hudson orogenic zircon populations which dominate the other samples. Igneous rocks formed between 1.4 and 1.8 Ga are only common to the south of the Sibley Basin and this agrees with paleocurrents for the Kama Hill Formation, conformably underlying the Outan Island Formation, showing flow from the south.

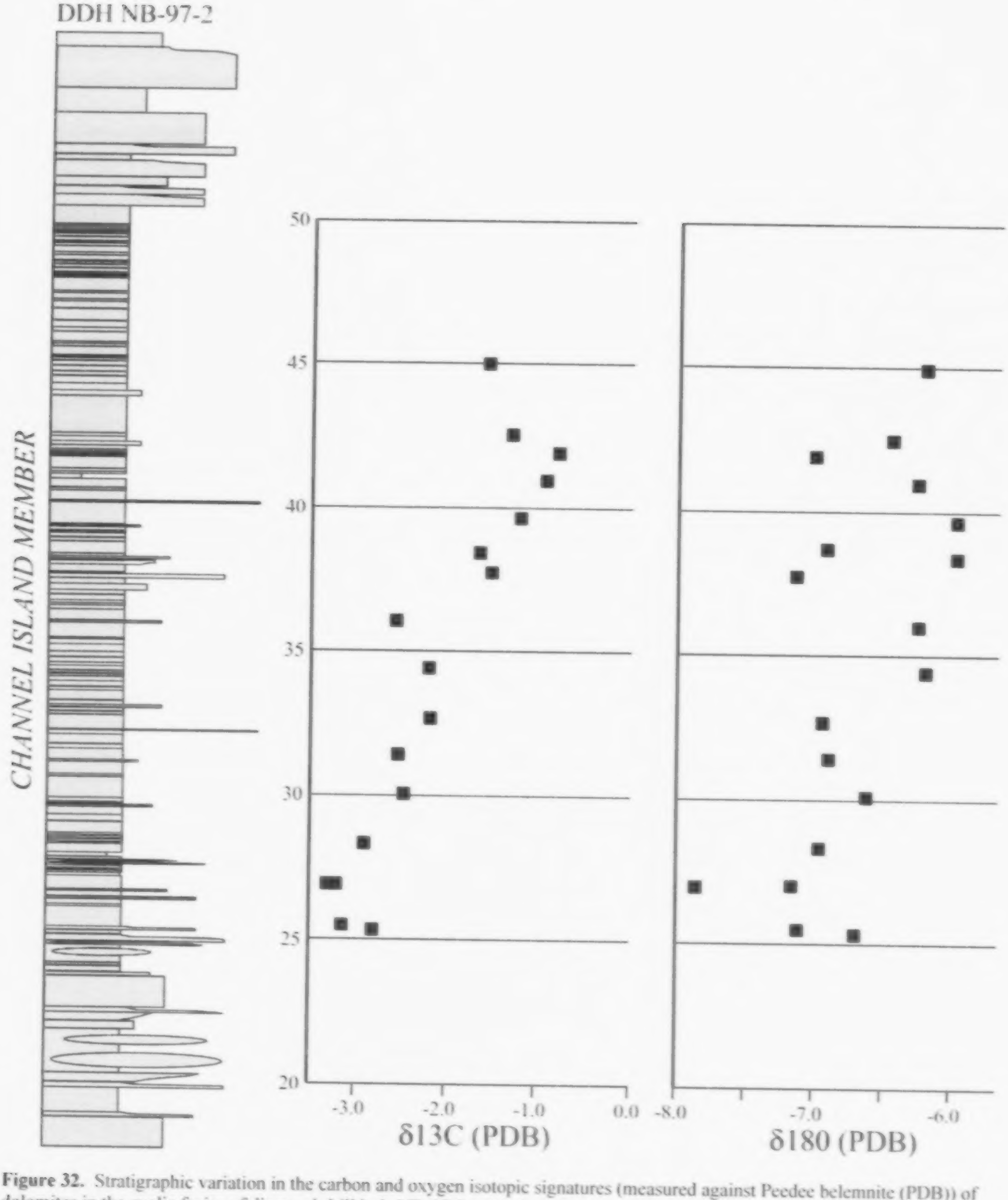

Figure 32. Stratigraphic variation in the carbon and oxygen isotopic signatures (measured against Peedee belemnite (PDB)) of dolomites in the cyclic facies of diamond-drill hole NB-97-2 in Nipigon Bay.

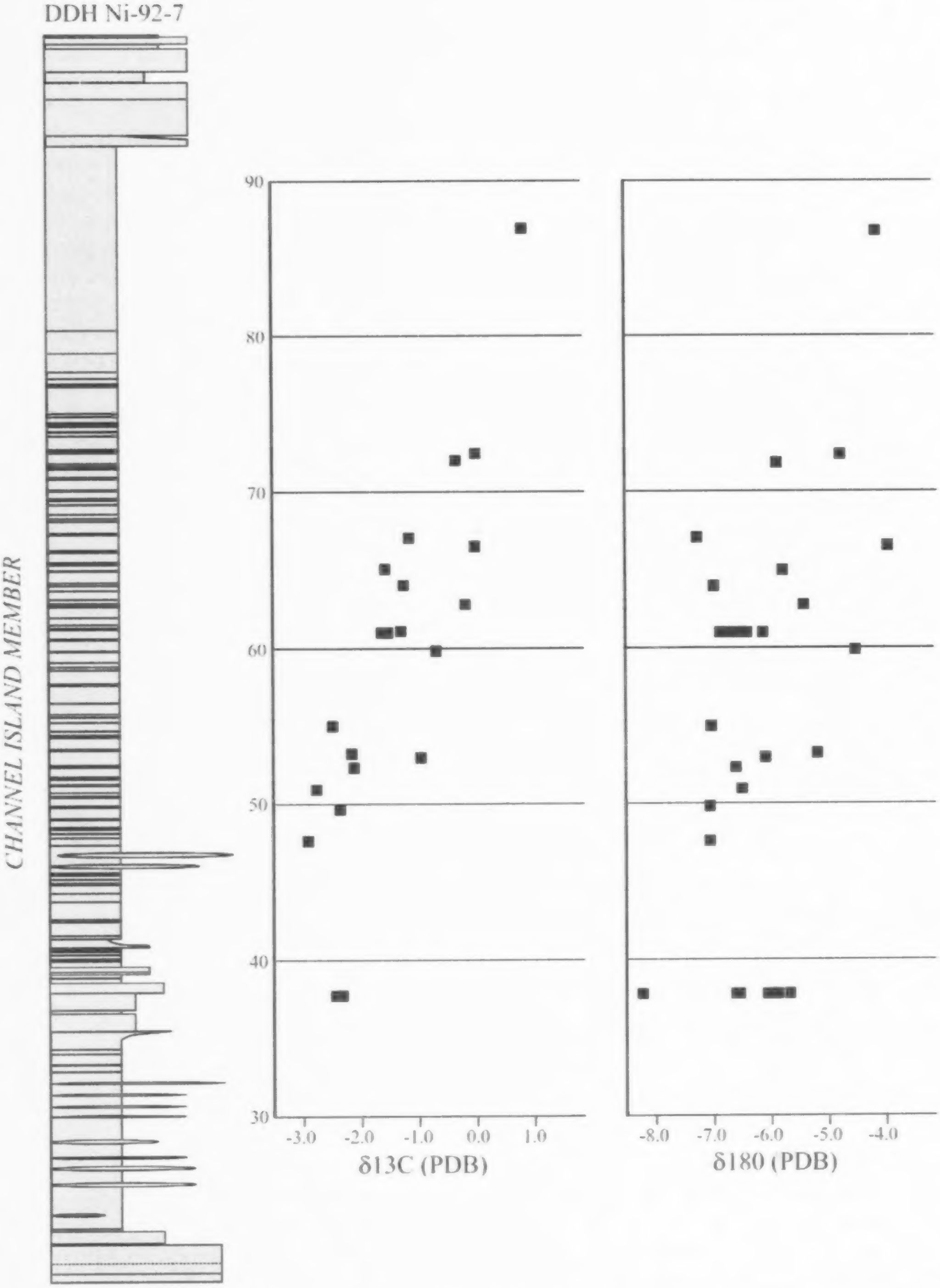

Figure 33. Stratigraphic variation in the carbon and oxygen isotopic signatures (measured against Peedee belemnite (PDB)) of dolomite in the cyclic facies of diamond-drill hole NI-92-7 in the south-central Sibley Basin.

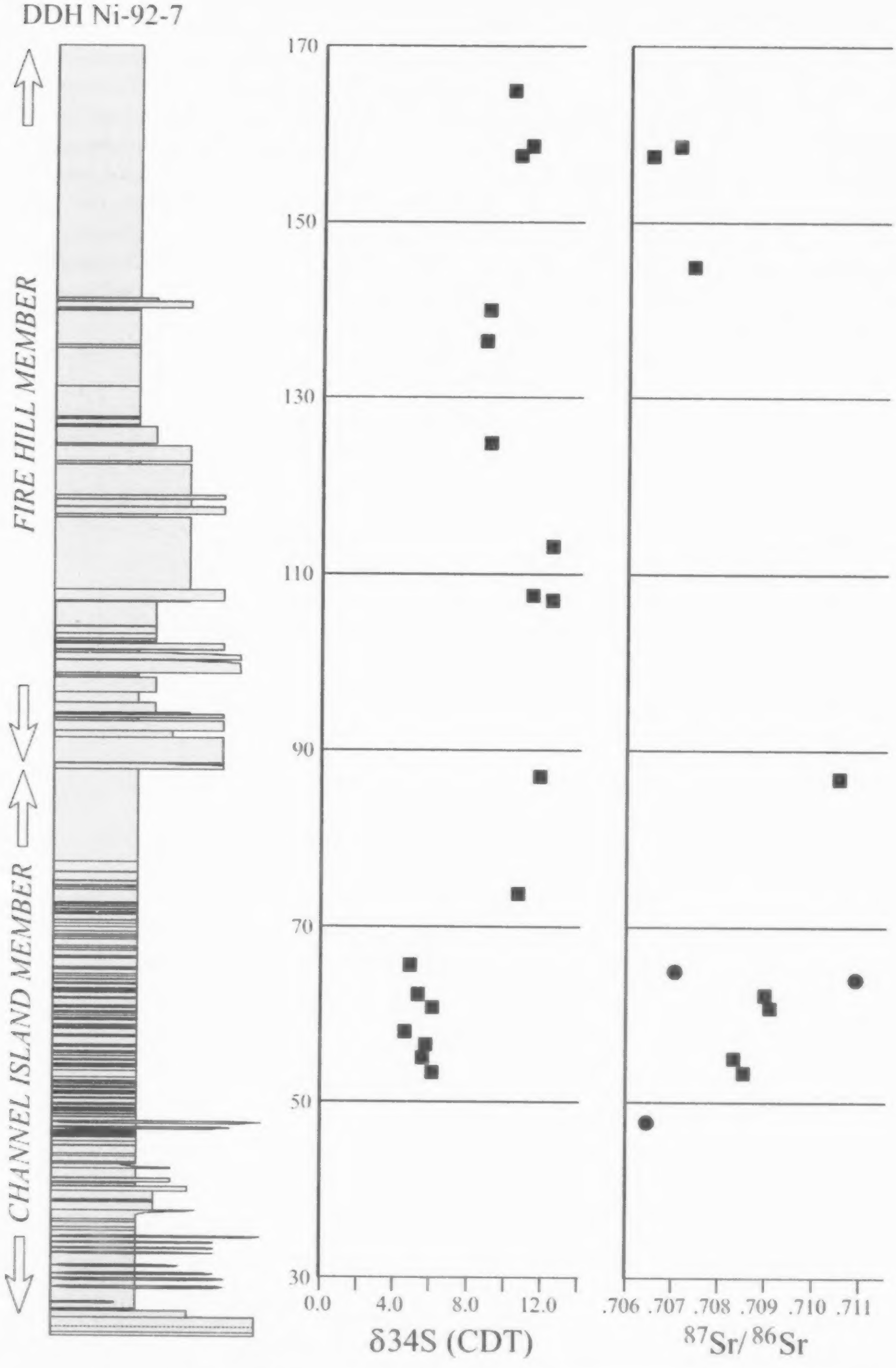

Figure 34. Stratigraphic variation in sulphur isotopic signature (sulphate in gypsum measured against Canyon Diablo Troilite (CDT)) and strontium isotopic ratios in the Rossport Formation present in diamond-drill hole NI-92-7.

The uppermost formation in the Sibley Basin, the Nipigon Bay Formation, has a distribution of U/Pb ages of detrital zircons similar to the Pass Lake Formation, based on analysis of 62 grains. The major difference is the presence of zircons in the time interval between 2.0 and 2.35 Ga. Felsic igneous rock units formed in this age bracket are unknown in the Superior Province in Ontario, as this was a time of post-rift passive margin development. Rocks of this age exist in the Baltic Shield, which was joined to eastern North America at this time. Rocks of this age also are present on the western side of the Trans-Hudson Orogen. As the paleocurrents for the eolian Nipigon Bay Formation indicate transport from the northeast, a Baltica source for these zircons is most likely. Most of the zircons in the Nipigon Bay Formation appear to be fairly locally derived.

ISOTOPE GEOCHEMISTRY

The isotope geochemistry of the Sibley Group exhibits some well-defined trends (Figures 32 and 33). Carbon becomes more enriched in the heavier isotope up through the cyclic facies of the Rossport Formation (Figures 32 (left) and 33 (left)). Oxygen also shows a similar trend (Figures 32 (right) and 33 (right)), but with considerably more scatter. This trend in carbon isotopic values can be used to construct detailed correlations between different exposures of the cyclic facies as the composition of the water from which the dolomite was precipitating was the control on the isotopic ratio. The cyclic facies in diamond-drill hole NI-92-7 is thicker than the lithically same interval in diamond-drill hole NB-97-2, and the heavier isotopic ratios in the top of the thicker succession indicate that deposition of the cyclic facies in NB-97-2 ended before it did in NI-92-7. The cause of the trend may be a local control, i.e., increasing salinity leading to evaporative loss of the lighter isotope from the water, or global, i.e., a general shift in the isotopic ratio driven by increased burial of isotopically light organic carbon in the deep ocean.

The sulphur isotopes also show an interesting trend (Figure 34 (left)). Most of the cyclic facies has a sulphur isotopic ratio of between 4 and 7, whereas the uppermost portion of the cyclic facies of the Channel Island Member and the Fire Hill Member have ratios from 10 to 13. The low ratios for the cyclic facies indicate that the water mass that deposited the sediment was probably not the ocean, as it would have deposited isotopically heavier sulphur in the precipitates. Thus, the Rossport Formation was probably deposited from a hypersaline lacustrine system. The reason for the increase in the isotopic ratio of sulphur is unknown, but it may be linked in some way to the higher salinity of the water that formed the evaporate minerals in the Fire Hill Member.

The strontium isotopic ratios are variable (Figure 34 (right)). This is probably caused by the difficulty in avoiding incorporating radiogenic strontium in the analyzed fraction. However, the lowest values are similar to low values from other rock units deposited at approximately this time period.

Work on this geochemical data set is ongoing.

Acknowledgments

This Open File Report relies heavily on work conducted by Becky Rogala and Riku Mesaranta during the thesis portion of their MSc studies (Rogala 2003; Metsaranta, in preparation). Mark Smyk and John Scott at the Thunder Bay Resident Geologist's Office of the Ministry of Northern Development and Mines, provided useful advice both in the office and field. Diagrams were drafted by Sam Spivak and the manuscript was compiled and proofread by Kristine Carey and Monica Easton, for which we are deeply indebted. Tom Hart and Michael Easton of the Ontario Geological Survey reviewed the manuscript and recommended many revisions that helped clarify the text.

References

Addison, W.D., Brumpton, G.R., Vallini, D.A., McNaughton, N.J., Davis, D.W., Kissin, S.A., Fralick, P.W. and Hammond, A.L. 2005. Discovery of detrital ejecta from the 1850 Ma Sudbury impact event; Geology, v.33, p.193-196.

Aleksandrov, S.M. 1996. Self-organization in prograde carbonate-rock metasomatism; Geochemistry International, v.33, no.8, p.129-145.

Allen, J.R.L. 1964. Studies in fluviatile sedimentation: six cyclothems from the lower Old Red Sandstone, Anglo-Welsh Basin; Sedimentology, v.3, p.163-198.

——— 1970. Studies in fluviatile sedimentation: a comparison of fining-upward cyclothems, with special reference to coarse-member composition and interpretation; Journal of Sedimentary Petrology, v.40, p.298-323.

Anglin, C.D., Franklin, J.M., Loveridge, W.D., Hunt, P.A. and Osterberg, S.A. 1988. Use of zircon U-Pb ages of felsic intrusive and extrusive rocks in eastern Wabigoon Subprovince, Ontario, to place constraints on base metal and gold mineralization; *in* Radiogenic Age and Isotopic Studies, Report 2, Geological Survey of Canada, Paper 88-2, p.109-115.

Barnett, P.J. 1991. Quaternary geology of Ontario; *in* Geology of Ontario, Ontario Geological Survey, Special Volume 4, Part 2, p.1011-1088.

Barrett, T.J. and Fralick, P.W. 1985. Sediment redeposition in Archean iron formation: examples from the Beardmore–Geraldton greenstone belt, Ontario; Journal of Sedimentary Petrology, v.55, p.205-212.

——— 1989. Turbidites and iron formations, Beardmore–Geraldton, Ontario: application of a combined ramp/fan model to Archean clastic and chemical sedimentation; Sedimentology, v.36, p.221-234.

Bell, R. 1870. Report of Mr. Robert Bell on lakes Superior and Nipigon; Geological Survey of Canada, Report of Progress 1866–69, Part IX, p.313-364.

Bigarella, J.J. 1972. Eolian environments: their characteristics recognition and importance; *in* Recognition of ancient sedimentary environments, Society of Economic Paleontologists and Mineralogists, Special Publication 16, p.13-62.

Blackburn, C.E., Johns, G.W., Ayer, J. and Davis, D.W. 1991. Wabigoon Subprovince; *in* Geology of Ontario, Ontario Geological Survey, Special Volume 4, Part 1, p.303-381.

Bucher, K. and Frey, M. 2002. Petrogenesis of metamorphic rocks, 7th ed.; Springer-Verlag, New York, 341p.

Cheadle, B.A. 1986a. Stratigraphy and sedimentation of the Middle Proterozoic Sibley Group, Thunder Bay District, Ontario; unpublished PhD thesis, University of Western Ontario, London, Ontario, 434p.

——— 1986b. Alluvial-playa sedimentation in the lower Keweenawan Sibley Group, Thunder Bay District, Ontario; Canadian Journal of Earth Sciences, v.23, p.527-541.

Clemmensen, L.B. and Abrahamsen, K. 1983. Aeolian stratification and facies association in desert sediments, Arran basin (Permian), Scotland; Sedimentology, v.30, p.311-339.

Coates, M.E. 1972. Geology of the Black Sturgeon River area, District of Thunder Bay; Ontario Department of Mines and Northern Affairs, Geological Report 98, 41p.

Coleman, J.M. and Prior, D.B. 1980. Deltaic sand bodies; American Association of Petroleum Geologists, Continuing Education Course Notes, No. 15, 171p.

Collinson, J.D. 1996. Alluvial sediments; *in* Sedimentary environments: processes, facies, and stratigraphy, 3rd edition, Blackwell Science, London, p.37-82.

Davis, D.W. and Sutcliffe, R.H. 1985. U-Pb ages from the Nipigon Plate and Northern Lake Superior; Geological Society of America Bulletin, v.96, p.1572-1579.

Devaney, J.R. and Williams, H.R. 1989. Evolution of an Archean subprovince boundary: a sedimentological and structural study of part of the Wabigoon–Quetico boundary in northern Ontario; Canadian Journal of Earth Sciences, v.26, p.1013-1026.

Eriksson, K.A., Krapez, B. and Fralick, P.W. 1994. Sedimentology of Archean greenstone belts: signatures of tectonic evolution; Earth Science Reviews, v.37, p.1-88.

——— 1997. Sedimentological aspects; *in* Greenstone belts, Clarendon Press, Oxford, United Kingdom, p.33-54.

Fralick, P.W. and Barrett, T.J. 1995. Depositional controls on iron formation associations in Canada; *in* Sedimentary facies analysis, International Association of Sedimentologists, Special Publication 22, p.137-156.

Fralick, P.W., Davis, D.W. and Kissin, S.A. 2002. The age of the Gunflint Formation, Ontario, Canada: single zircon U-Pb age determinations from reworked volcanic ash; Canadian Journal of Earth Sciences, v.39, p.1085-1091.

Fralick, P.W., Jinhua, W. and Williams, H.R. 1992. Trench and slope basin deposits in an Archean metasedimentary belt, Superior Province, Canadian Shield; Canadian Journal of Earth Sciences, v.29, p.2551-2557.

Fralick, P.W. and Kronberg, B.I. 1997. Geochemical discrimination of clastic sedimentary rock sources; Sedimentary Geology, v.113, p.111-124.

Fralick, P.W. and Miall, A.D. 1989. Sedimentology of the lower Huronian Supergroup (Early Proterozoic), Elliot Lake area, Ontario, Canada; Sedimentary Geology, v.63, p.127-153.

Franklin, J.M. 1970. Metallogeny of the Proterozoic rocks of Thunder Bay District, Ontario; unpublished PhD thesis, University of Western Ontario, London, Ontario, 317p.

——— 1978. The Sibley Group, Ontario; *in* Rubidium-Strontium Isotopic Age Studies, Report 2, Geological Survey of Canada, Paper 77-14, p.31-34.

Franklin, J.M., McIlwaine, W., Poulsen, K. and Wanless, R. 1980. Stratigraphy and depositional setting of the Sibley Group, Thunder Bay District, Ontario, Canada; Canadian Journal of Earth Sciences, v.17, p.633-650.

Hart, T.R. 2005. Precambrian geology of the southern Black Sturgeon River and Seagull Lake area, Nipigon Embayment, northwestern Ontario; Ontario Geological Survey, Open File Report 6165, 63p.

Hart, T.R. and Magyarosi, Z. 2004. Precambrian geology of the northern Black Sturgeon River and Disraeli Lake area, Nipigon Embayment, northwestern Ontario; Ontario Geological Survey, Open File Report 6138, 56p.

Haszeldine, R.S. 1984. Muddy delta in freshwater lakes, and tectonism in the Upper Carboniferous Coalfield of NE England; Sedimentology, v.31, p.811-822.

Heaman, L.M. and Easton, R.M. 2005. Proterozoic history of the Lake Nipigon area, Ontario: constraints from U-Pb zircon and baddeleyite dating; 51st Institute on Lake Superior Geology, Proceedings, Volume 51, Part 1, p.24-25.

Heaman, L.M., Easton, R.M., Hart, T.R., MacDonald, C.A., Fralick, P. and Hollings, P. 2005. Proterozoic history of the Lake Nipigon area, Ontario: constraints from U-Pb zircon and baddeleyite dating; abstract, Ontario Exploration and Geoscience Symposium, Toronto, Ontario, December 13-14, 2005.

Hollings, P., Fralick, P.W. and Kissin, S.A. 2004. Geochemistry and geodynamic implications of the Mesoproterozoic English Bay granite-rhyolite complex, northwestern Ontario; Canadian Journal of Earth Sciences, v.41, p.1329-1338.

Hubert, J.F. and Hyde, M.G. 1982. Sheet-flow deposit of graded beds and mudstones on an alluvial sandflat–playa system: Upper Triassic Blomidon redbeds, St. Mary's Bay, Nova Scotia; Sedimentology, v.29, p.457-474.

Hunt, T.S. 1873. The geonostical history of the metals; Transactions of the American Institute of Mining and Engineering, v.1, p.331-345.

Johnson, H.D. and Baldwin, C.T. 1996. Shallow clastic seas; *in* Sedimentary environments: processes, facies, and stratigraphy, 3rd edition, Blackwell Science, London, p.232-280.

Jones, C.M. and McCabe, P.J. 1980. Erosion surfaces within giant fluvial cross-beds of the Carboniferous in Northern England; Journal of Sedimentary Petrology, v.50, p.613-620.

Kocurek, G.A. 1996. Desert aeolian systems; *in* Sedimentary environments: processes, facies, and stratigraphy, 3rd edition, Blackwell Science, London, p.125-157.

Lafrance, B., DeWolfe, J.C. and Stott, G.M. 2004. A structural reappraisal of the Beardmore–Geraldton Belt at the southern boundary of the Wabigoon Subprovince, Ontario, and implications for gold mineralization; Canadian Journal of Earth Sciences, v.41, p.217-235.

Letargo, C.M.R., Lamb, W.M. and Park, J. 1995. Comparison of calcite + dolomite thermometry and carbonate + silica equilibria: constraints on the conditions of metamorphism of the Llano Uplift, Texas, U.S.A.; American Mineralogist, v.80, p.131-143.

Logan, Sir W.E., Murray, A., Hunt, T.S. and Billings, E. 1863. Geology of Canada—Report of Progress from its commencement to 1863; Geological Survey of Canada, Report of Progress, 1863, 983p.

MacDonald, C.A. 2004. Precambrian geology of the south Armstrong–Gull Bay area, Nipigon Embayment, northwestern Ontario; Ontario Geological Survey, Open File Report 6136, 42p.

MacDonald, C.A., Tremblay, E. and Easton, R.M. 2005. Precambrian geology of the west-central map area, Nipigon Embayment, northwestern Ontario: Lake Nipigon Region Geoscience Initiative; Ontario Geological Survey, Open File Report 6164, 49p.

Machette, M.N. 1985. Calcic soils of the southwestern United States; Geological Society of America, Special Paper 203, p.1-21.

Magyarosi, Z., Hart, T.R., Fralick, P., Metsaranta, R., Heggie, G.J., Hollings, P. and Richardson, A. 2004. Black Sturgeon River area geological cross-sections, Nipigon Embayment, northwestern Ontario; Ontario Geological Survey, Preliminary Map P.3540, scale 1:50 000.

McIlwaine, W.H. 1971a. McTavish Township (west part of north half), District of Thunder Bay; Ontario Division of Mines and Northern Affairs, Preliminary Map P.720, scale 1:15 840.

——— 1971b. McTavish Township (east part of north half), District of Thunder Bay; Ontario Division of Mines and Northern Affairs, Preliminary Map P.721, scale 1:15 840.

——— 1975. McTavish Township (southern half), District of Thunder Bay; Ontario Division of Mines and Northern Affairs, Preliminary Map P.990, scale 1:15 840.

Metsaranta, R. and Fralick, P.W. 2004. Lake Nipigon Region Geoscience Initiative. Stratigraphy of the Sibley Group and its relationship to sedimentary units of the basal Osler Group and the Nipigon Sills; *in* Summary of Field Work and Other Activities 2004, Ontario Geological Survey, Open File Report 6145, p.50-1 to 50-5.

Miall, A.D. 1977. A review of the braided-river depositional environment; Earth Science Reviews, v.13, p.1-62.

——— 1985. Architectural-element analysis: a new method of facies analysis applied to fluvial deposits; Earth Science Reviews, v.22, p.261-308.

——— 1996. The geology of fluvial deposits: sedimentary facies, basin analysis, and petroleum geology; Springer-Verlag, Berlin, 582p.

Nanson, G.C. 1980. Point bar and floodplain formation of the meandering Beatton River, northeastern British Columbia; Sedimentology, v.27, p.3-29.

Nesbitt, H.W. and Young, G.M. 1982. Early Proterozoic climates and plate motions inferred from major element chemistry of lutites; Nature, v.299, p.715-717.

Ojakangas, R., Morey, G.B. and Green, J.C. 2001. The Mesoproterozoic Midcontinent Rift System, Lake Superior Region, USA; Sedimentary Geology, v.141-142, p.421-442.

Ojakangas, R., Morey, G.B. and Southwick, D.L. 2001. Paleoproterozoic basin development and sedimentation in the Lake Superior region, North America; Sedimentary Geology, v.141-142, p.319-341.

Piper, D.J.W. and Panagos, A.G. 1981. Growth patterns of the Acheloos and Evinos deltas, western Greece; Sedimentary Geology, v.28, p.111-132.

Pufahl, P. and Fralick, P.W. 2000. Field Trip 4. Depositional environments of the Paleoproterozoic Gunflint Formation; Institute on Lake Superior Geology, 46th Annual Meeting, Thunder Bay, Ontario, Proceedings and Abstracts, Part 2 – Field Trip Guidebooks, v.46, pt.2.

——— 2004. Depositional controls on Paleoproterozoic iron formation accumulation, Gogebic Range, Lake Superior region, USA; Sedimentology, v.51, p.791-808.

Reading, H.G. and Collinson, J.D. 1996. Clastic coasts; *in* Sedimentary environments: processes, facies, and stratigraphy, 3rd edition, Blackwell Science, London, p.154-231.

Rice, J.M. 1977. Contact metamorphism of impure dolomitic limestone in the Boulder aureole, Montana; Contributions to Mineralogy and Petrology, v.59, p.237-259.

Rogala, B. 2000. A metamorphosed evaporite sequence from the Sibley Basin; unpublished BSc thesis, Lakehead University, Thunder Bay, Ontario, 38p.

——— 2003. The Sibley Group: a lithostratigraphic, geochemical, and paleomagnetic study; unpublished MSc thesis, Lakehead University, Thunder Bay, Ontario, 254p.

Rust, B.R. 1978. Depositional models for braided alluvium; *in* Fluvial sedimentology, Canadian Society of Petroleum Geologists, Memoir 5, p.605-625.

Salvany, J.M., Muñoz, A. and Pérez, A. 1994. Nonmarine evaporitic sedimentation and associated diagenetic processes of the southwestern margin of the Ebro Basin (Lower Miocene), Spain; Journal of Sedimentary Research, v.A64, p.190-203.

Schneider, D.A., Bickford, M.E., Cannon, W.F., Schulz, K.J. and Hamilton, M.A. 2002. Age of volcanic rocks and syndepositional iron formations, Marquette Range Supergroup: implications for the tectonic setting of Paleoproterozoic iron formations of the Lake Superior region; Canadian Journal of Earth Sciences, v.39, p.999-1012.

Schumm, S.A. 1963. Speculations concerning paleohydrologic controls of terrestrial sedimentation; Geological Society of America Bulletin, v.79, p.1573-1588.

Skippen, G. and Trommsdorff, V. 1986. The influence of NaCl and KCl on phase relations in metamorphosed carbonate rocks; American Journal of Science, v.286, p.81-104.

Smith, N.D. 1970. The braided stream depositional environment: comparison of the Platte River with some Silurian clastic rocks, north-central Appalachians; Geological Society of America Bulletin, v.81, p.2993-3013.

Smoot, J.P. and Castens-Seidell, B. 1994. Sedimentary features produced by efflorescent salt crusts, Saline Valley and Death Valley, California; *in* Sedimentology and geochemistry of modern and ancient saline lakes, Society of Economic Paleontologists and Mineralogists (SEPM), Special Publication 50, p.73-90.

Sutcliffe, R.H. 1986. Proterozoic rift-related igneous rocks at Lake Nipigon, Ontario; unpublished PhD thesis, University of Western Ontario, London, Ontario, 325p.

——— 1991. Proterozoic geology of the Lake Superior area; *in* Geology of Ontario, Ontario Geological Survey, Special Volume 4, Part 1, p.627-658.

Talbot, M.R. and Allen, P.A. 1996. Lakes; *in* Sedimentary environments: processes, facies, and stratigraphy, 3rd edition, Blackwell Science, London, p.154-231.

Tanton, T.L. 1931. Fort William and Port Arthur, and Thunder Cape map-area, Thunder Bay District, Ontario; Geological Survey of Canada, Memoir 167, 222p. with accompanying maps.

Thomas, M.D. and Teskey, D.J. 1994. An interpretation of gravity anomalies over the Midcontinent Rift, Lake Superior, constrained by GLIMPCE seismic and aeromagnetic data; Canadian Journal of Earth Sciences, v.31, p.682-697.

Tomlinson, K.Y., Davis, D.W., Stone, D. and Hart, T.R. 2003. U-Pb age and Nd isotopic evidence for Archean terrane development and crustal recycling in the south-central Wabigoon Subprovince, Canada; Contributions to Mineralogy and Petrology, v.144, p.684-702.

Tracy, R.J. and Frost, B.R. 1991. Phase equilibria and thermobarometry of calcareous, ultramafic and mafic rocks, and iron formations; *in* Contact metamorphism, Mineralogical Society of America, Reviews in Mineralogy, v.26, p.207-289.

Truc, G. 1978. Lacustrine sedimentation in an evaporate environment: the Ludian (Palaeogene) of the Mormoiron basin, southeastern France; International Association of Sedimentologists, Special Publication 2, p.189-203.

Van Hise, C.R. and Leith, C.K. 1909. Precambrian geology of North America; United States Geological Survey, Bulletin 360, 939p.

West, I.M., Ali, Y.A. and Hilmy, M.E. 1979. Primary gypsum nodules in a modern sabkha on the Mediterranean coast of Egypt; Geology, v.7, p.354-358.

White, A.H. and Youngs, B.C. 1980. Cambrian alkali playa-lacustrine sequence in the northeastern Officer Basin, South Australia; Journal of Sedimentary Petrology, v.50, p.1279-1286.

Williams, H.R. 1991. Quetico Subprovince; *in* Geology of Ontario, Ontario Geological Survey, Special Volume 4, Part 1, p.383-403.

Wilson, A.W.G. 1910. Geology of the Nipigon Basin, Ontario; Geological Survey of Canada, Memoir 1, 152p.

Winchester, J.A. and Floyd, P.A. 1977. Geochemical discrimination of different magma series and their differentiation products using immobile elements; Chemical Geology, v.20, p.325-343.

Winkler, H.G.F. 1974. Petrogenesis of metamorphic rocks; Springer-Verlag, New York, 320p.

Appendix 1

Major Element Analyses for the Sibley Group

Note:

Data are from medium-grained sandstones. Sampling is in stratigraphic order from 01-1 at the top of the Sibley Group to sample 01-43 at the bottom. Data were used to construct Figures 29, 30 and 31.

Universal Transverse Mercator (UTM) co-ordinates are North American Datum 1927 (NAD 27), Zone 16.

Appendix 1. Major element analyses for the Sibley Group.

Laboratory Lakehead University

Sample	Method	Detection Limit	01-1	01-2	01-3	01-4	01-5	01-6	01-7	01-8	01-9
SiO_2 (wt. %)	ICP–AES	0.01	83.56	89.29	91.06	89.16	87.83	90.05	88.78	88.15	91.68
TiO_2	ICP–AES	0.01	0.11	0.05	0.04	0.13	0.04	0.03	0.10	0.18	0.03
Al_2O_3	ICP–AES	0.01	7.38	5.18	4.65	5.01	3.86	3.93	4.82	5.37	3.80
Fe_2O_{3T}	ICP–AES	0.01	0.84	0.51	0.37	1.78	1.47	0.63	1.51	1.26	0.27
MnO	ICP–AES	0.01	0.05	0.02	0.02	0.01	0.04	0.02	0.03	0.02	0.01
MgO	ICP–AES	0.01	1.08	0.64	0.51	0.45	1.08	0.68	0.53	0.57	0.44
CaO	ICP–AES	0.01	1.15	0.47	0.34	0.13	1.43	0.74	0.35	0.24	0.41
K_2O	ICP–AES	0.01	3.80	2.56	1.80	2.39	1.82	2.49	2.77	3.09	2.36
Na_2O	ICP–AES	0.01	0.24	0.09	0.07	0.07	0.08	0.05	0.07	0.08	0.06
P_2O_5	ICP–AES	0.01	0.05	0.04	0.05	0.05	0.04	0.04	0.06	0.06	0.04
H_2O_P	ICP–AES	0.01	0.72	0.63	0.72	0.63	0.63	0.36	0.54	0.72	0.36
CO_2	ICP–AES	0.01	1.03	0.51	0.37	0.18	1.98	0.99	0.44	0.26	0.55
Total	ICP–AES	0.01	100.0	100.0	100.0	100.0	100.3	100.0	100.0	100.0	100.0
Nb (ppm)	ICP–AES	0.030	5.8	2.7	3.6	4.7	4.6	1.9	3.8	5.7	3.9
Sr	ICP–AES	0.005	46.1	28.3	17.8	26.8	22.8	24.7	28.7	26.6	25.1
Y	ICP–AES	0.005	14.9	6.6	6.0	12.1	7.1	5.2	10.7	14.0	4.5
Zr	ICP–AES	0.02	65.8	35.0	33.1	69.8	27.7	27.7	55.8	95.4	26.4
Ba	ICP–AES	0.006	387	476	281	233	351	268	377	325	297
V	ICP–AES	0.03	10.1	5.0	4.6	14.1	4.0	2.9	13.2	14.0	3.2
Co	ICP–AES	0.05	32.6	21.7	25.1	26.9	30.4	11.6	16.1	21.9	26.2
Ni	ICP–AES	0.03	6.4	4.0	5.5	5.9	2.9	3.3	5.6	6.6	3.5
Zn	ICP–AES	0.005	11.3	3.6	11.1	10.5	0.6	1.9	8.0	10.4	1.0

Sample	Method	Detection Limit	01-10	01-11	01-12	01-13	01-14	01-15	01-16	01-17	01-18
SiO_2 (wt. %)	ICP–AES	0.01	94.03	89.46	90.03	83.16	75.43	80.25	85.47	78.29	85.49
TiO_2	ICP–AES	0.01	0.03	0.07	0.06	0.16	0.11	0.15	0.23	0.26	0.19
Al_2O_3	ICP–AES	0.01	3.56	3.89	4.19	5.60	5.24	6.95	5.83	4.60	5.54
Fe_2O_{3T}	ICP–AES	0.01	0.30	1.40	1.53	2.66	1.85	2.75	2.36	4.45	2.93
MnO	ICP–AES	0.01	0.00	0.02	0.01	0.04	0.06	0.04	0.04	0.04	0.03
MgO	ICP–AES	0.01	0.26	0.75	0.42	1.56	2.86	2.49	0.39	2.12	0.67
CaO	ICP–AES	0.01	0.10	0.78	0.32	1.11	3.91	0.74	0.35	2.67	0.58
K_2O	ICP–AES	0.01	1.14	2.25	2.26	3.14	3.64	4.73	4.47	2.99	3.35
Na_2O	ICP–AES	0.01	0.02	0.06	0.09	0.09	1.22	0.12	0.11	0.09	0.06
P_2O_5	ICP–AES	0.01	0.03	0.04	0.04	0.04	0.04	0.06	0.07	0.07	0.06
H_2O_P	ICP–AES	0.01	0.36	0.36	0.72	0.90	0.72	0.99	0.27	0.54	0.36
CO_2	ICP–AES	0.01	0.18	0.92	0.33	1.54	6.01	0.73	0.40	3.89	0.73
Total	ICP–AES	0.01	100.0	100.0	100.0	100.0	101.1	100.0	100.0	100.0	100.0
Nb (ppm)	ICP–AES	0.030	3.5	5.0	5.5	8.1	11.1	6.8	9.4	11.4	9.4
Sr	ICP–AES	0.005	5.6	21.6	40.7	22.3	23.4	27.6	23.0	27.7	18.7
Y	ICP–AES	0.005	5.4	5.3	5.7	11.2	11.6	11.9	9.9	14.1	15.6
Zr	ICP–AES	0.02	26.4	68.0	51.2	79.6	58.6	67.6	89.4	96.0	101.3
Ba	ICP–AES	0.006	31	209	272	274	318	1277	539	240	225
V	ICP–AES	0.03	7.4	7.3	9.1	18.9	13.7	37.8	28.5	32.6	27.6
Co	ICP–AES	0.05	25.6	26.7	39.6	49.0	58.8	29.8	46.2	38.4	35.4
Ni	ICP–AES	0.03	3.5	3.8	3.6	6.8	3.3	14.7	2.7	6.1	6.5
Zn	ICP–AES	0.005	1.7	3.4	1.4	17.9	8.5	28.8	4.1	7.9	7.6

Appendix 1. continued

Laboratory Lakehead University

Sample	**Method**	**Detection Limit**	**01-19**	**01-20**	**01-21**	**01-22**	**01-23**	**01-24**	**01-25**	**01-26**	**01-27**
SiO_2 (wt. %)	ICP–AES	0.01	84.17	85.97	65.94	80.13	89.51	92.01	91.49	88.98	87.21
TiO_2	ICP–AES	0.01	0.16	0.13	0.28	0.54	0.49	0.08	0.05	0.03	0.09
Al_2O_3	ICP–AES	0.01	6.06	4.59	7.33	6.40	3.95	3.83	4.32	3.98	4.29
Fe_2O_{3T}	ICP–AES	0.01	2.34	2.95	0.94	3.07	2.26	0.41	0.75	0.32	1.66
MnO	ICP–AES	0.01	0.04	0.03	0.15	0.02	0.02	0.01	0.01	0.03	0.05
MgO	ICP–AES	0.01	0.79	0.67	5.71	5.26	0.58	0.53	0.36	0.89	1.00
CaO	ICP–AES	0.01	0.75	0.80	5.94	0.17	0.53	0.38	0.28	1.08	1.15
K_2O	ICP–AES	0.01	3.93	3.23	5.35	2.96	1.92	1.79	1.86	2.58	2.62
Na_2O	ICP–AES	0.01	0.09	0.07	0.18	0.13	0.04	0.05	0.04	0.07	0.07
P_2O_5	ICP–AES	0.01	0.07	0.06	0.14	0.09	0.03	0.03	0.02	0.03	0.03
H_2O_P	ICP–AES	0.01	0.54	0.45	0.09	1.08	0.63	0.45	0.45	0.54	0.36
CO_2	ICP–AES	0.01	1.06	1.06	7.96	0.15	0.44	0.44	0.37	1.47	1.47
Total	ICP–AES	0.01	100.0	100.0	100.0	100.0	100.4	100.0	100.0	100.0	100.0
Nb (ppm)	ICP–AES	0.030	8.9	8.6	8.5	8.2	3.3	4.0	5.3	3.8	4.6
Sr	ICP–AES	0.005	23.0	26.0	46.5	22.8	17.8	17.0	11.8	26.5	23.8
Y	ICP–AES	0.005	14.0	9.2	21.1	13.0	6.1	6.4	5.3	5.3	7.5
Zr	ICP–AES	0.02	84.3	75.0	129.4	132.0	66.2	65.9	32.7	30.3	69.1
Ba	ICP–AES	0.006	323	189	965	284	311	283	168	263	236
V	ICP–AES	0.03	22.7	29.3	63.8	60.0	12.3	20.5	4.8	5.2	9.2
Co	ICP–AES	0.05	40.1	45.9	20.4	28.2	13.7	25.2	45.3	23.0	23.6
Ni	ICP–AES	0.03	8.1	5.5	8.5	8.5	21.4	3.5	2.3	1.9	2.0
Zn	ICP–AES	0.005	8.9	4.7	38.6	121.0	3.2	0.4	0.9	0.5	5.9

Sample	**Method**	**Detection Limit**	**01-29**	**01-30**	**01-31**	**01-32**	**01-33**	**01-35**	**01-36**	**01-37**	**01-38**
SiO_2 (wt. %)	ICP–AES	0.01	91.41	92.26	81.75	83.15	71.31	59.81	53.90	79.44	77.24
TiO_2	ICP–AES	0.01	0.08	0.06	0.13	0.30	0.31	0.35	0.34	0.03	0.05
Al_2O_3	ICP–AES	0.01	4.09	3.44	3.61	4.95	5.57	8.72	9.19	1.44	1.27
Fe_2O_{3T}	ICP–AES	0.01	0.35	0.26	1.39	2.22	2.41	3.15	2.25	0.65	0.47
MnO	ICP–AES	0.01	0.00	0.01	0.04	0.03	0.06	0.09	0.08	0.00	0.03
MgO	ICP–AES	0.01	0.39	0.60	2.35	1.38	3.84	5.52	6.43	0.56	4.85
CaO	ICP–AES	0.01	0.17	0.55	3.19	1.73	4.78	6.46	8.75	15.81	6.07
K_2O	ICP–AES	0.01	2.22	1.82	2.42	3.33	4.07	6.06	5.87	1.00	0.63
Na_2O	ICP–AES	0.01	0.06	0.05	0.07	0.07	0.13	0.23	0.34	0.05	0.07
P_2O_5	ICP–AES	0.01	0.04	0.03	0.04	0.06	0.08	0.12	0.10	0.14	0.01
H_2O_P	ICP–AES	0.01	0.81	0.18	0.54	0.54	0.81	0.99	1.35	0.18	0.36
CO_2	ICP–AES	0.01	0.37	0.73	4.47	2.24	6.64	8.51	11.40	0.70	8.95
Total	ICP–AES	0.01	100.0	100.0	100.0	100.0	100.0	100.0	100.0	100.0	100.0
Nb (ppm)	ICP–AES	0.030	3.7	4.4	6.7	8.2	8.8	11.7	10.9	8.8	7.1
Sr	ICP–AES	0.005	31.9	18.0	23.8	24.0	88.9	99.9	188.0	925.8	538.5
Y	ICP–AES	0.005	6.4	5.7	10.7	14.6	16.3	30.7	24.1	3.4	6.9
Zr	ICP–AES	0.02	63.2	59.2	66.5	112.6	142.1	141.7	117.7	19.4	53.4
Ba	ICP–AES	0.006	239	365	450	218	2821	956	3028	234	7422
V	ICP–AES	0.03	6.1	7.3	12.8	25.8	29.0	60.2	37.7	7.1	18.4
Co	ICP–AES	0.05	14.4	25.4	27.2	20.7	22.1	16.8	13.6	4.2	21.8
Ni	ICP–AES	0.03	4.7	2.7	6.6	7.4	7.4	12.8	9.7	0.2	2.3
Zn	ICP–AES	0.005	4.7	188.9	12.3	17.2	22.6	31.0	25.9	0.0	0.9

Appendix 1. continued

Laboratory	Lakehead University						
Sample	**Method**	**Detection Limit**	**01-39**	**01-40**	**01-41**	**01-42**	**01-43**
SiO_2 (wt. %)	ICP–AES	0.01	75.85	70.78	75.46	78.19	66.99
TiO_2	ICP–AES	0.01	0.05	0.07	0.13	0.09	0.14
Al_2O_3	ICP–AES	0.01	1.45	1.81	3.86	2.77	4.51
Fe_2O_{3T}	ICP–AES	0.01	0.52	0.58	1.72	0.72	1.47
MnO	ICP–AES	0.01	0.03	0.03	0.02	0.07	0.04
MgO	ICP–AES	0.01	4.94	5.69	6.90	8.09	6.67
CaO	ICP–AES	0.01	6.94	8.15	9.40	4.70	10.29
K_2O	ICP–AES	0.01	0.73	0.94	1.83	0.73	2.29
Na_2O	ICP–AES	0.01	0.08	0.11	0.18	0.28	0.31
P_2O_5	ICP–AES	0.01	0.02	0.02	0.04	0.02	0.03
H_2O_P	ICP–AES	0.01	0.45	0.45	0.09	1.89	1.62
CO_2	ICP–AES	0.01	8.95	11.37	0.37	2.46	5.65
Total	ICP–AES	0.01	100.0	100.0	100.0	100.0	100.0
Nb (ppm)	ICP–AES	0.030	6.6	6.9	7.9	19.3	8.8
Sr	ICP–AES	0.005	380.5	149.9	150.5	52.0	83.3
Y	ICP–AES	0.005	5.2	7.4	8.1	6.3	7.6
Zr	ICP–AES	0.02	34.8	103.2	78.5	44.6	45.2
Ba	ICP–AES	0.006	5605	2807	1855	367	836
V	ICP–AES	0.03	23.6	69.1	19.8	12.1	18.2
Co	ICP–AES	0.05	16.0	11.8	10.7	8.6	11.3
Ni	ICP–AES	0.03	9.2	3.0	2.6	4.6	4.7
Zn	ICP–AES	0.005	15.7	0.9	5.2	17.0	21.1

Appendix 2

Geochemical Data for Channel Island Member Carbonate Rocks

Notes:
C and O stable isotope analyses conducted at Queen's University, Kingston, Ontario
Sr isotope analyses conducted at Carleton University, Ottawa, Ontario
Dilute acetic acid extractions were used for major and trace element analyses.
Universal Transverse Mercator (UTM) co-ordinates are North American Datum 1927 (NAD 27), Zone 16.

Appendix 2. Geochemical data for Channel Island Member (CIM) carbonate rocks

Sample			**RC1**	**RC2**
Lithostratigraphic Unit			CIM	CIM
Drill Hole			NI-92-7	NI-92-7
Stratigraphic Height (above basement) (m)			53.27	59.85
Easting (m)			353850	353850
Northing (m)			5443000	5443000
Description			red dolomitic mudstone	red dolomitic mudstone
$\delta^{13}C$ (PDB)			-2.2	-0.7
$\delta^{18}O$ (SMOW)			25.3	25.9
$\delta^{18}O$ (PDB)			-5.4	-4.8
	Method	**Detection Limit**		
Al (ppm)	ICP-MS	0.5	183.0	117.2
Fe	ICP-MS	2	35.6	44.0
Mn	ICP-MS	0.4	37.6	27.4
Mg	ICP-MS	250	46,751	35,027
Ca	ICP-MS	1000	79,500	59,260
Cs	ICP-MS	0.0015	0.0098	0.0491
Hf	ICP-MS	0.005	N.D.	N.D.
Rb	ICP-MS	0.35	N.D.	0.5
Sr	ICP-MS	10.00	18	14
Ta	ICP-MS	0.002	0.0041	N.D.
Nb	ICP-MS	0.004	0.005	0.005
Th	ICP-MS	0.005	0.196	0.145
U	ICP-MS	0.0035	0.248	0.093
Y	ICP-MS	0.015	2.666	1.786
Zr	ICP-MS	0.02	0.045	0.057
La	ICP-MS	0.005	1.082	0.867
Ce	ICP-MS	0.001	3.5873	2.4424
Pr	ICP-MS	0.0015	0.5138	0.3634
Nd	ICP-MS	0.02	2.451	1.692
Sm	ICP-MS	0.01	0.680	0.487
Eu	ICP-MS	0.0035	0.143	0.094
Gd	ICP-MS	0.005	0.670	0.442
Tb	ICP-MS	0.002	0.0988	0.0602
Dy	ICP-MS	0.005	0.533	0.348
Ho	ICP-MS	0.015	0.095	0.067
Er	ICP-MS	0.005	0.253	0.170
Tm	ICP-MS	0.0015	0.0354	0.0234
Yb	ICP-MS	0.004	0.220	0.148
Lu	ICP-MS	0.0015	0.0314	0.0248
Total REE			10.3937	7.2292

	Method	**Detection Limit**	**RC1** continued	**RC2** continued
Li (ppm)	ICP-MS	0.1	2.33	1.60
Be	ICP-MS	0.04	0.06	0.05
Sc	ICP-MS	0.3	1.12	0.63
V	ICP-MS	0.15	0.32	0.20
Mo	ICP-MS	0.025	0.070	0.050
Ba	ICP-MS	0.15	13.19	24.39
Tl	ICP-MS	0.001	0.0021	0.0020
Pb	ICP-MS	0.01	0.575	0.309
Ti	ICP-MS	0.005	0.642	1.936
Cr	ICP-MS	0.02	0.779	0.533
Co	ICP-MS	0.03	0.206	0.226
Ni	ICP-MS	0.4	1.5	1.4
Cu	ICP-MS	0.3	1.28	0.94
Zn	ICP-MS	0.5	5.2	11.1
Ag	ICP-MS	0.15	N.D.	N.D.
Cd	ICP-MS	0.01	0.027	0.031
Sn	ICP-MS	0.02	0.054	0.031
Sb	ICP-MS	0.015	N.D.	N.D.
W	ICP-MS	0.0035	0.017	0.007
Au	ICP-MS	0.05	N.D.	N.D.
Ga	ICP-MS	0.005	0.056	0.068

* blank cells = not analyzed; N.D. = not detected

Appendix 2. continued

Sample			**RC3**	**RC4**
Lithostratigraphic Unit			CIM	CIM
Drill Hole			NI-92-7	NI-92-7
Stratigraphic Height (above basement) (m)			66.54	62.79
Easting (m)			353850	353850
Northing (m)			5443000	5443000
Description			red dolomitic mudstone	red dolomitic mudstone
δ^{13}C (PDB)			0.0	-0.2
δ^{18}O (SMOW)			26.5	25.1
δ^{18}O (PDB)			-4.3	-5.7
	Method	**Detection Limit**		
Al (ppm)	ICP-MS	0.5	103.6	230.1
Fe	ICP-MS	2	32.3	36.2
Mn	ICP-MS	0.4	73.6	39.0
Mg	ICP-MS	250	31,942	32,368
Ca	ICP-MS	1000	54,380	54,180
Cs	ICP-MS	0.0015	0.0130	0.0125
Hf	ICP-MS	0.005	0.006	0.006
Rb	ICP-MS	0.35	N.D.	N.D.
Sr	ICP-MS	10.00	12	13
Ta	ICP-MS	0.002	N.D.	0.0029
Nb	ICP-MS	0.004	0.006	N.D.
Th	ICP-MS	0.005	0.154	0.167
U	ICP-MS	0.0035	0.076	0.078
Y	ICP-MS	0.015	2.203	2.341
Zr	ICP-MS	0.02	0.059	0.056
La	ICP-MS	0.005	0.760	0.869
Ce	ICP-MS	0.001	2.0365	2.6121
Pr	ICP-MS	0.0015	0.3793	0.4351
Nd	ICP-MS	0.02	1.945	2.251
Sm	ICP-MS	0.01	0.591	0.697
Eu	ICP-MS	0.0035	0.100	0.123
Gd	ICP-MS	0.005	0.558	0.663
Tb	ICP-MS	0.002	0.0790	0.0850
Dy	ICP-MS	0.005	0.423	0.475
Ho	ICP-MS	0.015	0.074	0.085
Er	ICP-MS	0.005	0.217	0.241
Tm	ICP-MS	0.0015	0.0310	0.0290
Yb	ICP-MS	0.004	0.182	0.179
Lu	ICP-MS	0.0015	0.0292	0.0276
Total REE			7.4050	8.7718

	Method	**Detection Limit**	**RC3** continued	**RC4** continued
Li (ppm)	ICP-MS	0.1	0.97	2.18
Be	ICP-MS	0.04	N.D.	0.07
Sc	ICP-MS	0.3	0.70	1.15
V	ICP-MS	0.15	N.D.	0.24
Mo	ICP-MS	0.025	0.068	0.070
Ba	ICP-MS	0.15	25.06	32.17
Tl	ICP-MS	0.001	0.0031	0.0012
Pb	ICP-MS	0.01	0.646	0.587
Ti	ICP-MS	0.005	0.800	0.754
Cr	ICP-MS	0.02	0.506	0.658
Co	ICP-MS	0.03	0.175	0.185
Ni	ICP-MS	0.4	1.8	2.0
Cu	ICP-MS	0.3	4.93	0.91
Zn	ICP-MS	0.5	9.1	12.1
Ag	ICP-MS	0.15	N.D.	N.D.
Cd	ICP-MS	0.01	0.034	0.036
Sn	ICP-MS	0.02	0.043	0.056
Sb	ICP-MS	0.015	N.D.	N.D.
W	ICP-MS	0.0035	0.013	0.010
Au	ICP-MS	0.05	N.D.	N.D.
Ga	ICP-MS	0.005	0.048	0.053

* blank cells = not analyzed; N.D. = not detected

Appendix 2. continued

Sample			**RC5**	***RC5***
Lithostratigraphic Unit			CIM	*duplicate*
Drill Hole			NI-92-7	
Stratigraphic Height (above basement) (m)				
Easting (m)			353850	
Northing (m)			5443000	
Description			red dolomitic mudstone	
δ^{13}C (PDB)				
δ^{18}O (SMOW)				
δ^{18}O (PDB)				
	Method	**Detection Limit**		
Al (ppm)	ICP–MS	0.5	157.9	*110.1*
Fe	ICP–MS	2	33.6	*19.2*
Mn	ICP–MS	0.4	39.7	*31.0*
Mg	ICP–MS	250	33,207	*24,190*
Ca	ICP–MS	1000	54,430	*41,180*
Cs	ICP–MS	0.0015	0.0520	*0.0234*
Hf	ICP–MS	0.005	N.D.	*N.D.*
Rb	ICP–MS	0.35	0.4	*N.D.*
Sr	ICP–MS	10.00	13	*11*
Ta	ICP–MS	0.002	0.0039	*N.D.*
Nb	ICP–MS	0.004	N.D.	*N.D.*
Th	ICP–MS	0.005	0.131	*0.088*
U	ICP–MS	0.0035	0.057	*0.080*
Y	ICP–MS	0.015	1.879	*1.479*
Zr	ICP–MS	0.02	0.042	*0.033*
La	ICP–MS	0.005	0.721	*0.583*
Ce	ICP–MS	0.001	1.9733	*1.5923*
Pr	ICP–MS	0.0015	0.3766	*0.2862*
Nd	ICP–MS	0.02	1.928	*1.529*
Sm	ICP–MS	0.01	0.612	*0.464*
Eu	ICP–MS	0.0035	0.130	*0.098*
Gd	ICP–MS	0.005	0.570	*0.437*
Tb	ICP–MS	0.002	0.0711	*0.0599*
Dy	ICP–MS	0.005	0.385	*0.330*
Ho	ICP–MS	0.015	0.067	*0.053*
Er	ICP–MS	0.005	0.162	*0.138*
Tm	ICP–MS	0.0015	0.0237	*0.0169*
Yb	ICP–MS	0.004	0.127	*0.111*
Lu	ICP–MS	0.0015	0.0172	*0.0141*
Total REE			7.1639	5.7124

	Method	**Detection Limit**	**RC5** continued	***RC5*** *duplicate* continued
Li (ppm)	ICP–MS	0.1	1.69	*1.39*
Be	ICP–MS	0.04	N.D.	*0.04*
Sc	ICP–MS	0.3	0.86	*0.68*
V	ICP–MS	0.15	0.23	*N.D.*
Mo	ICP–MS	0.025	N.D.	*N.D.*
Ba	ICP–MS	0.15	67.08	*45.61*
Tl	ICP–MS	0.001	0.0022	*0.0015*
Pb	ICP–MS	0.01	0.255	*0.167*
Ti	ICP–MS	0.005	1.800	*0.810*
Cr	ICP–MS	0.02	0.746	*0.249*
Co	ICP–MS	0.03	0.215	*0.138*
Ni	ICP–MS	0.4	2.0	*0.7*
Cu	ICP–MS	0.3	0.71	*0.50*
Zn	ICP–MS	0.5	11.0	*4.1*
Ag	ICP–MS	0.15	N.D.	N.D.
Cd	ICP–MS	0.01	0.024	*0.014*
Sn	ICP–MS	0.02	N.D.	*N.D.*
Sb	ICP–MS	0.015	N.D.	*N.D.*
W	ICP–MS	0.0035	0.012	*N.D.*
Au	ICP–MS	0.05	N.D.	*N.D.*
Ga	ICP–MS	0.005	0.055	*0.034*

* blank cells = not analyzed; N.D. = not detected

Appendix 2. continued

Sample			**RC6**	**RC7**
Lithostratigraphic Unit			CIM	CIM
Drill Hole			NI-92-7	NI-92-7
Stratigraphic Height (above basement) (m)				
Easting (m)			353850	353850
Northing (m)			5443000	5443000
Description			red dolomitic mudstone	red dolomitic mudstone
$\delta^{13}C$ (PDB)				
$\delta^{18}O$ (SMOW)				
$\delta^{18}O$ (PDB)				
	Method	**Detection Limit**		
Al (ppm)	ICP-MS	0.5	134.3	123.6
Fe	ICP-MS	2	34.4	127.4
Mn	ICP-MS	0.4	26.9	27.9
Mg	ICP-MS	250	30,121	33,252
Ca	ICP-MS	1000	50,690	56,770
Cs	ICP-MS	0.0015	0.0220	0.0239
Hf	ICP-MS	0.005	N.D.	0.005
Rb	ICP-MS	0.35	N.D.	N.D.
Sr	ICP-MS	10.00	13	31
Ta	ICP-MS	0.002	N.D.	0.0060
Nb	ICP-MS	0.004	N.D.	N.D.
Th	ICP-MS	0.005	0.128	0.139
U	ICP-MS	0.0035	0.051	0.083
Y	ICP-MS	0.015	1.705	2.043
Zr	ICP-MS	0.02	0.053	0.058
La	ICP-MS	0.005	0.786	0.907
Ce	ICP-MS	0.001	2.2523	2.4200
Pr	ICP-MS	0.0015	0.3796	0.4062
Nd	ICP-MS	0.02	1.866	1.968
Sm	ICP-MS	0.01	0.498	0.573
Eu	ICP-MS	0.0035	0.092	0.124
Gd	ICP-MS	0.005	0.473	0.594
Tb	ICP-MS	0.002	0.0625	0.0743
Dy	ICP-MS	0.005	0.352	0.410
Ho	ICP-MS	0.015	0.063	0.074
Er	ICP-MS	0.005	0.156	0.219
Tm	ICP-MS	0.0015	0.0183	0.0292
Yb	ICP-MS	0.004	0.138	0.180
Lu	ICP-MS	0.0015	0.0206	0.0282
Total REE			7.1573	8.0069

			RC6 continued	**RC7** continued
	Method	**Detection Limit**		
Li (ppm)	ICP-MS	0.1	1.74	1.27
Be	ICP-MS	0.04	0.07	0.07
Sc	ICP-MS	0.3	0.67	0.85
V	ICP-MS	0.15	N.D.	0.20
Mo	ICP-MS	0.025	N.D.	0.036
Ba	ICP-MS	0.15	29.46	18.29
Tl	ICP-MS	0.001	N.D.	N.D.
Pb	ICP-MS	0.01	0.251	0.597
Ti	ICP-MS	0.005	1.011	1.347
Cr	ICP-MS	0.02	0.362	0.498
Co	ICP-MS	0.03	0.161	0.173
Ni	ICP-MS	0.4	1.1	1.4
Cu	ICP-MS	0.3	0.55	0.74
Zn	ICP-MS	0.5	8.6	11.8
Ag	ICP-MS	0.15	N.D.	N.D.
Cd	ICP-MS	0.01	0.025	0.036
Sn	ICP-MS	0.02	N.D.	N.D.
Sb	ICP-MS	0.015	N.D.	0.015
W	ICP-MS	0.0035	0.007	0.007
Au	ICP-MS	0.05	N.D.	N.D.
Ga	ICP-MS	0.005	0.047	0.048

* blank cells = not analyzed; N.D. = not detected

Appendix 2. continued

Sample			03RM78-1	03RM78-2	03RM78-3
Lithostratigraphic Unit			CIM	CIM	CIM
Drill Hole			NI-92-7	NI-92-7	NI-92-7
Stratigraphic Height (above basement) (m)			61	61	61
Easting (m)			353850	353850	353850
Northing (m)			5443000	5443000	5443000
Description			dolomitic mudstone	dolomitic mudstone	dolomitic mudstone
$\delta^{13}C$ (PDB)			-1.63	-1.48	-1.48
$\delta^{18}O$ (SMOW)			23.92	23.88	24.37
$\delta^{18}O$ (PDB)			-6.8	-6.8	-6.4
	Method	Detection Limit			
Al (ppm)	ICP-AES	0.06	594.87	340.96	205.79
Ba	ICP-AES	0.006	215.044	95.351	65.430
Ca	ICP-AES	0.01	145317	127396	99987
Fe	ICP-AES	0.02	447.61	289.74	255.27
K	ICP-AES	0.25	1683.009	221.156	226.261
Mg	ICP-AES	0.01	88701	79241	60087
Mn	ICP-AES	0.003	136.283	84.846	65.282
Na	ICP-AES	0.01	753.10	120.15	188.28
P	ICP-AES	0.1	59.3	65.0	55.0
S	ICP-AES	0.1	597.5	137.9	71.4
Si	ICP-AES	0.025	1351.50	189.47	137.02
Sr	ICP-AES	0.005	63.186	29.988	22.033
V	ICP-AES	0.03	3.01	4.90	N.D.
Mn/Sr			2.16	2.83	2.96
Fe/Sr			7.08	9.66	11.59
Ca/Mg			1.64	1.61	1.66
Ca/Sr			2299.83	4248.27	4538.11
Al (ppm)	ICP-MS	0.5			186
Fe	ICP-MS	2			131
Mn	ICP-MS	0.4			53.1
Mg	ICP-MS	250			>20000
Ca	ICP-MS	1000			72,600
Cs	ICP-MS	0.0015			0.0229
Hf	ICP-MS	0.005			0.00634
Rb	ICP-MS	0.35			N.D.
Sr	ICP-MS	10.00			17.3
Ta	ICP-MS	0.002			N.D.
Nb	ICP-MS	0.004			N.D.
Th	ICP-MS	0.005			0.328
U	ICP-MS	0.0035			0.102
Y	ICP-MS	0.015			2.86
Zr	ICP-MS	0.02			0.0702
La	ICP-MS	0.005			1.15
Ce	ICP-MS	0.001			3.86
Pr	ICP-MS	0.0015			0.580
Nd	ICP-MS	0.02			2.94
Sm	ICP-MS	0.01			0.948
Eu	ICP-MS	0.0035			0.184
Gd	ICP-MS	0.005			0.863
Tb	ICP-MS	0.002			0.113
Dy	ICP-MS	0.005			0.597
Ho	ICP-MS	0.015			0.101
Er	ICP-MS	0.005			0.262
Tm	ICP-MS	0.0015			0.0337
Yb	ICP-MS	0.004			0.220
Lu	ICP-MS	0.0015			0.0322
Total REE					11.8839

	Method	Detection Limit	03RM78-3 continued
Li (ppm)	ICP-MS	0.1	1.61
Be	ICP-MS	0.04	0.0580
Sc	ICP-MS	0.3	1.17
V	ICP-MS	0.15	1.66
Mo	ICP-MS	0.025	0.278
Ba	ICP-MS	0.15	48.9
Tl	ICP-MS	0.001	0.00195
Pb	ICP-MS	0.01	0.984
Ti	ICP-MS	0.005	1.91
Cr	ICP-MS	0.02	0.899
Co	ICP-MS	0.03	0.232
Ni	ICP-MS	0.4	2.25
Cu	ICP-MS	0.3	2.83
Zn	ICP-MS	0.5	8.32
Ag	ICP-MS	0.15	N.D.
Cd	ICP-MS	0.01	N.D.
Sn	ICP-MS	0.02	N.D.
Sb	ICP-MS	0.015	N.D.
W	ICP-MS	0.0035	0.00634
Au	ICP-MS	0.05	N.D.
Ga	ICP-MS	0.005	0.0620

* blank cells = not analyzed; N.D. = not detected

Appendix 2. continued

Sample			**03RM78-4**	**03RM78-5**	**03RM78-6**	**03RM78-7**	**03RM30-1**	**03RM30-2**	**03RM30-3**
Lithostratigraphic Unit			CIM	CIM	CIM	CIM	CIM	CIM	CIM
Drill Hole			NI-92-7	NI-92-7	NI-92-7	NI-92-7	NI-92-7	NI-92-7	NI-92-7
Stratigraphic Height (above basement) (m)			61	61	61	61	37.76	37.76	37.76
Easting (m)			353850	353850	353850	353850	353850	353850	353850
Northing (m)			5443000	5443000	5443000	5443000	5443000	5443000	5443000
Description			dolomitic mudstone	dolomitic mudstone	dolomitic mudstone	dolomitic mudstone	dolomitic mudstone	dolomitic mudstone	dolomitic mudstone
$\delta^{13}C$ (PDB)			-1.60	-1.63	-1.47	-1.53	-2.37	-2.36	-2.26
$\delta^{18}O$ (SMOW)			24.08	23.82	23.63	23.74	24.82	24.62	23.92
$\delta^{18}O$ (PDB)			-6.6	-6.9	-7.1	-7.0	-5.9	-6.1	-6.8
	Method	**Detection Limit**							
Al (ppm)	ICP-AES	0.06		70.12	81.38	419.23	566.49	395.73	
Ba	ICP-AES	0.006		36.510	36.803	83.602	108.245	461.663	
Ca	ICP-AES	0.01		128555	126112	126357	129529	139817	
Fe	ICP-AES	0.02		226.46	200.70	291.01	333.11	347.69	
K	ICP-AES	0.25		45.668	56.990	208.221	524.691	615.935	
Mg	ICP-AES	0.01		79311	78169	78656	80944	84408	
Mn	ICP-AES	0.003		84.134	84.706	91.381	162.081	213.395	
Na	ICP-AES	0.01		90.82	82.03	128.73	112.43	414.09	
P	ICP-AES	0.1		59.7	50.4	58.9	22.5	96.3	
S	ICP-AES	0.1		260.1	368.7	195.0	79.6	246.7	
Si	ICP-AES	0.025		40.82	54.70	263.20	576.28	220.09	
Sr	ICP-AES	0.005		26.757	27.327	31.028	32.451	49.423	
V	ICP-AES	0.03		4.73	4.90	5.28	4.10	N.D.	
Mn/Sr				3.14	3.10	2.95	4.99	4.32	
Fe/Sr				8.46	7.34	9.38	10.26	7.04	
Ca/Mg				1.62	1.61	1.61	1.60	1.66	
Ca/Sr				4804.48	4614.99	4072.39	3991.46	2829.02	

* blank cells = not analyzed; N.D. = not detected

Appendix 2. continued

Sample			03RM30-4	*03RM30-4*	*03RM30-4*
Lithostratigraphic Unit			CIM	*duplicate*	*duplicate*
Drill Hole			NI-92-7		
Stratigraphic Height (above basement) (m)			37.76		
Easting (m)			353850		
Northing (m)			5443000		
Description			dolomitic mudstone		
$\delta^{13}C$ (PDB)			-2.27		
$\delta^{18}O$ (SMOW)			22.28		
$\delta^{18}O$ (PDB)			-8.4		
	Method	**Detection Limit**			
Al (ppm)	ICP-AES	0.06	221.63		
Ba	ICP-AES	0.006	460.848		
Ca	ICP-AES	0.01	137470		
Fe	ICP-AES	0.02	327.68		
K	ICP-AES	0.25	479.068		
Mg	ICP-AES	0.01	81452		
Mn	ICP-AES	0.003	568.567		
Na	ICP-AES	0.01	301.11		
P	ICP-AES	0.1	39.9		
S	ICP-AES	0.1	286.4		
Si	ICP-AES	0.025	100.76		
Sr	ICP-AES	0.005	63.978		
V	ICP-AES	0.03	8.69		
Mn/Sr			8.89		
Fe/Sr			5.12		
Ca/Mg			1.69		
Ca/Sr			2148.72		
Al (ppm)	ICP-MS	0.5	105	*105*	*101*
Fe	ICP-MS	2	97.4	*99.1*	*99.3*
Mn	ICP-MS	0.4	334	*333*	*324*
Mg	ICP-MS	250	>20000	*20000*	*20000*
Ca	ICP-MS	1000	75,800	*73,900*	*63,000*
Cs	ICP-MS	0.0015	0.0319	*0.0278*	*0.0301*
Hf	ICP-MS	0.005	0.0106	*0.0100*	*0.0110*
Rb	ICP-MS	0.35	0.391	*0.380*	*0.351*
Sr	ICP-MS	10.00	41.4	*41.6*	*41.6*
Ta	ICP-MS	0.002	N.D.	*N.D.*	*N.D.*
Nb	ICP-MS	0.004	0.00435	*0.0115*	*0.00766*
Th	ICP-MS	0.005	0.205	*0.204*	*0.214*
U	ICP-MS	0.0035	0.0309	*0.0306*	*0.0306*
Y	ICP-MS	0.015	4.83	*4.88*	*4.83*
Zr	ICP-MS	0.02	0.0536	*0.0522*	*0.0555*
La	ICP-MS	0.005	0.892	*0.886*	*0.913*
Ce	ICP-MS	0.001	2.63	*2.72*	*2.75*
Pr	ICP-MS	0.0015	0.699	*0.718*	*0.726*
Nd	ICP-MS	0.02	4.59	*4.71*	*4.60*
Sm	ICP-MS	0.01	2.00	*2.05*	*2.05*
Eu	ICP-MS	0.0035	0.378	*0.380*	*0.375*
Gd	ICP-MS	0.005	1.79	*1.74*	*1.73*
Tb	ICP-MS	0.002	0.216	*0.212*	*0.208*
Dy	ICP-MS	0.005	1.00	*0.990*	*1.04*
Ho	ICP-MS	0.015	0.162	*0.155*	*0.159*
Er	ICP-MS	0.005	0.395	*0.358*	*0.364*
Tm	ICP-MS	0.0015	0.0473	*0.0435*	*0.0474*
Yb	ICP-MS	0.004	0.262	*0.267*	*0.264*
Lu	ICP-MS	0.0015	0.0357	*0.0344*	*0.0330*
Total REE			15.0970	15.2639	15.2594

			03RM30-4	*03RM30-4*	*03RM30-4*
				duplicate	*duplicate*
			continued	continued	continued
	Method	**Detection Limit**			
Li (ppm)	ICP-MS	0.1	0.863	*0.823*	*0.667*
Be	ICP-MS	0.04	N.D.	*0.0440*	*0.0502*
Sc	ICP-MS	0.3	0.696	*0.664*	*0.520*
V	ICP-MS	0.15	2.42	*2.52*	*2.51*
Mo	ICP-MS	0.025	0.306	*0.271*	*0.240*
Ba	ICP-MS	0.15	357	*355*	*360*
Tl	ICP-MS	0.001	0.00193	*0.00191*	*0.00287*
Pb	ICP-MS	0.01	1.23	*1.22*	*1.27*
Ti	ICP-MS	0.005	2.45	*2.04*	*2.23*
Cr	ICP-MS	0.02	0.709	*0.866*	*0.894*
Co	ICP-MS	0.03	0.713	*0.712*	*0.725*
Ni	ICP-MS	0.4	3.79	*3.82*	*4.44*
Cu	ICP-MS	0.3	2.68	*2.75*	*2.75*
Zn	ICP-MS	0.5	19.0	*19.5*	*17.3*
Ag	ICP-MS	0.15	N.D.	*N.D.*	*N.D.*
Cd	ICP-MS	0.01	0.0271	*0.0144*	*0.0153*
Sn	ICP-MS	0.02	0.0246	*0.0230*	*N.D.*
Sb	ICP-MS	0.015	0.0193	*0.0177*	*0.0167*
W	ICP-MS	0.0035	0.0261	*0.0335*	*0.0124*
Au	ICP-MS	0.05	N.D.	*N.D.*	*N.D.*
Ga	ICP-MS	0.005	0.0739	*0.0818*	*0.0885*

* blank cells = not analyzed; N.D. = not detected

Appendix 2. continued

Sample			03RM32	03RM33
Lithostratigraphic Unit			CIM	CIM
Drill Hole			NI-92-7	NI-92-7
Stratigraphic Height (above basement) (m)			49.82	52.39
Easting (m)			353850	353850
Northing (m)			5443000	5443000
Description			dolomitic mudstone	dolomitic mudstone
$\delta^{13}C$ (PDB)			-2.44	-2.14
$\delta^{18}O$ (SMOW)			23.45	23.90
$\delta^{18}O$ (PDB)			-7.2	-6.8
	Method	Detection Limit		
Al (ppm)	ICP-AES	0.06	157.39	241.67
Ba	ICP-AES	0.006	75.802	69.729
Ca	ICP-AES	0.01	137017	134959
Fe	ICP-AES	0.02	302.79	283.19
K	ICP-AES	0.25	335.9	293.3
Mg	ICP-AES	0.01	83352	83353
Mn	ICP-AES	0.003	123.570	109.972
Na	ICP-AES	0.01	319.32	259.47
P	ICP-AES	0.1	80.5	71.5
S	ICP-AES	0.1	140.7	142.7
Si	ICP-AES	0.025	98.26	169.30
Sr	ICP-AES	0.005	28.452	25.855
V	ICP-AES	0.03	4.67	4.49
Mn/Sr			4.34	4.25
Fe/Sr			10.64	10.95
Ca/Mg			1.64	1.62
Ca/Sr			4815.73	5219.89
Al (ppm)	ICP-MS	0.5	98.8	141
Fe	ICP-MS	2	101	99.1
Mn	ICP-MS	0.4	76.7	78.5
Mg	ICP-MS	250	>20000	>20000
Ca	ICP-MS	1000	72,200	81,700
Cs	ICP-MS	0.0015	0.0259	0.0285
Hf	ICP-MS	0.005	0.00829	0.0100
Rb	ICP-MS	0.35	0.356	0.397
Sr	ICP-MS	10.00	18.9	18.9
Ta	ICP-MS	0.002	N.D.	N.D.
Nb	ICP-MS	0.004	0.0122	0.00800
Th	ICP-MS	0.005	0.300	0.316
U	ICP-MS	0.0035	0.0800	0.0700
Y	ICP-MS	0.015	2.80	2.96
Zr	ICP-MS	0.02	0.0585	0.0630
La	ICP-MS	0.005	1.07	1.18
Ce	ICP-MS	0.001	3.40	3.58
Pr	ICP-MS	0.0015	0.560	0.574
Nd	ICP-MS	0.02	2.79	2.97
Sm	ICP-MS	0.01	0.856	0.900
Eu	ICP-MS	0.0035	0.189	0.174
Gd	ICP-MS	0.005	0.790	0.845
Tb	ICP-MS	0.002	0.106	0.113
Dy	ICP-MS	0.005	0.583	0.602
Ho	ICP-MS	0.015	0.107	0.104
Er	ICP-MS	0.005	0.249	0.261
Tm	ICP-MS	0.0015	0.0332	0.0340
Yb	ICP-MS	0.004	0.213	0.221
Lu	ICP-MS	0.0015	0.0307	0.0320
Total REE			10.9769	11.5900

			03RM32 continued	03RM33 continued
	Method	Detection Limit		
Li (ppm)	ICP-MS	0.1	1.24	1.37
Be	ICP-MS	0.04	N.D.	0.0535
Sc	ICP-MS	0.3	0.846	1.07
V	ICP-MS	0.15	1.80	1.45
Mo	ICP-MS	0.025	0.0854	0.0620
Ba	ICP-MS	0.15	62.6	57.1
Tl	ICP-MS	0.001	0.00146	0.00250
Pb	ICP-MS	0.01	0.575	0.604
Ti	ICP-MS	0.005	2.72	2.59
Cr	ICP-MS	0.02	1.03	1.18
Co	ICP-MS	0.03	0.395	0.387
Ni	ICP-MS	0.4	1.62	1.86
Cu	ICP-MS	0.3	0.966	3.25
Zn	ICP-MS	0.5	1.50	3.52
Ag	ICP-MS	0.15	N.D.	N.D.
Cd	ICP-MS	0.01	N.D.	0.0200
Sn	ICP-MS	0.02	0.0278	N.D.
Sb	ICP-MS	0.015	N.D.	N.D.
W	ICP-MS	0.0035	0.0239	0.0155
Au	ICP-MS	0.05	N.D.	N.D.
Ga	ICP-MS	0.005	0.0585	0.0640

* blank cells = not analyzed; N.D. = not detected

Appendix 2. continued

Sample			**03RM34**	**03RM35**	**03RM44**
Lithostratigraphic Unit			CIM	CIM	CIM
Drill Hole			NI-92-7	NI-92-7	NI-92-7
Stratigraphic Height (above basement) (m)			71.97	86.93	64
Easting (m)			353850	353850	353850
Northing (m)			5443000	5443000	5443000
Description			dolomitic mudstone	dolomitic mudstone	dolomitic mudstone
$\delta^{13}C$ (PDB)			-0.36	0.8	-1.26
$\delta^{18}O$ (SMOW)			24.62	26.4	23.54
$\delta^{18}O$ (PDB)			-6.1	-4.4	-7.2
	Method	**Detection Limit**			
Al (ppm)	ICP–AES	0.06	319.85		
Ba	ICP–AES	0.006	54.230		
Ca	ICP–AES	0.01	157789		
Fe	ICP–AES	0.02	349.35		
K	ICP–AES	0.25	461.5		
Mg	ICP–AES	0.01	91516		
Mn	ICP–AES	0.003	400.976		
Na	ICP–AES	0.01	424.62		
P	ICP–AES	0.1	68.2		
S	ICP–AES	0.1	5344.1		
Si	ICP–AES	0.025	187.85		
Sr	ICP–AES	0.005	53.796		
V	ICP–AES	0.03	5.64		
Mn/Sr			7.45		
Fe/Sr			6.49		
Ca/Mg			1.72		
Ca/Sr			2933.10		
Al (ppm)	ICP–MS	0.5	155	53.3	
Fe	ICP–MS	2	105	163	
Mn	ICP–MS	0.4	187	159	
Mg	ICP–MS	250	>20000	19,700	
Ca	ICP–MS	1000	65,700	31,400	
Cs	ICP–MS	0.0015	0.0365	0.00773	
Hf	ICP–MS	0.005	0.00700	N.D.	
Rb	ICP–MS	0.35	0.408	N.D.	
Sr	ICP–MS	10.00	29.7	14.7	
Ta	ICP–MS	0.002	N.D.	N.D.	
Nb	ICP–MS	0.004	0.00800	N.D.	
Th	ICP–MS	0.005	0.266	0.119	
U	ICP–MS	0.0035	0.0695	0.0372	
Y	ICP–MS	0.015	2.57	1.64	
Zr	ICP–MS	0.02	0.0725	0.0304	
La	ICP–MS	0.005	0.907	0.619	
Ce	ICP–MS	0.001	3.01	1.34	
Pr	ICP–MS	0.0015	0.505	0.320	
Nd	ICP–MS	0.02	2.54	1.53	
Sm	ICP–MS	0.01	0.829	0.512	
Eu	ICP–MS	0.0035	0.166	0.0918	
Gd	ICP–MS	0.005	0.746	0.452	
Tb	ICP–MS	0.002	0.0980	0.0604	
Dy	ICP–MS	0.005	0.515	0.331	
Ho	ICP–MS	0.015	0.0895	0.0560	
Er	ICP–MS	0.005	0.233	0.148	
Tm	ICP–MS	0.0015	0.0275	0.0184	
Yb	ICP–MS	0.004	0.198	0.128	
Lu	ICP–MS	0.0015	0.0265	0.0169	
Total REE			9.8905	5.6235	

			03RM34 continued	**03RM35** continued
	Method	**Detection Limit**		
Li (ppm)	ICP–MS	0.1	1.14	0.501
Be	ICP–MS	0.04	N.D.	N.D.
Sc	ICP–MS	0.3	0.880	0.571
V	ICP–MS	0.15	2.26	0.305
Mo	ICP–MS	0.025	0.335	0.0353
Ba	ICP–MS	0.15	54.6	58.8
Tl	ICP–MS	0.001	0.00250	N.D.
Pb	ICP–MS	0.01	0.869	0.902
Ti	ICP–MS	0.005	2.46	0.610
Cr	ICP–MS	0.02	0.938	0.391
Co	ICP–MS	0.03	0.347	0.292
Ni	ICP–MS	0.4	2.57	1.77
Cu	ICP–MS	0.3	3.79	2.63
Zn	ICP–MS	0.5	8.97	8.79
Ag	ICP–MS	0.15	N.D.	N.D.
Cd	ICP–MS	0.01	0.0155	0.0111
Sn	ICP–MS	0.02	0.0235	0.0357
Sb	ICP–MS	0.015	N.D.	N.D.
W	ICP–MS	0.0035	0.0210	0.0140
Au	ICP–MS	0.05	N.D.	N.D.
Ga	ICP–MS	0.005	0.0880	0.0343

* blank cells = not analyzed, N.D. = not detected

Appendix 2. continued

Sample			**03RM30-5**	**03RM30-6**	**03RM30-7**	**04RM30**	**04RM31**	**04RM32**	**04RM33**	**04RM34**
Lithostratigraphic Unit			CIM	CIM	CIM	CIM	CIM	CIM	CIM	CIM
Drill Hole			NI-92-7	NI-92-7	NI-92-7	NI-92-7	NI-92-7	NI-92-7	NI-92-7	NI-92-7
Stratigraphic Height (above basement) (m)			37.76	37.76	37.76	51	67	55	65	53
Easting (m)			353850	353850	353850	353850	353850	353850	353850	353850
Northing (m)			5443000	5443000	5443000	5443000	5443000	5443000	5443000	5443000
Description			dolomitic mudstone	dolomitic mudstone	dolomitic mudstone	dolomitic mudstone	dolomitic mudstone	dolomitic mudstone	dolomitic mudstone	dolomitic mudstone
δ^{13}C (PDB)			-2.33	-2.29	-2.24	-2.8	-1.2	-2.5	-1.6	-1.0
δ^{18}O (SMOW)			24.49	23.91	24.45	24.0	23.2	23.5	24.7	24.4
δ^{18}O (PDB)			-6.2	-6.8	-6.3	-6.7	-7.5	-7.2	-6.0	-6.3
^{87}Sr/^{86}Sr							0.708288	0.70704		
2σ							0.000016	0.000021		
	Method	**Detection Limit**								
Al (ppm)	ICP-AES	0.06	133.74	112.65	391.02	187.91	277.22	133.11	149.28	119.78
Ba	ICP-AES	0.006	162.481	136.265	208.638	18.349	362.556	71.754	141.124	13.750
Ca	ICP-AES	0.01	135887	128183	129009	124325	141741	95336	133891	135891
Fe	ICP-AES	0.02	291.06	248.55	262.14	195.89	345.67	210.13	261.07	281.12
K	ICP-AES	0.25	266.9	163.7	294.6	138.3	126.4	106.3	97.3	81.9
Mg	ICP-AES	0.01	83457	78459	78915	81370	84444	58188	81448	81409
Mn	ICP-AES	0.003	214.715	191.432	150.839	79.770	161.556	66.930	70.693	105.216
Na	ICP-AES	0.01	228.04	101.86	86.38	74.74	97.33	53.55	94.12	77.37
P	ICP-AES	0.1	44.8	25.7	19.6	54.4	122.4	52.6	65.9	64.5
S	ICP-AES	0.1	96.5	49.3	64.7	8.7	79.6	135.1	36.4	25.0
Si	ICP-AES	0.025	91.68	138.30	431.49	113.01	133.44	91.54	99.14	85.39
Sr	ICP-AES	0.005	35.901	31.324	36.426	26.142	47.111	98.553	31.320	29.526
V	ICP-AES	0.03	5.16	4.49	4.20	4.76	6.00	4.21	4.86	5.78
Mn/Sr			5.98	6.11	4.14	3.05	3.43	0.68	2.26	3.56
Fe/Sr			8.11	7.93	7.20	7.49	7.34	2.13	8.34	9.52
Ca/Mg			1.63	1.63	1.63	1.53	1.68	1.64	1.64	1.67
Ca/Sr			3785.02	4092.21	3541.62	4755.75	3008.65	967.36	4274.91	4602.44

* blank cells = not analyzed; N.D. = not detected

Appendix 2. continued

Sample			**04RM2**	**04RM4**
Lithostratigraphic Unit			CIM	CIM
Drill Hole			NI-92-7	NI-92-7
Stratigraphic Height (above basement) (m)			47.69	72.45
Easting (m)			353850	353850
Northing (m)			5443000	5443000
Description			dolomitic mudstone	dolomitic mudstone
δ^{13}C (PDB)			-2.9	0.0
δ^{18}O (SMOW)			23.4	25.7
δ^{18}O (PDB)			-7.2	-5.1
^{87}Sr/^{86}Sr			0.706455	
2σ			0.000014	
	Method	**Detection Limit**		
Al (ppm)	ICP-AES	0.06	80.94	70.84
Ba	ICP-AES	0.006	7.862	37.511
Ca	ICP-AES	0.01	140294	136062
Fe	ICP-AES	0.02	259.81	182.62
K	ICP-AES	0.25	35.3	52.7
Mg	ICP-AES	0.01	84949	83025
Mn	ICP-AES	0.003	103.459	303.207
Na	ICP-AES	0.01	51.70	84.98
P	ICP-AES	0.1	39.1	48.5
S	ICP-AES	0.1	90.1	539.7
Si	ICP-AES	0.025	41.38	44.43
Sr	ICP-AES	0.005	23.396	61.561
V	ICP-AES	0.03	3.90	3.46
Mn/Sr			4.42	4.93
Fe/Sr			11.10	2.97
Ca/Mg			1.65	1.64
Ca/Sr			5996.42	2210.19
Al (ppm)	ICP-MS	0.5	59.4	36.1
Fe	ICP-MS	2	63.6	34.5
Mn	ICP-MS	0.4	87.1	159
Mg	ICP-MS	250	>20000	>20000
Ca	ICP-MS	1000	84,000	48,400
Cs	ICP-MS	0.0015	0.0158	0.00758
Hf	ICP-MS	0.005	0.00887	N.D.
Rb	ICP-MS	0.35	N.D.	N.D.
Sr	ICP-MS	10.00	17.8	12.5
Ta	ICP-MS	0.002	N.D.	N.D.
Nb	ICP-MS	0.004	0.00493	0.00404
Th	ICP-MS	0.005	0.237	0.146
U	ICP-MS	0.0035	0.0581	0.0273
Y	ICP-MS	0.015	3.11	1.49
Zr	ICP-MS	0.02	0.0665	0.0268
La	ICP-MS	0.005	1.48	0.507
Ce	ICP-MS	0.001	2.78	1.62
Pr	ICP-MS	0.0015	0.708	0.282
Nd	ICP-MS	0.02	3.64	1.45
Sm	ICP-MS	0.01	1.10	0.442
Eu	ICP-MS	0.0035	0.214	0.0924
Gd	ICP-MS	0.005	0.963	0.409
Tb	ICP-MS	0.002	0.128	0.0586
Dy	ICP-MS	0.005	0.659	0.308
Ho	ICP-MS	0.015	0.103	0.0556
Er	ICP-MS	0.005	0.279	0.141
Tm	ICP-MS	0.0015	0.0360	0.0162
Yb	ICP-MS	0.004	0.202	0.122
Lu	ICP-MS	0.0015	0.0286	0.0167
Total REE			12.3206	5.5205

	Method	**Detection Limit**	**04RM2** continued	**04RM4** continued
Li (ppm)	ICP-MS	0.1	1.12	0.592
Be	ICP-MS	0.04	N.D.	0.0465
Sc	ICP-MS	0.3	0.910	0.319
V	ICP-MS	0.15	1.23	0.345
Mo	ICP-MS	0.025	0.0764	0.0566
Ba	ICP-MS	0.15	8.27	8.21
Tl	ICP-MS	0.001	0.00148	0.00202
Pb	ICP-MS	0.01	1.67	1.24
Ti	ICP-MS	0.005	1.42	0.771
Cr	ICP-MS	0.02	0.738	0.406
Co	ICP-MS	0.03	0.395	0.225
Ni	ICP-MS	0.4	3.86	2.37
Cu	ICP-MS	0.3	2.26	0.913
Zn	ICP-MS	0.5	13.2	9.09
Ag	ICP-MS	0.15	N.D.	N.D.
Cd	ICP-MS	0.01	0.0192	N.D.
Sn	ICP-MS	0.02	0.0483	N.D.
Sb	ICP-MS	0.015	N.D.	N.D.
W	ICP-MS	0.0035	0.0133	0.00960
Au	ICP-MS	0.05	N.D.	N.D.
Ga	ICP-MS	0.005	0.0453	0.0364

* blank cells = not analyzed; N.D. = not detected

Appendix 2. continued

Sample			**NB-97-4-0**	**NB-97-4-1**	**NB-97-4-2**	**NB-97-4-2**	**NB-97-4-3**	**NB-97-4-4**	**NB-97-4-5**	**NB-97-4-6**	**NB-97-4-7**
Lithostratigraphic Unit			CIM	CIM	CIM	CIM	CIM	CIM	CIM	CIM	CIM
Drill Hole			NB-97-4	NB-97-4	NB-97-4	NB-97-4	NB-97-4	NB-97-4	NB-97-4	NB-97-4	NB-97-4
Stratigraphic Height (above basement) (m)			25.53	25.4	27.02	27.02	30.16	31.48	32.78	34.5	36.12
Easting (m)			425430	425430	425430	425430	425430	425430	425430	425430	425430
Northing (m)			5410540	5410540	5410540	5410540	5410540	5410540	5410540	5410540	5410540
Description			dolo mudstone	dolo mudstone	dolo mudstone	red dolo mudstone	dolo mudstone	dolo mudstone	dolo mudstone	dolo mudstone	dolo mudstone
$\delta^{13}C$ (PDB)			-3.1	-2.8	-3.2	-3.3	-2.5	-2.5	-2.2	-2.2	-2.6
$\delta^{18}O$ (SMOW)			23.9	24.3	23.1	23.8	24.4	24.1	24.1	24.8	24.8
$\delta^{18}O$ (PDB)			-6.8	-6.4	-7.5	-6.9	-6.3	-6.6	-6.6	-5.9	-6.0
	Method	**Detection Limit**									
Al (ppm)	ICP-AES	0.06	30.66	73.36	68.23		104.10	72.95	75.25	24.57	82.60
Ba	ICP-AES	0.006	4.805	3.512	10.160		131.530	2.856	15.688	3.400	31.154
Ca	ICP-AES	0.01	115129	133429	131818		133054	130567	128357	132956	136239
Fe	ICP-AES	0.02	229.14	261.09	233.56		257.26	221.81	266.69	168.54	229.72
K	ICP-AES	0.25	691.6	38.2	N.D.		38.1	24.9	30.8	59.0	92.2
Mg	ICP-AES	0.01	70548	80926	80777		82134	79949	79988	83253	83752
Mn	ICP-AES	0.003	128.345	171.683	139.532		111.901	141.537	187.438	105.266	112.780
Na	ICP-AES	0.01	522.99	132.50	179.93		266.69	197.30	207.63	61.06	25.24
P	ICP-AES	0.1	96.0	66.2	92.8		128.4	86.2	97.9	38.7	53.9
S	ICP-AES	0.1	6.9	12.0	N.D.		18.2	N.D.	N.D.	56.0	N.D.
Si	ICP-AES	0.025	34.25	96.27	80.79		108.50	78.61	66.25	17.50	50.15
Sr	ICP-AES	0.005	21.229	22.241	24.507		36.631	23.364	24.500	23.165	27.382
V	ICP-AES	0.03	2.80	3.29	3.26		4.33	4.36	4.81	4.42	5.20
Mn/Sr			6.05	7.72	5.69		3.05	6.06	7.65	4.54	4.12
Fe/Sr			10.79	11.74	9.53		7.02	9.49	10.89	7.28	8.39
Ca/Mg			1.63	1.65	1.63		1.62	1.63	1.60	1.60	1.63
Ca/Sr			5423.26	5999.29	5378.69		3632.32	5588.26	5239.08	5739.46	4975.46

Sample			**NB-97-4-8**	**NB-97-4-9**	**NB-97-4-10**	**NB-97-4-11**	**NB-97-4-12**	**NB-97-4-13**	**NB-97-4-14**	**NB-97-4-15**
Lithostratigraphic Unit			CIM	CIM	CIM	CIM	CIM	CIM	CIM	CIM
Drill Hole			NB-97-4	NB-97-4	NB-97-4	NB-97-4	NB-97-4	NB-97-4	NB-97-4	NB-97-4
Stratigraphic Height (above basement) (m)			37.8	38.45	39.68	40.98	41.92	42.57	45.01	28.34
Easting (m)			425430	425430	425430	425430	425430	425430	425430	425430
Northing (m)			5410540	5410540	5410540	5410540	5410540	5410540	5410540	5410540
Description			dolo	dolo	dolo	dolo	dolo	dolo	dolo	dolo
$\delta^{13}C$ (PDB)			-1.5	-1.6	-1.2	-0.9	-0.8	-1.3	-1.6	-2.9
$\delta^{18}O$ (SMOW)			23.9	25.0	25.0	24.8	24.0	24.6	24.8	24.0
$\delta^{18}O$ (PDB)			-6.8	-5.7	-5.7	-6.0	-6.7	-6.2	-5.9	-6.7
Al (ppm)	ICP-AES	0.06	56.54	46.46	63.56	33.28	54.35	17.38	133.50	56.42
Ba	ICP-AES	0.006	12.181	34.280	320.063	218.647	148.586	24.603	22.211	8.175
Ca	ICP-AES	0.01	131199	133377	132578	132899	135463	129466	126291	121898
Fe	ICP-AES	0.02	198.70	208.15	218.08	225.46	206.70	198.77	237.30	255.68
K	ICP-AES	0.25	84.8	82.4	106.7	57.7	129.7	N.D.	N.D.	N.D
Mg	ICP-AES	0.01	80606	82804	81619	80160	81643	81557	78447	76581
Mn	ICP-AES	0.003	139.717	81.257	90.709	93.133	161.257	94.682	79.368	112.919
Na	ICP-AES	0.01	104.87	59.33	104.25	120.40	146.70	114.38	298.76	347.92
P	ICP-AES	0.1	54.8	43.4	63.6	53.1	39.1	69.5	135.2	76.8
S	ICP-AES	0.1	2.8	9.6	121.2	47.5	N.D.	81.8	211.1	161.6
Si	ICP-AES	0.025	37.85	44.07	43.65	14.24	28.06	9.67	77.82	33.84
Sr	ICP-AES	0.005	24.023	28.256	66.016	44.812	39.162	21.319	22.312	20.351
V	ICP-AES	0.03	6.12	4.51	5.10	5.21	4.92	3.95	4.03	3.43
Mn/Sr			5.82	2.88	1.37	2.08	4.12	4.44	3.56	5.55
Fe/Sr			8.27	7.37	3.30	5.03	5.28	9.32	10.64	12.56
Ca/Mg			1.63	1.61	1.62	1.66	1.66	1.59	1.61	1.59
Ca/Sr			5461.48	4720.35	2008.27	2965.70	3459.01	6072.93	5660.28	5989.91

* blank cells = not analyzed; N.D. = not detected

Appendix 3

Whole Rock Analyses of Sibley Group Shale Samples from Diamond-Drill Hole NB-97-4

Note:
Universal Transverse Mercator (UTM) co-ordinates are North American Datum 1927 (NAD 27), Zone 16.

Appendix 3. Whole rock analyses of Sibley Group shale samples from diamond-drill hole NB-97-4.

Laboratory			Geoscience Laboratories			
Sample			**Nb-97-4-16**	**Nb-97-4-17**	**Nb-97-4-18**	**Nb-97-4-19**
Lithostratigraphic Unit			Pass Lake Fm.	Pass Lake Fm.	Fire Hill Mbr.	Fire Hill Mbr.
Drill Hole			NB-97-4	NB-97-4	NB-97-4	NB-97-4
Stratigraphic Height (above Sibley) (m)			24.15	14.9	47.7	67.15
Easting (m)			425430	425430	425430	425430
Northing (m)			5410540	5410540	5410540	5410540
Description			red silty mudstone	purple mudstone	red mudstone	red mudstone
	Method	**Detection Limit**				
SiO_2 (weight %)	XRF	0.01	25.42	42.32	40.64	30.63
TiO_2	XRF	0.01	0.19	0.23	0.35	0.26
Al_2O_3	XRF	0.01	5.34	8.16	11.03	6.9
Fe_2O_3	XRF	0.01	1.89	1.97	4.03	2.52
MnO	XRF	0.01	0.02	0.03	0.03	0.04
MgO	XRF	0.01	15.09	15.91	9.62	12.51
CaO	XRF	0.01	19.84	11.82	10.42	15.97
K_2O	XRF	0.01	1.46	3.5	4.86	3.07
Na_2O	XRF	0.01	0.05	0.11	0.07	0.07
P_2O_5	XRF	0.01	0.05	0.05	0.07	0.08
LOI		0.05	29.76	14.82	18.77	26.7
Total			99.11	98.92	99.89	98.75
Cr (ppm)	XRF	4	33	39	45	64
Nb	XRF	2	6	8	8	7
Ni	XRF	2	8	12	11	11
Rb	XRF	2	52	79	94	91
Sc	XRF	6	18	15	19	19
Sr	XRF	2	56	82	60	63
V	XRF	4	35	44	51	45
Y	XRF	1	10	20	13	14
Zr	XRF	3	58	118	111	102
Cs	ICP-MS	0.007	3.095	4.801	7.627	4.36
Hf	ICP-MS	0.10	1.8	3.6	3.2	3.3
Rb	ICP-MS	0.05	58.36	89.82	>150.00	97.97
Sr	ICP-MS	0.50	61.5	88.5	56.9	63.4
Ta	ICP-MS	0.17	0.35	0.53	0.7	0.48
Nb	ICP-MS	0.20	5.1	7.4	10	6.8
Th	ICP-MS	0.06	5.68	8.78	11.65	9.3
U	ICP-MS	0.007	1.651	3.288	4.474	2.877
Y	ICP-MS	0.02	10.64	19.91	16.26	14.11
Zr	ICP-MS	4.0	69.7	131	113.2	128.4
La	ICP-MS	0.02	15.35	22.23	25.05	24.18
Ce	ICP-MS	0.07	29.57	47.57	54.83	50.5
Pr	ICP-MS	0.006	3.326	4.862	4.903	5.627
Nd	ICP-MS	0.03	11.49	18.19	17.72	21.29
Sm	ICP-MS	0.01	2.11	3.46	3.13	3.7
Eu	ICP-MS	0.005	0.384	0.534	0.57	0.654
Gd	ICP-MS	0.009	1.829	3.202	2.62	3.009
Tb	ICP-MS	0.003	0.289	0.514	0.42	0.428
Dy	ICP-MS	0.008	1.764	3.414	2.718	2.535
Ho	ICP-MS	0.003	0.38	0.711	0.576	0.495
Er	ICP-MS	0.008	1.186	2.196	1.86	1.435
Tm	ICP-MS	0.003	0.182	0.337	0.277	0.213
Yb	ICP-MS	0.01	1.22	2.21	1.9	1.43
Lu	ICP-MS	0.003	0.185	0.332	0.285	0.215

Appendix 3. continued

Laboratory			Geoscience Laboratories			
Sample			**Nb-97-4-20**	**Nb-97-4-21**	**Nb-97-4-22**	**Nb-97-4-2 (red)**
Lithostratigraphic Unit			Fire Hill Mbr.	Fire Hill Mbr.	Fire Hill Mbr.	Channel Island Mbr.
Drill Hole			NB-97-4	NB-97-4	NB-97-4	NB-97-4
Stratigraphic Height (above Sibley) (m)			93.58	109.68	126.08	27.02
Easting (m)			425430	425430	425430	425430
Northing (m)			5410540	5410540	5410540	5410540
Description			red mudstone	red mudstone	red mudstone	red mudstone (cyclic facies)
	Method	**Detection Limit**				
SiO_2 (weight %)	XRF	0.01	36.15	58.6	51.82	30.75
TiO_2	XRF	0.01	0.25	0.48	0.41	0.24
Al_2O_3	XRF	0.01	7.24	14.18	11.1	8.66
Fe_2O_3	XRF	0.01	2.35	5.19	3.3	3.24
MnO	XRF	0.01	0.06	0.05	0.08	0.03
MgO	XRF	0.01	10.67	5.78	6.47	15.64
CaO	XRF	0.01	14.02	2.11	6.44	13.82
K_2O	XRF	0.01	4.35	6.13	6.64	2.03
Na_2O	XRF	0.01	0.14	0.1	0.13	0.05
P_2O_5	XRF	0.01	0.09	0.13	0.13	0.04
LOI		0.05	23.34	7.06	12.38	24.72
Total			98.65	99.81	98.9	99.21
Cr (ppm)	XRF	4	40	57	58	
Nb	XRF	2	8	10	11	
Ni	XRF	2	8	31	20	
Rb	XRF	2	95	164	146	
Sc	XRF	6	13	18	14	
Sr	XRF	2	96	43	60	
V	XRF	4	58	103	131	
Y	XRF	1	17	26	23	
Zr	XRF	3	137	139	164	
Cs	ICP–MS	0.007	3.446	8.671	5.954	4.491
Hf	ICP–MS	0.10	4	4.1	5.1	2.1
Rb	ICP–MS	0.05	102.02	>150.00	>150.00	74.89
Sr	ICP–MS	0.50	100.4	43.2	63.9	44.4
Ta	ICP–MS	0.17	0.51	0.6	0.71	0.41
Nb	ICP–MS	0.20	7.4	8.9	10.7	6
Th	ICP–MS	0.06	10.14	9.08	12.01	6.01
U	ICP–MS	0.007	2.929	4.701	5.446	1.719
Y	ICP–MS	0.02	17.71	20.92	24.6	10.45
Zr	ICP–MS	4.0	153.6	142.9	191	74.4
La	ICP–MS	0.02	38.37	28.68	38.26	12.78
Ce	ICP–MS	0.07	77.81	55.57	91.79	27.09
Pr	ICP–MS	0.006	9.604	5.762	10.78	3.028
Nd	ICP–MS	0.03	34.88	20.85	41.76	11.2
Sm	ICP–MS	0.01	4.71	4.03	7.06	2.07
Eu	ICP–MS	0.005	0.708	0.688	1.135	0.378
Gd	ICP–MS	0.009	3.34	3.559	5.006	1.794
Tb	ICP–MS	0.003	0.498	0.584	0.72	0.291
Dy	ICP–MS	0.008	2.977	3.707	4.355	1.761
Ho	ICP–MS	0.003	0.611	0.77	0.885	0.376
Er	ICP–MS	0.008	1.808	2.389	2.614	1.154
Tm	ICP–MS	0.003	0.28	0.38	0.393	0.176
Yb	ICP–MS	0.01	1.8	2.61	2.68	1.16
Lu	ICP–MS	0.003	0.275	0.395	0.4	0.179

Appendix 4

Whole Rock Analyses of Sibley Group Shale Samples from Outcrops

Note:
Universal Transverse Mercator (UTM) co-ordinates are North American Datum 1927 (NAD 27), Zone 16.

Appendix 4. Whole rock analyses of Sibley Group shale samples from outcrops.

Laboratory			University of Saskatchewan	
Sample			**03RM4**	**03RM5**
Lithostratigraphic Unit			Rossport Fm.	Rossport Fm.
Outcrop Locality			Pass Lake Hwy.	Pass Lake Hwy.
Easting (m)			372864	372864
Northing (m)			5377496	5377496
Description			red mudstone	purple mudstone
	Method	**Detection Limit**		
SiO_2 (weight %)	XRF	0.01	55.37	74.29
TiO_2	XRF	0.01	0.39	0.19
Al_2O_3	XRF	0.01	13.41	11.03
Fe_2O_3	XRF	0.01	5.4	3.35
MnO	XRF	0.01	0.03	<0.01
MgO	XRF	0.01	4.12	1.09
CaO	XRF	0.01	4.05	0.14
K_2O	XRF	0.01	10.16	8.47
Na_2O	XRF	0.01	0.14	0.08
P_2O_5	XRF	0.01	0.11	0.06
Cr_2O_3	XRF	0.01	<0.01	<0.01
LOI			7.05	1.2
Total			100.3	100.1
Nb (ppm)	XRF		9	8
Rb	XRF		131	93
Sr	XRF		32	30
Y	XRF		38	25
Zr	XRF		338	189
Ba	XRF		487	1040
Cs	ICP–MS	0.01	5.05	1.29
Hf	ICP–MS	0.04	8.53	5.27
Rb	ICP–MS	0.17	123.75	98.07
Sr	ICP–MS	0.19	30.95	30.24
Ta	ICP–MS	0.01	1.40	1.07
Nb	ICP–MS	0.02	20.87	14.09
Th	ICP–MS	0.02	21.66	16.96
U	ICP–MS	0.04	5.57	2.74
Y	ICP–MS	0.01	35.39	23.39
Zr	ICP–MS	0.04	276.59	170.09
La	ICP–MS	0.01	81.17	276.43
Ce	ICP–MS	0.01	157.10	446.81
Pr	ICP–MS	0.01	17.87	60.86
Nd	ICP–MS	0.08	60.19	206.64
Sm	ICP–MS	0.09	9.43	25.60
Eu	ICP–MS	0.03	1.38	2.79
Gd	ICP–MS	0.05	7.06	12.97
Tb	ICP–MS	0.01	0.96	0.94
Dy	ICP–MS	0.04	6.64	5.01
Ho	ICP–MS	0.01	1.29	0.91
Er	ICP–MS	0.02	4.21	2.88
Tm	ICP–MS	0.01	0.65	0.44
Yb	ICP–MS	0.05	4.67	3.23
Lu	ICP–MS	0.01	0.65	0.47

			03RM4 continued	**03RM5** continued
	Method	**Detection Limit**		
Li (ppm)	ICP–MS	4.03	43.72	38.76
Be	ICP–MS	1.83	2.73	2.62
Sc	ICP–MS	1.30	7.63	4.48
V	ICP–MS	0.34	44.93	31.78
Mo	ICP–MS	0.12	0.98	0.66
Ba	ICP–MS	0.20	423.33	1197.37
Tl	ICP–MS	0.02	0.62	0.48
Pb	ICP–MS	0.15	13.65	5.17
Bi	ICP–MS	0.02	0.45	0.19
P	ICP–MS	30.02	532.12	305.47
Ti	ICP–MS	0.36	2256.52	1131.39
Cr	ICP–MS	1.37	27.74	9.69
Co	ICP–MS	0.04	7.92	3.80
Ni	ICP–MS	0.28	7.81	2.03
Cu	ICP–MS	0.51	8.61	11.80
Zn	ICP–MS	1.07	12.51	1.89
As	ICP–MS	0.10	8.76	13.06
Ge	ICP–MS	0.04	1.94	2.70
Mo	ICP–MS	0.05	0.95	0.62
Ag	ICP–MS	0.01	0.17	0.07
Cd	ICP–MS	0.19	N.D.	N.D.
Sn	ICP–MS	0.03	4.81	5.11
Sb	ICP–MS	0.02	1.31	0.52
W	ICP–MS	0.08	6.33	3.61
Hg	ICP–MS	0.60	N.D.	N.D.

Appendix 5

Geochemical Data for Soil-Related Carbonates from Various Sibley Group Stratigraphic Units

Notes:
C and O stable isotope analyses conducted at Queen's University, Kingston, Ontario
Sr isotope analyses conducted at Carleton University, Ottawa, Ontario
Dilute acetic acid extractions were used for major and trace element analyses.
Universal Transverse Mercator (UTM) co-ordinates are North American Datum 1927 (NAD 27), Zone 16.

Appendix 5A. Geochemical data for soil-related carbonates from various Sibley Group stratigraphic units.

Sample	**04RM26 carb**	**04RM26 carb**
Lithostratigraphic Unit	Channel Island/ Fire Hill mbr.	continued
Drill Hole	n/a	
Outcrop Locality	Pass Lake Hwy	
Easting (m)	372820	
Northing (m)	5377714	
Description	carb nodule overlying carb breccia Pass Lake Rd	
$\delta^{13}C$ (PDB)	0.9	
$\delta^{18}O$ (SMOW)	28.1	
$\delta^{18}O$ (PDB)	-2.8	
$^{87}Sr/^{86}Sr$		
2σ		

	Method	**Detection Limit**			**Method**	**Detection Limit**	
Al (ppm)	ICP–MS	0.5	105	**Li (ppm)**	ICP–MS	0.1	0.587
Ca	ICP–MS	1000	37,500	**Be**	ICP–MS	0.04	0.0527
Fe	ICP–MS	0.3	87.5	**Sc**	ICP–MS	0.3	0.801
Mn	ICP–MS	0.4	176	**V**	ICP–MS	0.4	0.623
Mg	ICP–MS	250	>20000	**Mo**	ICP–MS	0.02	0.0418
Cs	ICP–MS	0.001	0.0995	**Ba**	ICP–MS	0.0015	63.8
Hf	ICP–MS	0.05	0.00746	**Tl**	ICP–MS	0.0035	0.00149
Rb	ICP–MS	0.02	N.D.	**Pb**	ICP–MS	0.15	0.890
Sr	ICP–MS	0.00	12.4	**Ti**	ICP–MS	0.005	1.20
Ta	ICP–MS	0.10%	N.D.	**Cr**	ICP–MS	0.03	0.509
Nb	ICP–MS	0.01	0.00498	**Co**	ICP–MS	0.5	0.373
Th	ICP–MS	0.02	0.202	**Ni**	ICP–MS	0.005	0.755
U	ICP–MS	2	0.0502	**Cu**	ICP–MS	0.35	1.68
Y	ICP–MS	0.025	2.09	**Zn**	ICP–MS	10	5.81
Zr	ICP–MS	0.2	0.109	**Ag**	ICP–MS	0.015	N.D.
La	ICP–MS	0.02	2.23	**Cd**	ICP–MS	0.0015	0.0159
Ce	ICP–MS	0.01	2.52	**Sn**	ICP–MS	0.15	N.D.
Pr	ICP–MS	0.0035	0.583	**Sb**	ICP–MS	0.005	N.D.
Nd	ICP–MS	0.002	2.27	**W**	ICP–MS	0.01	0.0144
Sm	ICP–MS	0.005	0.495	**Au**	ICP–MS	0.005	N.D.
Eu	ICP–MS	0.005	0.0915	**Ga**	ICP–MS	0.015	0.0567
Gd	ICP–MS	0.005	0.436				
Tb	ICP–MS	0.015	0.0736				
Dy	ICP–MS	0.0015	0.422				
Ho	ICP–MS	0.004	0.0791				
Er	ICP–MS	0.0015	0.229				
Tm	ICP–MS	0.005	0.0303				
Yb	ICP–MS	0.002	0.185				
Lu	ICP–MS	0.0035	0.0264				

* blank cells = not analyzed; N.D. = not detected

5A. continued

Sample	**04RM28a carb breccia**	***04RM28a***	**04RM28a carb breccia**	***04RM28a***
Lithostratigraphic Unit	Channel Island/ Fire Hill mbr.	*duplicate*	continued	continued
Drill Hole	n/a			
Outcrop Locality	Pass Lake Hwy			
Easting (m)	372820			
Northing (m)	5377714			
Description	clast in carb breccia. Pass Lake Rd. light green cloudy carb at edge			
δ^{13}C (PDB)	1.2			
δ^{18}O (SMOW)	27.9			
δ^{18}O (PDB)	-3.0			
^{87}Sr/^{86}Sr				
2σ				

	Method	**Detection Limit**		
Al (ppm)	ICP–MS	0.5	114	*36.0*
Ca	ICP–MS	1000	45,000	*57,900*
Fe	ICP–MS	0.3	63.0	*149*
Mn	ICP–MS	0.4	184	*664*
Mg	ICP–MS	250	>20000	*>20000*
Cs	ICP–MS	0.001	0.0470	*0.00829*
Hf	ICP–MS	0.05	0.00950	*N.D.*
Rb	ICP–MS	0.02	N.D.	*N.D.*
Sr	ICP–MS	0.00	14.4	*17.8*
Ta	ICP–MS	0.10%	N.D.	*N.D.*
Nb	ICP–MS	0.01	N.D.	*N.D.*
Th	ICP–MS	0.02	0.231	*0.0341*
U	ICP–MS	2	0.0400	*0.0668*
Y	ICP–MS	0.025	4.11	*1.62*
Zr	ICP–MS	0.2	0.0765	*0.0488*
La	ICP–MS	0.02	3.24	*0.885*
Ce	ICP–MS	0.01	3.99	*0.882*
Pr	ICP–MS	0.0035	0.911	*0.349*
Nd	ICP–MS	0.002	3.65	*1.49*
Sm	ICP–MS	0.005	0.859	*0.323*
Eu	ICP–MS	0.005	0.137	*0.0668*
Gd	ICP–MS	0.005	0.863	*0.381*
Tb	ICP–MS	0.015	0.134	*0.0434*
Dy	ICP–MS	0.0015	0.832	*0.232*
Ho	ICP–MS	0.004	0.157	*0.0449*
Er	ICP–MS	0.0015	0.481	*0.119*
Tm	ICP–MS	0.005	0.0680	*0.0151*
Yb	ICP–MS	0.002	0.452	*0.0824*
Lu	ICP–MS	0.0035	0.0695	*0.0112*

	Method	**Detection Limit**		
Li (ppm)	ICP–MS	0.1	0.576	*0.453*
Be	ICP–MS	0.04	0.0695	*0.0766*
Sc	ICP–MS	0.3	1.16	*0.361*
V	ICP–MS	0.4	0.349	*N.D.*
Mo	ICP–MS	0.02	0.0405	*0.120*
Ba	ICP–MS	0.0015	65.1	*6.92*
Tl	ICP–MS	0.0035	0.00150	*N.D.*
Pb	ICP–MS	0.15	0.845	*1.14*
Ti	ICP–MS	0.005	1.17	*0.621*
Cr	ICP–MS	0.03	0.446	*0.410*
Co	ICP–MS	0.5	0.444	*1.26*
Ni	ICP–MS	0.005	0.972	*1.54*
Cu	ICP–MS	0.35	3.49	*3.09*
Zn	ICP–MS	10	7.37	*25.0*
Ag	ICP–MS	0.015	N.D.	*N.D.*
Cd	ICP–MS	0.0015	0.0265	*0.160*
Sn	ICP–MS	0.15	N.D.	*0.0395*
Sb	ICP–MS	0.005	N.D.	*0.0180*
W	ICP–MS	0.01	0.0140	*0.0112*
Au	ICP–MS	0.005	N.D.	*N.D.*
Ga	ICP–MS	0.015	0.0650	*0.0659*

* blank cells = not analyzed; N.D. = not detected

5A. continued

Sample	**04RM28b carb breccia**	**03RM28 stromatolite**
Lithostratigraphic Unit	Channel Island/ Fire Hill mbr	Middlebrun Bay/Fire Hill mbr
Drill Hole	n/a	n/a
Outcrop Locality	Pass Lake Hwy	Kama Hill
Easting (m)	372820	425488
Northing (m)	5377714	5428453
Description	clast in carb breccia, Pass Lake Rd, massive dark green carb in centre	weathered horizon developed on stromatolitic unit at Kama Hill
δ^{13}C (PDB)	1.3	-1.5
δ^{18}O (SMOW)	28.0	24.6
δ^{18}O (PDB)	-2.8	-6.2
^{87}Sr/^{86}Sr		
2σ		

	Method	**Detection Limit**	**04RM28b carb breccia**	**03RM28 stromatolite**
Al (ppm)	ICP–MS	0.5		78.0
Ca	ICP–MS	1000		48,800
Fe	ICP–MS	0.3		100
Mn	ICP–MS	0.4		213
Mg	ICP–MS	250		>20000
Cs	ICP–MS	0.001		0.00900
Hf	ICP–MS	0.05		0.0100
Rb	ICP–MS	0.02		N.D.
Sr	ICP–MS	0.00		21.5
Ta	ICP–MS	0.10%		N.D.
Nb	ICP–MS	0.01		0.00600
Th	ICP–MS	0.02		0.0995
U	ICP–MS	2		0.0370
Y	ICP–MS	0.025		4.52
Zr	ICP–MS	0.2		0.0350
La	ICP–MS	0.02		1.81
Ce	ICP–MS	0.01		4.50
Pr	ICP–MS	0.0035		0.691
Nd	ICP–MS	0.002		2.86
Sm	ICP–MS	0.005		0.834
Eu	ICP–MS	0.005		0.136
Gd	ICP–MS	0.005		0.854
Tb	ICP–MS	0.015		0.151
Dy	ICP–MS	0.0015		0.909
Ho	ICP–MS	0.004		0.174
Er	ICP–MS	0.0015		0.479
Tm	ICP–MS	0.005		0.0665
Yb	ICP–MS	0.002		0.467
Lu	ICP–MS	0.0035		0.0695

	Method	**Detection Limit**	**04RM28b carb breccia continued**	**03RM28 stromatolite continued**
Li (ppm)	ICP–MS	0.1		0.235
Be	ICP–MS	0.04		N.D.
Sc	ICP–MS	0.3		1.17
V	ICP–MS	0.4		0.471
Mo	ICP–MS	0.02		0.0395
Ba	ICP–MS	0.0015		210
Tl	ICP–MS	0.0035		N.D.
Pb	ICP–MS	0.15		1.30
Ti	ICP–MS	0.005		0.385
Cr	ICP–MS	0.03		0.474
Co	ICP–MS	0.5		0.294
Ni	ICP–MS	0.005		2.75
Cu	ICP–MS	0.35		4.69
Zn	ICP–MS	10		20.7
Ag	ICP–MS	0.015		N.D.
Cd	ICP–MS	0.0015		0.0290
Sn	ICP–MS	0.15		0.0255
Sb	ICP–MS	0.005		0.0225
W	ICP–MS	0.01		0.0300
Au	ICP–MS	0.005		N.D.
Ga	ICP–MS	0.015		0.0645
Al (ppm)	ICP–AES		160.69	
Ba	ICP–AES		167.835	
Ca	ICP–AES		129422.18	
Fe	ICP–AES		264.70	
K	ICP–AES		187.4	
Mg	ICP–AES		78083.07	
Mn	ICP–AES		383.001	
Na	ICP–AES		265.29	
P	ICP–AES		123.3	
S	ICP–AES		128.4	
Si	ICP–AES		142.68	
Sr	ICP–AES		39.725	
V	ICP–AES		10.90	

* blank cells = not analyzed; N.D. = not detected

5A. continued

Sample	**04RM50**	**04-59 carb**	**04-60 silicified carb**	**04-61 carb**	**04RM50**
Lithostratigraphic Unit	Fire Hill Mbr	Middlebrun Bay/Fire Hill mbr	Middlebrun Bay/Fire Hill mbr	Middlebrun Bay/Fire Hill mbr	continued
Drill Hole	NB-97-4	n/a	n/a	n/a	
Outcrop Locality	n/a	Channel Island	Channel Island	Channel Island	
Easting (m)	425430	462992	462992	462992	
Northing (m)	5410540	5406020	5406020	5406020	
Description	green carbonate nodules in red siltstone	altered light gn carb from top of weathered carb unit	silicified carb nodule in weathered top of carb unit	mass flow carb rich matrix	
$\delta^{13}C$ (PDB)	0.1	-0.7	1.2	-1.0	
$\delta^{18}O$ (SMOW)	22.8	26.6	25.6	26.5	
$\delta^{18}O$ (PDB)	-7.9	-4.2	-5.2	-4.3	
$^{87}Sr/^{86}Sr$	0.712522				
2σ	0.000014				

	Method	**Detection Limit**	
Al (ppm)	ICP–MS	0.5	96.3
Ca	ICP–MS	1000	57,900
Fe	ICP–MS	0.3	17.8
Mn	ICP–MS	0.4	213
Mg	ICP–MS	250	>20000
Cs	ICP–MS	0.001	0.0121
Hf	ICP–MS	0.05	0.00707
Rb	ICP–MS	0.02	N.D.
Sr	ICP–MS	0.00	63.5
Ta	ICP–MS	0.10%	N.D.
Nb	ICP–MS	0.01	N.D.
Th	ICP–MS	0.02	0.134
U	ICP–MS	2	1.84
Y	ICP–MS	0.025	2.46
Zr	ICP–MS	0.2	0.0434
La	ICP–MS	0.02	0.815
Ce	ICP–MS	0.01	2.88
Pr	ICP–MS	0.0035	0.778
Nd	ICP–MS	0.002	4.34
Sm	ICP–MS	0.005	1.78
Eu	ICP–MS	0.005	0.313
Gd	ICP–MS	0.005	1.38
Tb	ICP–MS	0.015	0.142
Dy	ICP–MS	0.0015	0.586
Ho	ICP–MS	0.004	0.0929
Er	ICP–MS	0.0015	0.191
Tm	ICP–MS	0.005	0.0303
Yb	ICP–MS	0.002	0.158
Lu	ICP–MS	0.0035	0.0202

	Method	**Detection Limit**	
Li (ppm)	ICP–MS	0.1	0.800
Be	ICP–MS	0.04	0.0561
Sc	ICP–MS	0.3	0.794
V	ICP–MS	0.4	0.919
Mo	ICP–MS	0.02	0.143
Ba	ICP–MS	0.0015	227
Tl	ICP–MS	0.0035	0.00101
Pb	ICP–MS	0.15	1.78
Ti	ICP–MS	0.005	0.549
Cr	ICP–MS	0.03	0.346
Co	ICP–MS	0.5	0.455
Ni	ICP–MS	0.005	3.35
Cu	ICP–MS	0.35	8.90
Zn	ICP–MS	10	20.4
Ag	ICP–MS	0.015	N.D.
Cd	ICP–MS	0.0015	0.0399
Sn	ICP–MS	0.15	N.D.
Sb	ICP–MS	0.005	0.0283
W	ICP–MS	0.01	0.0232
Au	ICP–MS	0.005	N.D.
Ga	ICP–MS	0.015	0.0586

* blank cells = not analyzed; N.D. = not detected

5A. continued

Sample			**WL3a calcrete**	**WL3b**				**WL3a calcrete**	**WL3b**
Lithostratigraphic Unit			Loon Mbr.	Loon Mbr.				continued	continued
Drill Hole			n/a	n/a					
Outcrop Locality			West Loon	West Loon					
Easting (m)			368006	368006					
Northing (m)			5387586	5387586					
Description			calcrete horizon in basal conglomerate, pink matrix material, silicified?	silicified carb matirx					
δ^{13}C (PDB)			-1.1	-1.2					
δ^{18}O (SMOW)			28.4	27.5					
δ^{18}O (PDB)			-2.4	-3.3					
^{87}Sr/^{86}Sr				0.704284					
2σ				0.000012					
	Method	**Detection Limit**				**Method**	**Detection Limit**		
Al (ppm)	ICP-MS	0.5	38.0	79.3	**Li (ppm)**	ICP-MS	0.1	0.355	0.716
Ca	ICP-MS	1000	47,600	82,800	**Be**	ICP-MS	0.04	0.103	0.116
Fe	ICP-MS	0.3	141	301	**Sc**	ICP-MS	0.3	N.D.	0.436
Mn	ICP-MS	0.4	579	750	**V**	ICP-MS	0.4	N.D.	N.D.
Mg	ICP-MS	250	>20000	>20000	**Mo**	ICP-MS	0.02	0.256	0.0485
Cs	ICP-MS	0.001	0.00990	0.0193	**Ba**	ICP-MS	0.0015	6.37	3.42
Hf	ICP-MS	0.05	N.D.	N.D.	**Tl**	ICP-MS	0.0035	N.D.	0.00297
Rb	ICP-MS	0.02	N.D.	N.D.	**Pb**	ICP-MS	0.15	1.18	1.18
Sr	ICP-MS	0.00	15.3	29.5	**Ti**	ICP-MS	0.005	0.693	1.11
Ta	ICP-MS	0.10%	N.D.	N.D.	**Cr**	ICP-MS	0.03	0.391	0.340
Nb	ICP-MS	0.01	N.D.	N.D.	**Co**	ICP-MS	0.5	1.09	1.97
Th	ICP-MS	0.02	0.0332	0.0574	**Ni**	ICP-MS	0.005	4.18	5.24
U	ICP-MS	2	0.0599	0.130	**Cu**	ICP-MS	0.35	3.68	10.7
Y	ICP-MS	0.025	1.37	2.84	**Zn**	ICP-MS	10	36.4	40.8
Zr	ICP-MS	0.2	0.0609	0.0881	**Ag**	ICP-MS	0.015	N.D.	N.D.
La	ICP-MS	0.02	0.772	1.61	**Cd**	ICP-MS	0.0015	0.142	0.221
Ce	ICP-MS	0.01	0.756	1.88	**Sn**	ICP-MS	0.15	0.0401	0.0574
Pr	ICP-MS	0.0035	0.306	0.614	**Sb**	ICP-MS	0.005	0.0233	0.0208
Nd	ICP-MS	0.002	1.27	2.57	**W**	ICP-MS	0.01	N.D.	0.0119
Sm	ICP-MS	0.005	0.290	0.558	**Au**	ICP-MS	0.005	N.D.	N.D.
Eu	ICP-MS	0.005	0.0604	0.126	**Ga**	ICP-MS	0.015	0.0629	0.121
Gd	ICP-MS	0.005	0.295	0.622					
Tb	ICP-MS	0.015	0.0401	0.0817					
Dy	ICP-MS	0.0015	0.202	0.420					
Ho	ICP-MS	0.004	0.0376	0.0772					
Er	ICP-MS	0.0015	0.104	0.188					
Tm	ICP-MS	0.005	0.0104	0.0262					
Yb	ICP-MS	0.002	0.0644	0.154					
Lu	ICP-MS	0.0035	0.0114	0.0223					

* blank cells = not analyzed; N.D. = not detected

5A. continued

5B. Geochemical data for Fire Hill Member carbonates

Sample	Method	Detection Limit	WL3c	BM90	BM91	04rm40	BRO1-3	03RM37 dolo mudstone
Lithostratigraphic Unit			Loon Mbr	on basement	on basement	Fire Hill Member	Fire Hill Mbr	Fire Hill Mbr
Drill Hole			n/a	n/a	n/a	n/a	NI-92-7	n/a
Outcrop Locality			West Loon	Beardmore	Beardmore	Red Rock Railway	n/a	Kama Hill
Easting (m)			368006			407703	353850	425488
Northing (m)			5387586			5423237	5443000	5428453
Description			massive pink silic calcrete	carb nodule, soil	discont. soil carb layer	dolo siltstone/mudstone, a few m above Middlebrun Bay Member	dissemminated carbonate associated with sulphates	massive fine-grained dolo, overlies stromatolite unit at Kama Hill
$\delta^{13}C$ (PDB)			-1.3	-1.2	-1.5	-1.4	-0.7	1.198142857
$\delta^{18}O$ (SMOW)			27.2	14.8	14.0	26.3	15.3	25.41328571
$\delta^{18}O$ (PDB)			-3.6	-15.7	-16.4	-4.5	-15.1	-5.3
$^{87}Sr/^{86}Sr$						0.707028		
2σ						0.000013		
Al (ppm)	ICP-AES	0.06	47.98	756.77	313.96	193.95	1037.09	
Ba	ICP-AES	0.006	27.457	25.521	10.239	43.627	28.074	
Ca	ICP-AES	0.01	122265.33	454804.17	200854.26	135189.02	130742.62	
Fe	ICP-AES	0.02	461.51	1553.12	784.31	308.16	120.90	
K	ICP-AES	0.25	17.5	N.D.	N.D.	60.2	N.D.	
Mg	ICP-AES	0.01	77384.05	15539.06	8688.70	76724.98	12798.98	
Mn	ICP-AES	0.003	1680.606	917.708	411.968	279.057	356.967	
Na	ICP-AES	0.01	85.78	3445.31	2437.10	369.00	N.D.	
P	ICP-AES	0.1	28.4	1118.7	872.3	133.7	1027.0	
S	ICP-AES	0.1	74.1	4393.1	1256.7	176.3	83794.8	
Si	ICP-AES	0.025	21.76	891.67	378.72	73.85	681.15	
Sr	ICP-AES	0.005	33.864	N.D.	11.170	37.459	1302.459	
V	ICP-AES	0.03	4.41	10.42	4.26	9.59	8.20	

* blank cells = not analyzed; N.D. = not detected

Appendix 6

Geochemical Data for Sibley Group Stromatolites

Notes:

C and O stable isotope analyses conducted at Queen's University, Kingston, Ontario

Sr isotope analyses conducted at Carleton University, Ottawa, Ontario

Dilute acetic acid extractions were used for major and trace element analyses.

Universal Transverse Mercator (UTM) co-ordinates are North American Datum 1927 (NAD 27), Zone 16.

Appendix 6. Geochemical data for Sibley Group stromatolites.

Sample	**BO2-4a**	***BO2-4a***
Lithostratigraphic Unit	Middlebrun Bay Mbr	*duplicate*
Drill Hole	n/a	
Stratigraphic Height (above basement) (m)	n/a	
Outcrop Locality	Channel Island	
Easting (m)	462992	
Northing (m)	5406020	
Description	stromatolite, massive white layer	
$\delta^{13}C$ (PDB)	-0.1	
$\delta^{18}O$ (SMOW)	15.7	
$\delta^{18}O$ (PDB)	-14.7	
$^{87}Sr/^{86}Sr$	0.709386	
2σ	0.000016	

	Method	**Detection Limit**		
Al (ppm)	ICP–MS	0.5	24.0	*21.1*
Fe	ICP–MS	0.3	83.0	*84.1*
Mn	ICP–MS	0.4	499	*475*
Mg	ICP–MS	250	>20000	*>20000*
Ca	ICP–MS	1000	96,400	*72,600*
Cs	ICP–MS	0.001	0.00198	*0.00396*
Hf	ICP–MS	0.05	N.D.	*N.D.*
Rb	ICP–MS	0.02	N.D.	*N.D.*
Sr	ICP–MS	0.004	37.2	*36.8*
Ta	ICP–MS	0.10%	N.D.	*N.D.*
Nb	ICP–MS	0.01	N.D.	*N.D.*
Th	ICP–MS	0.02	0.0144	*0.0134*
U	ICP–MS	2	0.0802	*0.0807*
Y	ICP–MS	0.025	2.33	*2.36*
Zr	ICP–MS	0.15	N.D.	*N.D.*
La	ICP–MS	0.02	4.35	*4.52*
Ce	ICP–MS	0.01	2.70	*2.82*
Pr	ICP–MS	0.0035	0.992	*0.991*
Nd	ICP–MS	0.002	3.84	*3.85*
Sm	ICP–MS	0.005	0.651	*0.619*
Eu	ICP–MS	0.005	0.112	*0.111*
Gd	ICP–MS	0.005	0.623	*0.657*
Tb	ICP–MS	0.015	0.0703	*0.0708*
Dy	ICP–MS	0.0015	0.383	*0.365*
Ho	ICP–MS	0.004	0.0624	*0.0614*
Er	ICP–MS	0.0015	0.150	*0.148*
Tm	ICP–MS	0.005	0.0168	*0.0158*
Yb	ICP–MS	0.002	0.0807	*0.0822*
Lu	ICP–MS	0.0035	0.0114	*0.00990*

			BO2-4a	***BO2-4a***
			continued	continued
	Method	**Detection Limit**		
Li (ppm)	ICP–MS	0.1	0.192	*0.122*
Be	ICP–MS	0.04	0.0634	*0.0525*
Sc	ICP–MS	0.3	0.433	*N.D.*
V	ICP–MS	0.4	2.00	*1.73*
Mo	ICP–MS	0.02	0.0465	*0.0332*
Ba	ICP–MS	0.0015	290	*295*
Tl	ICP–MS	0.0035	N.D.	*N.D.*
Pb	ICP–MS	0.15	0.837	*0.938*
Ti	ICP-MS	0.005	2.52	*4.18*
Cr	ICP–MS	0.03	0.266	*0.276*
Co	ICP–MS	0.5	0.450	*0.447*
Ni	ICP–MS	0.005	1.09	*1.68*
Cu	ICP–MS	0.35	1.18	*1.32*
Zn	ICP–MS	10	5.84	*4.83*
Ag	ICP–MS	0.015	N.D.	*N.D.*
Cd	ICP–MS	0.0015	0.0312	*0.0267*
Sn	ICP–MS	0.15	0.0861	*0.101*
Sb	ICP–MS	0.005	0.0213	*0.0203*
W	ICP–MS	0.01	0.0183	*0.0104*
Au	ICP–MS	0.005	N.D.	*N.D.*
Ga	ICP–MS	0.015	0.0812	*0.0673*

* blank cells = not analyzed; N.D. = not detected

Appendix 6. continued

Sample	BO2-4b	BO2-4c	BO2-4b	BO2-4c
Lithostratigraphic Unit	Middlebrun Bay Mbr	Middlebrun Bay Mbr	continued	continued
Drill Hole	n/a	n/a		
Stratigraphic Height (above basement) (m)	n/a	n/a		
Outcrop Locality	Channel Island	Channel Island		
Easting (m)	462992	462992		
Northing (m)	5406020	5406020		
Description	stromatolite, massive white layer	fine dark krinkly laminae		
$\delta^{13}C$ (PDB)	-0.1	0.4		
$\delta^{18}O$ (SMOW)	18.5	16.4		
$\delta^{18}O$ (PDB)	-12.1	-14.1		
$^{87}Sr/^{86}Sr$	0.711604	0.712309		
2σ	0.000025	0.000023		

	Method	Detection Limit		
Al (ppm)	ICP–MS	0.5		
Fe	ICP–MS	0.3		
Mn	ICP–MS	0.4		
Mg	ICP–MS	250		
Ca	ICP–MS	1000		
Cs	ICP–MS	0.001		
Hf	ICP–MS	0.05		
Rb	ICP–MS	0.02		
Sr	ICP–MS	0.004		
Ta	ICP–MS	0.10%		
Nb	ICP–MS	0.01		
Th	ICP–MS	0.02		
U	ICP–MS	2		
Y	ICP–MS	0.025		
Zr	ICP–MS	0.15		
La	ICP–MS	0.02		
Ce	ICP–MS	0.01		
Pr	ICP–MS	0.0035		
Nd	ICP–MS	0.002		
Sm	ICP–MS	0.005		
Eu	ICP–MS	0.005		
Gd	ICP–MS	0.005		
Tb	ICP–MS	0.015		
Dy	ICP–MS	0.0015		
Ho	ICP–MS	0.004		
Er	ICP–MS	0.0015		
Tm	ICP–MS	0.005		
Yb	ICP–MS	0.002		
Lu	ICP–MS	0.0035		

	Method	Detection Limit		
Li (ppm)	ICP–MS	0.1		
Be	ICP–MS	0.04		
Sc	ICP–MS	0.3		
V	ICP–MS	0.4		
Mo	ICP–MS	0.02		
Ba	ICP–MS	0.0015		
Tl	ICP–MS	0.0035		
Pb	ICP–MS	0.15		
Ti	ICP–MS	0.005		
Cr	ICP–MS	0.03		
Co	ICP–MS	0.5		
Ni	ICP–MS	0.005		
Cu	ICP–MS	0.35		
Zn	ICP–MS	10		
Ag	ICP–MS	0.015		
Cd	ICP–MS	0.0015		
Sn	ICP–MS	0.15		
Sb	ICP–MS	0.005		
W	ICP–MS	0.01		
Au	ICP–MS	0.005		
Ga	ICP–MS	0.015		

* blank cells = not analyzed; N.D. = not detected

Appendix 6. continued

Sample	**CIIb**	**CIIa**
Lithostratigraphic Unit	Middlebrun Bay Mbr	Middlebrun Bay Mbr
Drill Hole	n/a	n/a
Stratigraphic Height (above basement) (m)	n/a	n/a
Outcrop Locality	Channel Island	Channel Island
Easting (m)	462992	462992
Northing (m)	5406020	5406020
Description	stromatolite	stromatolite
δ^{13}C (PDB)	0.71	0.22
δ^{18}O (SMOW)	23.37	23.47
δ^{18}O (PDB)	-7.3	-7.2
^{87}Sr/^{86}Sr		0.708152
2σ		0.000013

	Method	**Detection Limit**		
Al (ppm)	ICP–MS	0.5	51.7	45.5
Fe	ICP–MS	0.3	160	427
Mn	ICP–MS	0.4	420	386
Mg	ICP–MS	250	>20000	>20000
Ca	ICP–MS	1000	113,000	77,600
Cs	ICP–MS	0.001	0.00300	0.00297
Hf	ICP–MS	0.05	N.D.	N.D.
Rb	ICP–MS	0.02	N.D.	N.D.
Sr	ICP–MS	0.004	27.5	32.6
Ta	ICP–MS	0.10%	N.D.	N.D.
Nb	ICP–MS	0.01	0.00550	N.D.
Th	ICP–MS	0.02	0.0230	0.0144
U	ICP–MS	2	0.169	0.273
Y	ICP–MS	0.025	2.17	2.63
Zr	ICP–MS	0.15	0.0230	N.D.
La	ICP–MS	0.02	1.85	2.01
Ce	ICP–MS	0.01	2.36	2.93
Pr	ICP–MS	0.0035	0.564	0.692
Nd	ICP–MS	0.002	2.29	2.90
Sm	ICP–MS	0.005	0.471	0.602
Eu	ICP–MS	0.005	0.112	0.125
Gd	ICP–MS	0.005	0.440	0.620
Tb	ICP–MS	0.015	0.0610	0.0782
Dy	ICP–MS	0.0015	0.370	0.505
Ho	ICP–MS	0.004	0.0660	0.0837
Er	ICP–MS	0.0015	0.167	0.208
Tm	ICP–MS	0.005	0.0210	0.0272
Yb	ICP–MS	0.002	0.108	0.138
Lu	ICP–MS	0.0035	0.0145	0.0168

	Method	**Detection Limit**	**CIIb** continued	**CIIa** continued
Li (ppm)	ICP–MS	0.1	0.227	0.122
Be	ICP–MS	0.04	N.D.	N.D.
Sc	ICP–MS	0.3	0.482	0.564
V	ICP–MS	0.4	6.55	4.91
Mo	ICP–MS	0.02	0.0790	0.111
Ba	ICP–MS	0.0015	523	433
Tl	ICP–MS	0.0035	0.00150	0.00149
Pb	ICP–MS	0.15	0.925	0.825
Ti	ICP–MS	0.005	0.925	0.549
Cr	ICP–MS	0.03	0.315	0.623
Co	ICP–MS	0.5	0.555	0.503
Ni	ICP–MS	0.005	1.73	1.55
Cu	ICP–MS	0.35	4.71	4.83
Zn	ICP–MS	10	11.3	2.99
Ag	ICP–MS	0.015	N.D.	N.D.
Cd	ICP–MS	0.0015	0.0225	0.0223
Sn	ICP–MS	0.15	0.0530	0.0327
Sb	ICP–MS	0.005	N.D.	N.D.
W	ICP–MS	0.01	0.0175	0.0144
Au	ICP–MS	0.005	N.D.	N.D.
Ga	ICP–MS	0.015	0.0605	0.0733

* blank cells = not analyzed; N.D. = not detected

Appendix 6. continued

Sample	**TH1**	**TH2**
Lithostratigraphic Unit	Kama Hill Fm/upper Fire Hill	Kama Hill Fm/upper Fire Hill
Drill Hole	n/a	n/a
Stratigraphic Height (above basement) (m)	n/a	n/a
Outcrop Locality	boulder, SW of Moraine Lake	boulder, SW of Moraine Lake
Easting (m)	363774	363774
Northing (m)	5425172	5425172
Description	recrystallized	recrystallized

	TH1	**TH2**
$\delta^{13}C$ (PDB)	1.3	1.3
$\delta^{18}O$ (SMOW)	24.8	25.0
$\delta^{18}O$ (PDB)	-6.0	-5.7
$^{87}Sr/^{86}Sr$	0.707031	
2σ	0.000023	

	Method	**Detection Limit**	**TH1**	**TH2**
Al (ppm)	ICP–MS	0.5	41.8	
Fe	ICP–MS	0.3	335	
Mn	ICP–MS	0.4	750	
Mg	ICP–MS	250	>20000	
Ca	ICP–MS	1000	105,000	
Cs	ICP–MS	0.001	0.120	
Hf	ICP–MS	0.05	N.D.	
Rb	ICP–MS	0.02	N.D.	
Sr	ICP–MS	0.004	19.1	
Ta	ICP–MS	0.10%	N.D.	
Nb	ICP–MS	0.01	N.D.	
Th	ICP–MS	0.02	0.0367	
U	ICP–MS	2	0.0141	
Y	ICP–MS	0.025	1.11	
Zr	ICP–MS	0.15	0.0402	
La	ICP–MS	0.02	0.519	
Ce	ICP–MS	0.01	0.818	
Pr	ICP–MS	0.0035	0.327	
Nd	ICP–MS	0.002	1.50	
Sm	ICP–MS	0.005	0.300	
Eu	ICP–MS	0.005	0.0538	
Gd	ICP–MS	0.005	0.266	
Tb	ICP–MS	0.015	0.0312	
Dy	ICP–MS	0.0015	0.177	
Ho	ICP–MS	0.004	0.0281	
Er	ICP–MS	0.0015	0.0759	
Tm	ICP–MS	0.005	0.00854	
Yb	ICP–MS	0.002	0.0518	
Lu	ICP–MS	0.0035	0.00754	

	Method	**Detection Limit**	**TH1** continued	**TH2** continued
Li (ppm)	ICP–MS	0.1	0.333	
Be	ICP–MS	0.04	N.D.	
Sc	ICP–MS	0.3	0.491	
V	ICP–MS	0.4	0.208	
Mo	ICP–MS	0.02	N.D.	
Ba	ICP–MS	0.0015	3.60	
Tl	ICP–MS	0.0035	0.00151	
Pb	ICP–MS	0.15	0.783	
Ti	ICP–MS	0.005	1.95	
Cr	ICP–MS	0.03	1.92	
Co	ICP–MS	0.5	0.956	
Ni	ICP–MS	0.005	2.16	
Cu	ICP–MS	0.35	1.18	
Zn	ICP–MS	10	9.56	
Ag	ICP–MS	0.015	N.D.	
Cd	ICP–MS	0.0015	0.0462	
Sn	ICP–MS	0.15	0.0623	
Sb	ICP–MS	0.005	N.D.	
W	ICP–MS	0.01	0.00754	
Au	ICP–MS	0.005	N.D.	
Ga	ICP–MS	0.015	0.0754	

* blank cells = not analyzed; N.D. = not detected

Appendix 6. continued

Sample			**GF7-L**	**GF7-W**	**04RM10**	**04RM15a**	**04RM15b**	**04RM77**
Lithostratigraphic Unit			Kama Hill Fm?	Kama Hill Fm?	Kama Hill Fm?	Kama Hill Fm?	Kama Hill Fm?	Middlebrun Bay Mbr
Drill Hole			n/a	n/a	NI-92-7	HE-02-02	HE02-02	n/a
Stratigraphic Height (above basement) (m)			n/a	n/a	165.5	78 (above base of hole)	78 (above base of hole)	n/a
Outcrop Locality			Hwy 11-17, near Dorion	Hwy 11-17, near Dorion	n/a	n/a	n/a	Red Rock Railway
Easting (m)			384322	384322	353850	393007	393007	407703
Northing (m)			5401639	5401639	5443000	5449701	5449701	5423237
Description			finely laminated pink carbonate	weathered top of finely laminated pink carbonate	with abundant diagenetic gypsum	finely laminated pink carbonate from strmatolitic horizon in core	clast of massive white carb in breccia above 15a	stromatolitic chert/limstone
δ^{13}C (PDB)			1.3	1.4	1.5	1.7	1.5	0.2
δ^{18}O (SMOW)			26.7	26.3	25.5	27.3	26.9	23.9
δ^{18}O (PDB)			-4.1	-4.5	-5.3	-3.5	-3.9	-6.8
^{87}Sr/^{86}Sr								
2σ								
	Method	**Detection Limit**						
Al (ppm)	ICP–AES	0.06	2.21	39.07	N.D.	100.06	83.28	105.76
Ba	ICP–AES	0.006	9.735	402.932	1.384	3.779	2.486	185.312
Ca	ICP–AES	0.01	131026.40	129657.95	150235.12	127831.04	139814.58	124741.32
Fe	ICP–AES	0.02	324.63	340.71	437.02	751.48	849.04	309.00
K	ICP–AES	0.25	N.D.	N.D.	N.D.	102.2	N.D.	N.D.
Mg	ICP–AES	0.01	80517.33	78320.83	70719.29	71860.55	74565.82	77503.13
Mn	ICP–AES	0.003	1371.165	1061.282	950.952	785.189	1046.497	336.800
Na	ICP–AES	0.01	68.29	67.54	87.11	173.53	252.37	247.32
P	ICP–AES	0.1	4.7	N.D.	N.D.	15.0	68.2	61.7
S	ICP–AES	0.1	N.D.	94.1	28060.9	85.6	14.6	203.4
Si	ICP–AES	0.025	14.23	73.66	N.D.	90.67	98.70	46.15
Sr	ICP–AES	0.005	15.044	33.002	45.329	39.069	30.960	26.541
Y	ICP–AES	0.03	4.65	7.50	0.52	4.49	4.52	4.76

* blank cells = not analyzed; N.D. = not detected

Appendix 7

Geochemical Data for Sibley Group Sulphate Samples

Notes:
Sr isotope analyses conducted at Carleton University, Ottawa, Ontario
Universal Transverse Mercator (UTM) co-ordinates are North American Datum 1927 (NAD 27), Zone 16.

Appendix 7. Geochemical data for Sibley Group sulphate samples.

Sample			**03RM27**	**03RM28**	**03RM29**	**BR0136**	**BR0138**	**BR0144**
Lithostratigraphic Unit			Fire Hill Mbr	Fire Hill Mbr	Fire Hill Mbr	Fire Hill Mbr	Fire Hill Mbr	Fire Hill Mbr
Drill Hole			NI-92-7	NI-92-7	NI-92-7	NI-92-7	NI-92-7	NI-92-7
Stratigraphic Height (above basement) (m)			157.45	158.6	145.2	107.6	125	136.48
Easting (m)			353850	353850	353850	353850	353850	353850
Northing (m)			5443000	5443000	5443000	5443000	5443000	5443000
Description			gyp/anh nodule	gyp/anh nodule	gyp/anh nodule	gyp/anh nodule	gyp/anh nodule	gyp/anh nodule
$^{87}Sr/^{86}Sr$			0.70647	0.707047	0.707383			
2σ			0.000037	0.000012	0.000013			
Approximate %S			18	18		22	15	20
$\delta^{34}S$ (CDT)			10.6	11.2		11.4	9.0	8.9
	Method	**Detection Limit**						
Al (ppm)	ICP-AES	0.06	N.D.	N.D.		28.77	N.D.	11.84
Ba	ICP-AES	0.006	20.301	7.451		5.802	4.366	3.596
Ca	ICP-AES	0.01	273239.01	80151.71		289816.05	226325.35	256974.56
Fe	ICP-AES	0.02	7.18	N.D.		67.28	N.D.	37.63
K	ICP-AES	0.25	N.D.	71.8		175.1	N.D.	N.D.
Mg	ICP-AES	0.01	107.37	55.25		263.95	49.86	426.67
Mn	ICP-AES	0.003	0.712	0.033		21.975	0.563	8.947
Na	ICP-AES	0.01	83.70	98.93		295.68	360.99	229.91
P	ICP-AES	0.1	44.6	23.6		N.D.	N.D.	N.D.
S	ICP-AES	0.1	232934.8	67271.7		220985.7	184110.4	209507.4
Si	ICP-AES	0.025	23.67	12.63		43.46	113.80	53.33
Sr	ICP-AES	0.005	1253.699	429.605		712.222	641.549	1459.912
Y	ICP-AES	0.03	N.D.	N.D.		N.D.	N.D.	N.D.

Sample			**BR0146**	**04RM5**	**04RM8**	**M-14**	**CFG1**	**CFG2**
Lithostratigraphic Unit			Fire Hill Mbr	Fire Hill Mbr	Fire Hill Mbr	Fire Hill Mbr	Channel Island Mbr	Channel Island Mbr
Drill Hole			NI-92-7	NI-92-7	NI-92-7	NI-92-7	NI-92-7	NI-92-7
Stratigraphic Height (above			140	107.27	113.32	165	53.36	60.72
Easting (m)			353850	353850	353850	353850	353850	353850
Northing (m)			5443000	5443000	5443000	5443000	5443000	5443000
Description			gyp/anh nodule	sulphate cement	gyp/anh nodule	gyp nodule	cyclic gypsum	cyclic gypsum
$^{87}Sr/^{86}Sr$							0.708522	0.709063
2σ							0.000011	0.000008
Approximate %S			16	25	33	24	22	23
$\delta^{34}S$ (CDT)			9.0	12.4	12.2	10.3	6.0	6.0
	Method	**Detection Limit**						
Al (ppm)	ICP-AES	0.06	N.D.	N.D.	N.D.	11.38	16.58	N.D.
Ba	ICP-AES	0.006	N.D.	2326.429	N.D.	0.331	14.188	58.387
Ca	ICP-AES	0.01	229057.53	2474302.86	230382.51	250774.59	253386.32	204878.97
Fe	ICP-AES	0.02	17.42	N.D.	N.D.	46.30	15.21	19.23
K	ICP-AES	0.25	N.D.	N.D.	N.D.	N.D.	454.7	N.D.
Mg	ICP-AES	0.01	3153.88	3725.00	124.79	1348.95	1740.17	3116.06
Mn	ICP-AES	0.003	33.596	10.000	N.D.	14.586	6.496	40.903
Na	ICP-AES	0.01	194.33	3487.86	337.63	49.83	814.19	217.23
P	ICP-AES	0.1	73.5	477.1	39.8	N.D.	N.D.	46.2
S	ICP-AES	0.1	187287.6	2070656.2	192842.7	200771.7	203313.5	168059.3
Si	ICP-AES	0.025	42.47	491.43	10.79	32.04	107.69	102.45
Sr	ICP-AES	0.005	1295.281	19242.857	2093.023	799.448	541.026	363.613
Y	ICP-AES	0.03	N.D.	N.D.	N.D.	N.D.	N.D.	N.D.

* blank cells = not analyzed; N.D. = not detected

Appendix 7. continued

Sample			**CFG3**	**CFG4**	**CFG5**	**CFG6**	**03RM35g**	**03RM26**	**04RM32**
Lithostratigraphic Unit			Channel Island Mbr	Channel Island Mbr	Channel Island Mbr	Channel Island Mbr	Channel Island Mbr	Channel Island Mbr	Channel Island Mbr
Drill Hole			NI-92-7	NI-92-7	NI-92-7	NI-92-7	NI-92-7	NI-92-7	NI-92-7
Stratigraphic Height (above basement) (m)			62.32	56.53	58.18	65.86	86.93	74.04	55
Easting (m)			353850	353850	353850	353850	353850	353850	353850
Northing (m)			5443000	5443000	5443000	5443000	5443000	5443000	5443000
Description			cyclic gypsum	cyclic gypsum	cyclic gypsum	cyclic gypsum	cyclic gypsum	cyclic gypsum	cyclic gypsum
^{87}Sr/^{86}Sr			0.708999				0.710492		
2σ			0.000005				0.000008		
Approximate %S			18	26	15	24	13	46	21
δ^{34}S (CDT)			5.3	5.7	4.5	4.9	11.9	10.7	5.5
	Method	**Detection Limit**							
Al (ppm)	ICP-AES	0.06	N.D.	14.09	61.64	24.67	25.18	7.36	3.88
Ba	ICP-AES	0.006	11.818	353.960	38.630	6.000	788.684	27.917	45.426
Ca	ICP-AES	0.01	262793.51	265706.04	252687.67	245454.67	442764.04	376876.39	280637.21
Fe	ICP-AES	0.02	16.49	111.28	9.04	4.13	82.37	158.47	N.D.
K	ICP-AES	0.25	213.0	811.5	N.D.	N.D.	N.D.	N.D.	N.D.
Mg	ICP-AES	0.01	1481.56	2094.77	2951.23	1582.13	2106.14	4770.83	1849.61
Mn	ICP-AES	0.003	3.896	8.591	4.384	6.667	49.298	31.944	4.651
Na	ICP-AES	0.01	221.95	584.30	44.66	344.40	325.00	318.19	127.91
P	ICP-AES	0.1	N.D.	N.D.	N.D.	N.D.	14.0	N.D.	N.D.
S	ICP-AES	0.1	212309.6	209393.8	194132.6	198904.5	320560.0	271608.9	226013.0
Si	ICP-AES	0.025	39.48	63.89	203.29	97.07	108.77	45.00	65.74
Sr	ICP-AES	0.005	220.909	439.060	381.096	1094.267	1091.316	1322.917	623.411
Y	ICP-AES	0.03	N.D.	N.D.	N.D.	N.D.	N.D.	N.D.	N.D.

Sample			**03RM44g**	**03RM26**	**03RM61**	**03RM62**	**03rm63**	**03rm64**
Lithostratigraphic Unit			Channel Island Mbr	Fire Hill Mbr	Fire Hill Mbr	Fire Hill Mbr	Fire Hill Mbr	Fire Hill Mbr
Drill Hole			NI-92-7	NI-92-7	D00-02	D00-03	D00-04	D00-05
Stratigraphic Height (above			64	74.04	n/a	n/a	n/a	n/a
Easting (m)			353850	353850	357206	357206	357206	357206
Northing (m)			5443000	5443000	5440995	5440995	5440995	5440995
Description			cyclic gypsum	gyp/anh nodule	gyp/anh nodule	gyp/anh nodule	gyp/anh nodule	gyp/anh nodule
^{87}Sr/^{86}Sr			0.710899		0.708836	0.708186	0.707788	0.708799
2σ			0.000018		0.000015	0.000013	0.000018	0.000015
Approximate %S					19	20	19	16
δ^{34}S (CDT)					12.0	12.0	11.2	11.9
	Method	**Detection Limit**						
Al (ppm)	ICP-AES	0.06			N.D.	N.D.	N.D.	N.D.
Ba	ICP-AES	0.006			8.357	2.440	3.348	5.413
Ca	ICP-AES	0.01			263201.71	234329.08	230140.17	236367.71
Fe	ICP-AES	0.02			1.00	N.D.	N.D.	20.12
K	ICP-AES	0.25			N.D.	91.69	N.D.	N.D.
Mg	ICP-AES	0.01			320.79	28.48	45.17	12.20
Mn	ICP-AES	0.003			8.429	N.D.	N.D.	N.D.
Na	ICP-AES	0.01			256.21	179.78	165.35	9.14
P	ICP-AES	0.1			123.4	41.1	71.0	70.8
S	ICP-AES	0.1			219722.8	199181.6	195222.6	199208.5
Si	ICP-AES	0.025			70.00	16.62	36.00	13.70
Sr	ICP-AES	0.005			926.286	278.164	185.565	574.067
Y	ICP-AES	0.03			N.D.	N.D.	N.D.	N.D.

* blank cells = not analyzed; N.D. = not detected

Appendix 8

Trace and Rare Earth Element Analyses of Hydrochloric Acid (10%) Soluble Portions of Various Sibley Group Carbonate Rocks

Note:
Universal Transverse Mercator (UTM) co-ordinates are North American Datum 1927 (NAD 27), Zone 16.

Appendix 8. Trace and rare earth element analyses of hydrochloric acid (10%) soluble portions of various Sibley Group carbonate rocks (N.D. = not detected).

Laboratory			University of Saskatchewan		
Sample			**M6 (HCl)**	**03RM6 (HCl)**	**BO2-1 (HCl)**
Lithostratigraphic Unit			Channel Island Mbr.	Channel Island Mbr.	Channel Island Mbr.
Drill Hole			NI-97-2	n/a	n/a
Outcrop Locality			n/a	Pass Lake Hwy.	Channel Island
Easting (m)			353850	372820	462992
Northing (m)			5443000	5377714	5406020
Description			dolomitic mudstone	dolomitic mudstone	stromatolite
	Method	**Detection Limit**			
Cs (ppm)	ICP–MS	0.01	0.53	2.96	0.15
Hf	ICP–MS	0.04	0.09	0.12	N.D.
Rb	ICP–MS	0.17	7.17	31.75	0.43
Sr	ICP–MS	0.19	209.09	33.46	225.99
Ta	ICP–MS	0.01	N.D.	N.D.	N.D.
Nb	ICP–MS	0.02	0.04	0.05	N.D.
Th	ICP–MS	0.02	2.08	3.67	0.04
U	ICP–MS	0.04	0.32	1.78	0.72
Y	ICP–MS	0.01	8.01	11.80	4.24
Zr	ICP–MS	0.04	3.40	5.35	0.27
La (ppm)	ICP–MS	0.01	4.97	23.19	5.65
Ce	ICP–MS	0.01	12.03	45.24	5.37
Pr	ICP–MS	0.01	1.87	6.11	0.95
Nd	ICP–MS	0.08	7.78	21.97	3.46
Sm	ICP–MS	0.09	1.87	4.16	0.71
Eu	ICP–MS	0.03	0.34	0.64	0.14
Gd	ICP–MS	0.05	1.56	3.39	0.67
Tb	ICP–MS	0.01	0.20	0.43	0.07
Dy	ICP–MS	0.04	1.12	2.38	0.43
Ho	ICP–MS	0.01	0.21	0.43	0.08
Er	ICP–MS	0.02	0.54	1.11	0.20
Tm	ICP–MS	0.01	0.07	0.15	0.03
Yb	ICP–MS	0.05	0.48	1.04	0.18
Lu	ICP–MS	0.01	0.05	0.13	N.D.
Li (ppm)	ICP–MS	4.03	32.32	29.94	N.D.
Be	ICP–MS	1.83	N.D.	N.D.	N.D.
Sc	ICP–MS	1.30	3.46	5.47	1.54
V	ICP–MS	0.34	13.71	23.00	11.24
Mo	ICP–MS	0.12	N.D.	N.D.	N.D.
Ba	ICP–MS	0.20	353.48	384.73	2802.21
Tl	ICP–MS	0.02	0.62	0.29	0.15
Pb	ICP–MS	0.15	1.64	1.75	0.84
Bi	ICP–MS	0.02	0.13	0.42	0.13
P	ICP–MS	30.02	189.36	517.73	48.99
Ti	ICP–MS	0.36	85.79	173.89	19.49
Cr	ICP–MS	1.37	21.74	38.67	14.83
Co	ICP–MS	0.04	3.01	6.23	5.32
Ni	ICP–MS	0.28	5.26	13.04	1.55
Cu	ICP–MS	0.51	5.41	12.69	34.59
Zn	ICP–MS	1.07	5.78	21.21	2.92
As	ICP–MS	0.10	8.29	11.29	6.75
Ge	ICP–MS	0.04	N.D.	N.D.	N.D.
Mo	ICP–MS	0.05	0.15	0.15	N.D.
Ag	ICP–MS	0.01	N.D.	N.D.	N.D.
Cd	ICP–MS	0.19	0.24	N.D.	N.D.
Sn	ICP–MS	0.03	0.43	0.83	1.47
Sb	ICP–MS	0.02	N.D.	0.02	N.D.
W	ICP–MS	0.08	1.62	0.14	18.46
Hg	ICP–MS	0.60	N.D.	N.D.	N.D.

Appendix 9

Whole Rock Geochemical Data for Possible Weathered Granite at the Base of Diamond-Drill Hole NB-97-2

Note:
Universal Transverse Mercator (UTM) co-ordinates are North American Datum 1927 (NAD 27), Zone 16.

Appendix 9. Whole rock geochemical data for possible weathered granite at the base of diamond-drill hole NB-97-2.

Laboratory			Geoscience Laboratories			
Sample			**03RM10**	**03RM11**	**03RM13**	**03RM15**
Lithostratigraphic Unit			n/a	n/a	n/a	n/a
Drill Hole			NB-97-2	NB-97-2	NB-97-2	NB-97-2
Distance below Sibley Group contact (cm)			10	100	372	737
Easting (m)			426990	426990	426990	426990
Northing (m)			5416241	5416241	5416241	5416241
	Method	**Detection Limit**				
SiO_2 (weight %)	XRF	0.01	66.73	63.14	61.45	65.01
TiO_2	XRF	0.01	0.48	0.92	0.65	0.63
Al_2O_3	XRF	0.01	14.32	15.93	15.2	15.21
Fe_2O_3	XRF	0.01	2.57	3.15	5.5	3.17
MnO	XRF	0.01	0.02	0.04	0.04	0.02
MgO	XRF	0.01	2.33	2.68	4.34	2.1
CaO	XRF	0.01	0.48	1.36	0.64	0.97
K_2O	XRF	0.01	10.4	6.56	7.66	5.78
Na_2O	XRF	0.01	0.15	2.84	1.02	3.85
P_2O_5	XRF	0.01	0.33	0.75	0.44	0.45
LOI		0.05	1.88	1.55	2.82	1.77
Total			99.69	98.91	99.76	98.96
Cr (ppm)	XRF	4	8	5	17	26
Nb	XRF	2	26	29	27	26
Ni	XRF	2	8	10	10	8
Rb	XRF	2	194	184	140	136
Sc	XRF	6	N.D.	8	6	6
Sr	XRF	2	61	113	78	163
V	XRF	4	59	84	74	111
Y	XRF	1	28	26	16	26
Zr	XRF	3	466	649	377	394
Cs	ICP–MS	0.007	1.982	2.369	2.871	1.588
Hf	ICP–MS	0.10	9.5	9	16.6	16.5
Rb	ICP–MS	0.05	>150.00	>150.00	109.28	>150.00
Sr	ICP–MS	0.50	55.5	91	86.2	173.7
Ta	ICP–MS	0.17	1.77	1.34	1.54	1.47
Nb	ICP–MS	0.20	28.3	26	28.6	27.8
Th	ICP–MS	0.06	11.54	11.17	12.15	19.57
U	ICP–MS	0.007	1.916	1.826	2.669	2.15
Y	ICP–MS	0.02	18.98	19.79	17.57	44.58
Zr	ICP–MS	4.0	414.4	438.8	762.8	757.9
La	ICP–MS	0.02	63.44	>100.00	88.06	>100.00
Ce	ICP–MS	0.07	135.04	>200.00	193.46	>200.00
Pr	ICP–MS	0.006	14.356	>25.000	20.544	>25.000
Nd	ICP–MS	0.03	48.2	>100.00	68.7	>100.00
Sm	ICP–MS	0.01	7.17	17.37	8.73	20.97
Eu	ICP–MS	0.005	1.097	2.6	1.406	3.369
Gd	ICP–MS	0.009	4.709	8.805	4.654	12.234
Tb	ICP–MS	0.003	0.641	0.946	0.634	1.548
Dy	ICP–MS	0.008	3.574	4.321	3.575	8.011
Ho	ICP–MS	0.003	0.711	0.739	0.645	1.466
Er	ICP–MS	0.008	2.087	2.056	1.857	4
Tm	ICP–MS	0.003	0.305	0.298	0.276	0.543
Yb	ICP–MS	0.01	2	2.01	1.89	3.49
Lu	ICP–MS	0.003	0.294	0.297	0.283	0.51

Appendix 10

Whole Rock Geochemical Data for Possible Weathered Archean Metasedimentary Rocks below Sibley Group in Diamond-Drill Hole NI-92-7

Note:
Universal Transverse Mercator (UTM) co-ordinates are North American Datum 1927 (NAD 27), Zone 16.

Appendix 10. Whole rock geochemical data for possible weathered Archean metasedimentary rocks below Sibley Group in diamond-drill hole NI-92-7 (blank = not analyzed; N.D. = not detected).

Laboratory			Geoscience Laboratories				
Sample			**03RM18**	**03RM19**	**03RM21**	**03RM23**	**03RM25**
Lithostratigraphic Unit			n/a	n/a	n/a	n/a	n/a
Drill Hole			NI-92-7	NI-92-7	NI-92-7	NI-92-7	NI-92-7
Distance below Sibley Group contact (cm)			50	185	395	645	895
Easting (m)			353850	353850	353850	353850	353850
Northing (m)			5401639	5401639	5401639	5401639	5401639
Description			weathered Quetico sandstone				
	Method	**Detection Limit**					
SiO_2 (weight %)	XRF	0.01	57.74	61.02	59.87	55.71	68.26
TiO_2	XRF	0.01	0.76	0.58	0.49	0.47	0.07
Al_2O_3	XRF	0.01	16.91	14.76	16.76	15.02	15.43
Fe_2O_3	XRF	0.01	8.6	7.8	6.68	4.67	1.1
MnO	XRF	0.01	0.01	0.03	0.03	0.04	0.03
MgO	XRF	0.01	3.25	3.99	5.87	5.14	0.86
CaO	XRF	0.01	0.52	2.36	1.73	3.58	3.53
K_2O	XRF	0.01	6.7	5.77	6.35	6.11	1.93
Na_2O	XRF	0.01	0.14	1.01	0.4	0.67	5.51
P_2O_5	XRF	0.01	0.23	0.17	0.19	0.22	1.15
LOI		0.05	4.86	2.4	2.21	8.13	0.97
Total			99.72	99.89	100.58	99.76	98.84
Cr (ppm)	XRF	4	613	549		609	20
Nb	XRF	2	8	5		7	8
Ni	XRF	2	83	49		119	10
Rb	XRF	2	172	116		149	95
Sc	XRF	6	27	29		30	N.D.
Sr	XRF	2	26	37		22	441
V	XRF	4	111	45		232	15
Y	XRF	1	8	8		6	N.D.
Zr	XRF	3	160	149		132	52
Cs	ICP-MS	0.007	17.78	10.951	14.825	14.785	11.006
Hf	ICP-MS	0.10	6.6	3.9	3.3	4.5	1.7
Rb	ICP-MS	0.05	80.76	129.19	81.95	140.56	101.11
Sr	ICP-MS	0.50	23.9	31.5	24.4	31.6	445
Ta	ICP-MS	0.17	0.42	0.42	0.28	0.27	4.89
Nb	ICP-MS	0.20	5.4	4.8	4.5	3.6	7.4
Th	ICP-MS	0.06	1.46	7.11	0.91	6.09	0.52
U	ICP-MS	0.007	5.134	5.977	3.065	5.032	1.412
Y	ICP-MS	0.02	5.56	7.32	2.68	9.96	1.17
Zr	ICP-MS	4.0	263.8	147.4	127.9	181.3	44.6
La	ICP-MS	0.02	1.17	3.6	0.74	6.29	1.69
Ce	ICP-MS	0.07	2.36	6.46	1.7	10.9	3.9
Pr	ICP-MS	0.006	0.375	1.233	0.242	2.017	0.513
Nd	ICP-MS	0.03	1.81	5.45	1.04	8.85	2.1
Sm	ICP-MS	0.01	0.59	1.92	0.31	2.34	0.47
Eu	ICP-MS	0.005	0.195	0.547	0.099	0.62	0.206
Gd	ICP-MS	0.009	0.884	1.859	0.378	2.316	0.355
Tb	ICP-MS	0.003	0.143	0.281	0.064	0.327	0.043
Dy	ICP-MS	0.008	0.862	1.52	0.429	1.849	0.214
Ho	ICP-MS	0.003	0.173	0.285	0.101	0.373	0.042
Er	ICP-MS	0.008	0.502	0.808	0.315	1.037	0.105
Tm	ICP-MS	0.003	0.076	0.122	0.052	0.16	0.017
Yb	ICP-MS	0.01	0.54	0.83	0.4	1.12	0.11
Lu	ICP-MS	0.003	0.083	0.129	0.066	0.181	0.016

Appendix 11

Whole Rock Geochemical Data for Possible Weathered Rove Formation Shale near Pass Lake, Ontario

Note:
Universal Transverse Mercator (UTM) co-ordinates are North American Datum 1927 (NAD 27), Zone 16.

Appendix 11. Whole rock geochemical data for possible weathered Rove Formation shale near Pass Lake, Ontario.

Laboratory			Geoscience Laboratories			
Sample			**03RM44**	**03RM45**	**03RM46**	**03RM47**
Lithostratigraphic Unit			Rove Fm?	Rove Fm?	Rove Fm?	Rove Fm?
Distance below Sibley Group contact (cm)			20	60	120	170
Outcrop Locality			Pass Lake	Pass Lake	Pass Lake	Pass Lake
Easting (m)			371803	371803	371803	371803
Northing (m)			5380488	5380488	5380488	5380488
Description			weathered shale	weathered shale	weathered shale	weathered shale
	Method	**Detection Limit**				
SiO_2 (weight %)	XRF	0.01	55.94	59.71	77.71	66.85
TiO_2	XRF	0.01	0.72	0.75	0.37	0.71
Al_2O_3	XRF	0.01	15.5	16.61	7.92	14.82
Fe_2O_3	XRF	0.01	5.24	10.7	4.9	3.97
MnO	XRF	0.01	0.08	0.02	0.03	0.03
MgO	XRF	0.01	5.02	3.37	1.85	3.23
CaO	XRF	0.01	3.11	0.4	0.84	0.37
K_2O	XRF	0.01	5.17	5.54	2.64	5.04
Na_2O	XRF	0.01	0.03	0.04	N.D.	0.03
P_2O_5	XRF	0.01	0.15	0.16	0.1	0.15
LOI		0.05	8.65	2.34	3.01	4.75
Total			99.61	99.64	99.35	99.95
Cr (ppm)	XRF	4	152	145	82	165
Nb	XRF	2	14	14	7	14
Ni	XRF	2	81	86	41	77
Rb	XRF	2	151	151	70	137
Sc	XRF	6	20	20	9	17
Sr	XRF	2	35	33	16	30
V	XRF	4	214	201	160	330
Y	XRF	1	30	28	13	23
Zr	XRF	3	196	189	102	179
Cs	ICP–MS	0.007	9.765	9.336	4.182	7.653
Hf	ICP–MS	0.10	5.2	5.1	2.9	4.8
Rb	ICP–MS	0.05	>150.00	88.99	73.36	69.56
Sr	ICP–MS	0.50	34.9	32.7	17	27.9
Ta	ICP–MS	0.17	0.94	0.94	0.48	0.91
Nb	ICP–MS	0.20	13.9	14.3	6.7	13.7
Th	ICP–MS	0.06	12.96	11.28	6.64	7.73
U	ICP–MS	0.007	5.81	8.063	3.099	5.402
Y	ICP–MS	0.02	30.14	24.31	12.06	11.21
Zr	ICP–MS	4.0	203.3	195.5	111.5	189.2
La	ICP–MS	0.02	38.08	35.88	20.83	19.59
Ce	ICP–MS	0.07	69.04	67.43	33.84	38.21
Pr	ICP–MS	0.006	8.022	7.812	3.894	4.564
Nd	ICP–MS	0.03	28.83	27.76	14.35	16.67
Sm	ICP–MS	0.01	5.49	5.12	2.61	2.85
Eu	ICP–MS	0.005	1.13	1.015	0.566	0.495
Gd	ICP–MS	0.009	5.362	4.474	2.436	2.287
Tb	ICP–MS	0.003	0.828	0.698	0.35	0.338
Dy	ICP–MS	0.008	4.986	4.134	2.104	2.05
Ho	ICP–MS	0.003	1	0.857	0.415	0.413
Er	ICP–MS	0.008	2.935	2.547	1.22	1.242
Tm	ICP–MS	0.003	0.452	0.38	0.179	0.188
Yb	ICP–MS	0.01	3.06	2.63	1.14	1.29
Lu	ICP–MS	0.003	0.468	0.397	0.181	0.2

Appendix 12

Whole Rock Analyses of Various Sibley Group Carbonate Rocks

Note:
Universal Transverse Mercator (UTM) co-ordinates are North American Datum 1927 (NAD 27), Zone 16.

Appendix 12. Whole rock analyses of various Sibley Group carbonate rocks.

Laboratory	University of Saskatchewan	
Sample	**M6**	**M6**
Lithostratigraphic Unit	Channel Island Mbr.	continued
Drill Hole	NI-97-2	
Stratigraphic Height (above Sibley) (m)	?	
Outcrop Locality	n/a	
Easting (m)	353850	
Northing (m)	5443000	
Description	dolomitic mudstone	

	Method	**Detection Limit**	
SiO_2 (weight %)	XRF	0.01	15.2
TiO_2	XRF	0.01	0.11
Al_2O_3	XRF	0.01	1.99
Fe_2O_3	XRF	0.01	0.32
MnO	XRF	0.01	0.04
MgO	XRF	0.01	18.75
CaO	XRF	0.01	25.48
K_2O	XRF	0.01	0.52
Na_2O	XRF	0.01	0.22
P_2O_5	XRF	0.01	0.03
Cr_2O_3	XRF	0.01	<0.01
LOI			37.5
Total			100.4
Nb (ppm)	XRF		<2
Rb	XRF		17
Sr	XRF		222
Y	XRF		4
Zr	XRF		42
Ba	XRF		1630
Cs	ICP–MS	0.01	0.82
Hf	ICP–MS	0.04	0.81
Rb	ICP–MS	0.17	18.66
Sr	ICP–MS	0.19	245.28
Ta	ICP–MS	0.01	0.15
Nb	ICP–MS	0.02	1.63
Th	ICP–MS	0.02	3.16
U	ICP–MS	0.04	0.52
Y	ICP–MS	0.01	7.43
Zr	ICP–MS	0.04	24.75
La	ICP–MS	0.01	10.21
Ce	ICP–MS	0.01	19.82
Pr	ICP–MS	0.01	2.50
Nd	ICP–MS	0.08	9.50
Sm	ICP–MS	0.09	2.03
Eu	ICP–MS	0.03	0.44
Gd	ICP–MS	0.05	1.76
Tb	ICP–MS	0.01	0.23
Dy	ICP–MS	0.04	1.29
Ho	ICP–MS	0.01	0.25
Er	ICP–MS	0.02	0.71
Tm	ICP–MS	0.01	0.09
Yb	ICP–MS	0.05	0.56
Lu	ICP–MS	0.01	0.09

	Method	**Detection Limit**	
Li (ppm)	ICP–MS	4.03	38.84
Be	ICP–MS	1.83	N.D.
Sc	ICP–MS	1.30	3.91
V	ICP–MS	0.34	11.97
Mo	ICP–MS	0.12	0.34
Ba	ICP–MS	0.20	1571.87
Tl	ICP–MS	0.02	0.09
Pb	ICP–MS	0.15	1.36
Bi	ICP–MS	0.02	0.05
P	ICP–MS	30.02	239.62
Ti	ICP–MS	0.36	575.68
Cr	ICP–MS	1.37	8.62
Co	ICP–MS	0.04	3.22
Ni	ICP–MS	0.28	5.66
Cu	ICP–MS	0.51	7.12
Zn	ICP–MS	1.07	2.82
As	ICP–MS	0.10	2.00
Ge	ICP–MS	0.04	1.08
Mo	ICP–MS	0.05	0.32
Ag	ICP–MS	0.01	0.06
Cd	ICP–MS	0.19	N.D.
Sn	ICP–MS	0.03	0.97
Sb	ICP–MS	0.02	0.16
W	ICP–MS	0.08	5.03
Hg	ICP–MS	0.60	N.D.

* N.D. = not detected

Appendix 12. continued

Laboratory	University of Saskatchewan	
Sample	**03RM6**	**03RM6**
Lithostratigraphic Unit	Channel Island Mbr.	continued
Drill Hole	n/a	
Stratigraphic Height (above Sibley) (m)	n/a	
Outcrop Locality	Pass Lake Hwy	
Easting (m)	372820	
Northing (m)	5377714	
Description	dolomitic mudstone	

	Method	Detection Limit	
SiO_2 (weight %)	XRF	0.01	42.29
TiO_2	XRF	0.01	0.36
Al_2O_3	XRF	0.01	8.53
Fe_2O_3	XRF	0.01	1.14
MnO	XRF	0.01	0.08
MgO	XRF	0.01	10.1
CaO	XRF	0.01	12.56
K_2O	XRF	0.01	5.04
Na_2O	XRF	0.01	0.2
P_2O_5	XRF	0.01	0.11
Cr_2O_3	XRF	0.01	<0.01
LOI			19.85
Total			100.4
Nb (ppm)	XRF		7
Rb	XRF		109
Sr	XRF		60
Y	XRF		27
Zr	XRF		170
Ba	XRF		733
Cs	ICP–MS	0.01	4.96
Hf	ICP–MS	0.04	3.93
Rb	ICP–MS	0.17	102.09
Sr	ICP–MS	0.19	55.85
Ta	ICP–MS	0.01	0.63
Nb	ICP–MS	0.02	9.91
Th	ICP–MS	0.02	9.33
U	ICP–MS	0.04	3.36
Y	ICP–MS	0.01	23.03
Zr	ICP–MS	0.04	142.76
La	ICP–MS	0.01	25.27
Ce	ICP–MS	0.01	50.75
Pr	ICP–MS	0.01	6.68
Nd	ICP–MS	0.08	24.54
Sm	ICP–MS	0.09	4.75
Eu	ICP–MS	0.03	0.85
Gd	ICP–MS	0.05	4.49
Tb	ICP–MS	0.01	0.64
Dy	ICP–MS	0.04	4.03
Ho	ICP–MS	0.01	0.75
Er	ICP–MS	0.02	2.19
Tm	ICP–MS	0.01	0.33
Yb	ICP–MS	0.05	2.17
Lu	ICP–MS	0.01	0.32

	Method	Detection Limit	
Li (ppm)	ICP–MS	4.03	40.51
Be	ICP–MS	1.83	2.43
Sc	ICP–MS	1.30	8.44
V	ICP–MS	0.34	34.89
Mo	ICP–MS	0.12	0.31
Ba	ICP–MS	0.20	649.15
Tl	ICP–MS	0.02	0.45
Pb	ICP–MS	0.15	5.39
Bi	ICP–MS	0.02	0.48
P	ICP–MS	30.02	593.85
Ti	ICP–MS	0.36	1938.83
Cr	ICP–MS	1.37	34.52
Co	ICP–MS	0.04	7.50
Ni	ICP–MS	0.28	14.47
Cu	ICP–MS	0.51	14.74
Zn	ICP–MS	1.07	14.74
As	ICP–MS	0.10	5.35
Ge	ICP–MS	0.04	1.58
Mo	ICP–MS	0.05	0.30
Ag	ICP–MS	0.01	0.05
Cd	ICP–MS	0.19	N.D.
Sn	ICP–MS	0.03	2.49
Sb	ICP–MS	0.02	0.31
W	ICP–MS	0.08	2.13
Hg	ICP–MS	0.60	N.D.

* N.D. = not detected

Appendix 12.	continued	
Laboratory	University of Saskatchewan	
Sample	**BO2-1**	**BO2-1**
Lithostratigraphic Unit	Middlebrun Bay Mbr.	continued
Drill Hole	n/a	
Stratigraphic Height (above Sibley) (m)	n/a	
Outcrop Locality	Channel Island	
Easting (m)	462992	
Northing (m)	5406020	
Description	stromatolite	

	Method	**Detection Limit**	
SiO_2 (weight %)	XRF	0.01	67.92
TiO_2	XRF	0.01	0.01
Al_2O_3	XRF	0.01	0.07
Fe_2O_3	XRF	0.01	0.08
MnO	XRF	0.01	0.05
MgO	XRF	0.01	5.73
CaO	XRF	0.01	10.83
K_2O	XRF	0.01	0.05
Na_2O	XRF	0.01	<0.01
P_2O_5	XRF	0.01	<0.01
Cr_2O_3	XRF	0.01	<0.01
LOI			14.3
Total			100.4
Nb (ppm)	XRF		2
Rb	XRF		5
Sr	XRF		402
Y	XRF		4
Zr	XRF		<2
Ba	XRF		>10000
Cs	ICP–MS	0.01	0.53
Hf	ICP–MS	0.04	0.13
Rb	ICP–MS	0.17	1.75
Sr	ICP–MS	0.19	761.47
Ta	ICP–MS	0.01	0.05
Nb	ICP–MS	0.02	0.81
Th	ICP–MS	0.02	0.17
U	ICP–MS	0.04	0.92
Y	ICP–MS	0.01	10.23
Zr	ICP–MS	0.04	4.70
La	ICP–MS	0.01	24.35
Ce	ICP–MS	0.01	14.98
Pr	ICP–MS	0.01	2.60
Nd	ICP–MS	0.08	9.84
Sm	ICP–MS	0.09	1.78
Eu	ICP–MS	0.03	0.78
Gd	ICP–MS	0.05	1.73
Tb	ICP–MS	0.01	0.20
Dy	ICP–MS	0.04	1.16
Ho	ICP–MS	0.01	0.24
Er	ICP–MS	0.02	0.57
Tm	ICP–MS	0.01	0.08
Yb	ICP–MS	0.05	0.37
Lu	ICP–MS	0.01	0.04

	Method	**Detection Limit**	
Li (ppm)	ICP–MS	4.03	N.D.
Be	ICP–MS	1.83	N.D.
Sc	ICP–MS	1.30	2.66
V	ICP–MS	0.34	15.22
Mo	ICP–MS	0.12	N.D.
Ba	ICP–MS	0.20	17731.95
Tl	ICP–MS	0.02	N.D.
Pb	ICP–MS	0.15	0.57
Bi	ICP–MS	0.02	0.05
P	ICP–MS	30.02	110.17
Ti	ICP–MS	0.36	36.05
Cr	ICP–MS	1.37	N.D.
Co	ICP–MS	0.04	4.23
Ni	ICP–MS	0.28	1.30
Cu	ICP–MS	0.51	38.05
Zn	ICP–MS	1.07	3.67
As	ICP–MS	0.10	0.43
Ge	ICP–MS	0.04	18.19
Mo	ICP–MS	0.05	N.D.
Ag	ICP–MS	0.01	0.02
Cd	ICP–MS	0.19	N.D.
Sn	ICP–MS	0.03	1.64
Sb	ICP–MS	0.02	0.22
W	ICP–MS	0.08	19.65
Hg	ICP–MS	0.60	N.D.

* N.D. = not detected

Appendix 12. continued

Laboratory	University of Saskatchewan	
Sample	**03RM27**	**03RM27**
Lithostratigraphic Unit	Fire Hill Mbr.	continued
Drill Hole	NI-92-7	
Stratigraphic Height (above Sibley) (m)	157.45	
Outcrop Locality	n/a	
Easting (m)	353850	
Northing (m)	5443000	
Description	nodular gyp/anh	

	Method	Detection Limit	
SiO_2 (weight %)	XRF	0.01	1.08
TiO_2	XRF	0.01	0.02
Al_2O_3	XRF	0.01	0.26
Fe_2O_3	XRF	0.01	0.2
MnO	XRF	0.01	<0.01
MgO	XRF	0.01	0.19
CaO	XRF	0.01	34.6
K_2O	XRF	0.01	0.15
Na_2O	XRF	0.01	0.03
P_2O_5	XRF	0.01	0.02
Cr_2O_3	XRF	0.01	<0.01
LOI			2.93
Total			39.58
Nb (ppm)	XRF		<2
Rb	XRF		<2
Sr	XRF		939
Y	XRF		<2
Zr	XRF		<2
Ba	XRF		175
Cs	ICP–MS	0.01	0.16
Hf	ICP–MS	0.04	0.08
Rb	ICP–MS	0.17	3.58
Sr	ICP–MS	0.19	857.62
Ta	ICP–MS	0.01	0.02
Nb	ICP–MS	0.02	0.32
Th	ICP–MS	0.02	0.21
U	ICP–MS	0.04	0.51
Y	ICP–MS	0.01	2.32
Zr	ICP–MS	0.04	2.66
La	ICP–MS	0.01	0.92
Ce	ICP–MS	0.01	1.83
Pr	ICP–MS	0.01	0.17
Nd	ICP–MS	0.08	0.54
Sm	ICP–MS	0.09	0.10
Eu	ICP–MS	0.03	0.02
Gd	ICP–MS	0.05	0.11
Tb	ICP–MS	0.01	0.02
Dy	ICP–MS	0.04	0.10
Ho	ICP–MS	0.01	0.02
Er	ICP–MS	0.02	N.D.
Tm	ICP–MS	0.01	0.01
Yb	ICP–MS	0.05	0.10
Lu	ICP–MS	0.01	N.D.

	Method	Detection Limit	
Li (ppm)	ICP–MS	4.03	N.D.
Be	ICP–MS	1.83	N.D.
Sc	ICP–MS	1.30	2.49
V	ICP–MS	0.34	9.58
Mo	ICP–MS	0.12	0.90
Ba	ICP–MS	0.20	30.35
Tl	ICP–MS	0.02	0.03
Pb	ICP–MS	0.15	1.85
Bi	ICP–MS	0.02	0.14
P	ICP–MS	30.02	167.05
Ti	ICP–MS	0.36	124.83
Cr	ICP–MS	1.37	N.D.
Co	ICP–MS	0.04	0.54
Ni	ICP–MS	0.28	5.92
Cu	ICP–MS	0.51	2.28
Zn	ICP–MS	1.07	2.18
As	ICP–MS	0.10	0.70
Ge	ICP–MS	0.04	0.06
Mo	ICP–MS	0.05	0.80
Ag	ICP–MS	0.01	0.02
Cd	ICP–MS	0.19	N.D.
Sn	ICP–MS	0.03	0.12
Sb	ICP–MS	0.02	0.07
W	ICP–MS	0.08	0.09
Hg	ICP–MS	0.60	N.D.

* N.D. = not detected

Appendix 12.	continued	
Laboratory	University of Saskatchewan	
Sample	**03RM29**	**03RM29**
Lithostratigraphic Unit	Fire Hill Mbr.	continued
Drill Hole	NI-92-7	
Stratigraphic Height (above Sibley) (m)	158.6	
Outcrop Locality	n/a	
Easting (m)	353850	
Northing (m)	5443000	
Description	nodular gyp/anh	

	Method	**Detection Limit**	
SiO_2 (weight %)	XRF	0.01	0.49
TiO_2	XRF	0.01	<0.01
Al_2O_3	XRF	0.01	0.02
Fe_2O_3	XRF	0.01	0.06
MnO	XRF	0.01	<0.01
MgO	XRF	0.01	0.23
CaO	XRF	0.01	33.12
K_2O	XRF	0.01	0.03
Na_2O	XRF	0.01	0.04
P_2O_5	XRF	0.01	0.02
Cr_2O_3	XRF	0.01	<0.01
LOI			1.65
Total			35.73
Nb (ppm)	XRF		<2
Rb	XRF		<2
Sr	XRF		584
Y	XRF		<2
Zr	XRF		2
Ba	XRF		<20
Cs	ICP–MS	0.01	N.D.
Hf	ICP–MS	0.04	0.10
Rb	ICP–MS	0.17	0.55
Sr	ICP–MS	0.19	738.80
Ta	ICP–MS	0.01	0.02
Nb	ICP–MS	0.02	0.32
Th	ICP–MS	0.02	0.05
U	ICP–MS	0.04	0.09
Y	ICP–MS	0.01	1.93
Zr	ICP–MS	0.04	2.24
La	ICP–MS	0.01	0.38
Ce	ICP–MS	0.01	0.67
Pr	ICP–MS	0.01	0.10
Nd	ICP–MS	0.08	0.42
Sm	ICP–MS	0.09	0.10
Eu	ICP–MS	0.03	N.D.
Gd	ICP–MS	0.05	0.09
Tb	ICP–MS	0.01	N.D.
Dy	ICP–MS	0.04	0.06
Ho	ICP–MS	0.01	N.D.
Er	ICP–MS	0.02	N.D.
Tm	ICP–MS	0.01	0.01
Yb	ICP–MS	0.05	0.06
Lu	ICP–MS	0.01	N.D.

	Method	**Detection Limit**	
Li (ppm)	ICP–MS	4.03	N.D.
Be	ICP–MS	1.83	N.D.
Sc	ICP–MS	1.30	2.72
V	ICP–MS	0.34	1.75
Mo	ICP–MS	0.12	N.D.
Ba	ICP–MS	0.20	5.12
Tl	ICP–MS	0.02	N.D.
Pb	ICP–MS	0.15	0.61
Bi	ICP–MS	0.02	0.04
P	ICP–MS	30.02	180.27
Ti	ICP–MS	0.36	82.78
Cr	ICP–MS	1.37	N.D.
Co	ICP–MS	0.04	0.67
Ni	ICP–MS	0.28	3.78
Cu	ICP–MS	0.51	14.44
Zn	ICP–MS	1.07	2.21
As	ICP–MS	0.10	N.D.
Ge	ICP–MS	0.04	0.04
Mo	ICP–MS	0.05	N.D.
Ag	ICP–MS	0.01	0.03
Cd	ICP–MS	0.19	N.D.
Sn	ICP–MS	0.03	2.30
Sb	ICP–MS	0.02	N.D.
W	ICP–MS	0.08	1.79
Hg	ICP–MS	0.60	N.D.

* N.D. = not detected

Appendix 12. continued

Laboratory	University of Saskatchewan	
Sample	**03RM44**	**03RM44**
Lithostratigraphic Unit	Channel Island Mbr.	continued
Drill Hole	NI-92-7	
Stratigraphic Height (above Sibley) (m)	64	
Outcrop Locality	n/a	
Easting (m)	353850	
Northing (m)	5443000	
Description	nodular gyp/anh	

	Method	**Detection Limit**	
SiO_2 (weight %)	XRF	0.01	
TiO_2	XRF	0.01	
Al_2O_3	XRF	0.01	
Fe_2O_3	XRF	0.01	
MnO	XRF	0.01	
MgO	XRF	0.01	
CaO	XRF	0.01	
K_2O	XRF	0.01	
Na_2O	XRF	0.01	
P_2O_5	XRF	0.01	
Cr_2O_3	XRF	0.01	
LOI			
Total			
Nb (ppm)	XRF		
Rb	XRF		
Sr	XRF		
Y	XRF		
Zr	XRF		
Ba	XRF		
Cs	ICP–MS	0.01	0.10
Hf	ICP–MS	0.04	0.14
Rb	ICP–MS	0.17	2.18
Sr	ICP–MS	0.19	1281.69
Ta	ICP–MS	0.01	0.02
Nb	ICP–MS	0.02	0.47
Th	ICP–MS	0.02	0.18
U	ICP–MS	0.04	0.10
Y	ICP–MS	0.01	3.69
Zr	ICP–MS	0.04	5.08
La	ICP–MS	0.01	1.14
Ce	ICP–MS	0.01	2.71
Pr	ICP–MS	0.01	0.36
Nd	ICP–MS	0.08	1.39
Sm	ICP–MS	0.09	0.33
Eu	ICP–MS	0.03	0.04
Gd	ICP–MS	0.05	0.29
Tb	ICP–MS	0.01	0.03
Dy	ICP–MS	0.04	0.19
Ho	ICP–MS	0.01	0.03
Er	ICP–MS	0.02	0.11
Tm	ICP–MS	0.01	0.02
Yb	ICP–MS	0.05	0.09
Lu	ICP–MS	0.01	N.D.

	Method	**Detection Limit**	
Li (ppm)	ICP–MS	4.03	N.D.
Be	ICP–MS	1.83	N.D.
Sc	ICP–MS	1.30	4.73
V	ICP–MS	0.34	1.88
Mo	ICP–MS	0.12	N.D.
Ba	ICP–MS	0.20	47.60
Tl	ICP–MS	0.02	0.04
Pb	ICP–MS	0.15	0.52
Bi	ICP–MS	0.02	N.D.
P	ICP–MS	30.02	564.54
Ti	ICP–MS	0.36	164.61
Cr	ICP–MS	1.37	2.59
Co	ICP–MS	0.04	0.44
Ni	ICP–MS	0.28	5.62
Cu	ICP–MS	0.51	2.25
Zn	ICP–MS	1.07	7.02
As	ICP–MS	0.10	N.D.
Ge	ICP–MS	0.04	0.19
Mo	ICP–MS	0.05	N.D.
Ag	ICP–MS	0.01	0.02
Cd	ICP–MS	0.19	N.D.
Sn	ICP–MS	0.03	0.38
Sb	ICP–MS	0.02	N.D.
W	ICP–MS	0.08	N.D.
Hg	ICP–MS	0.60	N.D.

* N.D. = not detected

Metric Conversion Table

Conversion from SI to Imperial			Conversion from Imperial to SI		
SI Unit	*Multiplied by*	*Gives*	*Imperial Unit*	*Multiplied by*	*Gives*
		LENGTH			
1 mm	0.039 37	inches	1 inch	**25.4**	mm
1 cm	0.393 70	inches	1 inch	**2.54**	cm
1 m	3.280 84	feet	1 foot	**0.304 8**	m
1 m	0.049 709	chains	1 chain	20.116 8	m
1 km	0.621 371	miles (statute)	1 mile (statute)	**1.609 344**	km
		AREA			
1 cm^2	0.155 0	square inches	1 square inch	**6.451 6**	cm^2
1 m^2	10.763 9	square feet	1 square foot	**0.092 903 04**	m^2
1 km^2	0.386 10	square miles	1 square mile	2.589 988	km^2
1 ha	2.471 054	acres	1 acre	0.404 685 6	ha
		VOLUME			
1 cm^3	0.061 023	cubic inches	1 cubic inch	**16.387 064**	cm^3
1 m^3	35.314 7	cubic feet	1 cubic foot	0.028 316 85	m^3
1 m^3	1.307 951	cubic yards	1 cubic yard	0.764 554 86	m^3
		CAPACITY			
1 L	1.759 755	pints	1 pint	0.568 261	L
1 L	0.879 877	quarts	1 quart	1.136 522	L
1 L	0.219 969	gallons	1 gallon	**4.546 090**	L
		MASS			
1 g	0.035 273 962	ounces (avdp)	1 ounce (avdp)	28.349 523	g
1 g	0.032 150 747	ounces (troy)	1 ounce (troy)	**31.103 476 8**	g
1 kg	2.204 622 6	pounds (avdp)	1 pound (avdp)	**0.453 592 37**	kg
1 kg	0.001 102 3	tons (short)	1 ton (short)	**907.184 74**	kg
1 t	1.102 311 3	tons (short)	1 ton (short)	**0.907 184 74**	t
1 kg	0.000 984 21	tons (long)	1 ton (long)	**1016.046 908 8**	kg
1 t	0.984 206 5	tons (long)	1 ton (long)	**1.016 046 90**	t
		CONCENTRATION			
1 g/t	0.029 166 6	ounce (troy)/ ton (short)	1 ounce (troy)/ ton (short)	34.285 714 2	g/t
1 g/t	0.583 333 33	pennyweights/ ton (short)	1 pennyweight/ ton (short)	1.714 285 7	g/t

OTHER USEFUL CONVERSION FACTORS

	Multiplied by	
1 ounce (troy) per ton (short)	31.103 477	grams per ton (short)
1 gram per ton (short)	0.032 151	ounces (troy) per ton (short)
1 ounce (troy) per ton (short)	20.0	pennyweights per ton (short)
1 pennyweight per ton (short)	0.05	ounces (troy) per ton (short)

Note: Conversion factors which are in bold type are exact. The conversion factors have been taken from or have been derived from factors given in the Metric Practice Guide for the Canadian Mining and Metallurgical Industries, published by the Mining Association of Canada in co-operation with the Coal Association of Canada.

ISSN 0826-9580
ISBN 0-7794-9212-9